**Title**
The effects of wavelength, metals, and reactive oxygen species on the sunlight inactivation of microorganisms: observations and applications to the solar disinfection of drinking water



**Author**
Fisher, Michael Benjamin

**Publication Date**
2011

Peer reviewed|Thesis/dissertation

# The effects of wavelength, metals, and reactive oxygen species on the sunlight inactivation of microorganisms: observations and applications to the solar disinfection of drinking water

By

Michael Benjamin Fisher

A dissertation submitted in partial satisfaction of the

Requirements for the degree of

Doctor of Philosophy

In

Engineering - Civil and Environmental Engineering

In the

Graduate Division

Of the

University of California, Berkeley

Committee in charge:

Professor Kara L. Nelson, Chair

Professor Stuart Linn

Professor David L. Sedlak

Professor Bettina M. Voelker

Spring, 2011

The effects of wavelength, metals, and reactive oxygen species on the sunlight inactivation of microorganisms: observations and applications to the solar disinfection of drinking water



by Michael Benjamin Fisher

Abstract

The effects of wavelength, metals, and reactive oxygen species on the sunlight inactivation of microorganisms: observations and applications to the solar disinfection of drinking water

By Michael Benjamin Fisher
Doctor of Philosophy
In
Engineering - Civil and Environmental Engineering
University of California, Berkeley
Professor Kara L. Nelson, Chair

Sunlight has long been known to inactivate microorganisms in natural waters and engineered systems. However, the mechanisms of inactivation are not yet fully understood. Solar disinfection (SODIS) is a treatment technology that relies on the germicidal effects of sunlight to inactivate pathogens in drinking water at the point of use. The objective of this work was to explore the roles of wavelengths, transition metals, and reactive oxygen species in the inactivation of indicator microorganisms in water, and discuss the implications of these findings for solar water disinfection. Alternative container materials and hydrogen-peroxide-producing additives were found to accelerate the sunlight inactivation of MS2 bacteriophage as well as *E. coli* and *Enterococcus* bacteria during field trials. Furthermore, it was observed that the inactivation of *E. coli* and *Enterococcus* derived from local wastewater was significantly slower than the inactivation of laboratory-cultures of the same organisms, while the inactivation of MS2 was slowest of all. The inactivation of all organisms appeared to be heavily dependent on the UVB-transparency of the container material used. To investigate these apparent wavelength effects in more depth, sunlight action spectra were measured in clear water for bacteriophage and *E. coli*. Both UVA (320 - 400 nm) and UVB (280 - 320 nm) light were found to contribute to the inactivation of PRD1 bacteriophage, while only UVB inactivated MS2. The inactivation of three laboratory *E. coli* strains and three *E. coli* strains isolated from wastewater was also studied. Both UVB and UVA wavelengths contributed to the inactivation of all strains, which exhibited strong similarities in their inactivation characteristics, while *E. coli* naturally present in fresh wastewater was found to be less sensitive to UVA than a cultured laboratory strain. A computational model was developed for interpreting the action spectra of these viruses and bacteria with 3-nm resolution. Studies were also conducted to investigate the roles of iron and reactive oxygen species in the photoinactivation of *E. coli*. Mutants lacking peroxidase and superoxide dismutase enzymes were found to be more sensitive to polychromatic simulated sunlight, while cells grown with low iron concentrations were more resistant to photoinactivation. Furthermore, prior exposure to light sensitized *E. coli* to subsequent exposure to hydrogen peroxide in the dark, an effect which was diminished for cells grown on low-iron media. Collectively, these results provide further evidence for the involvement of both UVA and UVB wavelengths in driving *E. coli* photoinactivation through a mechanism that appears to be consistent with intracellular photoFenton chemistry. These findings also reinforce the critical role of UVB wavelengths in the

sunlight inactivation of viruses and, to a lesser extent, wastewater-derived bacteria. The approach to measuring photoaction spectra used in this work may be applicable to investigations of a variety of photobiological and photochemical systems. Finally, the fieldwork results suggest that additives and alternative container materials may be able to greatly accelerate the photoinactivation of microorganisms in drinking water.

Dedication

This work is dedicated to my parents, whose love, support, encouragement, and patience made my efforts possible, and to my grandfather, who encouraged my enthusiasm for science and exploration throughout my childhood.

## Contents

## Figures

## Tables

## Terms and Abbreviations

Ahp: Alkyl hydroperoxide reductase: one of several enzymes responsible for degrading peroxides
ATP: Adenosine triphosphate
BP: Base pair (DNA or RNA)
CFU: colony-forming unit: amount of a culturable organism required to form a single colony on culture media
DFO: Desferrioxamine Mesylate (iron chelator)
DPD: N, N-diethyl-p-phenylene diamine
EBSS: Earle's Balanced Salt Solution
HP (I, II): Hydroperoxidases I and II: a class of catalase enzymes responsible for degrading peroxides
LB: Luria-Bertani
MEM: Minimal Essential Medium
NADH: Nicotinamide Adenine Dinucleotide
NADPH: Nicotinamide Adenine Dinucleotide Phosphate
NUV: near-UV (280-400 nm)
PBS: Phosphate Buffered Saline
PC: polycarbonate
PET: polyethylene terephthalate
POU: point-of-use
PP: polypropylene
PPCO: polypropylene copolymer
PS: polystyrene
ROS: reactive oxygen species
SODIS: solar disinfection
UV: ultraviolet
UVA: 320-400 nm
UVB: 280-320 nm
UVC: 100-280 nm
Visible Light: 400-700 nm
WT: wild-type (nonmutant) strain

Acknowledgements

Many thanks to the National Science Foundation, the American Society for Engineering Education, the American Water Works Association, and the U.C. Berkeley Blum Center for Developing Economies for their generous support of this work.

Many thanks to Alberto Castro, Maria Luisa Chavez, Cecilia Decker, Wilbur Hinojosa Delgadillo, Dr. James Imlay, Erin Inglish, Mercedes Iriarte, Alexandro Canaza Jorges, Dr. Tamar Kohn, Dr. David Love, Don Emilio Mamani, Fernando Arias Meneses, Ing. Alvaro Mercado, Dr. Kara Nelson, Dr. Brian Pecson, Fermin Reygadas, Scott Remine, Leidy Rocha, Ing. Ana Maria Romero, Matthias Saladin, Elsa Sanchez, Rudi Schuech, Michael Schulte, Andrea Silverman, Dr. Gordon Williams, and the countless other individuals who made this work possible!

# 1. Introduction

## 1.1. Focus of this Work

This work focuses on the ability of sunlight to inactivate microorganisms in water. It is therefore relevant both to point-of-use drinking water treatment techniques utilizing sunlight and to attempts to understand photoinactivation processes in natural and engineered environmental systems. While the inactivation of all microorganisms is of interest, particular attention will be given to *E. coli*, as much of the work in this study and the literature has utilized this species as an indicator microorganism. Much of this work focuses on applications of sunlight-mediated microbial inactivation to SODIS, the solar disinfection of drinking water at the point-of-use (i.e. at the household scale).

In the following introduction, point-of-use drinking water technologies will be broadly reviewed, followed by a more detailed review of the applied and mechanistic aspects of solar disinfection of drinking water. The applied review discusses the technical aspects and microbiological efficacy of this disinfection technique, the behavioral aspects determining user uptake of and adherence to solar disinfection, and epidemiological studies that have explored the health impact of previous intervention trials. The mechanistic review will cover not only studies concerned with point-of-use water treatment applications, but general explorations of the wavelength-dependence and photochemical mechanisms of sunlight inactivation of microorganisms in general, and of *E. coli* in particular.

These studies provide the foundation for the current work. Specifically, prior work on the wavelength dependence of photoinactivation informs the current studies of the ability of alternative container materials with different UV-visible transmittance spectra to accelerate the inactivation of bacteria and MS2 bacteriophage (Chapter 2), as well as our more fundamental studies of the wavelength dependence of the photoinactivation of MS2 and PRD1 bacteriophage (Chapter 3), as well as *E. coli* (Chapter 4). Furthermore, previous studies of the role of different sensitizers, targets, reactive intermediates, and cellular defenses in the inactivation of *E. coli* and other organisms informs both our current work on the ability of additives to accelerate the photoinactivation of indicator organisms in the field (Chapter 2) and our more mechanistic explorations of the roles of iron, hydrogen peroxide, and superoxide in the photoinactivation of *E. coli* (Chapter 5).

### 1.1.1. Drinking Water Treatment

Solar disinfection (SODIS) is a point of use drinking water treatment technology that relies on sunlight to inactivate pathogens in water. Understanding the applied and mechanistic features of this process may help facilitate future efforts to demonstrate and enhance the impact of solar disinfection. Specifically, understanding the wavelength dependence and putative mechanisms of inactivation for different classes of microorganisms may inform decisions on the types of materials and additives, if any, used for SODIS. In addition, understanding these dimensions may provide insights into the operating procedures, meteorological conditions, and geographic settings under which SODIS may produce optimal results for users.

#### 1.1.2. Understanding photoinactivation in natural and engineered systems

Light and oxygen are present in aquatic systems ranging from lakes, rivers, and oceans to natural and constructed wetlands, as well as waste stabilization ponds for the treatment of wastewater. Photooxidative stress affects the viability and infectivity of countless microorganisms in each of these systems. Better understanding the processes driving this form of stress may be important both to understanding and predicting the behavior of organisms in existing systems, as well as to better targeting efforts to control inputs of microbial pollutants into natural systems and potentially designing engineered systems to more effectively inactivate pathogens.

## 1.2. Point-of-Use Drinking Water Treatment

### 1.2.1. The Right to Safe Water

In addition to being essential for human survival and development, access to enough safe drinking water is a fundamental human right (Mintz 2001; WHO 2003). However, nearly 1 billion people in developing countries currently lack access to an improved water source, and 2.6 billion lack access to improved sanitation (WHO/UNICEF, 2010). Moreover, many of those who have nominal access to improved water sources may be exposed to unsafe water as a result of poorly maintained and intermittently pressurized systems (Vairavamoorthy et al., 2008). Diarrheal diseases are especially prevalent in communities without access to safe water, adequate hygiene, and improved sanitation. These diseases account for an estimated 2.2 million deaths each year, 6% of the total disease burden in developing countries and 17% of all mortality in children under the age of five (Mathers et al., 2009; WHO, 2009).

Point-of-use (POU) water treatment technologies have received increasing attention as valuable tools for improving drinking water quality and reducing diarrheal illness (Clasen et al., 2007a; Clasen et al., 2007b; Mintz et al., 2001; Sobsey, 2002). However, it is often difficult to prove a direct link between water treatment and health, and some researchers have suggested that in areas where sanitation and hygiene are poor, improvements in water quality may not lead to appreciable improvements in health (Cairncross, 2003; Eisenberg et al., 2007; Schmidt and Cairncross, 2009). However, in combination with hygiene education and hand washing practices, studies suggest that point-of-use improvements in drinking water quality can frequently lead to improved health (Clasen et al., 2007b; Sobsey, 2002; Sobsey et al., 2008). The World Health Organization asserts that safe water is essential not only for health, but also for effective education, economic prosperity, and human dignity (WHO 2003).

### 1.2.2. Limitations of Centralized Safe Water Systems

Continuously-pressurized piped distribution of treated drinking water is among the most reliable and cost-effective means of providing safe water to communities. However, there are many settings in which such systems are absent or so poorly maintained and operated that they do not provide safe water to their end users (Vairavamoorthy et al., 2008). In emergency settings, in settings without functional governments, or where resources are extremely scarce, safe and properly-operating centralized distribution systems are frequently lacking. Hundreds of millions of individuals in such settings are

likely to lack access to safe, piped treated water for the foreseeable future (Mintz et al., 2001). Therefore, point-of-use drinking water treatment may be a valuable set of technologies for reducing harm to those individuals.

### 1.2.3. Review of POU Technologies

A number of point-of-use (POU) drinking water treatment technologies are currently in use in developing countries worldwide, and many of these have been reviewed by Sobsey (Sobsey, 2002; Sobsey et al., 2008) and others. Some of the most widely used POU technologies include boiling, ceramic filtration, slow sand filtration, POU micro-and ultrafiltration devices, chlorination, and combined chlorination and flocculation (ibid).

#### 1.2.3.1. Characteristics of an Ideal POU

An ideal POU water treatment technology would be one that is highly effective, simple to use and maintain, low cost, acceptable to users, highly sustainable, and with high potential for dissemination (Sobsey, 2002). Oates adds that a POU technology should be effective against a broad range of pathogens, should not make water unpalatable, should involve only minor concentrations of any chemicals, should provide residual protection against recontamination, and should utilize locally available equipment (Oates, 2001). A POU system should be robust, breaking down infrequently if at all, and should require readily available parts and expertise for maintenance. Moreover, it must be obvious to the user when a system is malfunctioning. Finally, while an acceptable system should not significantly alter the taste, odor, or appearance of water to the point of making it unappealing to users, the ability to smell, taste, or see evidence that a POU technology is "working" may be indispensable for inspiring confidence in users (Lukacs, 2001). While no single POU technology meets all of these criteria, several have been demonstrated to be effective at reducing waterborne illness and to be readily adopted by users in developing country settings.

#### 1.2.3.2. Boiling

Boiling is simple and highly effective at inactivating pathogens, and is the most commonly used POU water treatment technology (Clasen et al., 2008). However, in addition to being time- and labor-intensive, boiling can require prohibitive and unsustainable amounts of fuel (Clasen et al., 2008; Mintz et al., 2001). Moreover, boiling can alter the taste of water, making it potentially unpalatable to users (Clark, 1956), while the additional time required for boiled water to cool is an added inconvenience. Furthermore, because boiling water does not provide any residual disinfecting power, and because boiled water is often stored unsafely in open containers or in containers where unwashed hands and cups may be easily introduced, recontamination of boiled drinking water is often a problem (Clasen et al., 2008).

#### 1.2.3.3. Chlorination

Point-of-use chlorination is the second most widely used POU water treatment technology. Chlorine in the form of aqueous sodium hypochlorite solutions, calcium hypochlorite tablets, or tablets containing sodium dichloro- or trichloro isocyanurates can be added to water to inactivate most bacteria and viruses, as well as some protozoans. Different dosing procedures can produce free chlorine concentrations ranging from less

than 1 mg/L at the low end to over 10 mg/L at the upper limit, but concentrations are generally on the order of 2-4 mg/L, depending on source water quality (CDC, 2000). At lower concentrations, all the available free chlorine may be lost to reactions with dissolved organic matter in contaminated water, while at higher concentrations the chlorine taste becomes unpalatable to most users. Advantages of chlorine include low cost, rapid inactivation of most bacteria and viruses, and low shipping weight per dose. This technology has several drawbacks, however, including limited shelf life (particularly for sodium hypochlorite), low efficacy against eukaryotic parasites such as *Cryptosporidium* species, and a tendency for free chlorine to be consumed by dissolved organic matter (Arnold and Colford, 2007; McLaughlin et al., 2009; Sobsey et al., 2008). Chlorination of water with high organic content can also lead to the formation of carcinogenic disinfection byproducts (Morris et al., 1992), although these are generally considered vastly preferable to the presence of infectious waterborne pathogens.

#### 1.2.3.4. Filtration

Four types of point-of-use filtration are commonly employed: ceramic filtration, slow sand filtration, cartridge micro- and ultrafiltration, and superficial filtration through fabric or other coarse porous media. Superficial filtration may remove sediment and other particulates, upon which significant concentrations of pathogens are thought to be sorbed (Huo et al., 1996). However, this is generally not sufficient to adequately remove most pathogens.

##### 1.2.3.4.1. Ceramic Filters

Ceramic filters are used in numerous forms, primarily pot and candle filters. These can remove parasites and some bacteria, but viruses are too small to be adequately removed by the pores in most ceramic filters (although many of the particles to which they are adsorbed may be removed) (Sobsey et al., 2008). Many ceramic filters are also characterized by low flow rates and can develop cracks, which may be undetectable to the naked eye while permitting the passage of unfiltered water. Some ceramic filters are impregnated with silver, which has been reported to enhance the biocidal effect (Oyanedel-Craver and Smith, 2007). Manufacturers maintain that silver inactivates pathogens on contact, while other researchers have suggested that dissolved silver ions may be responsible for much of the disinfecting power of this additive.

##### 1.2.3.4.2. Slow Sand Filters

Slow sand filters remove most protozoan cysts and helminth eggs, as well as some bacteria, but significant concentrations of bacteria and viruses may pass through. However, the ability of the *schmutzdecke*, or slime layer, on the surface of a properly-operated, ripened slow sand filter to degrade organic pollutants and some microorganisms is significant. Sand filters are characterized by variable performance, however, which varies as a function of filter ripening and other factors. Drawbacks of slow sand filters include their large size and weight, as well as the relatively high cost of many designs (Sobsey et al., 2008).

##### 1.2.3.4.3. Microfiltration and Ultrafiltration

Microfiltration and ultrafiltration cartridges are used primarily in mass-produced filters. Microfiltration devices include the Hindustan Unilever Pure-IT®, which combines a carbon block filter capable of removing protozoan cysts and helminth eggs with trichloroisocyanurate tablets capable of inactivating bacteria and viruses (Patterson et al., 2010). This filter requires quarterly replacement of the filter cartridge, chlorine tablets, and other parts, but is robust, attractive, and has a reasonably high flow rate. Ultrafiltration systems include the Vestergaard Frandsen Lifestraw Family® and the Lifesaver® water purifier. These filters are reported to efficiently remove all classes of pathogens, as well as particulate matter, and to filter up to 20,000 liters before needing to be replaced (Clasen et al., 2009). Ultrafiltration systems typically have acceptable flow rates; however, because they need a significant amount of pressure to achieve these flow rates, the Lifestraw Family® requires a roughly one-meter vertical drop, making it potentially awkward to use. Other designs utilize mechanical pumps, which may fail or prove too tiring for sustained use.

#### 1.2.3.5. Metal Ion Disinfectants

Several metal-ion-based disinfectants exist, including silver-based disinfectants, silver- and copper-based disinfectants, and proprietary metal ion disinfectants such as One Drop®. The mechanisms of action of these disinfectants are not entirely understood. However, some have been reported to inactivate bacteria and viruses (Hiser et al., 2009). Moreover, unlike chemical oxidants such as chlorine, metal ion disinfectants provide a lasting residual. However, the solubility and efficacy of metal ions may depend on solution chemistry, while the dosages required to achieve adequate inactivation of all pathogen classes in a timely manner is a subject of some uncertainty.

#### 1.2.3.6. UV Disinfection

Ultraviolet radiation, particularly the UVC light emitted by medium-pressure mercury vapor lamps (~254 nm), has long been known to inactivate all classes of pathogens. This inactivation occurs through the direct absorption of light by bonds in the genomic DNA or RNA of each organism, resulting in the formation of lesions which interfere with replication (Harm, 1980). Thus, while organisms may remain viable for some time, they are rendered noninfectious. A number of point-of-use water treatment technologies based on UVC light have been developed and promoted, including UV Waterworks (Drescher et al., 2001), the UV Tube, and the Mesita Azul—an integrated UV disinfection and safe water storage system developed by Fundación Cantaro Azul and based on the UV tube design developed at UC Berkeley and Lawrence Berkeley National Laboratory (Brownell et al., 2008; Reygadas et al., 2009). A similar system, the UVeta, likewise integrates a UV light source with a bucket fitted for safe storage of treated water (Barstow, 2010). Numerous other POU UV systems are commercially available worldwide. While all known organisms are susceptible to UV light, double stranded DNA viruses such as Adenovirus have much higher thresholds for inactivation than do most other organisms (Gerba et al., 2002), particularly if they are capable of undergoing host-mediated repair. In addition, pathogens present in highly turbid water or trapped within particles may not be efficiently inactivated by UV light (Qualls et al., 1983).

### 1.2.4. Efficacy of POU Technologies

The efficacy of a number of promising POU technologies has been reviewed by Sobsey (Sobsey et al., 2008) and others, and selected results are presented in Table 1.1.

Table 1.1 Efficacy of several point-of-use water treatment technologies

| Intervention | Log Removal/Inactivation | | | Diarrhea Reduction | Reference |
|---|---|---|---|---|---|
| | Bacteria | Viruses | Protozoan Cysts | | |
| **Ceramic Filter** | 2-6 | 0.5-4 | 4-6 | 50% | **(Sobsey et al., 2008)** |
| **Biosand Filter** | 1-3 | 0.5-3 | 2-4 | 45% | **(Sobsey et al., 2008)** |
| **SODIS** | 3-5.5+ | 2-4+ | 1-3+ | 26-37% | **(King et al., 2008; Sobsey et al., 2008)** |
| **Free Chlorine** | 3-6+ | 3-6+ | 3-6+ | 13-42% | **(Arnold and Colford, 2007; Sobsey et al., 2008)** |
| **Coagulation/ Chlorination** | **7-9** | **2-6** | **3-5** | **19-59%** | **(Sobsey et al., 2008)** |

#### 1.2.4.1. Evaluating POU Technologies

The effectiveness of POU technologies, both individually and as a group, is a challenging and contentious topic of ongoing research. This subject is complicated by the difficulty of accurately measuring outcomes and of agreeing on an objective definition of effectiveness. For the purpose of this work, we will define "efficacy" as the ability of an intervention to function properly when used correctly and with perfect adherence. We will likewise define "effectiveness" as the ability of introducing an intervention at the intention-to-treat level to produce the desired results when used by typical end users with actual (nonideal) levels of adherence.

Determining effectiveness also requires clearly defining and measuring the desired outcomes. It is reasonable to assume that the primary objective of any POU is to reduce the health impact of contaminated drinking water. However, apportioning the appropriate emphasis on morbidity and mortality presents a challenge: some interventions may reduce infant mortality without significantly affecting waterborne diarrheal illness rates in adults, or vice versa. For the purpose of this work, we will envision effectiveness as some combination of reduced morbidity and mortality in children under the age of five. This definition is helpful, since the most severe impairments to life, health, and development from waterborne illness impact this age group disproportionately (Mathers et al., 2009).

However, even measuring these variables is complicated. The cost of directly observing such relatively infrequent events as diarrhea and mortality in a sample size large enough to measure an effect of POU interventions can be considered prohibitive. As a result, most studies rely on questionnaire-based surveys administered to mothers and heads of household with some periodic frequency. This introduces several potentially

confounding factors, particularly in unblinded studies (a category which includes the majority of POU intervention trials to date). Such confounders include recall bias (Hunter, 2009; Schmidt and Cairncross, 2009), socially desirable response bias, and survey effects (Zwane et al., 2011). These biases may partially explain the finding that the reported effect size of point-of-use drinking water chlorination and solar disinfection studies tended to decrease with increasing trial duration (Arnold and Colford, 2007; Hunter, 2009). One recent meta analysis of unblinded epidemiological studies of POU trials found significant bias accounting for much, if not all, of the reported effects of several POU interventions (Hunter, 2009).

This bias may take several forms, including publication bias (Easterbrook et al., 1991). To the extent that negative results of epidemiological field trials are under-published by journals and that researchers studying POU interventions may be predisposed to confirmation biases regarding the efficacy of the intervention in question, an inadvertent tendency toward favorable results may be inevitable, particularly where researchers are not blinded to study conditions. Thus, even when all researchers act in good faith and the highest levels of professional integrity are observed, bias in unblinded studies may be unavoidable.

Finally, integrating across the numerous health outcomes that may occur or be prevented by interventions at different rates is a complex task. One often-cited approach to this challenge is the use of disability-adjusted life years, or DALYs (Murray, 1994), as a metric of the health-adjusted lifespan lost by individuals to disease and other factors. Thus, it may be helpful to think of an intervention's effectiveness as the number of DALY's whose loss is avoided by adding one additional "user" at the intention to treat level.

Another difficulty with measuring the effectiveness of a POU is the scale of analysis of that POUs implementation. For example, one could consider the results of a given study as measuring the effectiveness of a ceramic filter, or of a given implementation of that ceramic filter, or of an implementation of that filter in a given setting. Clearly, the task of measuring and comparing POU performance is a complex one. However, valuable comparisons may be possible with the careful application of statistical and epidemiological methods and the correct interpretation of their results.

Finally, cost metrics can be problematic in interpreting studies of POU interventions. The value of a POU is not only in its ability to prevent disease, but also in its ability to prevent disease more effectively and economically than the next-best alternative given real-world environmental conditions and actual user compliance rates. Since POUs are designed to be implemented in resource-constrained settings, their goal is not only to deliver high efficacy, but to deliver the greatest efficacy to the greatest number for the greatest period of time with a given level of investment. As the number of potentially effective POU interventions increases, the ability to compare efficacy-per-dollar among potential options becomes critical. A recent study found POU water treatment in general to be highly cost-effective (Clasen et al., 2007a). However, weighing the marginal benefits of individual treatments remains a complex and politically fraught task. Thus, the

need for blinded randomized trials and objective evaluation procedures by which POU and non-POU water treatment technologies can be evaluated is significant.

### 1.2.5. Effectiveness of POU Technologies

#### 1.2.5.1. Chlorination

Point-of-use chlorination has been reported to significantly reduce diarrheal disease, with average reductions in incidence of roughly 30%. However, compliance was variable in these studies, with fewer than 50% of households having detectable chlorine residuals in their water storage containers during random visits conducted in several trials (Sobsey et al., 2008). Moreover, there was a notable, if not necessarily significant, trend towards smaller observed reductions in diarrhea risk with increasing trial length (Arnold and Colford, 2007; Hunter, 2009). These findings suggest that compliance may be an obstacle to the successful implementation of point-of-use chlorination.

#### 1.2.5.2. Filters

Trials of ceramic candle filters found diarrhea reductions on the order of 50-70%, while trials of ceramic pot filters found 30-60% reductions and biosand filters found diarrhea reductions of approximately 45%. Adherence in these trials was generally high, although breakage was a significant issue in some ceramic filter trials (Sobsey et al., 2008). Interestingly, one 6-month RCT of a biosand filter implementation found significantly greater diarrhea reductions of children 2-4 years old than those under 2 and over 5 years old (Stauber et al., 2009). This finding was attributed to the protective effects of breastfeeding.

Specifically, it was hypothesized that many children under two were exclusively breastfed for a significant period of time. Since exclusive breastfeeding would reduce the exposure of children under two to the unsafe water that ceramic filters are intended to treat, and since exclusive breastfeeding has been reported to be highly protective against diarrhea (Arifeen et al., 2001), the authors suggested that the unadjusted impact of ceramic filters on diarrhea in children under two years old might be overshadowed by these breastfeeding effects.

#### 1.2.5.3. Chlorination-Flocculation

Trials of combined chlorination/flocculation have found reductions in diarrhea of 19-59% (Sobsey et al., 2008). It is worth noting that some of these trials received direct support from manufacturers of the chlorination/flocculation products being studied (ibid).

### 1.2.6. Challenges in Evaluating POUs

While most published POU intervention trials have found significant reductions in diarrhea, recent studies have suggested that, as noted above, a variety of biases must be considered when interpreting the results of unblinded field trials (Schmidt and Cairncross, 2009). These biases may account for significant fractions of the disease reduction rates reported for point-of-use chlorination and SODIS studies (Hunter, 2009). Regardless of the effects of any biases, however, it seems clear that filtration-based POUs such as ceramic and slow sand filtration have higher reported diarrhea reduction rates

than point-of-use chlorination and SODIS, while the variability of reported reductions for chlorination plus coagulation make this POU difficult to compare (Sobsey et al., 2008). It seems possible that these differences in health impacts may in part be related to differences in adherence rates among users of filters vs. other POUs (ibid). If so, it is interesting to note that one common feature of these high-adherence POUs is that they consist of a single, fixed device, to which raw water can simply be added and from which treated water can be directly consumed. By contrast, the lower-adherence POUs such as SODIS and chlorination share the feature that they represent more abstract and precise (and by extension more complex and demanding) processes that a user must regularly perform, as compared to simply "refilling the filter when it's empty."

#### 1.2.7. Impact of POU Technologies in the Context of the MDGs

POU drinking water treatment technologies are an important part of the international effort to meet the millennium development goal of reducing by half the number of individuals lacking access to safe drinking water by 2015 (United_Nations, 2000). Moreover, POUs may represent important auxiliary treatment methods for households that have access to nominally improved water sources yet are at significant risk from waterborne diseases. These include individuals with access to intermittently pressurized piped water of dubious quality (Vairavamoorthy et al., 2008).

### 1.3. Solar Disinfection

Solar water disinfection, or SODIS, is one important point-of-use technology for drinking water treatment. It has been implemented in numerous countries, with millions of individuals reported to have been trained in its use (EAWAG/SANDEC, 2011).

#### 1.3.1. History

Sunlight has long been known to improve water quality. Sanskrit texts dating back to 2000 B.C. recommend treating water by exposure to sunlight, filtering it through charcoal, and storing it in copper vessels (Baker, 1981). The first controlled study on the ability of sunlight to inhibit bacterial growth was reported in 1877 by Downes and Blunt, who demonstrated that light was able to both inactivate bacteria and inhibit their growth in nutrient broth (Downes, 1877). In 1943, Hollaender conducted the first quantitative study of near-UV inactivation of *E. coli* (Hollaender, 1943), while in 1946 Lukiesh specifically reported the ability of natural sunlight to inactivate *E. coli* (Luckiesh, 1946). More recently, Calkins et al. reported that simulated solar UV-B rapidly inactivated both *E. coli* and other indicator organisms, in good agreement with the inactivation rates they observed in sunlit Kentucky waste stabilization ponds (Calkins et al., 1976).

In the 1980s, Acra et al. at the American University in Beirut, Lebanon, published the first quantitative studies on solar disinfection of drinking water and oral rehydration solutions (Acra et al., 1980; Acra, 1984). Since then, a number of groups have studied the SODIS process, with the Swiss Federal Institute for Environmental Science and Technology taking the lead in many areas of the applied research, as well as in disseminating practical SODIS information (EAWAG/SANDEC, 2011; Wegelin et al., 1994). To date, SODIS has been used and studied in two dozen countries in Africa, Asia, and Latin America (EAWAG/SANDEC, 2011).

### 1.3.2. Procedure

SODIS relies upon the combined putative abilities of ultraviolet and visible light, as well as elevated temperatures, to inactivate microorganisms. While the precise mechanisms responsible for SODIS are not yet fully understood, the efficiency of this treatment has been studied by a number of researchers, and has been characterized for representative bacteria and viruses (Wegelin et al., 1994). The process begins with pouring low-turbidity raw water into a clean, transparent PET (polyethylene terephthalate) plastic bottle, oxygenating the water by shaking, and exposing the bottle to sunlight for a period of at least one day (EAWAG/SANDEC, 2011). Recent work (Oates, 2001) suggests that two days may be preferable for ensuring adequate disinfection, and many SODIS proponents currently recommend exposing bottles for two days to ensure adequate treatment. The water is allowed to cool overnight and is ready to drink the next morning. SODIS has been reported to work best with clear water in containers with a depth of less than 10 cm (EAWAG/SANDEC, 2011; Wegelin et al., 1994).

### 1.3.3. Advantages and Drawbacks

The primary advantage of SODIS over other technologies is its simplicity. This method requires only plastic bottles, considered by many of its proponents to be ubiquitous and inexpensive or free in developing countries. A second advantage is its low cost, since additional chemicals, apparatus, and fuel are not required. Perhaps the most important aspect in terms of acceptability, according to proponents, is that SODIS does not alter the odor, taste, or appearance of the water and has no associated risks of an overdose. Some drawbacks of SODIS are labor inputs, potential scarcity of bottles, and the variable effectiveness of disinfection, especially in cloudy weather conditions (Fisher et al., 2008; Oates, 2001), all of which may tend to reduce the technology's acceptance. An additional drawback is the low adherence of users to the SODIS procedure in some contexts (Mausezahl et al., 2009).

### 1.3.4. Efficacy

#### 1.3.4.1. Bacteria

Most SODIS trials have reported greater than 3-log inactivation of *E. coli* and other cultured enteric bacteria in fewer than 6 hours under suitable field conditions (Acra, 1984; Dejung et al., 2007; Keenan, 2001; Kehoe et al., 2001; Reed et al., 2000; Wegelin et al., 1994). However, naturally occurring fecal coliforms have shown much slower inactivation rates in some cases (Fisher et al., 2008; Sinton et al., 2002b; Sommer et al., 1997), while light-resistant subpopulations of cultured *E. coli* were found to be inactivated considerably more slowly than light-sensitive organisms within the same trial (McGuigan et al., 1998).

#### 1.3.4.2. Viruses

Studies have also evaluated the efficacy of SODIS against human and bacterial viruses. Davies-Colley et al. (Davies-Colley et al., 2005) have reported rapid sunlight inactivation of somatic coliphage in pond waters. By contrast, Dejung et al. (Dejung et al., 2007) found that roughly 8-11 h of sunlight exposure were required to achieve a 1-log reduction

of three different classes of coliphage in cistern water under field conditions in Bolivia. Polio virus has been inactivated under simulated SODIS laboratory conditions (4.4-log reduction in 6 hours, 850$Wm^{-2}$, water temp. = 25$^{o}$ C) (Heaselgrave et al., 2006). Similarly, Wegelin et al. (Wegelin et al., 1994) found that at 20° C, three-log inactivation of bacteriophage f2, bovine rotavirus, and encephalomyocarditis virus occurred after 3.3, 2.5, and 12.5 h of simulated sunlight exposure, respectively. Walker *et al.* (Walker et al., 2004b) found that a solar disinfection (SODIS) pouch constructed from food-grade, commercially available packaging materials was slightly less efficient at reducing viable plaques of the F-specific RNA bacteriophage MS2 ( 3.5 log units) than at inactivating enterotoxigenic *E. coli* O18:H11 (5.0 log reduction) after 6 hours' exposure to natural sunlight. However, viable FRNA coliphages were detected in SODIS reactors fitted with reflectors (increasing the water temperature by an additional 8-10$^{o}$ C to 64-75$^{o}$ C) even though *E. coli* was easily disinfected under identical conditions (Rijal and Fujioka, 2003). Similarly, Safapour and Metcalf (Safapour and Metcalf, 1999) did not find significant sunlight inactivation of T2 phage after 8 hours' exposure. These findings suggest that under some conditions, viruses may prove to be quite resistant to solar disinfection.

#### 1.3.4.3. Protozoan Cysts

Several studies have reported significant rates of inactivation for protozoan cysts. King et al. (King et al., 2008) found rates of *Cryptosporidium parvum* oocyst inactivation ranging from 0.15 to 2.5 log units per hour. The same authors also observed that inactivation rates were highly dependent on solar UV, and on UVB in particular. Mendez-Hermida et al. (Mendez-Hermida et al., 2005) found that 6 h of simulated sunlight reduced the infectivity of *Cryptosporidium parvum* oocysts by 1.1 logs, while 8 h of natural sunlight reduced the concentration of viable cysts (as measured by vital dye staining) by 0.93 logs (Mendez-Hermida et al., 2007). McGuigan et al (McGuigan et al., 2006) found that the infectivity of *Cryptosporidium parvum* oocysts toward mice was reduced by 1.2 logs after 8 h exposure to sunlight, while 4 h of sunlight rendered *Giardia lamblia* cysts completely noninfectious and reduced *in vitro* excystation rates by approximately 0.7 logs. Mtapuri-Zinyowera et al. (Mtapuri-Zinyowera et al., 2009) found 1.3- and 0.7-log inactivation of *Giardia duodenalis* and *Entamoeba histolitica*, respectively, by vital dye staining, after 7 h of sunlight exposure in PET bottles. Meanwhile, Heaselgrave (Heaselgrave et al., 2006) found no inactivation of Acanthamoeba polyphaga cysts at temperatures below 50° C, but at 55° C observed a 2.1-log reduction in cyst viability after 6 h exposure to simulated sunlight.

#### 1.3.4.4. Helminth Eggs

Inactivation of helminth eggs by sunlight has been studied less extensively than other classes of pathogens. However, Spindler (Spindler, 1940) observed complete inactivation of *Ascaris suis* [*suum*] eggs after 3 h exposure to tropical sunlight.

#### 1.3.4.5. Fungi and Spores

Lonnen et al. (Lonnen et al., 2005) observed complete (5.4-log) inactivation of *Candida albicans* after 6 h exposure to simulated sunlight, and complete (5.5-log) inactivation of *Fusarium solani* following 8 h exposure. By contrast, the same group found only 1.7-log inactivation of Bacillus subtilis spores following 8 h exposure to simulated sunlight.

These findings suggest that while fungi and vegetative bacteria may be relatively sensitive to sunlight inactivation, bacterial spores appear to be much more resistant.

### 1.3.5. Adoption and Adherence

SODIS adoption rates have not been extensively studied. However, several field trials have measured adherence rates of study participants over the course of the trial. While some studies reported high levels of user compliance (Conroy et al., 1996), one randomized trial of 425 households found mean compliance rates of 32% (Mausezahl et al., 2009), while other groups have found sustained adoption rates as low as 9%, with up to 85% of users also consuming untreated water on a regular basis (Rainey and Harding, 2005a; b). One contributing factor in the varying level of user compliance may have been the buy-in and participation of influential opinion leaders in the Conroy study (op cit).

### 1.3.6. Health Impact Studies

SODIS health impact trials have found variable diarrhea reductions (Table 1.2). The majority of trials have found reductions in disease incidence of between 26-37% (Sobsey et al., 2008). Conroy et al. (Conroy et al., 1996) conducted one of the first SODIS RCTs, observing a 34% reduction in diarrhea and 35% decrease in severe diarrhea over 12 weeks. A follow-up trial by the same group found a sustained 16% reduction in diarrhea incidence over one year (Conroy et al., 1999). Furthermore, during a cholera outbreak the same authors observed that SODIS reduced cholera incidence by approximately 88% in children under 6 (95% CI: 35-98% reduction), while the effect in children 6-15 years old was not statistically significant (95% CI: 42% reduction-105% increase) (Conroy et al., 2001).

Studies conducted in rural Pakistan, rural Cambodia, and the periurban Kibera slum in Nairobi, Kenya found average reductions of diarrhea incidence in children of 41%, 31%, and 42%, respectively (Gurung et al., 2009), while a study in rural Uzbekistan found a reduction of 47% in diarrhea rates (Grimm, 2003). Some of these studies were observational in nature and appeared to lack adequate controls, while others may not have been adequately powered to detect effects at the levels they reported.

Furthermore, some of the previous SODIS trials were conducted in high-compliance settings such as Massai communities, in which the buy-in of Massai elders ensured high compliance rates among community members (Conroy et al., 1996; Conroy et al., 1999; 2001). A recent trial in a low-compliance setting found positive but statistically-insignificant reductions in diarrheal disease (Mausezahl et al., 2009). This is unsurprising, since the intention to treat individuals with an intervention is unlikely to affect health outcomes unless the intervention is actually used by study participants. A recent meta-analysis also concluded that the protective effects of SODIS after 1 year's implementation could not be confirmed as being significantly different from zero (Hunter, 2009). This is not to say that the study proves that SODIS is ineffective at the one year mark. Rather, the study calls for additional blinded trials of longer duration to better quantify the health impacts of SODIS and other interventions in trials of longer duration.

Table 1.2 Results of selected SODIS health impact studies

| Mean % Reduction (95% CI) | Outcome | Type of Study | Population | Sample Size | Age | Location | Adherence | Duration | Reference |
|---|---|---|---|---|---|---|---|---|---|
| 34* | Diarrhea | RCT | Massai, Rural | 206 children | 5-15 | Kenya | High | 12 weeks | (Conroy et al., 1996) |
| 16* | Diarrhea | RCT | Massai, Rural | 349 children | <6 | Kenya | High | 52 weeks | (Conroy et al., 1999) |
| 88* (35:98) | Cholera | RCT | Massai children <6, Rural | 299 children | <6 | Kenya | High | 8 weeks | (Conroy et al., 2001) |
| 41* | Diarrhea | | Rural | | | Pakistan | | | (Gurung et al., 2009) |
| 31* | Diarrhea | | Rural | | | Cambodia | | | (Gurung et al., 2009) |
| 42* | Diarrhea | | Kibera Slum, Periurban | | | Kenya | | | (Gurung et al., 2009) |
| 47* | Diarrhea | | Rural | 419 | All | Uzbekistan | 38% | 2 years | (Grimm, 2003) |
| 19 (-12:41) | Diarrhea | RCT | Rural | 22 clusters (725 children) | <5 | Bolivia | Moderate (32%) | 52 weeks | (Mausezahl et al., 2009) |

*Statistically significant reduction at the 95% confidence level (as calculated by the original study authors)

### 1.3.7. Social and Behavioral Studies

Several groups have studied social and behavioral factors linked to SODIS adoption, diffusion, and adherence. Heri and Mosler (Heri et al., 2005; Heri and Mosler, 2008; Moser and Mosler, 2008) conducted a study of 644 households in 8 Bolivian communities and found that reported SODIS use rates ranged from 2.5% to 92%, while the fraction of households with SODIS-treated water available on request during unannounced visits ranged from 0% to 55%. The authors further observed that the reported percentage of total water consumed by respondents that was treated using SODIS ranged from 1.5% to 56.9%. The authors found several factors affecting SODIS use, and calculated beta weights (that is, the amount by which SODIS water consumption increased when each factor increased by one standard deviation) for these factors as shown in Table 1.3. Kraemer and Mosler (Kraemer and Mosler, 2010) also studied similar factors affecting intentions and SODIS use, and selected results from their work are also presented below. While the authors of the last study conclude that both habits and persuasion influence SODIS adoption, the results regarding the amount of SODIS water consumed per household seem consistent with the findings of behavioral researchers such as Wood and others who report that habits are often stronger predictors of consumption behavior than intentions (Ji and Wood, 2007; Neal et al., 2006).

Table 1.3 Selected results from SODIS adoption studies

| Factor | B weight | Reference |
|---|---|---|
| Habits (degree of automaticity of SODIS) | 0.29* | (Heri et al., 2005) |
| Number of others seen using SODIS | 0.21* | (Heri et al., 2005) |
| Conviction SODIS water safe to drink | 0.20* | (Heri et al., 2005) |
| Perceived vulnerability to diarrhea | 0.16* | (Heri et al., 2005) |
| Belief that SODIS is fastest way to treat water | 0.13* | (Heri et al., 2005) |
| Compatibility with daily routine | 0.165* | (Heri and Mosler, 2008) |
| Perceived Vulnerability | 0.10* | (Heri and Mosler, 2008) |
| Availability of PET bottles | 0.10* | (Heri and Mosler, 2008) |
| % Peers Using SODIS | 0.123* | (Heri and Mosler, 2008) |
| Other Safe Water Sources | -0.547* | (Heri and Mosler, 2008) |
| SODIS habit strength | 0.24* | (Kraemer and Mosler, 2010) |
| Perceived benefit | 0.04 | (Kraemer and Mosler, 2010) |
| Knowledge about bacteria | 0.12 | (Kraemer and Mosler, 2010) |
| Perceived health risk of raw water | 0.02 | (Kraemer and Mosler, 2010) |

* Indicates result significantly different from 0 at the 95% confidence level according to authors' calculations.

Tamas et al. (Tamas et al., 2009) also found pronounced differences in the effectiveness of various SODIS promotion strategies in an observational study of four communities. Specifically, they found that both utilizing designated SODIS promoters and leveraging community opinion leaders increased SODIS use. However, while the use of promoters had a greater effect on short-term SODIS knowledge and use, opinion leaders had a stronger effect on sustained SODIS use. These findings are consistent with the observations of Heri et al. that adoption is correlated with the rate of SODIS use within potential users' social networks (Heri and Mosler, 2008).

### 1.3.8. Safety and Properties of PET Bottles

A variety of container materials have been used for solar water disinfection, but by far the most common container type has been 1-2 L polyethylene terephthalate (PET) bottles. This is currently the container type recommended by Fundación SODIS and the Swiss Federal Agency for Water Science and Technology. Studies have found that PET bottles do not leach significant concentrations of detectable compounds during SODIS (Wegelin et al., 2001), nor does water disinfected in PET bottles exhibit increased genotoxicity as measured by an Ames mutagenesis assay (Ubomba-Jaswa et al., 2010). PET bottles are inexpensive, thermostable at all relevant environmental temperatures, and can be reused multiple times for SODIS, typically lasting 3-6 months before accumulated scratches render them too opaque for effective use (Altherr, 2004). However, while PET is transparent to visible light and transmits significant amounts of UVA light, most PET bottles screen out UVB light and the shortest UVA wavelengths in sunlight. While earlier

researchers observed that the light excluded by PET only represents a small fraction of typical solar energy flux, these wavelengths may nevertheless be important for disinfection. Thus, the advantages and drawbacks of PET bottles as SODIS containers remain ongoing subjects of research and discussion.

### 1.3.9. Beyond PET Bottles: Approaches to Advanced Solar Disinfection

Several groups have studied disinfection in reactors with a variety of geometries and materials, and a small subset of these studies is summarized in Table 4. These trials can be divided into studies of batch and continuous flow reactors with a variety of reactor materials, as well as studies with or without the addition of additives or photocatalysts. For convenience, the term "window material" will be used to denote any material through which light must pass to reach the water to be treated, whether that material is the wall of a bottle or the covering of a tank or other reactor.

#### 1.3.9.1. Alternative Container Materials and Morphologies

Batch reactor studies have been performed in tubes, bottles, bags, and tanks made from quartz, borosilicate glass, PET, polystyrene (PS), polycarbonate (PC), polyethylene (PE), and other materials. It should be noted that in the case of plastics, two containers may be made from the same nominal polymer (e.g., PET) but contain different plasticizers and UV stabilizers that result in markedly different optical properties. That is true in the case of the polycarbonates used by Noble (Noble et al., 2004) and Davies (Davies et al., 2009). In the first case, UV-visible absorbance measurements of similar containers suggest that the 2 L PC bottle used by Noble et al. blocked significant amounts of UVB and some UVA light (Noble et al., 2004), while in the second case, manufacturer's specifications indicate that the PC material used in this study transmitted > 80% of all solar UV wavelengths (Davies et al., 2009). It can be seen that while significant variability exists, trials using uncovered reactors or UVAB-transparent window materials appeared to produce faster inactivation than those using less transparent materials such as PET (Table 1.4). Furthermore, trials using extremely thin layers of window material such as those performed in plastic bags tended to produce extremely rapid inactivation (Acra and Demerrell, 2001). Finally, studies using simple and compound parabolic reflectors found that these tended to enhance inactivation rates as well (Mani et al., 2006; Navntoft et al., 2008).

Table 1.4 Inactivation parameters and rates for organisms exposed to natural and artificial sunlight in reactors of various materials and configurations with and without additives and/or photocatalysts. [a]Values calculated for this work from data presented or referenced in the cited publication. [b]Values estimated for this work based on independent measurements of similar parameters. [c]Values estimated for this work from reports of similar parameters elsewhere in the literature. [d]Values integrated over 300-400 nm. [e]Values integrated over 320-400 nm. $F_{99.9}$ denotes the fluence (in megaJoules per square meter) required to achieve a 3-log inactivation of the organism studied. $t_{99.9}$ denotes the analogous time-based measurement (in hours).

| Reactor Config. | Organism (s) | Container/ Window Material (50% Transmittance wavelength [nm]) | Additive/ Catalyst | Max. Temp. (°C) | Light source | Intensity (W/m2) | $F_{99.9}$ (MJ/m2) | $t_{99.9}$ (h) | Reference |
|---|---|---|---|---|---|---|---|---|---|
| Batch<br>(30L tank) | *E. faecalis* | PC (< 280[a])<br>PC<br>PC<br>PS (~320[b]) | N/A<br>TiO2 (powdered)<br>TiO2 (immob)<br>N/A | 39 | Sun | 610[a] | 1.9<br>2.1<br>2.5<br>5.4 | 0.86[a]<br>0.97[a]<br>1.13[a]<br>2.45[a] | (Davies et al., 2009) |
| Batch<br>(30L tank) | P22 phage | PC<br>PC<br>PC<br>PS | N/A<br>TiO2 (powdered)<br>TiO2 (immob)<br>N/A | 39 | Sun | 610[a] | 4.5<br>7.2<br>6.6<br>12 | 2.05[a]<br>3.27[a]<br>3.00[a]<br>5.45[a] | (Davies et al., 2009) |
| Batch<br>(30L tank) | B. subtilis spores | PC<br>PC<br>PC<br>PS | N/A<br>TiO2 (powdered)<br>TiO2 (immob)<br>N/A | 39 | Sun | 610[a] | 5.7<br>9.0<br>5.7<br>8.1 | 2.59[a]<br>4.09[a]<br>2.59[a]<br>3.68[a] | (Davies et al., 2009) |
| Batch<br>(1L) | *E. coli*<br>ATCC11775 | PET (337[a])<br>PET + reflector<br>PET black back | N/A<br>N/A<br>N/A | 48<br>47.7<br>54.6 | Sun | >700 | >7.3[a]<br>>6.0[a]<br>>6.2[a] | 2.90<br>2.40<br>2.45 | (Mani et al., 2006) |
| Batch | *E. coli* K12<br>ATCC 23631 | PET Bottle<br>Glass Tube<br>Glass Tube + CPC reflector | N/A<br>N/A<br>N/A | 33 | Sun | 35<br>(320-400 nm) | 0.20 [a,e]<br>0.12 [a,e]<br>0.09 [a,e] | 1.93[a]<br>1.28[a]<br>0.89[a] | (Navntoft et al., 2008) |
| Batch<br>(50 mL) | *E. coli* K12<br>ATCC 23716 | Pyrex Bottle | N/A<br>TiO2 (powdered) | 32 | Solar sim | 1000 | 2.3<br>0.7 | 0.65<br>0.20 | (Rincón and Pulgarin, 2004a) |
| Batch<br>(50 mL) | Wastewater *E. coli* | Pyrex Bottle | N/A<br>TiO2 (powdered) | 32 | Solar sim | 1000 | 5.2<br>2.6 | 1.44<br>0.73 | (Rincón and Pulgarin, 2004a) |
| Recirc. (35L, 20L/m) | *E. coli* K12<br>ATCC 23716 | Glass Tube + CPC reflector | N/A<br>TiO2 (powdered) | N.R.<br>(35[c]) | Sun | 759<br>878 | 0.13[a]<br>0.09[a] | 1.71[a]<br>0.87[a] | (Rincon and Pulgarin, 2007) |
| Batch<br>(1 L) | *E. coli* | PET<br><br>BSG | N/A<br>Immob. $TiO_2$<br>N/A<br>Immob. $TiO_2$<br>Annealed $TiO_2$ | N.R. | Sun | 28.6[a] (300-400 nm) | 0.21[a,d]<br>0.13[a,d]<br>0.13[a,d]<br>0.13[a,d]<br>0.18[a,d] | 1.83[a]<br>1.17[a]<br>1.17[a]<br>1.17[a]<br>1.58[a] | (Duffy et al., 2004) |

### 1.3.9.2. $TiO_2$-Catalyzed Photoinactivation

In addition to alternative reactor materials and morphologies, a number of studies have used additives and titanium dioxide-based photocatalysts in batch and flow reactors, and these studies are described in a number of reviews (Blanco-Galvez et al., 2007; Malato et al., 2007; Rincón and Pulgarin, 2010). In the case of batch reactors, immobilized $TiO_2$ tended to accelerate inactivation in glass and PET reactors in a manner proportional to the surface-area-to-volume ratio of the reactor (Duffy, 2004), while the addition of powdered $TiO_2$ was found to accelerate inactivation in a concentration-dependent manner (up to a maximum of 1-1.5 g/L) (Rincón and Pulgarin, 2010). In general, powdered $TiO_2$ appeared to accelerate inactivation in glass reactors more effectively than an equivalent amount of $TiO_2$ immobilized on a Nafion® membrane (Rincón and Pulgarin, 2003). Interestingly, Davies et al. found that powdered and immobilized $TiO_2$ did not accelerate the batch photoinactivation of bacteria, viruses, and spores when a UVAB-transparent window material was used, and may even have slowed disinfection (Davies et al., 2009). Thus, it seems possible that while $TiO_2$ enhances photoinactivation when UVB

wavelengths are absent, the light screening effects of $TiO_2$ may outweigh its catalytic activity when UVB wavelengths are present. Furthermore, while Rincon and Pulgarin found that powdered $TiO_2$ dramatically accelerated the solar disinfection of laboratory cultured *E. coli* in glass bottles exposed to simulated sunlight, they observed that $TiO_2$ appeared to have a diminished or even inhibitory effect on the disinfection of indicator bacteria naturally present in wastewater, and that regrowth occurred in some cases when irradiated wastewater bacteria were allowed to stand in the dark for 48 h (Rincón and Pulgarin, 2004a). Studies further investigated the effects of additives such as $Fe^{3+}$ in batch reactors, which were found to accelerate inactivation, presumably by means of photoFenton reactions. In addition, the addition of hydrogen peroxide has been found to accelerate photoinactivation in batch reactors (Fisher et al., 2008; Keenan, 2001; Rincón and Pulgarin, 2004b), as has the addition of copper in combination with ascorbate (Fisher et al., 2008).

Flow reactor studies have also investigated the effects of immobilized and powdered $TiO_2$, as well as $Fe^{3+}$. These studies found similar results, with enhanced inactivation from the addition of powdered $TiO_2$ and also from $Fe^{3+}$, particularly when $H_2O_2$ was also added in addition to $Fe^{3+}$ (Rincón and Pulgarin, 2007a). Slower inactivation was observed in the presence of immobilized as compared to suspended $TiO_2$ (Rincón and Pulgarin, 2003), perhaps due to the far greater mean diffusion distance photoproduced reactive species must travel to reach a target organism. Interestingly, both flow rate and the presence of a catalyst appeared to have some effect on inactivation rates, with faster uncatalyzed sunlight inactivation occurring when the flow rate was increased (Rincón and Pulgarin, 2007a; b; c), but faster photocatalytic inactivation occurring when the flow rate was decreased (Sichel et al., 2007a; Sichel et al., 2007b).

### 1.4. Mechanisms of Photoinactivation

Sunlight inactivation of microorganisms is not entirely understood, but studies have demonstrated the importance of key wavelength regions, disinfection parameters, and reactive intermediates.

#### 1.4.1. Characteristics of Sunlight

Sunlight reaching the earth's surface varies significantly with factors such as the time of day, season, elevation, and latitude, as well as the stratospheric ozone concentration above the region of interest. Models such as SMARTS (Gueymard, 1995) and others have been designed to allow researchers to rapidly characterize these variations and predict their effects on sunlight spectra. However, despite this variation, several characteristics of sunlight remain relatively constant. Specifically, only a few percent of total solar irradiance is concentrated in the UV region, while UVB accounts for only one percent of total sunlight (Davies-Colley et al., 1999). Ozone and molecular oxygen dramatically attenuate UVC wavelengths, ensuring that intensity below 280 nm is virtually 0 at the earth's surface. Moreover, cloud cover disproportionately attenuates longer wavelengths relative to UV light, so that UV fluences on cloudy days may be higher than might otherwise be anticipated based on visible irradiance (Frederick and Erlick, 1997).

### 1.4.2. Wavelength Dependence of Photoinactivation

Despite the small fraction of sunlight intensity in the UV region, these wavelengths are by far the most important in driving the photoinactivation of microorganisms. Photoaction spectra are plots of the rate at which a chemical transformation or biological response occurs as a function of wavelength. Spectra measuring inactivation as a function of the wavelength of light emitted from a monochromatic source have shown UVB wavelengths to be far more important than UVA wavelengths in the inactivation of bacteria and viruses (Peak et al., 1984; Webb and Brown, 1979; Webb and Tuveson, 1982). By contrast, some studies using polychromatic light and optical cutoff filters have also shown UVA wavelengths to be highly important in the photoinactivation of bacteria (and some viruses) (Wegelin et al., 1994), although others have found wavelengths above 340 nm to be relatively unimportant (Davies-Colley et al., 1997; Sinton et al., 2002b). The discrepancies between early photoaction spectra and polychromatic experiments may be due to a number of factors, including synergies between different wavelengths. However, all studies are in agreement that UV light is far more important than visible wavelengths, and few groups dispute that, to the extent that it is able to reach organisms, UVB light is highly effective at inactivating them.

### 1.4.3. Photolysis Pathways

Photoinactivation of microorganisms is believed to proceed by a photolytic process in which sunlight results in the breaking or reorganization of chemical bonds within the target organism. Photolysis may proceed via direct or indirect pathways. In both pathways, a bond or delocalized electron cloud in a chromophore (i.e., light-absorbing molecule) accepts energy in the form of a photon, exciting the chromophore (A) and promoting bonding electrons to higher-energy antibonding orbitals (A*). These electrons may then subsequently relax without undergoing any chemical change by releasing heat or emitting a photon (no reaction), or they may relax by breaking or reorganizing bonds in a type I reaction, as a result of which the molecule (A*) is said to undergo direct photolysis. In indirect photolysis, the chromophore (A) becomes excited as before, but relaxes by transferring energy or electrons to another species (B) in solution (type II reaction) via electronic energy transfer, direct electron transfer, or hydrogen atom transfer (Zepp, 1984; Halliwell, 1999). Molecule A may also convert to a longer-lived triplet state via a process known as “intersystem crossing” before either transferring energy or electrons to B via a type II reaction or relaxing via a type I or no-reaction pathway.

When a second excited species (B*) is produced, this intermediate may in turn relax via each of the pathways described above (no reaction, type I reaction, type II reaction). A special case of this situation is when the excited species (A*) transfers charge/energy to a small, rapidly diffusible species (B) such as water, oxygen, or some nitrogen and organic species, in which case a reactive intermediate is formed, which may in turn react with and modify another target molecule in solution (C). When any species (B or C) other than the original chromophore (A) is modified as a result of these processes, that species is said to undergo indirect photolysis. We will refer to the special case in which the target species oxidized by the reactive intermediate (B*) is the original photosensitizer (A) as indirect autophotolysis. Since it may be difficult to distinguish between direct photolysis and

indirect autophotolysis without careful mechanistic studies, it is convenient to refer to these two cases collectively as simply “autophotolysis”.

#### 1.4.3.1. Extracellular

A variety of key photosensitizers are commonly present in the aquatic environment, and many of these can accelerate the inactivation of organisms by sunlight. These extracellular sensitizers include dissolved organic matter (DOM) such as humic substances (HSs), algal and microbial exudates (Zepp and Schlotzhauer, 1983), complexed transition metals (Blough, 1995), and others. Humic substances include humic and fulvic acids and can sensitize the production of a range of reactive species, including hydrogen peroxide, superoxide, and possibly singlet oxygen (Blough, 1995; Voelker et al., 1997). Humic substances can also react directly with other constituents in their photoexcited triplet states (Zepp et al., 1985). In addition to their ability to transform chemical species (Zepp et al., 1984), recent studies have shown that aqueous photosensitizers can accelerate the sunlight inactivation of bacteria (Kadir, 2010) and viruses (Kohn et al., 2007).

#### 1.4.3.2. Intracellular

Photosensitizers that are contained within microorganisms are referred to as intracellular, or endogenous, photosensitizers. A variety of biological macromolecules can absorb sunlight and potentially react to damage key targets within organisms. Although some of the principles discussed are applicable to viruses, eukaryotes, spores, and fungi, this discussion will focus primarily on vegetative bacteria, as more is known about potential sensitizers within these organisms than within other classes of microbes. The catalog of potential intracellular sensitizers is nearly as varied as the list of macromolecules and cofactors that make up microorganisms. A selection of potential sensitizers are presented below.

##### 1.4.3.2.1. DNA

DNA is known to absorb sunlight in the UVB region, leading to the formation of a variety of lesions including cyclobutane-pyrimidine dimers, 6-4 photoproducts, and single-stranded DNA breaks (Eisenstark et al., 1989; Harm, 1980; Sinha and Hader, 2002). Photoaction spectra for bacterial inactivation have found much of the DNA damage at wavelengths below 313 nm to be oxygen-independent, suggesting that direct DNA damage may be an important mechanism in this region (Webb and Brown, 1976). Although less than 1% of sunlight energy is present in the UVB region (Davies-Colley et al., 1999), these wavelengths may nonetheless be quite important. However, the absorbance of DNA is 3 orders of magnitude lower at 320 than at 260 nm (Jagger, 1985a), and it has been suggested that direct DNA damage is unlikely to account for all the mutations observed at UVA wavelengths and the longest UVB wavelengths (Peak et al., 1984). Furthermore, the oxygen dependence of DNA damage at longer UVB wavelengths suggests that even in cases where DNA may be a critical chromophore, much of the autooxidative damage that occurs may be indirect, possibly occurring via a Fenton reaction (Eisenstark et al., 1989). Interestingly, UVB DNA damage has been reported to be more easily repaired by cells than damage at higher wavelengths (Harm, 1980).

#### 1.4.3.2.2. Proteins

The amino acid tryptophan can absorb sunlight at the shorter UVB wavelengths (McCormick et al., 1976; McCormick and Thomason, 1978), potentially resulting in direct protein damage and/or the production of reactive oxygen species. Kochevar (Kochevar, 1990) has reported UVB-induced damage to human erythrocyte membrane proteins, while Sidorkina et al. (Sidorkina et al., 1999) have reported tryptophan-sensitized UVB damage to proteins in *E. coli*. Furthermore, excitation of tryptophan can contribute to the formation of reactive photoproducts which may be able to damage proteins (Zigman et al., 1976) and inhibit cell growth (Zigman and Hare, 1976), while other researchers have suggested that tryptophan acts to shield DNA from harmful UV wavelengths (Oladepo and Loppnow, 2010). Furthermore, studies suggest that in the presence of oxygen, near-UV photoproducts of tryptophan can in turn photosensitize the production of reactive oxygen species such as superoxide and hydrogen peroxide (McCormick and Thomason, 1978).

#### 1.4.3.2.3. NADH/NADPH

NAD and NADP are critical cofactors for a number of biological enzymes in cells. NADH has been identified as a potential endogenous photosensitizer, capable of producing hydrogen peroxide in the presence of UVA light (Ito et al., 2007). Both NADH and NADPH have also been reported to photosensitize the production of superoxide in the presence of monochromatic light at near-UV wavelengths (Cunningham et al., 1985b; Cunningham et al., 1985c). In addition to sensitizing the production of reactive intermediates, NADH is critical in a number of intracellular repair mechanisms and vital metabolic functions, making autophotolysis of this cofactor an extremely deleterious event. However, studies have also reported the ability of NADH to protect molecules in solution from superoxide-mediated UV photooxidation (240-410 nm) (Makareyeva et al., 1997).

#### 1.4.3.2.4. Flavins

Like NAD(P)H, flavins are critical redox cofactors in a wide variety of metabolic and repair functions. Flavins have been shown to sensitize the production of superoxide (Cunningham et al., 1985a) and hydrogen peroxide (Sato et al., 1995) when exposed to sunlight in vitro, although the superoxide quantum yields were lower than those reported for NAD(P). Furthermore, in the presence of oxygen, Riboflavin and other flavins produce singlet oxygen with extremely high quantum yields (0.1-0.5) when irradiated with 355 nm light (Baier et al., 2006a). Riboflavin has been shown to sensitize mammalian cells to inactivation and to increase the frequency of DNA lesions and mutations in the presence of UVA light (Besaratinia et al., 2007). This damage was prevented by prior treatment with vitamin C (ibid). Finally, *E. coli* mutants unable to synthesize riboflavin were shown to be sensitive to near UV light in proportion to their level of riboflavin supplementation, while supplementation had little effect on the NUV sensitivity of wild-type cells (Lloyd et al., 1990).

#### 1.4.3.2.5. Porphyrins

Porphyrins are a class of colored molecules containing four pyrrole rings joined by methene bridges with their N heteroatoms oriented so that their lone pair electrons are available to bind metal atoms. When an iron atom is complexed by the porphyrin ring, a heme group is formed. The bound iron atom can switch between the $Fe^{2+}$ and $Fe^{3+}$ oxidation states with an oxidation potential that depends on the functional groups attached to the pyrrole rings, making the heme family an extremely useful and versatile class of enzymatic cofactors (White, 2000). Furthermore, hemes are believed to form Fe(IV)-oxo intermediates during reactions with dioxygen (Nam, 2007). Hemes are present in cytrochromes, a class of membrane-bound redox enzymes present in bacterial (and eukaryotic) electron transport chains. Because of their large delocalized pi electron clouds, porphyrins and cytochromes are highly colored molecules, absorbing strongly in characteristic visible wavelength regions known as Soret bands. Each cytochrome has three such bands, an α, β, and γ band, with the α band typically occurring at approximately 400 nm and the β and γ bands between 500 and 600 nm (ibid). Tuveson et al. (Tuveson and Sammartano, 1986a) have suggested that the contributions of visible wavelengths to the inactivation of bacteria may be related to photosensitization by cytochromes.

Porphyrins are known to naturally photosensitize damage to microorganisms (Jagger, 1985a; Sies, 1985). Porphyrins and light have also been used to target tumors in vivo via a process known as photodynamic therapy, in which singlet oxygen formation at visible wavelengths has been identified as the key mechanism of photosensitized membrane damage in these applications (Weishaupt et al., 1976). Furthermore, mutants deficient in the synthesis of the porphyrin precursor δ-ALA have been found to be highly resistant to near-UV doses that produced 5-log inactivation in wild-type strains. These hemA8 mutants became more sensitive to NUV light with increasing δ-ALA supplementation in a dose-dependent manner (Tuveson and Sammartano, 1986a). Furthermore, supplementation with δ-ALA was not found to have a significant effect on wild-type cells. As the authors note, disruption of porphyrin synthesis may have inhibited the synthesis or function of the electron transport chain, a source of many other possible chromophores and ROSs (ibid). However, the strong dose-dependence observed with δ-ALA at all levels of supplementation seems difficult to explain if porphyrins are not critical photosensitizers. Interestingly, although it functions as a scavenger of the reactive oxygen species hydrogen peroxide, the porphyrin-containing protein catalase has also been reported to behave as an intracellular photosensitizer (Eisenstark and Perrot, 1987).

#### 1.4.3.2.6. Quinones

Quinones are a class of aromatic diones that participate in electron transport chains. It has been suggested that quinones may act as photosensitizers, absorbing light at the shortest solar UVB wavelengths to yield hydroxyl radicals, superoxide, and singlet oxygen (Alegra et al., 1999). Other groups have suggested that the hydroxylating effect of excited quinones is due to the formation of a hydroxyl radical-semiquinone complex, and not necessarily a free hydroxyl radical (Pochon et al., 2002).

#### 1.4.3.2.7. FeS clusters

Iron sulfur clusters are critical cofactors in many proteins within the electron transport chain, and have been identified as potential photosensitizers. One study found that irradiation of natural and artificial FeS proteins by blue light resulted in singlet oxygen formation and damage to cellular constituents (Kim and Jung, 1992).

#### 1.4.3.2.8. tRNA

Transfer RNA in *E. coli*, salmonella, and other organisms contains thiolated bases such as 4-thiouridine that are capable of absorbing light at UVA wavelengths (Favre et al., 1985; Kramer et al., 1988). This results in damage to the tRNA and transient cessation of protein synthesis, producing a characteristic growth delay effect. Since protein synthesis is involved in the SOS response (a response in which bacteria induce the production of ROS scavengers and other defenses against oxidative damage), this effect has been implicated in exacerbating oxidative stress (Favre et al., 1985).

### 1.4.4. Targets

A number of potential targets exist for damage photosensitized by the above chromophores. These include the chromophores themselves, as well as membranes, proteins, and DNA (all potential chromophores themselves, but also possible targets of damage mediated by other photosensitizers). Several groups have found evidence for membrane damage in bacteria exposed to near-UV light. Peak (Peak et al., 1987) found evidence that mutants deficient in porphyrin synthesis were sensitized to NUV light by δ-ALA addition, which resulted in membrane damage, as indicated by leakage of rubidium introduced into the irradiated cells. Moss and Smith (Moss and Smith, 1981) likewise found membrane damage to be critical in bacterial photoinactivation. Other studies have suggested that DNA damage is the dominant mechanism of near-UV photoinactivation (Eisenstark, 1987; Sinha and Hader, 2002; Tyrrell and Webb, 1973; Tyrrell, 1978a; Webb and Lorenz, 1972; Webb and Brown, 1976; 1979).

### 1.4.5. Intermediates

As noted above, in addition to direct photolysis and electronic energy transfer, excited chromophores can modify target molecules (including themselves) indirectly by producing reactive intermediates. These can include excited oxygen, nitrogen, and organic species. The observed oxygen-dependence of bacterial inactivation at wavelengths above 313 nm (Webb and Brown, 1979) has drawn particular attention to the class of reactive oxygen species (ROS). These include singlet oxygen as well as all of the one-electron reduction intermediates between molecular oxygen and water.

#### 1.4.5.1. Reactive Oxygen Species

##### 1.4.5.1.1. Singlet Oxygen

When chromophores absorb photons to reach excited triplet states they can readily react with molecular oxygen, which exists as a triplet in its ground state. As a result of this reaction, a lone electron is promoted from one of oxygen's bonding molecular orbitals to an antibonding orbital to produce the excited singlet oxygen species (Schwartzenbach, 2003). Singlet oxygen is rapidly quenched by water ($t_{1/2}$ ~ 3.8 μs), or can rapidly react

with species containing double bonds, including heme-containing proteins and lipids containing polyunsaturated fatty acids (PUFAs) (Halliwell, 1999). Furthermore, singlet oxygen can damage key scavengers of other reactive oxygen species, including catalase (ibid) and, in one *in-vitro* study, superoxide dismutase (Kim et al., 2001). Studies have also suggested that singlet oxygen may be a key species in the sunlight inactivation of bacteria (Curtis et al., 1992) and MS2 bacteriophage (Kohn and Nelson, 2007b), as well as human fibroblasts (Tyrrell and Pidoux, 1989). Studies with singlet-oxygen scavengers such as histidine have produced mixed results, possibly owing to the limited ability of these scavengers to compete with the dominant intracellular scavenger of $^1O_2$, water, which quenches singlet oxygen at a rate of approximately $10^5$ $s^{-1}$ (Wilkinson et al., 1995). Thus, while the relative rates at which $^1O_2$ reacts with various membrane-permeable quenchers are well known, some studies may not have added sufficiently high concentrations of these quenchers to significantly affect sunlight inactivation rates. Studies such as those of Tyrrell (Tyrrell and Pidoux, 1989), which use a deuterated medium to enhance the lifetime of singlet oxygen (via the kinetic isotope effect), are thus more convincing, since they reduce the rate of quenching by singlet oxygen's primary sink, rather than introducing a competing sink that may or may not significantly alter steady-state concentrations of $^1O_2$.

#### 1.4.5.1.2. Superoxide

Superoxide radical anion ($O_2\bullet^-$) is the one-electron reduction product of molecular oxygen. Dissolved organic matter can photosensitize the production of superoxide in natural waters (Blough, 1995), while in aerobic biological systems, superoxide is produced in the electron transport chain. Although the production of reactive intermediates such as superoxide is undesirable for organisms, it is a "cost of doing business" for aerobically-respiring cells. Specifically, because molecular oxygen exists in an unpaired triplet state, spin-paired redox enzymes in the electron transport chain must reduce dioxygen one electron at a time. Superoxide can be formed when the reduced flavins of these enzymes are adventitiously oxidized by molecular oxygen rather than the adjacent enzyme in the ETC (Imlay, 2003; 2006). This process occurs at rates up to 5 $\mu M\ s^{-1}$ in aerobically respiring *E. coli* (Halliwell, 1999). Superoxide production has also been reported from the photooxidation of tryptophan by NUV light (McCormick and Thomason, 1978). While superoxide does not directly damage most cellular constituents, it reacts with enzymatic iron-sulfur clusters, which are highly conserved throughout all kingdoms of life, at rates on the order of $10^6$ $M^{-1}s^{-1}$, inactivating these enzymes and releasing free intracellular iron (Fridovich, 1998; Imlay, 2003; 2006). Superoxide also undergoes dismutation (one molecule oxidizes another) to generate hydrogen peroxide. This reaction can be catalyzed by transition metal ions in solution (Blough, 1995), or by superoxide dismutases, a nearly ubiquitous class of enzymes whose sole known function is to reduce steady-state intracellular concentrations of superoxide (Fridovich, 1998; Halliwell, 1999; Imlay, 2003; 2006). Finally, superoxide can reduce intracellular Fe(III) to Fe(II), perpetuating the Fenton reaction (Halliwell, 1999).

Studies have shown that mutants lacking superoxide dismutases are sensitized to mutations and inactivation by near-UV light from a mercury vapor source, suggesting that superoxide may play an important role in photooxidative damage (Hoerter et al.,

1989; Knowles and Eisenstark, 1994). While trials have not demonstrated an effect of exogenously-added superoxide dismutase on the photoinactivation of microorganisms (Curtis et al., 1992; Gourmelon et al., 1994), this is not surprising. The putative role of superoxide in oxidative stress is an intracellular one, and it is highly unlikely that large proteins such as SODs or charged radicals such as superoxide could cross plasma membranes or significantly interact, given the short diffusion distance of superoxide and the high activity of cells' endogenous superoxide dismutase enzymes. Thus, significant evidence exists for the participation of superoxide in photooxidative damage. Furthermore, the dismutation product of superoxide, hydrogen peroxide, is also a potentially important reactive oxygen species.

1.4.5.1.3. Hydrogen Peroxide

Hydrogen peroxide is present at concentrations on the order of 0.1-1 μM in typical surface waters and can be formed at rates on the order of 0.1-10 μM/h in sunlit natural waters (Cooper et al., 1988) by the photoexcitation of DOM (Blough, 1995; Cooper et al., 1988). The primary sink for hydrogen peroxide in natural systems is believed to be microbial catalases, which efficiently scavenge hydrogen peroxide from the extracellular milieu (Blough, 1995). In aerobic biological systems, the dismutation of adventitiously-produced superoxide contributes to the formation of significant amounts of hydrogen peroxide (Seaver and Imlay, 2001a). Production rates of 3 μM/s were measured in stationary phase *E. coli*, and rates as high as 15 μM/s were measured in exponentially growing cells (ibid). The activities of enzymes such as urate oxidase and D-amino acid oxidase may also contribute to intracellular $H_2O_2$ production (Halliwell, 1999). Added hydrogen peroxide has been shown to sensitize bacterial cells and viruses to inactivation by natural and simulated sunlight (Ahmad, 1981; Craggs et al., 1994; Eisenstark et al., 1986; Fisher et al., 2008; Hartman and Eisenstark, 1978; Hartman et al., 1979; Hartman and Eisenstark, 1980; Keenan, 2001), while $H_2O_2$ scavengers have been found to protect cells from irradiation (Curtis et al., 1992; Gourmelon et al., 1994; Sammartano and Tuveson, 1984). The mechanism of this activity is believed to be related to DNA damage (Hartman and Eisenstark, 1978), and Fenton-mediated DNA damage has been shown to be the mechanism of hydrogen peroxide toxicity in the dark (Imlay et al., 1988b). Furthermore, this mechanism has been shown to contribute to bimodal killing, with mode one killing occurring at lower $H_2O_2$ doses and mode two occurring at higher concentrations and via a different mechanism (Imlay and Linn, 1987). In addition, exogenously-added hydrogen peroxide can also damage lipids and proteins, including Fe and CuZn superoxide dismutases, presumably via Fenton mechanisms (Halliwell, 1999). Unlike charged and singlet ROSs, $H_2O_2$ has a half-life on the order of hours in natural waters (Draper and Crosby, 1983) and can cross cell membranes both via diffusion and through aquaporins (Halliwell, 1999; Seaver and Imlay, 2001a).

1.4.5.1.4. Other Peroxides

Organic peroxides can be formed via lipid peroxidation (Halliwell, 1999), and may be highly reactive in the presence of transition metals and heme groups, with potentially cytotoxic effects (Akaike et al., 1992; Termini, 2000). These peroxides are rapidly degraded by scavengers such as alkyl hydroperoxide reductase, but have been shown to inhibit growth in strains lacking these scavengers (Storz et al., 1989). Imlay has noted

that bacteria lack the polyunsaturated fatty acids that are precursors to lipid peroxidation (Imlay, 2002), thus if lipid peroxidation does occur in bacterial systems, it may be initiated and propagated by unknown mechanisms.

#### 1.4.5.1.5. Hydroxyl Radical

Hydroxyl radicals can be formed in natural waters via the excitation of constituents such as dissolved organic matter, nitrate, and nitrite, although the high reactivity of this species makes its steady-state concentrations extremely low (Halliwell, 1999). In biological systems, hydroxyl reacts at near diffusion-limited rates with all classes of biological molecules. As a result, the lifetime of hydroxyl radical is extremely short in all types of systems, approximately $10^{-9}$ s in vivo (Sies, 1993). As noted above, Fenton-mediated hydroxyl radical formation and subsequent DNA damage has been proposed as a mechanism of oxidative stress in bacteria exposed to hydrogen peroxide, sunlight, or both. Attempts to measure the effect of hydroxyl radical scavengers on microbial inactivation rates (Curtis et al., 1992; Gourmelon et al., 1994) have produced mixed results. However, such attempts are complicated by the observation that, as with singlet oxygen, the ubiquity of natural quenchers makes reducing the steady-state intracellular hydroxyl radical concentration a challenging task. This is especially true if hydroxyl radicals are formed at or near the site of their lethal action, as is almost certainly the case.

### 1.4.5.2. Other Reactive Species

As noted above, researchers have proposed that the active species produced by intracellular Fenton reactions may not a free hydroxyl radical, but rather an iron radical species such as a ferryl ($Fe(IV)O^{2+}$) species (Imlay et al., 1988a). However, this distinction may be arbitrary, as ferryl species may react to yield hydroxyl radicals and $Fe^{3+}$, and vice versa (Henle and Linn, 1997), and the reaction rates and products of these two species in complex systems may also be quite similar (Vermilyea and Voelker, 2009).

### 1.4.5.3. Reactive Nitrogen Species

Reactive nitrogen species such as peroxynitrite have also been implicated in intracellular damage (Halliwell, 1999). Peroxynitrite is formed through the reactions of nitric oxide with reactive oxygen species such as superoxide, and has a half-life on the order of 2 s (Beckman et al., 1990; Neeley, 2006), although this half-life is greatly reduced in the presence of $CO_2$. Peroxynitrite can decompose to form hydroxyl radicals or react with $CO_2$ to form nitrosoperoxycarbonate, which can in turn decompose to form radicals capable of damaging DNA bases (Neeley, 2006). Since the dominant mode of peroxynitrite formation involves superoxide, which may be a photoproduct of bacterial irradiation, it is likely that sunlight accelerates the formation of reactive nitrogen species, although the importance of these species relative to other ROSs is unknown.

### 1.4.5.4. Transition Metals

As noted above, the critical biological roles of many reactive intermediates are intimately linked with transition metals, particularly as they relate to the Fenton reaction and other analogous reactions.

#### 1.4.5.4.1. Iron

Iron is earth's most abundant element (if the core is included), and the fourth most abundant in the earth's crust. However, the development of an aerobic atmosphere reduced the availability of iron to aquatic microorganisms, while the host tactic of strategically limiting iron availability further reduced its availability to enteric and intracellular pathogens (Imlay, 2006). The importance of iron in biological systems stems both from its role as a critical cofactor in enzymes ranging from porphyrins and FeS clusters to superoxide dismutase, and from its ability to catalyze the Fenton reaction. The Fenton reaction was first described in 1876, and can be written as:

$$Fe^{2+} + H_2O_2 \rightarrow Fe^{3+} + OH\bullet + OH^- \quad (1)$$

$$Fe^{3+} + Red \rightarrow Fe^{2+} + Ox \quad (2)$$

Where Red represents any reducing species that recycles oxidized Fe(III), frequently NAD(P)H in the case of intracellular oxidative DNA damage (Brumaghim et al., 2003; Imlay et al., 1988a). Iron complexes can also be photoreduced via a ligand-to-metal charge transfer process (Blough, 1995). Furthermore, Fenton-like reactions can occur with ROOH in place of $H_2O_2$ (Akaike et al., 1992; Termini, 2000) and other transition metal ions in place of $Fe^{2+}$, because both organic and hydrogen peroxides can react with iron, copper, and other transitions metals via analogous mechanisms (Goldstein et al., 1993). Finally, it should be noted that free intracellular iron readily binds to DNA, membranes, and other potential targets and undergoes the Fenton reaction at much higher rates when complexed by these species than when dissolved in solution (Imlay, 2003; Rush et al., 1990).

#### 1.4.5.4.2. Copper

As noted above, copper can also catalyze Fenton-like reactions in the presence of hydrogen peroxide and organic peroxides (Goldstein et al., 1993; Halliwell, 1999; Stohs and Bagchi, 1995). Like $Fe^{2+}$, $Cu^+$ can also be recycled via photoreduction, particularly when complexed with amino acids, and can also be recycled by ascorbate and other biological reductants (Halliwell, 1999). The copper-ascorbate-peroxide system is well-known, and has been reported to oxidize DNA, lipids, and a range of other biomolecules in the dark (Halliwell, 1999; Orr, 1967a; b; Sagripanti and Kraemer, 1989; Sagripanti et al., 1997). Copper, hydrogen peroxide, and ascorbate have been shown to inactivate fecal coliforms (Ragab_depre, 1982) and Herpes simplex virus (Sagripanti et al., 1997) in the dark, while in the light this system has been shown to accelerate the inactivation of *E. coli* (Fisher et al., 2008).

### 1.4.6. Cellular Defenses

In order to survive in aerobic environments, organisms have evolved a variety of defense mechanisms to minimize the oxidative damage caused by transition metals and reactive oxygen and nitrogen species. The ROS scavengers catalase, peroxidase, and superoxide dismutase are of great interest to the study of sunlight inactivation of prokaryotes, as are the DNA repair and protection mechanisms of bacteria.

#### 1.4.6.1. Catalase

Catalase is a class of enzymes used by a range of organisms to scavenge hydrogen peroxide. Catalase reacts with its substrate at near diffusion-limited rates and is extremely efficient at scavenging exogenously-added $H_2O_2$ at high concentrations, although this enzyme may not be the most important scavenger of lower intracellular concentrations of hydrogen peroxide (Halliwell, 1999; Seaver and Imlay, 2001b). Catalase is vulnerable to inactivation by singlet oxygen (Halliwell, 1999), as well as by its substrate (Brumaghim et al., 2003). Finally, mutants lacking *katF*, which is necessary for the production of catalase HPII and the exonuclease ExoIII, have been shown to be more sensitive to near-UV radiation (Tuveson and Sammartano, 1986a), but this sensitivity appears to be unrelated to catalase activity (Eisenstark et al., 1989; Sak et al., 1989). Other studies have found no protective effect of catalases HPI and HPII induced by other genes (Eisenstark and Perrot, 1987; Smyk-Randall et al., 1993), and catalase may even sensitize cells to photoinactivation (Eisenstark and Perrot, 1987). Hoerter et al also observed that catalase HPII is more sensitive to inactivation by UVA than HPI (Hoerter et al., 2005a).

#### 1.4.6.2. Peroxidase

As noted above, alkyl hydroperoxide reductase (Ahp) is believed to be the most important scavenger of hydrogen peroxide (Seaver and Imlay, 2001a; b) and organic peroxides (Akaike et al., 1992; Termini, 2000) inside *E. coli* cells. Ahp is a flavoprotein that efficiently scavenges peroxides while oxidizing either NADH or NADPH in the process. Since NADH is believed to be a major reductant driving the intracellular Fenton reaction, cells are believed to expend ATP to convert NADH to NADPH (Brumaghim et al., 2003). Thus, depletion of ATP, NADPH, or both could diminish the concentration of reducing equivalents available to support the peroxidase activity of Ahp, potentially allowing steady-state concentrations of hydrogen peroxide to increase, and accelerating Fenton-mediated DNA damage in the presence of free intracellular iron. Furthermore, Ahp absorbs light in the NUV and visible regions (maxima at 280, 380 and 448 nm) (Jacobson et al., 1989), and has been shown to be photoinactivated in vitro (this work). Thus, photoinactivation of peroxidase may contribute to photoFenton damage in *E. coli* and other organisms.

#### 1.4.6.3. Superoxide Dismutase

Superoxide dismutases are a widely conserved family of enzymes that react with superoxide at diffusion-limited rates (Halliwell, 1999). Despite relatively high levels of production in the electron transport chain, SODs are able to reduce steady-state superoxide concentrations to $10^{-10}$ M in *E. coli* cells (Gort and Imlay, 1998). Several SODs have been found in *E. coli*, including CuZn, Fe, and Mn SODs, of which the first and second can be inactivated by hydrogen peroxide. SODs may also be vulnerable to attack by singlet oxygen (Halliwell, 1999). As noted above, SOD mutants are highly susceptible to mutations and inactivation as a result of near UV irradiation from mercury vapor sources (Hoerter et al., 1989; Hoerter et al., 2005a; Knowles and Eisenstark, 1994). Furthermore, mutants with inducible plasmid copies of Mn- (but not Fe-) SOD were found to be slightly protected from NUV irradiation by mercury vapor sources, as reviewed by Eisenstark (Eisenstark, 1989). These findings seem to suggest that Fe SODs may be degraded in the presence of near-UV light.

#### 1.4.6.4. DNA Binding Proteins

DNA binding proteins such as Dps (so called because it is a DNA binding protein isolated from starved cells) can also play a protective role in responding to oxidative stress. Dps is the most abundant protein in stationary-phase *E. coli*, and can be induced under redox-stressed conditions by OxyR to bind free intracellular iron (Ahmad, 1981; Chiancone et al., 2004; Ilari et al., 2002; Zhao et al., 2002). In addition to its iron-binding capacity, Dps binds DNA during stationary phase in a stable, protective complex known as a "biocrystal" and can degrade hydrogen peroxide. Dps mutants were found to be more sensitive to iron, copper, high levels of hydrogen peroxide, high temperatures, extreme pH, and UVC radiation than wild-type cells (Nair and Finkel, 2004). Dps may also act as a sacrificial substrate for oxidative damage, preferentially oxidizing in order to protect DNA from oxidative damage (ibid).

#### 1.4.6.5. Gene Regulation

Gene regulation in response to near-UV and solar radiation has been extensively reviewed (Berney et al., 2006a; Eisenstark, 1989). However, it should be noted that bacteria rely on the transcription of certain key genes to respond to photooxidative stress. *oxyR* and *perR* are activated in response to hydrogen peroxide, resulting in the upregulation of catalase, peroxidase, Dps, and other proteins (Halliwell, 1999; Helmann et al., 2003; Park et al., 2005; Zheng et al., 2001). Meanwhile, *soxR* is activated in response to high superoxide levels, resulting in upregulation of MnSOD and superoxide-resistant forms of several FeS-containing proteins (Halliwell, 1999; Imlay, 2006). Although not necessarily activated in response to oxidative stress, the *fur* gene is involved in iron regulation within cells, and *fur* mutants are highly sensitive to oxygen (Halliwell, 1999; Touati, 2000).

#### 1.4.6.6. DNA Repair

DNA repair is critical to microbial survival, particularly in sunlit aerobic environments. One study (Harm, 1980) found greater than two-log inactivation of *E. coli* mutants deficient in two key DNA repair enzymes (UvrA and RecA) after one minute's exposure to natural sunlight. This study also found that much of this damage could be repaired by light-dependent DNA repair mechanisms. Interestingly, RecA has been reported to be potentially inhibited by hydrogen peroxide (Hartman and Eisenstark, 1978). Moreover, since RecA is an ATPase, the depletion of the proton motive force and ATP pools reported during sunlight irradiation of *E. coli* (Berney et al., 2006c) might also interfere with RecA-mediated repair. Furthermore, mutants deficient in exonuclease III and polymerase I are highly sensitive to NUV light and hydrogen peroxide (Demple et al., 1986), suggesting that base excision repair is also important in protecting cells from these stresses (Eisenstark, 1989). Thus, while DNA damage is not necessarily the primary mechanism of all sunlight inactivation in wild-type cells, it is certainly an important consequence of exposure to near-UV light that can inactivate mutants deficient in DNA repair.

### 1.4.7. Physical Conditions Affecting Inactivation Rates

The rate at which organisms are inactivated by sunlight can also depend on the physical conditions under which exposure occurs. Extreme conditions have been shown to sensitize bacteria to sunlight inactivation, although it is unknown whether this effect is due to mechanistic synergies or to an accumulation of unrelated stresses.

#### 1.4.7.1. Temperature

Most cells are sensitive to extreme temperatures, probably due to decreased enzyme function as proteins begin to denature, and perhaps also due to increased membrane permeability (Madigan, 2002). *E. coli* has a maximum growth temperature of approximately 48º C, above which it cannot survive for prolonged periods. Thus, it is perhaps unsurprising that studies have found the sunlight inactivation of *E. coli* and other bacteria to be more effectively at temperatures above 45-50º C (Wegelin et al., 1994).

#### 1.4.7.2. pH

Enteric bacteria such as *E. coli* are adapted to life at circum-neutral pH, and can only survive for limited periods under conditions that are more than a few pH units outside of that range. Extreme pH can disrupt membrane integrity and interfere with the cellular proton motive force, which is essential for ATP production (Madigan, 2002). Thus, the observation that extreme pH values of 9.5 (Curtis et al., 1992) and 2.5 (Fisher et al., 2008) could accelerate the inactivation rates of enteric bacteria are not surprising. Whether light-induced membrane damage sensitizes cells to extreme pH (Davies-Colley et al., 1999) or extreme transmembrane proton gradients interfere with cellular metabolism and microbial oxidative stress defenses remains unknown. It seems unlikely, however, that intracellular pH is significantly displaced from neutral during photoinactivation, since such a thorough loss of membrane integrity would likely result in immediate cell death.

#### 1.4.7.3. Salinity

While *E. coli* and other enteric bacteria may be able to survive in hypertonic saline environments for a limited time, they are eventually either killed by such conditions or become dehydrated and dormant (Madigan, 2002). The observation that incubation in seawater reduces the metabolic activity of *E. coli* (Gourmelon et al., 1994) may partially explain the finding that saline conditions sensitized these bacteria to sunlight inactivation (Davies and Evison, 1991; Shah et al., 1996). Furthermore, hypotonic solutions may also contribute to osmotic stress that could accelerate the inactivating effects of sunlight on bacteria.

#### 1.4.7.4. Growth Conditions

Bacterial growth conditions may also affect photoinactivation. The inactivation rate of *E. coli* cultured in a chemostat by simulated sunlight has been shown to be lower for cells that were grown more slowly than for cells with higher relative growth rates (Berney et al., 2006d). While the mechanisms of this effect are not fully understood, bacterial protein production rates are known to depend on growth rates (Pedersen et al., 1978), and the synthesis of flavins and other potential endogenous chromophores is tied to protein transcription levels (Wilson and Pardee, 1962). Furthermore, the abundance of FeS

clusters, which are known to be critical targets for superoxide (Imlay, 2003; 2006) is highly dependent on iron availability during growth (McHugh et al., 2003). Thus, there are a variety of ways in which bacterial growth conditions might affect the sensitivity of cells to sunlight and oxidative damage.

#### 1.4.7.5. Incubation Conditions

Finally, it should be noted that studies of microbial inactivation rely on imperfect techniques to quantify the abundance and viability of the organisms in question. The effects of media and growth conditions on the apparent rate of sunlight inactivation of bacteria have been observed by a number of researchers. The recovery of bacteria exposed to sunlight has been observed to be dramatically different when these cells were cultured on selective vs. nonselective media (Rincón and Pulgarin, 2004a; Shah et al., 1996), while Reed et al. observed that incubation in anaerobic cabinets and/or on plates containing the hydrogen peroxide scavengers catalase or pyruvate dramatically reduced the apparent inactivation rates of bacteria exposed to sunlight (Kehoe et al., 2004; Reed, 2004). This sensitivity to culture conditions may be attributable to the tendency of rapid aerobic growth on rich media to result in a burst of intracellular ROS production that may inactivate sublethally-damaged bacteria (Aldsworth et al., 1999; Dodd et al., 1997).

The ideal solution to these growth and culture condition effects might be to develop laboratory protocols for each organism of interest that reproduce the loss of infectivity that would be observed for fecal-derived pathogens exposed to the same conditions before being ingested by immunocompetent human hosts. However, such a task would obviously represent an enormous effort, and the absence of such protocols should not be considered an impediment to ongoing research. Thus, while the search for culture and growth protocols that reproduce environmental conditions remains an ongoing task, current and prior studies must simply be interpreted carefully in the context of these phenomena.

## 1.5. Opportunities for Accelerating SODIS

The above findings suggest several possible opportunities for enhancing applied solar disinfection. Specifically, the strong wavelength dependence of inactivation suggests that if a low-cost, UVA- and UVB-transparent (UVAB-transparent) material can be identified, it could represent an improved material for use in SODIS reactors. Furthermore, the apparent roles of singlet oxygen, superoxide, and hydrogen peroxide in the sunlight inactivation of microorganisms suggest that, while the first two species are fairly transient, addition of the stable oxidant hydrogen peroxide should accelerate inactivation, as found by other groups previously. One possible innovation on prior work might be the use of a stable source of hydrogen peroxide, such as the solid compound sodium percarbonate, which might be more practical to use and transport under field conditions. Furthermore, the excellent results achieved in batch and flow reactor studies using Fenton and Fenton-like reagents suggest that the introduction of Fenton-like reagents might further enhance microbial inactivation. Finally, the apparent higher rates of sustained adoption and adherence for filters relative to behavior-based interventions suggest that any steps that might make SODIS more automatic and structurally-integrated with users' living spaces might enhance its uptake and success at the household level.

## 2. Solar Disinfection (SODIS) of *E. coli*, *Enterococcus*, and MS2 phage: Effects of Additives and Alternative Container Materials.

### 2.1. Chapter Summary

The use of alternative container materials and added oxidants accelerated the inactivation of MS2 bacteriophage and *E. coli* and *Enterococcus* bacteria during solar water disinfection (SODIS) trials. Specifically, bottles made from polypropylene copolymer (PPCO), a UVB-transparent plastic, resulted in three log inactivation of these organisms in approximately half the time required for disinfection in bottles made from PET, polycarbonate, or Tritan®, which absorb most UVB light. Furthermore, the addition of 125 mg/L sodium percarbonate in combination with either citric acid or copper plus ascorbate accelerated the inactivation of most organisms in most trials, with mean enhancement factors ranging from 1.4 to 19. Finally, it was observed that the inactivation of *E. coli* and *Enterococcus* derived from local wastewater was far slower than the inactivation of laboratory-cultured *E. coli* and *Enterococcus* strains, while the inactivation of MS2 was slowest of all. These results highlight the importance of UVB in SODIS under certain conditions, and also the greater sunlight resistance of viruses and bacteria of fecal origin, as compared to the laboratory cultures commonly used to model their inactivation. Furthermore, this study illustrates promising new avenues for accelerating the inactivation of bacteria and viruses by solar disinfection.

### 2.2. Introduction

Diarrheal diseases are prevalent in communities with inadequate access to safe water, hygiene, and sanitation. These diseases account for an estimated 2.2 million deaths each year, representing 3-4% of the burden of disease worldwide, and over 6% of the disease burden in developing countries. Furthermore, diarrheal diseases disproportionately affect infants and small children, accounting for 1.75 million deaths, or 17% of all mortality in children under the age of 5 (Mathers et al., 2009; WHO, 2009). Nearly 90% of deaths from diarrheal diseases are attributed to lack of safe water, sanitation, and hygiene (Mathers et al., 2009). Point-of-use (POU) water treatment technologies have received increasing attention as valuable tools for improving drinking water quality (Clasen et al., 2007a; Mintz et al., 2001; Sobsey, 2002). A variety of POU water treatment technologies have been implemented, including solar disinfection (SODIS) —the use of sunlight to inactivate pathogens in drinking water.

The ability of sunlight to inactivate microorganisms in natural surface waters (Boehm et al., 2009b; Davies and Evison, 1991; Sinton et al., 2002b) and drinking water (Wegelin et al., 1994) is well known. However, studies on the microbiological efficacy of SODIS, as well as its effectiveness at reducing diarrhea, have yielded mixed results. While many studies report rapid inactivation of indicator organisms with a few hours' exposure to natural sunlight (Boyle et al., 2008; Mani et al., 2006; McGuigan et al., 1998; Ubomba-Jaswa et al., 2009; Wegelin et al., 1994), others have found that detectible indicator bacteria may still remain in contaminated environmental samples, even after a full day's exposure under field conditions (Fisher et al., 2008; Oates et al., 2003). One study found

that only a minority of households with contaminated source water (20-34%) achieved 1-log inactivation of bacteria in exposed SODIS bottles (Du Preez et al., 2010). A wide range of three-log inactivation times spanning nearly two orders of magnitude have been reported for various types of coliform bacteria exposed to natural and simulated sunlight in PET bottles (Table 2.1, Figure 2.1). Furthermore, previous studies have found low rates of inactivation of viruses and bacteriophage (viruses that infect bacteria) in PET bottles (Dejung et al., 2007; Rijal and Fujioka, 2003). While several field trials have shown that SODIS significantly reduced diarrheal disease burdens under field conditions (Conroy et al., 1996; Conroy et al., 1999; Rose et al., 2006), a recent study failed to detect statistically significant health impacts under low-compliance conditions (Mausezahl et al., 2009). Variability in findings regarding the health impacts of SODIS may be related to variable compliance among users. Du Preez et al. found among households who completed daily diarrhea diaries on > 75% of days, assignment to the SODIS condition was associated with a significant reduction in dysentery, while effects among households reporting their diarrhea episodes with less regularity were not significant (Du Preez et al., 2010). They attributed these findings to greater motivation among households with high diary compliance, although it is not known whether diary compliance and SODIS compliance were correlated. Variability in health impact data may also be related to variations in the efficacy of SODIS under different field conditions, and/or the influence of other transmission routes of diarrheal disease and other underlying health conditions. Specifically, in communities with high levels of exposure to diarrheal disease-causing pathogens from unsafe food, inadequate hygiene, and/or poor sanitation, an incremental change in drinking water quality may have a smaller health impact than in a community with lower non-drinking-water pathogen loads.

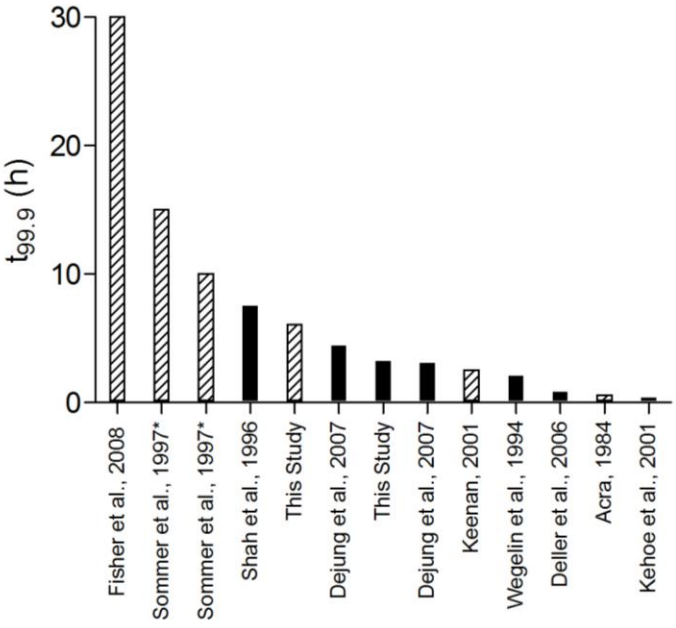


Figure 2.1 Three log inactivation times (h) for *E. coli* and total coliforms (denoted by *) calculated from data in published solar disinfection field studies performed in PET bottles. Striped bars represent studies using wild or fecal organisms, shaded bars represent studies using laboratory cultured organisms.

Table 2.1 Three-log inactivation times (h) For *E. coli* (EC), Total Coliforms (TC), Fecal Coliforms (FC), and bacteriophage in various sunlight laboratory and field studies. ǂ Denotes intensity values that were calculated based on published plots of intensity vs. time.

| Organism | Type | Source | $T_{99.9\%}$ (h) | $F_{99.9\%}$ ($MJ/m^2$) | Container | Sunlight Source | $I_{ave}$ ($W/m^2$) | $T_{max}$ (ºC) | Location | Reference |
|---|---|---|---|---|---|---|---|---|---|---|
| EC | Wild | WSP | 27.6 | 88 | Open Tank | Natural | 888* | 14 | Christchurch, NZ | (Sinton et al., 2002b) |
| EC | Wild | Raw Sewage | 9.9 | 24 | Open Tank | Natural | 673* | 14 | Christchurch, NZ | (Sinton et al., 2002b) |
| EC | Wild | Ditch Water | 30.0 | | PET bottle | Natural | 11000 Lux | 29.5 | Mumbai, India | (Fisher et al., 2008) |
| TC | Wild | | 15.0 | | PET bottle | Natural | | 30 | Cali, Colombia | (Sommer et al., 1997) |
| TC | Wild | | 10.0 | | PET bottle | Natural | | 48 | Cali, Colombia | (Sommer et al., 1997) |
| EC | Lab | ATCC 11229 | 7.5 | | PET bottle | Natural | | 30 | Ontario, Canada | (Shah et al., 1996) |
| EC | Wild | WW | 6.1 | 13.5 | PET bottle | Natural | 617 | 48 | Cochabamba, BO | This Study |
| EC | Lab | K12 MG1655 | 3.2 | 7.1 | PET bottle | Natural | 617 | 48 | Cochabamba, BO | This Study |
| EC | Lab | Bolivian Isolate | 3.1 | 7.5 | PET bottle | Natural | 670ǂ | 44 | Cochabamba, BO | (Dejung et al., 2007) |
| EC | Wild | River Water | 2.5 | | PET bottle | Natural | | 44 | Jolivert, Haiti | (Keenan, 2001) |
| EC | Lab | Lab | 2.1 | 6.3 | PET bottle | Natural | 835 | | Dubendorf, CH | (Wegelin et al., 1994) |
| FC | Wild | Wild | 1.1 | | Plastic Container | Natural | | 26 | Jaipur, India | (Reed et al., 2000) |
| FC | Wild | Wild | 1.9 | | Plastic Container | Natural | | 18 | Mabopane, ZA | (Reed et al., 2000) |
| EC | Lab | ATCC 11775 | 1.0 | | | Natural | | 43 | Kochi, India | (Mani et al., 2006) |
| EC | Lab | Local Isolate | 0.94 | | Glass Test Tube | Natural | | | Muscat, Oman | (Salih, 2002) |
| EC | Lab | ATCC 25922 | 0.83 | | PET bottle | Natural | | 32 | Graz, Austria | (Deller et al., 2006) |
| EC | Wild | WW | 0.55 | | PET bottle | Natural | | | Beirut, Lebanon | (Acra, 1984) |
| EC | Lab | Lab | 0.36 | | PET bottle | Natural | | | | (Kehoe et al., 2001) |
| EC | Wild | WW | 72 | 163 | PC bottle | Natural | 630ǂ | 20 | Los Angeles, US | (Noble et al., 2004) |
| Entero. | Wild | WSP | 9.0 | 25 | Open Tank | Natural | 778* | 14 | Christchurch, NZ | (Sinton et al., 2002b) |
| Entero. | Wild | Raw Sewage | 19.2 | 50 | Open Tank | Natural | 729* | 14 | Christchurch, NZ | (Sinton et al., 2002b) |
| Entero. | Wild | WW | 5.9 | 13.1 | PET bottle | Natural | 617 | 48 | Cochabamba, BO | This Study |
| Entero. | Lab | ATCC 19433 | 3.3 | 7.3 | PET bottle | Natural | 617 | 48 | Cochabamba, BO | This Study |
| Entero. | Lab | ATCC 29212 | 2.5 | | PET bottle | Natural | | 32 | Graz, Austria | (Deller et al., 2006) |
| E. faecalis | Wild | WW | 53 | 120 | PC bottle | Natural | 630ǂ | 20 | Los Angeles, US | (Noble et al., 2004) |
| E. faecalis | Lab | ATCC 19433 | 0.9 | 1.9 | Reactor (UVB transp.) | Natural | 610* | 39 | NSW, Australia | (Davies et al., 2009) |
| F2 coliphage | Lab | | 5.0 | | Quartz Tubes | Natural | | | Dubendorf, CH | (Wegelin et al., 1994) |
| Somatic Coliphages | Wild | WSP | 34.8 | 90 | Open Tank | Natural | 718* | 14 | Christchurch, NZ | (Sinton et al., 2002b) |
| Somatic Coliphages | Wild | Raw Sewage | 24.9 | 70 | Open Tank | Natural | 783* | 14 | Christchurch, NZ | (Sinton et al., 2002b) |
| F-RNA Phages | Wild | WSP | 39.9 | 98 | Open Tank | Natural | 685* | 14 | Christchurch, NZ | (Sinton et al., 2002b) |
| F-RNA Phages | Wild | Raw Sewage | 37.5 | 93 | Open Tank | Natural | 687* | 14 | Christchurch, NZ | (Sinton et al., 2002b) |
| Coliphages | Lab | WSP | 40.8 | 98 | PET bottle | Natural | 670ǂ | 44 | Cochabamba, BO | (Dejung et al., 2007) |
| MS2 Coliphage | Lab | | 34.3 | 76 | PET bottle | Natural | 617 | 48 | Cochabamba, BO | This Study |
| F+-spec. coliphage | Wild | WW | 71 | 161 | PC bottle | Natural | 630ǂ | 20 | Los Angeles, US | (Noble et al., 2004) |
| P22 Phage | Lab | | 2.0 | 4.5 | Reactor (UVB transp.) | Natural | 610* | 39 | NSW, Australia | (Davies et al., 2009) |

Methods for accelerating inactivation may enhance the efficacy of solar disinfection as a point-of-use method for water treatment. Such work could also provide new insights into the interactions of sunlight and microorganisms in a range of natural and engineered environmental systems.

Previous laboratory studies have demonstrated the ability of hydrogen peroxide to accelerate the photoinactivation of *E. coli* (Fisher et al., 2008; Hartman and Eisenstark, 1978; 1980; Keenan, 2001; Rincón and Pulgarin, 2004b) and bacteriophage (Ananthaswamy and Eisenstark, 1976; Eisenstark et al., 1986; Hartman et al., 1979), while copper-based additives have also been shown to accelerate the inactivation of *E. coli* alone and in combination with hydrogen peroxide (Fisher et al., 2008). However, hydrogen peroxide is unstable in aqueous solutions, particularly in combination with copper, and thus not conducive to storage and dosing by potential users. Thus, we investigated the ability of premeasured granular solid additives to accelerate inactivation under real field conditions. Similarly, while other groups have investigated the effects of alternative containers and materials (e.g. pouches made from food grade polymers, reactors with antifog-coated, UV-transparent polycarbonate lids) on inactivation rates (Davies et al., 2009; Walker et al., 2004a), we measured the effect of multiple commercially-available container materials on multiple indicator organisms using natural sunlight under real field conditions. Materials with different degrees of transparency to solar UV light were of particular interest.

The ability of UVB to play a critical role in solar water disinfection has received limited attention in the literature. Previous groups reported that UVA light was responsible for the majority of inactivation during solar disinfection with a smaller (potentially synergistic) contribution from visible light (Acra, 1984; McGuigan et al., 1998; Wegelin et al., 1994). While some groups noted the biocidal activity of UVB light (Davies et al., 2009; McGuigan et al., 1998), the high attenuation of these wavelengths by the earth's atmosphere and PET bottles resulted in less consideration being given to the role of these wavelengths in solar disinfection. Moreover, the small amount of additional UVB light transmitted by polystyrene, glass, and other materials was not considered significant based on its small fraction of total irradiance and its minor contribution to the inactivation of laboratory-cultured bacteria (McGuigan et al., 2006). Thus, many prior studies considered UVA light to be the most important variable driving the photoinactivation of microorganisms in optically transparent containers, while the potential for UVB-transparent materials was largely overlooked.

In this work, we studied the effects of five different container materials and two sets of additives on the rate at which laboratory-cultured *E. coli*, *Enterococcus faecalis*, and MS2 bacteriophage as well as *E. coli* and enterococci naturally present in local wastewater were inactivated by exposure to natural sunlight in the Cochabamba department of Bolivia. This study was undertaken in the hopes of developing procedures for more rapid solar disinfection that might be simple and low-cost, with demonstrable efficacy under field conditions.

## 2.3. Materials and Methods

### 2.3.1. Bacteria

Bacteria were naturally present in wastewater and were obtained fresh daily from the second of three primary settling basins receiving untreated wastewater from the Center for Environmental Water and Sanitation (CASA) building on the campus of the Universidad Mayor de San Simon, Cochabamba, Bolivia. Laboratory *Escherichia coli* (*E. coli*) K12 MG1655 (generously provided by Dr. James Imlay, UIUC) and *Enterococcus faecalis* (*E. faecalis*) (ATCC, #19433) were grown fresh daily in Luria Bertani (LB) broth at 37 C. Laboratory and wastewater *E. coli* and enterococci were enumerated by spread-plate and membrane filtration methods. The spread plate technique (20 µL of sample plated on 47 mm plates) was used to enumerate samples with concentrations > approximately 500 CFU/mL, while membrane filtration (0.45-µm filter on 47mm plates) was used to enumerate samples with concentrations < 500 CFU/mL. For *E. coli* enumerated by either technique, samples were plated on LB agar supplemented with 0.1% SDS (a well-known inhibitor of Gram-positive bacteria), 0.05% sodium pyruvate (Khaengraeng and Reed, 2005), and 0.05 g/L X-gluc (5-Bromo-3-Chloro-β-Glucuronide). For *Enterococcus* enumerated by either technique, samples were plated on M Enterococcus agar supplemented with 0.05% sodium pyruvate. The decision to enumerate each sample by the spread-plate technique, by membrane filtration, or both was made using best judgment as well as the results of previous trials under similar conditions. CFU concentrations from samples measured by both spread-plate and membrane filtration techniques were generally in good agreement.

### 2.3.2. MS2 Bacteriophage

MS2, a single stranded $F^+$ RNA coliphage was propagated in *E. coli* $F_{amp}$ (ATCC #700891) by broth enrichment (EPA Method 1601). Bacteriophage plaque assays were performed using 100 µL virus inocula and the double agar layer (DAL) method (Adams, 1959a) to titer stocks and to enumerate viruses after exposure to simulated sunlight. Concentrations of phage present in the wastewater used for the current study were too low for reliable quantification by the above technique, and thus only cultured MS2 bacteriophage were used.

### 2.3.3. Containers

1-L bottles made from transparent polyethylene terephthalate (PET), polystyrene (PS), polypropylene copolymer (PPCO), polycarbonate (PC), and copolyester (Tritan®) were used in the study. Several 1-2 L PET bottles containing bottled water and other soft drinks were purchased locally from a supermarket in Cochabamba, Bolivia, and all were produced by Embol, S.A., La Paz, Bolivia. The PET containers used for disinfection experiments in this study were 1-L bottles containing bottled water. PS bottles were purchased from Corning Incorporated, Corning NY (mfr. part number 8396). Nalgene NVision® PPCO packaging bottles (mfr. part number 342080-1000), PC bottles (2205-0032), and Eastman Tritan® bottles (2178-2027) were purchased from Nalge Nunc International, Rochester, NY. UV-visible transmittance spectra of bottles were obtained by cutting sections from each bottle and measuring on a Beckman Lambda 14 UV-Vis spectrometer (Figure 2.2).

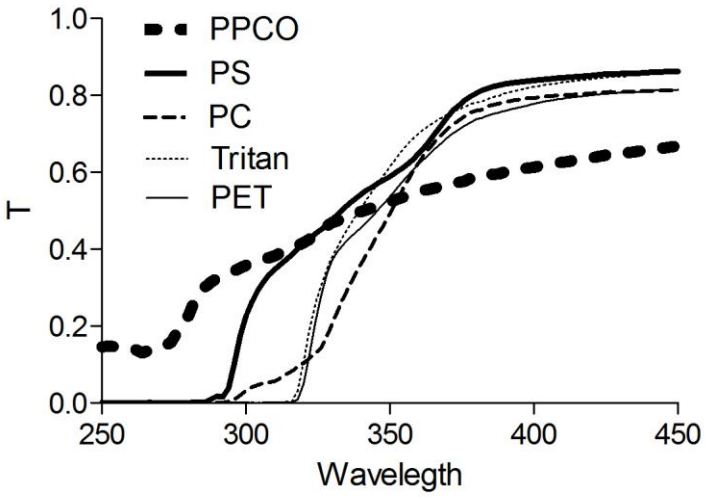


Figure 2.2 Transmittance spectra of cross-sections of Eastman Tritan (Tritan), polycarbonate (PC), polypropylene copolymer (PPCO), polystyrene (PS), and polyethylene terephthalate (PET) bottles used in this study.

### 2.3.4. Additives

Two sets of additives were prepared. Additive A included 100 mg sodium percarbonate and 100 mg citric acid. Sodium percarbonate is a granular solid used in laundry detergents, food processing, and toothpastes that reacts with water to produce 1.5 moles of hydrogen peroxide per mole of percarbonate (thus a final concentration of 125 mg/L produces approximately 1.20 mM $H_2O_2$). Since the reaction of sodium percarbonate with water also produces carbonate ions, raising pH, citric acid was added to maintain circum-neutral pH. Additive B included 100 mg sodium percarbonate along with 100 mg ascorbic acid and 20 µg copper sulfate. Copper and ascorbate have previously been shown to accelerate SODIS, both alone and in the presence of hydrogen peroxide (Fisher et al., 2008). Both additives were formulated to produce concentrations of all reagents that were below levels deemed to be safe for consumption (copper is regulated at 1.3 mg/L (USEPA, 2003) while hydrogen peroxide is Generally Regarded as Safe by the US FDA, and approved for use in milk at concentrations up to 0.05%, roughly 15 mM (CSTEE, 2001; USFDA, 2009).

### 2.3.5. Sample Preparation

1-L PET, PS, PPCO, PC, or Tritan® bottles were washed, rinsed with sterile distilled water, sterilized with absolute ethanol, and rinsed with sterile 20 mM, phosphate buffered saline (PBS, pH 7) prior to each experiment. Samples were prepared daily in 800 mL of PBS unless otherwise indicated. Wastewater was allowed to settle for 1 h before the supernatant was added to all samples at an approximate concentration of 5% (v/v: ~40 mL wastewater to 800 mL PBS). Typical *E. coli* and *Enterococcus* concentrations in the resulting diluted wastewater ranged from $10^2$-$10^3$ CFU/mL. Laboratory *E. coli* and *E. faecalis* strains were spiked into selected samples of diluted wastewater at approximate concentrations of $10^6$-$10^7$ CFU/mL. Laboratory MS2 stock was spiked into all samples at an approximate concentration of $10^3$ PFU/mL.

### 2.3.6. Sunlight Exposure

Samples were irradiated on a corrugated steel platform on the roof of the Center for Environmental Water and Sanitation (CASA) at the Universidad Mayor de San Simon in Cochabamba, Bolivia (UMSS). Bottles were exposed on a 2 x 10 m piece of North-facing corrugated steel inclined at an angle of 30 degrees. Bottles were typically exposed from 10 AM (+/- 30 minutes) to 4 PM. Aliquots were decanted into sterile tubes containing 100 μL sodium pyruvate (5% wt/wt) at regular intervals and diluted in PBS, as necessary, before enumeration by the spread-plate or membrane filtration technique.

Air temperature was measured using Fisher Scientific digital thermometers (Model 15-077-50), while water temperatures were measured in a subset of exposed bottles (usually in a total of four to five bottles per experiment) using a SPER Scientific Model 800024 four channel digital thermometer with K-type flexible thermocouple electrodes. Sunlight intensity was recorded at 5-min intervals throughout all experiments by a LI-COR LI DataLogger pyranometer measuring total irradiance. Sunlight spectra were modeled using the Simple Model of the Atmospheric Radiative Transfer of Sunshine (SMARTS) (Gueymard, 1995).

### 2.3.7. Experimental Design

Bottle material experiments were conducted by simultaneously exposing two bottles of each material type (PET, PS, PPCO, PC, Tritan), for a total of 10 bottles per trial. For each material type, one bottle contained diluted wastewater while the other contained diluted wastewater spiked with *E. coli*, *Enterococcus*, and MS2 (Table 2.2). It is unlikely that the different initial concentrations of wastewater and laboratory bacteria, $10^3$ versus $10^6$ CFU/mL, respectively, affected the observed inactivation rates due to screening effects, as a control experiment comparing the inactivation of lab *E. coli* in PBS with initial concentrations of $10^5$ and $10^6$ CFU/mL produced similar inactivation rates (Figure 2.3 A). Trials were performed for each condition on three separate days (total of 30 bottles).

Table 2.2 Experimental conditions for bottles exposed to sunlight in container material trials. All bottles were filled with sterile 20 mM PBS spiked with wastewater.

| Bottle | Material | Spiked |
|---|---|---|
| 1 | PET | No |
| 2 | PET | Yes |
| 3 | PS | No |
| 4 | PS | Yes |
| 5 | PPCO | No |
| 6 | PPCO | Yes |
| 7 | PC | No |
| 8 | PC | Yes |
| 9 | Tritan | No |
| 10 | Tritan | Yes |

Combined additive/bottle material experiments were conducted by simultaneously exposing six PET bottles and six PPCO bottles, for a total of 12 bottles per trial. Three PET and three PPCO bottles contained diluted wastewater, while the other three bottles of each type contained diluted wastewater spiked with *E. coli*, *Enterococcus*, and MS2. Of the three unspiked PET bottles, one contained no additives, one contained 100 mg sodium percarbonate + 100 mg citric acid (Additive A), and one contained 100 mg sodium percarbonate, 100 mg ascorbic acid, and 20 μg $CuSO_{4(aq)}$ (Additive B). The same additives (Nothing, A, B) were added to the three spiked PET bottles, as well as the three spiked and three unspiked PPCO bottles (Table 2.3). Three trials were performed for each condition on three separate days (total of 36 bottles).

Table 2.3 Experimental conditions for bottles exposed to sunlight in additive trials. All bottles were filled with sterile 20 mM PBS and spiked with wastewater.

| Bottle | Material | Spiked | Additives |
|---|---|---|---|
| 1 | PET | No | None |
| 2 | PET | No | A |
| 3 | PET | No | B |
| 4 | PET | Yes | None |
| 5 | PET | Yes | A |
| 6 | PET | Yes | B |
| 7 | PPCO | No | None |
| 8 | PPCO | No | A |
| 9 | PPCO | No | B |
| 10 | PPCO | Yes | None |
| 11 | PPCO | Yes | A |
| 12 | PPCO | Yes | B |

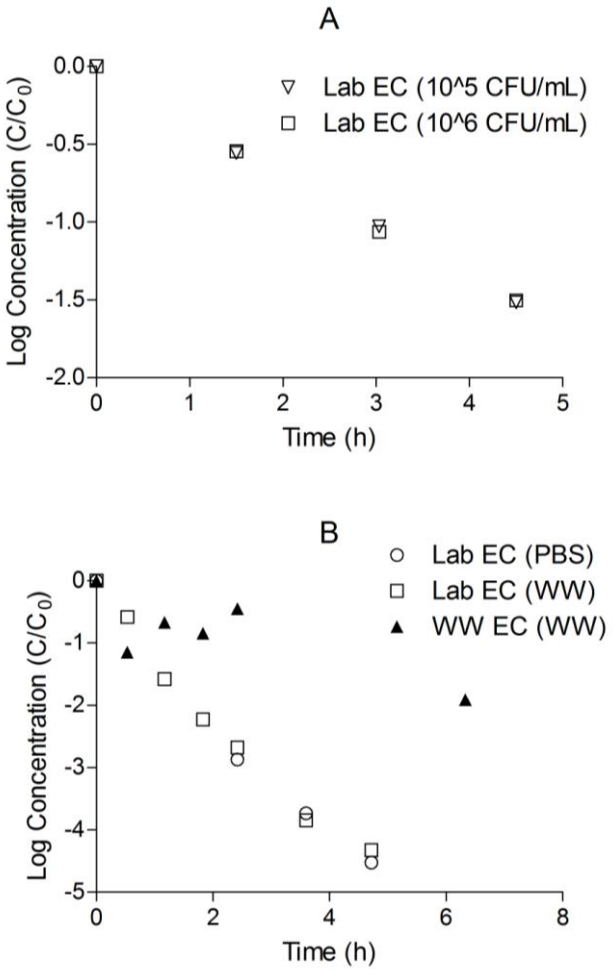


Figure 2.3 Representative inactivation curves for laboratory-cultured and wastewater-derived E. coli exposed to natural sunlight in PET bottles. A) Inactivation of laboratory-cultured E. coli added to PBS at initial concentrations of either $10^5$ or $10^6$ CFU/mL. B) inactivation of laboratory-cultured E. coli added to either PBS or diluted wastewater at initial concentrations of $10^6$ CFU/mL, as well as inactivation of E. coli naturally present in diluted wastewater at concentrations of $10^3$ CFU/mL.

### 2.3.8. Inactivation Rate Coefficients

For MS2 coliphage, inactivation rate coefficients (k) were determined assuming first order kinetics according to the equation:

$$N = N_0 \exp(-kt) \quad (1)$$

Where F can be substituted for t to determine fluence-based inactivation rates. Inactivation curves of enteric bacteria such as *E. coli* and *Enterococcus* are known to follow shoulder curves as described by the equations presented by Wegelin et al. (Wegelin et al., 1994) and Harm et al. (Harm, 1980):

$$N = N_0[1 - (1 - \exp(-kt))^m] \quad (2)$$

Where k and m are fitting parameters, and again, F can be substituted for t in Fluence-based calculations. However, small shoulder periods were observed in many trials, particularly those with additives, and the combined effects of changing additive concentrations and varying sunlight intensity frequently resulted in inactivation curves that were not well-described by either Equation 1 or 2 (Figure 2.4). Thus, linear interpolation between data points was used to estimate three-log inactivation times and fluences. In the rare cases where no data were obtained beyond 99.9% inactivation, the slope between the last two points was used to extrapolate a three-log inactivation time.

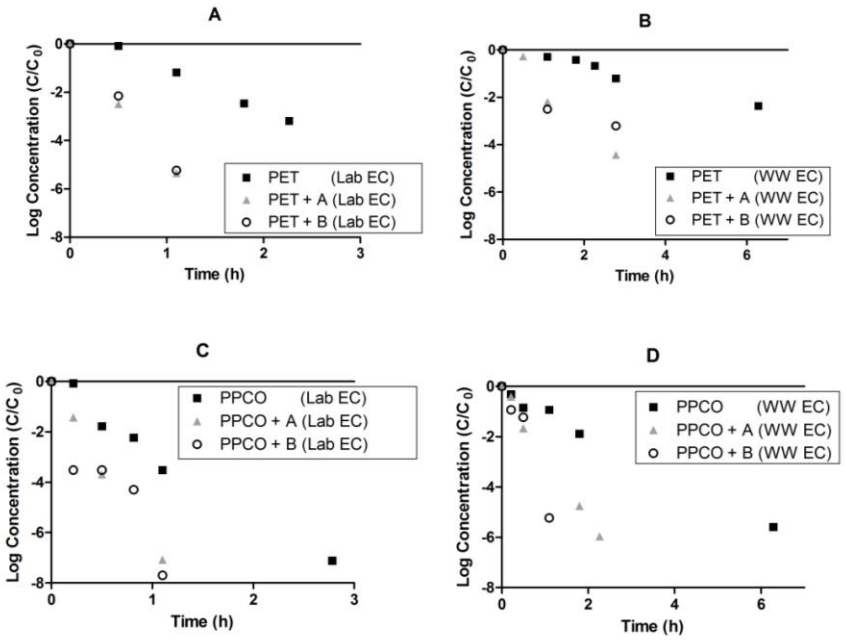


Figure 2.4 Representative inactivation curves for laboratory-cultured and wastewater-derived *E. coli* exposed to natural sunlight in containers of different materials with and without additives. A) Laboratory-cultured *E. coli* in PET bottles. B) Laboratory-cultured *E. coli* in PPCO bottles. C) Wastewater-derived *E. coli* in PET bottles. D) Wastewater-derived *E. coli* in PPCO bottles.

### 2.3.9. Enhancement Factors

To facilitate comparison of inactivation rates across different conditions, we calculated "Enhancement Factors" for three-log inactivation times and fluences, EF(3). These factors were calculated as the ratio of the time or fluence required to achieve three-log inactivation under two conditions in the same trial on the same day. Thus, if I and II are two conditions within a single trial, the time-based enhancement factor for condition II relative to condition I is calculated as shown in Equation 3.

$$EF(3)_{II/I} = \frac{t_{99.9\%}(I)}{t_{99.9\%}(II)} \quad (3)$$

Fluence-based EF(3) values were calculated analogously. Mean EF(3) values for replicate experiments were computed by first calculating the EF(3)s for each individual

experiment, then averaging these EF(3) values. This approach eliminated some of the variability due to different conditions (such as sunlight intensity) on different days.

### 2.3.10. Analytical Methods: Turbidity, pH, Conductivity

Turbidity was measured using an H.F. Scientific DRT-15 CE turbidimeter. pH was measured using a Thermo-Orion 3-star benchtop pH meter. Conductivity was measured using an Extech EC400 conductivity/TDS/salinity meter. Samples of diluted wastewater were found to have pH values ranging between 6.5 and 7.5, with samples containing additives having slightly lower pH values (typically between 6.5-7.0) than unamended samples (typically 7.0-7.5). Turbidity values ranged from 2-8 NTU, well below the recommended SODIS limit of 30 NTU (Dejung et al., 2007). Conductivity values were between 100 and 120 μS for samples without additives, and between 200 and 300 μS for samples with additives. Pure PBS with and without additives was found to have a conductivity of approximately 100 and 200 μS, respectively.

### 2.3.11. Use of Published Inactivation Data

Inactivation data from the literature were used as presented or adapted for comparison to other studies as necessary. Specifically, published three-log inactivation times and/or fluences were used without modification while inactivation curves and other metrics of inactivation rate, time, or fluence were used to extrapolate three log inactivation times. First-order kinetics were assumed when no additional kinetic data were available. Where light intensity data were published, these were used without modification. Where such data were not available, they were extrapolated from literature references (e.g. for solar simulators) or from averaging published plots of intensity Vs. time using the Graph Grabber software package (Quintessa, 2009).

### 2.3.12. Sources of Variability

Sunlight intensity and temperature varied significantly within and between days, largely due to differences in cloud cover (Figures 2.5 and 2.6), while Additives A and B reacted over the course of each trial. The combination of changing additive concentrations and fluctuating sunlight intensity and water temperatures produced significant variability in inactivation rates both within and between days.

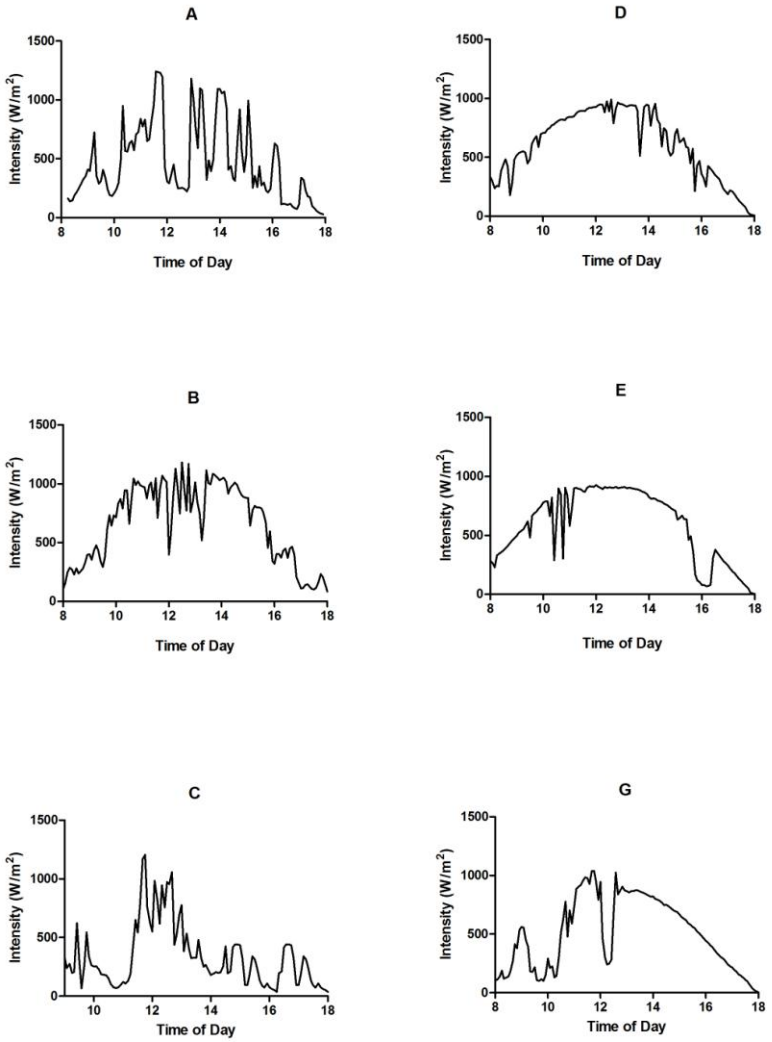


Figure 2.5 Sunlight intensity ($W/m^2$) as a function of time of day for trials in this study: A) 03.25.2009; B) 03.27.2009; C) 04.01.2009; D) 04.21.2009; E) 04.25.2009; F) 04.30.2009

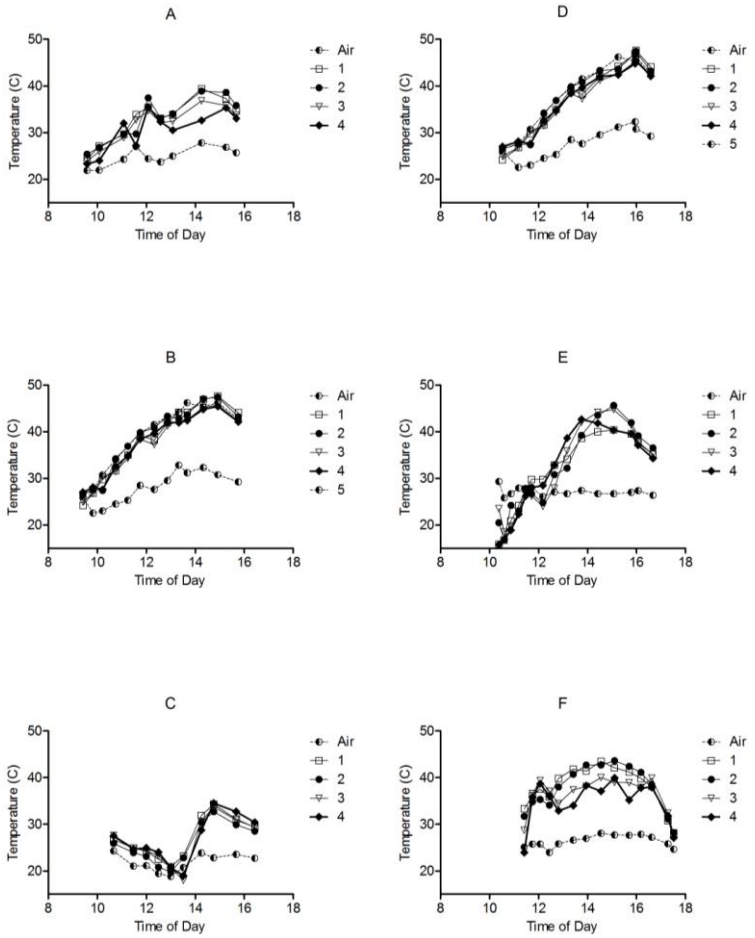


Figure 2.6 Air and water temperatures (degrees C) as a function of time of day for trials in this study. Air temperatures represent the averaged readings of two temperature sensors located beneath the exposure platform in the shade. Individual water temperatures (corresponding to the numbers in each legend) represent the readings of thermocouples inserted into 4-5 bottles in each experiment. A) 03.25.2009; B) 03.27.2009; C) 04.01.2009; D) 04.21.2009; E) 04.25.2009; F) 04.30.2009

## 2.4. Results

### 2.4.1. Organism Source

In all trials, laboratory-cultured *E. coli* and *E. faecalis* were inactivated more rapidly than wastewater organisms (Tables 2.4-2.8, Figures 2.7 and 2.8). In the case of PET and PPCO containers (without additives), the ratios of $t_{99.9}$ values for wastewater versus laboratory *E. coli* and *Enterococcus* were significantly different from one at the 90 or 95% confidence level (Tables 2.4, 2.6). Fluence-based calculations showed similar trends (Tables 2.5, 2.7). A two-tailed paired t test comparing three-log inactivation times and fluences of wastewater vs. laboratory bacteria showed significant differences at the 95% confidence level for all trials without additives in PET and PPCO containers (Table 2.8; the PET and PPCO conditions had 6 replicates, while all other conditions had 3). Note that the difference in inactivation rates between laboratory-cultured and wastewater organisms was not due to matrix effects; cultured cells spiked into diluted wastewater

were inactivated by sunlight at the same rate as cultured cells in unamended buffer (Figure 2.3 B).

Table 2.4 Three-log inactivation times (h) for all conditions studied in this paper. Values in parentheses represent standard deviations. * and ** Denote values that are significantly lower than the corresponding control condition at the 90 and 95% confidence levels, respectively. For container material studies and PET additive studies, the control condition is PET container without additives. For PPCO additive studies, the control condition is PPCO container without additives. ‡ Denotes values for laboratory strains that are significantly lower than the corresponding wastewater condition at the 95% confidence level.

| Organism | PET (n=6) | Tritan (n=3) | PC (n=3) | PS (n=3) | PPCO (n=6) | PET+ A (n=3) | PET+B (n=3) | PPCO+A (n=3) | PPCO+B (n=3) |
|---|---|---|---|---|---|---|---|---|---|
| *E. coli* K12 | 2.93‡ (1.55) | 4.10 (1.09) | 3.50 (0.88) | 3.15 (0.76) | 1.68 (1.09) | 1.03 (0.58) | 1.95 (1.54) | 0.41 (0.19) | 0.61 (0.75) |
| WW *E.C.* | 6.82 (1.27) | 7.54 (4.93) | 6.96 (4.28) | 4.34 (1.58) | 3.00 ** (1.17) | 1.78** (0.87) | 2.89* (1.12) | 2.42 (0.75) | 1.07 (0.37) |
| *E. fecalis* | 2.86‡ (1.30) | 3.27 (1.26) | 2.96 (1.09) | 2.79 (0.91) | 1.80‡ (0.78) | 1.96 (0.27) | 3.07 (3.13) | 0.85* (0.10) | 1.69 (0.99) |
| WW Ent. | 6.24 (1.95) | 6.56 (3.85) | 5.39 (2.59) | 3.89 (1.60) | 2.79 (1.37) | 2.77** (0.25) | 5.15 (2.53) | 1.51 (0.64) | 2.52 (0.81) |
| MS2 | 33.1 (16.6) | 25.0 (12.6) | 40.5 (25.2) | 19.1 (2.97) | 11.5 (3.59) | 4.12* (5.48) | 13.6 (14.2) | 1.71* (1.18) | 4.44 (1.25) |

Table 2.5 Three-log inactivation fluences (MJ/m$^2$) for all conditions studied in this paper. Values in parentheses represent standard deviations. * and ** Denote values that are significantly lower than the corresponding control condition at the 90 and 95% confidence levels, respectively. For container material studies and PET additive studies, the control condition is PET container without additives. For PPCO additive studies, the control condition is PPCO container without additives. ‡ Denotes values for laboratory strains that are significantly lower than the corresponding wastewater condition at the 95% confidence level.

| Organism | PET (n=6) | Tritan (n=3) | PC (n=3) | PS (n=3) | PPCO (n=6) | PET+A (n=3) | PET+B (n=3) | PPCO+A (n=3) | PPCO+B (n=3) |
|---|---|---|---|---|---|---|---|---|---|
| *E. coli* K12 | 7.40‡ (2.67) | 9.61 (1.26) | 8.09 (0.87) | 6.95 (0.44) | 3.83‡* (1.40) | 3.08 (1.64) | 6.07 (4.90) | 1.32* (0.51) | 1.92 (2.40) |
| WW *E.C.* | 17.8 (2.85) | 16.1 (8.41) | 12.7 (4.28) | 9.88* (2.37) | 7.35** (2.17) | 5.32** (2.41) | 8.75* (3.60) | 3.40** (0.59) | 3.29* (1.28) |
| *E. fecalis* | 7.09‡ (1.91) | 7.14 (2.11) | 6.07 (2.00) | 6.05 (1.35) | 4.15‡* (1.22) | 5.91‡ (0.44) | 8.91 (8.72) | 2.65 (0.33) | 5.03 (2.75) |
| WW Ent. | 14.9 (3.25) | 14.1 (6.66) | 12.1 (4.67) | 8.68 (2.90) | 7.07** (2.46) | 8.51** (0.79) | 13.4 (4.72) | 4.73 (2.12) | 7.66 (2.18) |
| MS2 | 80.5 (36.3) | 59.5 (24.4) | 105.7 (64.2) | 48.0 (10.1) | 28.2** (8.08) | 10.5* (13.3) | 35.0 (34.2) | 5.06** (3.26) | 13.1 (3.26) |

Table 2.6 Time-based three-log enhancement factors for the inactivation of laboratory-cultured bacteria relative to wastewater-derived bacteria for all conditions studied. Values in parentheses represent standard deviations. * and ** Denote values that are significantly different from 1.00 at the 90 and 95% confidence levels, respectively.

| Organism | PET (n=6) | Tritan (n=3) | PC (n=3) | PS (n=3) | PPCO (n=6) | PET+A (n=3) | PET+B (n=3) | PPCO+A (n=3) | PPCO+B (n=3) |
|---|---|---|---|---|---|---|---|---|---|
| *E. coli* | 2.85** (1.29) | 1.71 (0.75) | 1.43 (0.35) | 1.35 (0.23) | 2.13** (0.85) | 1.86 (0.84) | 2.00 (1.25) | 7.05 (4.14) | 3.58 (2.24) |
| enterococci | 2.39** (0.87) | 1.89 (0.65) | 1.75* (0.33) | 1.37* (0.21) | 1.56** (0.31) | 1.42** (0.16) | 2.68 (1.57) | 1.72 (0.53) | 1.65 (0.41) |

Table 2.7 Fluence-based three-log enhancement factors for the inactivation of laboratory-cultured bacteria relative to wastewater-derived bacteria for all conditions studied. Values in parentheses represent standard deviations. * and ** Denote values that are significantly different from one at the 90 and 95% confidence levels, respectively.

| Organism | PET (n=6) | Tritan (n=3) | PC (n=3) | PS (n=3) | PPCO (n=6) | PET+A (n=3) | PET+B (n=3) | PPCO+A (n=3) | PPCO+B (n=3) |
|---|---|---|---|---|---|---|---|---|---|
| *E. coli* | 2.85** (1.30) | 1.71 (0.75) | 1.43 (0.35) | 1.35 (0.23) | 2.13** (0.71) | 1.87 (0.85) | 2.00 (1.25) | 7.05 (4.14) | 3.59 (2.24) |
| enterococci | 2.40** (0.87) | 1.89 (0.66) | 1.75* (0.33) | 1.38* (0.21) | 1.56** (0.31) | 1.42** (0.17) | 2.69 (1.58) | 1.73 (0.54) | 1.65 (0.41) |

Table 2.8 Results of paired t test for three-log inactivation times and fluences of laboratory-cultured and wastewater-derived bacteria for all conditions studied. Values represent P values of two-tailed t tests. * and ** Denote conditions for which inactivation rates are significantly different at the 90 and 95% confidence levels, respectively.

| | Organism | PET (n=6) | Tritan (n=3) | PC (n=3) | PS (n=3) | PPCO (n=6) | PET + A (n=3) | PET + B (n=3) | PPCO + A (n=3) | PPCO + B (n=3) |
|---|---|---|---|---|---|---|---|---|---|---|
| Time-based | *E. coli* | 0.005** | 0.26 | 0.18 | 0.14 | 0.022** | 0.13 | 0.12 | 0.06* | 0.18 |
| | Entero. | 0.006** | 0.18 | 0.11 | 0.16 | 0.030** | 0.035** | 0.076* | 0.18 | 0.050** |
| Fluence-based | *E. coli* | 0.001** | 0.26 | 0.14 | 0.12 | 0.015** | 0.14 | 0.17 | 0.08* | 0.18 |
| | Entero. | 0.001** | 0.16 | 0.11 | 0.12 | 0.012** | 0.036** | 0.26 | 0.20 | 0.052* |

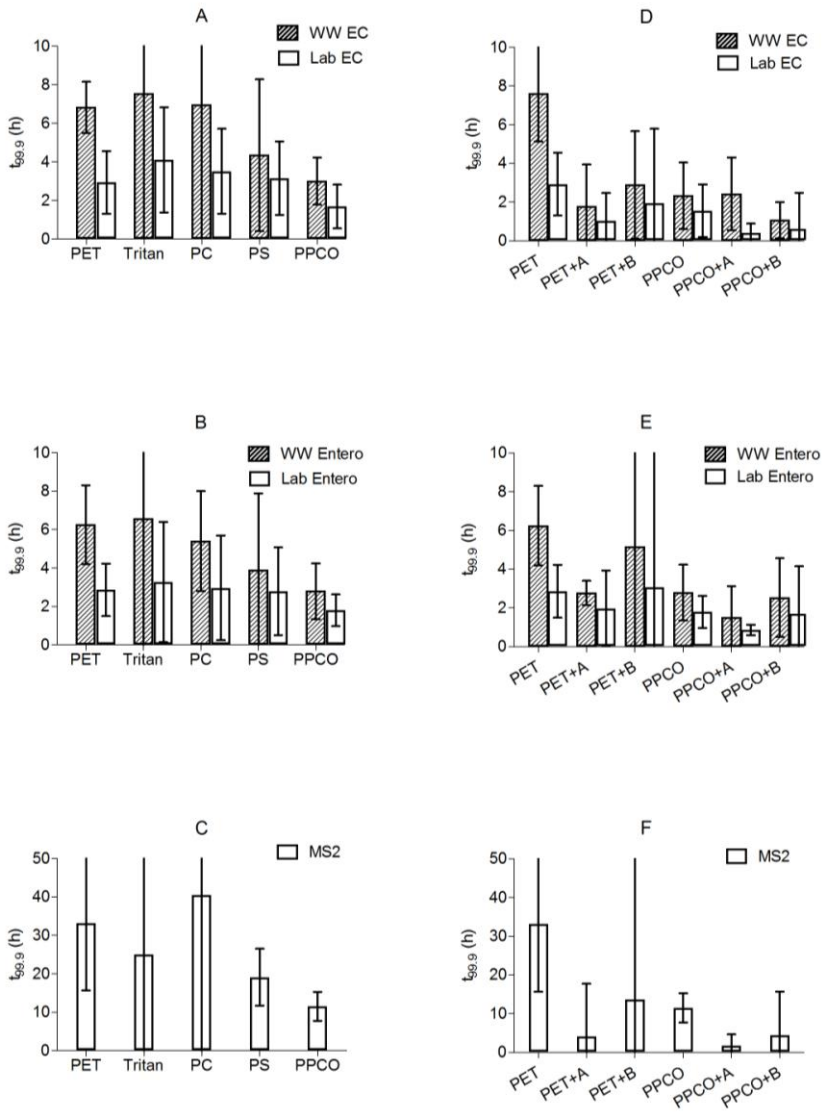


Figure 2.7 Calculated exposure time (based on Equation 2) to natural sunlight (under the field conditions studied) required to achieve 99.9% (three-log) inactivation in containers of different materials (Tritan, PC, PPCO, PS, and PET bottles) with and without additives (Additive A: 100 mg sodium percarbonate + 100 mg citric acid. Additive B: 100 mg sodium percarbonate + 100 mg ascorbic acid + 20 µg copper sulfate). Error bars represent 95% confidence intervals. N=6 for PET and PPCO trials without additives. N=3 for all other trials.

A) Laboratory-cultured *E. coli* K12 and wastewater-derived *E. coli* without additives

B) Laboratory-cultured *Enterococcus faecalis* and wastewater-derived enterococci without additives

C) Laboratory-cultured MS2 coliphage without additives

D) Laboratory-cultured *E. coli* K12 and wastewater-derived *E. coli* with additives

E) Laboratory-cultured *Enterococcus faecalis* and wastewater-derived enterococci with additives

F) MS2 coliphage with additives.

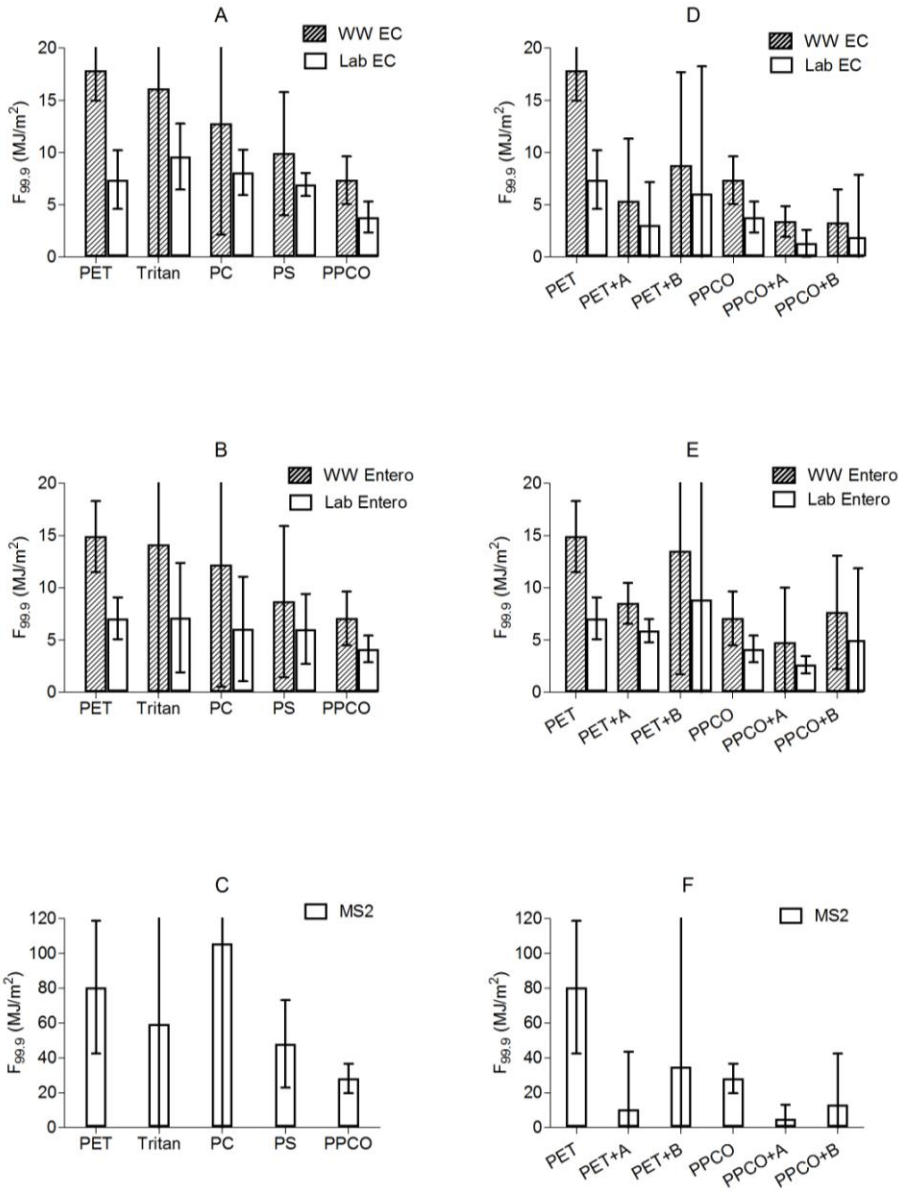


Figure 2.8 Calculated natural sunlight fluence (under the field conditions studied) required to achieve 99.9% (three-log) inactivation in containers of different materials (Tritan, PC, PPCO, PS, and PET bottles) with and without additives (Additive A: 100 mg sodium percarbonate + 100 mg citric acid. Additive B: 100 mg sodium percarbonate + 100 mg ascorbic acid + 20 µg copper sulfate). Error bars represent 95% confidence intervals. N=6 for PET and PPCO trials without additives. N=3 for all other trials.
A) Laboratory-cultured *E. coli* K12 and wastewater-derived *E. coli* without additives
B) Laboratory-cultured *Enterococcus faecalis* and wastewater-derived enterococci without additives
C) Laboratory-cultured MS2 coliphage without additives
D) Laboratory-cultured *E. coli* K12 and wastewater-derived *E. coli* with additives
E) Laboratory-cultured *Enterococcus faecalis* and wastewater-derived enterococci with additives
F) MS2 coliphage with additives.

### 2.4.2. Container Material

Container material had a large effect on inactivation rate (Figure 2.7 A, B, C, Figure 2.8 A, B, C). For all organisms studied, inactivation was fastest in PPCO containers, and all organisms had statistically significant differences in the time- and fluence-based EF(3) values for PPCO vs. PET (Table 2.9, 2.10). In the case of $t_{99.9}$ values, the difference between PPCO and PET was statistically significant for wastewater *E. coli* but not for other organisms (Table 2.4), while $F_{99.9}$ values were significantly different for all organisms (Table 2.5). Time-based EF(3) values for PS vs PET were significantly >1 for laboratory *E. coli* and wastewater enterococci, while only the latter had a significant fluence-based value. Three log inactivation times/fluences in PC and Tritan were not significantly different from PET for any organisms.

Table 2.9 Time-based three-log enhancement factors relative to the corresponding control condition for all conditions studied. For container material studies and PET additive studies, the control condition was PET container without additives. For PPCO additive studies, the control condition was PPCO container without additives. Values in parentheses represent standard deviations. * and ** Denote values that are significant at the 90 and 95% confidence levels, respectively.

| Organism | Tritan (n=3) | PC (n=3) | PS (n=3) | PPCO (n=6) | PET+A (n=3) | PET+B (n=3) | PPCO+A (n=3) | PPCO+B (n=3) |
|---|---|---|---|---|---|---|---|---|
| *E. coli* K12 | 0.97 (0.08) | 1.14 (0.12) | 1.27* (0.13) | 1.84** (0.30) | 4.26** (1.08) | 2.86 (1.49) | 7.65 (6.57) | 10.3 (9.77) |
| WW *E.C.* | 1.21 (0.86) | 1.47 (0.72) | 1.68 (0.71) | 2.48** (0.72) | 4.34 (2.17) | 2.47* (0.84) | 1.72 (1.19) | 3.40** (0.96) |
| *E. fecalis* | 1.08 (0.10) | 1.19 (0.18) | 1.25 (0.19) | 1.62** (0.33) | 1.83 (0.80) | 2.94 (3.71) | 2.68 (1.08) | 1.61 (1.06) |
| WW Ent. | 1.00 (0.35) | 1.13 (0.24) | 1.49** (0.19) | 2.60** (1.25) | 2.10 (0.87) | 1.41 (1.13) | 2.97 (1.93) | 1.68 (1.15) |
| MS2 | 1.13 (0.24) | 0.90 (0.70) | 1.40 (0.47) | 2.91** (0.97) | 19.1 (16.0) | 5.38 (6.04) | 5.99* (2.30) | 2.27* (0.19) |

Table 2.10 Fluence-based three-log enhancement factors relative to the corresponding control condition for all conditions studied. For container material studies and PET additive studies, the control condition was PET container without additives. For PPCO additive studies, the control condition was PPCO container without additives. Values in parentheses represent standard deviations. * and ** Denote values that are significant at the 90 and 95% confidence levels, respectively.

| Organism | Tritan (n=3) | PC (n=3) | PS (n=3) | PPCO (n=6) | PET+A (n=3) | PET+B (n=3) | PPCO+A (n=3) | PPCO+B (n=3) |
|---|---|---|---|---|---|---|---|---|
| *E. coli* K12 | 0.97 (0.09) | 1.15 (0.12) | 1.34 (0.22) | 1.93** (0.19) | 3.39** (0.95) | 2.31 (1.43) | 4.30 (2.40) | 6.56 (5.09) |
| WW *E.C.* | 1.35 (0.84) | 1.55 (0.78) | 1.91 (0.74) | 2.60** (0.79) | 3.67* (1.08) | 2.34 (1.14) | 2.43 (1.40) | 2.35** (0.05) |
| *E. fecalis* | 1.07 (0.09) | 1.28 (0.32) | 1.25 (0.17) | 1.75** (0.38) | 1.31 (0.47) | 2.18 (2.71) | 1.61 (0.50) | 1.05 (0.73) |
| WW Ent. | 1.04 (0.35) | 1.15 (0.28) | 1.56* (0.28) | 2.33** (0.98) | 1.57 (0.44) | 1.10 (0.61) | 2.15 (1.32) | 1.24 (0.74) |
| MS2 | 1.14 (0.27) | 0.87 (0.66) | 1.39 (0.49) | 2.89** (0.96) | 16.7 (12.9) | 3.94 (4.31) | 5.03* (1.95) | 1.66* (0.08) |

We believe the more rapid inactivation of organisms in PPCO is due to the higher UVB-transmittance of that material as compared to the PET, PC, and Tritan containers, which blocked virtually all UVB light (Table 2.11, Figure 2.6). It is significant that PPCO containers accelerated inactivation for all organisms studied despite transmitting only 19% of UVB light and substantially less UVA light than PET (Table 2.11, Figure 2.6). Furthermore, while we found that UVB irradiance was 50% greater at 2500 m than at sea level (Table 2.11, Figure 2.9) (Gueymard, 1995), the UVB/UVA ratio did not vary greatly across elevations and latitudes, suggesting that the effects of container material are expected to occur at lower elevations and at most latitudes (Table 2.11). Finally, while the differences were not significant in many cases, the overall trend in inactivation rates across all organisms (PPCO > PS > PC > PET ~ Tritan) matched the trend in UVB transmittances of the materials studied (Figure 2.6).

Table 2.11 Sunlight intensities calculated using SMARTS. Intensities in W/m2 are displayed in the UVA, UVB, and Visible ranges for the US ASTM 1976 standard sunlight spectrum. These are compared to values for Cochabamba, Bolivia (-17.4º S latitude) at 0 and 2500 m elevation, using temperature and humidity conditions reported for Cochabamba on April 21, 2009, as well as to mid-latitude (45º N) summer and winter conditions at sea level. Values are also compared to those for the standard ASTM spectrum filtered through the PET and PPCO bottle materials used in this study. Comparisons were made between Cochabamba and the equator at 0 and 2500m, but were found to be identical, and thus the latter set of values are not shown.

| Intensities (W/m2) | ASTM 1976 | Coch. 4.21.09 0m | Coch. 4.21.09 2500m | Mid Lat. Winter 0m | Mid Lat. Summer 0m | ASTM PET | ASTM PPCO |
|---|---|---|---|---|---|---|---|
| UVB | 1.62 | 1.62 | 2.37 | 1.53 | 1.66 | 0.01 | 0.31 |
| UVA | 59.4 | 59.6 | 73.2 | 59.8 | 59.8 | 19.2 | 16.8 |
| VIS | 431.9 | 433.4 | 456.9 | 435.5 | 431.1 | 312.8 | 277.1 |
| Norm. UVA | 1.00 | 1.00 | 1.23 | 1.01 | 1.01 | 0.32 | 0.28 |
| Norm. UVB | 1.00 | 1.00 | 1.47 | 0.95 | 1.03 | 0.00 | 0.19 |

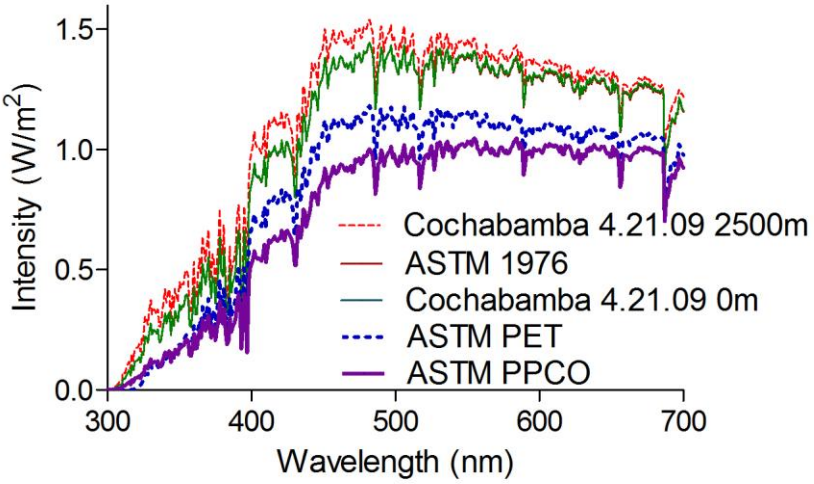


Figure 2.9 Modeled sunlight intensity spectra. Irradiance in $W/m^2$ is shown as a function of wavelength for the US ASTM standard solar spectrum (1976), and for April 21, 2009 at the latitude of Cochabamba, Bolivia (17.4 degrees S) at either sea level or 2500m elevation. The ASTM spectrum is also shown after correction for transmittance through the PET or PPCO bottle materials used in this study. The uncorrected ASTM spectrum may be difficult to observe, as it overlaps almost exactly with the sea level Cochabamba spectrum. Spectra were produced using the SMARTS model V.2.9.5.

### 2.4.3. Additives in PET bottles

Several groups of additives were found to enhance inactivation rates in PET bottles.

#### 2.4.3.1. Additive A

In PET containers Additive A, the combination of citric acid (100 mg) and sodium percarbonate (100 mg), increased the inactivation rate of all organisms (Figure 2.7 D, E, F and Figure 2.8 D, E, F). The effects were particularly pronounced for MS2 and *E. coli*, where the mean three-log inactivation times and fluences decreased by a factor of two or more (Tables 2.4, 2.9, 2.5, 2.10).

#### 2.4.3.2. Additive B

Likewise, the addition of ascorbic acid (100 mg), sodium percarbonate (100 mg), and copper sulfate (20 µg) (Additive B) accelerated the inactivation of all organisms except for laboratory-cultured *E. faecalis* (Figure 2.7 D, E, F and Figure 2.8 D, E, F). Only wastewater-derived *E. coli* had a time-based EF(3) that was significantly greater than 1 (Table 2.9), and no fluence-based values were significantly > 1 (Table 2.10).

### 2.4.4. Additives in PPCO

#### 2.4.4.1. Additive A

In PPCO, the addition of citric acid and sodium percarbonate (Additive A) appeared to result in faster inactivation of all organisms (Figure 2.7 D, E, F and Figure 2.8 D, E, F). Time- and fluence-based enhancement factors (relative to PPCO without additives) were greater than one for all organisms, but were only significant for MS2.

#### 2.4.4.2. Additive B

The addition of copper, ascorbate, and sodium percarbonate (Additive B) also appeared to result in faster inactivation of all organisms (Figure 2.7 D, E, F and Figure 2.8 D, E, F). Time- and fluence-based enhancement factors were significantly greater than one for wastewater-derived *E. coli* and MS2, while three-log inactivation times were not significantly faster for any organisms, and only wastewater-derived *E. coli* had an $F_{99.9}$ significantly lower than for PPCO without additives (Tables 2.4, 2.9, 2.5, 2.10).

## 2.5. Discussion

Additives and alternative container materials offer new opportunities for accelerating SODIS. These opportunities are particularly relevant in light of the slower inactivation observed for wastewater bacteria and MS2 bacteriophage, as compared to laboratory-cultured indicator bacteria in PET bottles.

### 2.5.1. Effect of Additives

Simple, low-cost additives were found to increase solar disinfection rates. Time-based three-log enhancement factors ranging from 1.4 to 19 were observed for Additives A and B (Table 2.9), while fluence-based EF(3)s were slightly lower (Table 2.10). The results presented in this paper were based on a formulation of Additive A including 20 µg of copper, but preliminary testing with 200 µg Cu (well below drinking water guidelines (USEPA, 2003)) resulted in inactivation rates that were too high to be accurately measured, with no detectable organisms remaining after 2 h (data not shown). Thus, higher concentrations of Cu may be extremely efficacious in the field.

Previous research has provided some insight into the mechanisms by which these additives accelerate inactivation. Hydrogen peroxide has been shown previously to accelerate the photoinactivation of indicator bacteria (Ananthaswamy and Eisenstark, 1977; Fisher et al., 2008; Hartman and Eisenstark, 1978; 1980; Keenan, 2001; Khaengraeng and Reed, 2005; Sciacca et al., 2010), viruses (Ananthaswamy and Eisenstark, 1976; Eisenstark et al., 1986; Hartman et al., 1979), and spores (Sichel et al., 2009), while the accelerating effects of copper in combination with ascorbate and/or hydrogen peroxide have been documented (Fisher et al., 2008; Nieto-Juarez et al., 2010). With bacteria, photo-Fenton mechanisms are implicated, either within organisms, on their outer surfaces, or both. Because the mechanisms of the additives are fairly non-specific, it seems likely that they may accelerate the photoinactivation of pathogenic bacteria and viruses under environmental conditions, although more research is needed.

### 2.5.2. Effect of Materials

The ability of alternative container materials to accelerate inactivation was adequately demonstrated in this study, with enhancement factors greater than 1.5 for all organisms in PPCO. Similarly, PS containers produced faster inactivation than PET for some organisms. It seems overwhelmingly likely that these results are due to differences in the

UVB transmittances of the materials used. Thus, SODIS containers with reduced thicknesses and/or even more UVB-transparent materials should facilitate still faster inactivation of laboratory and wastewater organisms than demonstrated in our research, consistent with the reactor optimization study by Davies et al. (Davies et al., 2009).

### 2.5.3. Role of UVB

In this study, the effects of alternative materials were particularly significant for MS2 bacteriophage, which exhibited low UVA sensitivity (Table 2.4), consistent with the findings of previous research (Love et al., 2010). Likewise, Dejung et al. and Noble et al. found low inactivation rates for wild coliphages exposed to sunlight in PET and Nalgene© PC bottles, respectively (Dejung et al., 2007; Noble et al., 2004) (Table 2.1), both materials that block virtually all UVB light (Table 2.11, Figure 2.2). These findings have mechanistic and applied implications for the sunlight inactivation of viruses.

UVB is known to be directly absorbed by the genomic material of both bacteria and viruses, and can participate in inactivation via direct DNA/RNA damage through the production of pyrimidine dimers and other lesions (Harm, 1980; Jaegger, 1985; Sinha and Hader, 2002). However, studies of viruses exposed to UVC found that direct genome damage cannot fully explain the observed decreases in infectivity (Pecson et al., 2009), and further implicated direct and nucleic acid-sensitized protein damage as additional mechanisms of inactivation (Wiggington et al., 2010). Similar pathways may participate in UVB-mediated damage to viruses (and potentially to other organisms as well), along with possible photosensitization by exogenous sensitizers present in the water matrices (Kohn and Nelson, 2007b). Reported three-log inactivation times for virus indicators are variable (Table 2.1), and the sensitivities of human viruses and bacteriophage to different sunlight wavelengths have been found to vary significantly (Fisher et al., Manuscript in Preparation-b; Love et al., 2010; Sinton et al., 2002b). Specifically, bacteriophage PRD1 and PhiX174 were inactivated by simulated sunlight in the presence and absence of a UVB-blocking filter while MS2, adenovirus 2, and poliovirus 3 were not inactivated when the filter was used (Love et al., 2010).

Understanding the mechanisms by which UVB damages bacteria is important for interpreting the results of this work. As noted above, direct absorption of light by bacterial DNA can lead to the formation of cytotoxic lesions. However, bacteria also possess endogenous photosensitizers, including proteins, porphyrins, flavins, quinones, FeS clusters, and others that can sensitize the photoinactivation of cells via direct or indirect photolysis (Curtis et al., 1992; Eisenstark, 1987; Jagger, 1967; 1981; Kramer and Ames, 1987; Lloyd et al., 1990; Smyk-Randall et al., 1993; Tuveson and Sammartano, 1986b). UVA has long been considered the critical wavelength range for these mechanisms (Wegelin et al., 1994), but the role of UVB has not been extensively studied and may also be significant. Genetic factors, growth conditions, sorbed particles and chromophores, and other factors could also affect the sensitivities of cells to direct and indirect damage by UV wavelengths.

### 2.5.4. Effect of Growth Conditions

Growth conditions in particular may affect UVA sensitivity; laboratory cultures grown aerobically on rich media may produce more photosensitizing respiratory proteins containing flavins, porphyrins and FeS clusters than wastewater cells growing in the mammalian gut under nutrient-limited anaerobic conditions, particularly if iron is limiting (McHugh et al., 2003). Bacteria may also have lower specific growth rates in the mammalian gut, increasing sunlight sensitivity (Berney et al., 2006d) and influencing the rate of protein biosynthesis (Pedersen et al., 1978), which can in turn regulate the production of potential photosensitizers (Wilson and Pardee, 1962). A review of prior studies suggests that indicator bacteria of fecal origin tend to be more resistant to inactivation than laboratory cultures (Table 2.1, Figure 2.10). However, published results for fecal bacteria are highly variable. Several groups observed rapid inactivation of indicator bacteria from wastewater or contaminated surface water in PET bottles (Acra, 1984; Keenan, 2001; Reed et al., 2000), while others reported three-log inactivation times for indicator bacteria of likely fecal origin (in open tanks or PET containers) ranging from 10 to 35 h (Table 2.1) (Fisher et al., 2008; Sinton et al., 2002b; Sommer et al., 1997). Noble et al. reported three-log sunlight inactivation times in excess of 48 h for indicator bacteria and viruses of fecal origin in polycarbonate bottles (Noble et al., 2004).

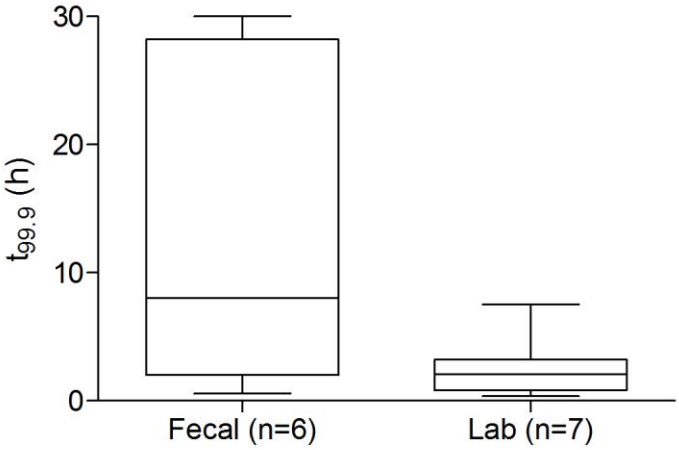


Figure 2.10 Box plot of three-log sunlight inactivation times for coliform bacteria from laboratory cultures or of probable fecal origin in PET bottles. Values for the seven studies using laboratory cultures and the six studies using indicator bacteria of probable fecal origin are presented in Table 2.1 and Figure 2.1.

The question of why MS2 bacteriophage and wastewater bacteria appear more resistant than laboratory *E. coli* to sunlight in general and wavelengths > 320 nm in particular has critical applied significance for SODIS. If pathogens of concern are similarly resistant to inactivation, that information could be helpful in optimizing and monitoring the effectiveness of solar water disinfection under field conditions. Specifically, more conservative disinfection indicators may be needed, and measures to enhance SODIS performance may be called for under some field conditions.

### 2.5.5. Reported UVA/B Sensitivities of True Pathogens

Recent studies suggest that some pathogenic human viruses may be fairly insensitive to wavelengths > 320 nm. As noted above, Love et al. observed an inactivation rate for Adenovirus type 2 that was similar to MS2, whereas the inactivation rate of Poliovirus type 3 was much faster; however, virtually no inactivation was observed when a UVB-blocking filter was used (Table 2.12, Love et al. studies) (Love et al., 2010). Likewise, researchers have shown that *Cryptosporidium* cysts are inactivated far more rapidly when solar UVB is present. King et al. observed that *Cryptosporidium parvum* oocysts exposed to 28 MJ/m$^2$ of full natural sunlight underwent 2.7-log inactivation, compared to 1.3 logs in the absence of UVB (King et al., 2008). Although Gomez-Couso et al. were not specifically studying wavelength effects, they observed a 0.94 log inactivation of *Cryptosporidium* oocysts after a comparable level of exposure (28.3 MJ/m$^2$) in PET bottles (Table 2.13) (Gómez-Couso et al., 2009). These studies show that UVB plays a critical role in the inactivation of some human viruses and protozoan cysts, and that such pathogens can be expected to undergo substantially slower inactivation in PET bottles than in UVB-transparent containers. Thus, while laboratory-cultured indicator bacteria are quite sensitive to sunlight inactivation in PET bottles, they differ in this respect from critical pathogens of concern.

Table 2.12 Log-inactivation levels, inactivation times and fluences, and $t_{99.9}$ values (h) for viral pathogens exposed to natural and simulated sunlight in laboratory and field inactivation trials. Where fluences, times, and/or $t_{99.9}$ values were not given, they were extrapolated from information in the literature sources.

| Organism | $Log_{10}$ Red. Viability (infect.) | Fluence: kJ/m$^2$ (time: h) | $t_{99.9}$ inact (inf.) | Fluence Integration Range (nm) | Container Material | Light Source | Temp (C) | Ref. |
|---|---|---|---|---|---|---|---|---|
| Coliphage f2 | 3 | 9,000 (3.3) | 3.3 | 350-450 | Quartz | TQ718 Hg Lamp | 20 | (Wegelin et al., 1994) |
| Rotavirus | 3 | 6,800 (2.5) | 2.5 | 350-450 | Quartz | TQ718 Hg Lamp | 20 | (Wegelin et al., 1994) |
| Encephalomyocarditis virus | 3 | 34,300 (12) | 12 | 350-450 | Quartz | TQ718 Hg Lamp | 20 | (Wegelin et al., 1994) |
| MS2 | 1.5 | 8,703 (8) | 16 | 200-750 | Open reactor | 1000W solar simulator | 20 | (Love et al., 2010) |
| MS2 | 0 | 8,173 (8) | | 200-750 | Open Reactor (UVB filter) | 1000W solar simulator | 20 | (Love et al., 2010) |
| Adenovirus type 2 | 3.1 | 13,055 (12) | 11.6 | 200-750 | Open reactor | 1000W solar simulator | 20 | (Love et al., 2010) |
| Adenovirus | 0 | 8,173 (8) | | 200-750 | Open Reactor (UVB filter) | 1000W solar simulator | 20 | (Love et al., 2010) |
| Poliovirus type 3 | 5.6 | 6,528 (6) | 3.2 | 200-750 | Open reactor | 1000W solar simulator | 20 | (Love et al., 2010) |
| Poliovirus type 3 | 0 | 8,173 (8) | | 200-750 | Open Reactor (UVB filter) | 1000W solar simulator | 20 | (Love et al., 2010) |
| Polio virus (NCPV #503) | 3.0 | 12,240 (4) | 4 | 300-1020 | PS Multiwell Plate | 1000W solar simulator | 40 | (Heaselgrave, 2006) |

Table 2.13 Log-inactivation levels, inactivation times and fluences, and $t_{99.9}$ values (h) for protozoan pathogens exposed to natural and simulated sunlight in laboratory and field inactivation trials. Where fluences, times, and/or $t_{99.9}$ values were not given, they were extrapolated from information in the literature sources.

| Organism | $Log_{10}$ Red. Viability (infect.) | Fluence: $kJ/m^2$ (time: h) | $T_{99.9}$ inact (inf.) | Fluence Integration Range (nm) | Container Material | Light Source | Temp. (C) | Ref. |
|---|---|---|---|---|---|---|---|---|
| *C. parvum* oocysts | 1.3 (1.1) | 17,928 (6) | 13.8 (16.4) | 300-1020 | PS Multiwell Plate | 1000W solar simulator | 40 | (Mendez-Hermida et al., 2005) |
| *C. parvum* oocysts | 1.0 | 56,000 (24) | 72 | 310-2800 | Borosilicate glass | Natural Sunlight | 30 | (Mendez-Hermida et al., 2007) |
| *C. parvum* oocysts | (2.7) | 28,000 | | 305-2800 | Acrylic cuvette | Natural Sunlight | 13-28 | (King et al., 2008) |
| *C. parvum* oocysts | (1.3) | 28,000 | | 305-2800 | Acrylic cuvette w/ 323 nm filter | Natural Sunlight | 13-28 | (King et al., 2008) |
| *C. parvum* oocysts | 1.7 (1.2) | 25,056 (8) | 14.1 (20.0) | 300-1020 | PS Multiwell Plate | 1000W solar simulator | 40 | (McGuigan et al., 2006) |
| *C. parvum* oocysts | 0.94 | 28,280 (12) | 38.4 | 310-2800 | PET bottle | Natural Sunlight | 46 | (Gomez-Couso et al., 2009) |
| *Giardia* muris cysts | (>3.7) | 12,528 (4) | < 3.2 | 300-1020 | PS Multiwell Plate | 1000W solar simulator | 40 | (McGuigan et al., 2006) |
| *A. polyphaga* cysts | 0.0 | 5,760 (8) | | 300-400 | Borosilicate Glass | 1000W solar simulator | 40 | (Lonnen et al., 2005) |
| *A. polyphaga* cysts | 0.0 | 18,360 (6) | | 300-1020 | PS Multiwell Plate | 1000W solar simulator | 40 | (Heaselgrave, 2006) |
| *A. polyphaga* cysts | 3.6 | 18,360 (6) | 5.0 | 300-1020 | PS Multiwell Plate | 1000W solar simulator | 50 | (Heaselgrave, 2006) |

By contrast, laboratory-cultured, non-sporulating bacterial pathogens appear relatively sensitive to sunlight inactivation in a variety of containers (including glass and PET). In one study, laboratory-cultured *Salmonella typhimurium* were only somewhat less sensitive to natural sunlight than *E. coli*, while *V. cholerae* and *S. flexneri* were more sensitive (Table 2.14) (Berney et al., 2006e). Additional groups studying these and other bacterial pathogens in a range of materials found that all were as sensitive as nonpathogenic *E. coli* to inactivation under a variety of conditions (Table 2.14) (Bosshard et al., 2009; Dejung et al., 2007; Kehoe et al., 2004; Lonnen et al., 2005; Smith et al., 2000; Ubomba-Jaswa et al., 2009; Wegelin et al., 1994). These findings demonstrate that laboratory-cultured pathogens remain sensitive to inactivation in PET bottles and other UVB-blocking containers.

Table 2.14 Log-inactivation levels, inactivation times and fluences, and $t_{99.9}$ values (h) for *E. coli* and bacterial and fungal pathogens exposed to natural and simulated sunlight in laboratory and field inactivation trials. Where fluences, times, and/or $t_{99.9}$ values were not given, they were extrapolated from information in the literature sources.

| Organism | $Log_{10}$ Red. Viability (infect.) | Fluence: $kJ/m^2$ (time: h) | $t_{99.9}$ inact (inf.) | Fluence Integration Range (nm) | Container Material | Light Source | Temp. (C) | Ref. |
|---|---|---|---|---|---|---|---|---|
| *Salmonella typhimurium* | 2 | 2,431 (6.0) | 9 | 350-450 | Quartz | Sunlight | 37 | (Berney et al., 2006e) |
| *Salmonella typhimurium* | 2 (>3) | 5,724 (1.5) | 2.3 (<1.5) | 300-1020 | Polystyrene | Xe arc lamp | 42 | (Smith et al., 2000) |
| *Salmonella typhimurium* | 6 | 10,000 (3.2) | 1.6 | 300-400 | Polystyrene | Xe arc lamp | 42 | (Kehoe et al., 2004) |
| *Salmonella* | 3 | 2,300 | | 350-450 | Quartz | Sunlight | 37 | (Bosshard et |

| | | | | | | | | |
|---|---|---|---|---|---|---|---|---|
| *typhimurium* | | | | | | | | al., 2009) |
| *Salmonella typhimurium* | 3 | 3,000 | | 350-450 | Quartz | TQ718 Hg Lamp | 37 | (Bosshard et al., 2009) |
| *Salmonella typhimurium* | 3 | 7,700 (3.2) | 3.2 | 300-1800 | PET Bottle | Sunlight | 44 | (Dejung et al., 2007) |
| *Salmonella typhi* | 3 | 6,000 (2.5) | 2.5 | 300-1800 | PET Bottle | Sunlight | 44 | (Dejung et al., 2007) |
| *Salmonella enteritidis* | 3 | 8,000 (3.3) | 3.3 | 300-1800 | PET Bottle | Sunlight | 44 | (Dejung et al., 2007) |
| *E. coli* MG 1655 | 2 | 1,530 (3.8) | 5.7 | 350-450 | Quartz | Sunlight | 37 | (Berney et al., 2006e) |
| *E. coli* MG 1655 | 3 | 1,700 | | 350-450 | Quartz | Sunlight | 37 | (Bosshard et al., 2009) |
| *E. coli* MG 1655 | 3 | 1,700 | | 350-450 | Quartz | TQ718 Hg Lamp | 37 | (Bosshard et al., 2009) |
| *E. coli* DH5α | 5.5 | 1,800 (2.5) | 1.4 | 300-400 | Borosilicate Glass | 1000W solar simulator | 40 | (Lonnen et al., 2005) |
| *E. coli* K12 | 6 | 9,558 (3) | 1.5 | 300-1020 | Polystyrene | 1000W solar simulator | 44 | (E Ubomba-Jaswa, 2008) |
| *E. coli* O157 (23631) | 4.9 | 12,754 (4) | 2.4 | 300-1020 | Polystyrene | 1000W solar simulator | 44 | (E Ubomba-Jaswa, 2008) |
| *E. coli* (Bolivian isolate) | 3 | 10,600 (4.4) | 4.4 | 300-1800 | PET Bottle | Sunlight | 44 | (Dejung et al., 2007) |
| *Shigella flexneri* | 2 | 1,194 (2.9) | 4.4 | 350-450 | Quartz | Sunlight | 37 | (Berney et al., 2006e) |
| *Shigella flexneri* | 6 | 4,914 (6) | 3 | 300-400 | Polystyrene | Xe arc lamp | 42 | (Kehoe et al., 2004) |
| *Shigella flexneri* | 3 | 1,800 | | 350-450 | Quartz | Sunlight | 37 | (Bosshard et al., 2009) |
| *Shigella flexneri* | 3 | 1,800 | | 350-450 | Quartz | TQ718 Hg Lamp | 37 | (Bosshard et al., 2009) |
| *Shigella dysenteriae* | 6 | 2,268 (1.5) | 0.8 | 300-400 | Polystyrene | Xe arc lamp | 42 | (Kehoe et al., 2004) |
| *V. cholerae* 01 (Ogawa) | 2 | 304 (0.8) | 1.2 | 350-450 | Quartz | Sunlight | 37 | (Berney et al., 2006e) |
| *V. cholerae* 01 (Ogawa) | 3 | 22,550 (5.2) | 5.2 | 300-400 | Polystyrene | Xe arc lamp | 45 | (Kehoe et al., 2004) |
| *Streptococcus faecalis* | 3 | 1,850 | | 350-450 | Quartz | TQ718 Hg Lamp | 20 | (Wegelin et al., 1994) |
| *Streptococcus faecalis* | 3 | 1,390 (3.2) | 3.2 | 350-450 | Quartz | Sunlight | 20 | (Wegelin et al., 1994) |
| *Pseudomonas aeruginosa* | 5.0 | 1,440 (2) | 1.2 | 300-400 | Borosilicate Glass | 1000W solar simulator | 40 | (Lonnen et al., 2005) |
| *Pseudomonas aeruginosa* | 3 | 12,000 (5) | 5 | 300-1800 | PET Bottle | Sunlight | 44 | (Dejung et al., 2007) |
| *Streptococcus faecalis* | 3 | 11,000 (4.6) | 4.6 | 300-1800 | PET Bottle | Sunlight | 44 | (Dejung et al., 2007) |
| *Bacillus subtilis* spores | 1.7 | 5,760 (8) | 14.1 | 300-400 | Borosilicate Glass | 1000W solar simulator | 40 | (Lonnen et al., 2005) |
| *Bacillus subtilis* spores | 1 | 29,900 (12.4) | 37.2 | 300-1800 | PET Bottle | Sunlight | 44 | (Dejung et al., 2007) |
| *Candida albicans* | 5.4 | 4,320 (6) | 3.3 | 300-400 | Borosilicate Glass | 1000W solar simulator | 40 | (Lonnen et al., 2005) |
| *Fusarium solani* (conidia) | 5.4 | 5,760 (8) | 4.4 | 300-400 | Borosilicate Glass | 1000W solar simulator | 40 | (Lonnen et al., 2005) |

However, pathogenic bacteria in contaminated water are likely to be of fecal origin (although some enteric bacteria can also grow in soil and other environments (Hardina and Fujioka, 1991; Ishii et al., 2006; Ishii et al., 2007)) and few groups have studied the inactivation of true pathogens of fecal origin by natural sunlight in PET bottles. If pathogenic bacteria are similar to bacterial indicators in being less sensitive to UVA when incubated in mammalian digestive tracts than in rich culture media, they also may be resistant to inactivation in containers made from UVB-blocking materials.

### 2.5.6. Quantifying Adequate Disinfection

The need to increase the disinfection achieved by SODIS depends on the level of pathogen inactivation required for effective water treatment. Three-log inactivation times and fluences are convenient and routinely-cited benchmarks (Bosshard et al., 2009; Dejung et al., 2007; Wegelin et al., 1994), but recent health-based recommendations advocate 4, 5, and 4 $\log_{10}$ reductions in viable bacteria, viruses, and protozoan cysts, respectively, to achieve "highly protective" drinking water treatment (Brown and Sobsey, 2010) (Table 2.15). Based on the inactivation rates observed for pathogens with low sensitivities to wavelengths > 320 nm (Tables 2.12, 2.13 (Gomez-Couso et al., 2009; Love et al., 2010)), it seems unlikely that one day's exposure in PET bottles without additives at temperatures below 45° C would meet these stringent inactivation benchmarks with respect to viral and protozoan pathogens under most conditions. While literature evidence is too scarce to predict how wastewater-derived bacterial pathogens will fare, indicator data suggest that the 4-log benchmark may be similarly difficult to consistently achieve.

Table 2.15 Preliminary inactivation levels for point-of-use drinking water disinfection as proposed by Brown and Sobsey in their draft Guidance Document (Brown and Sobsey, 2010).

| | $\text{Log}_{10}$ Reduction | | |
|---|---|---|---|
| Rating | Bacteria | Viruses | Protozoa |
| Highly Protective | 4 | 5 | 4 |
| Protective | 2 | 3 | 2 |
| Minimally Protective | 1 | 1 | 1 |

While SODIS in PET bottles may not always meet stringent disinfection benchmarks, it may dramatically reduce the infectivity of waterborne pathogens. Smith et al. demonstrated that sublethally damaged *Salmonella typhimurium* were rendered noninfectious by exposure to sunlight (Table 2.14) (Smith et al., 2000). Furthermore, the above-cited health-based guidelines also note that even one-log inactivation of pathogens may provide some protection against waterborne illness (Brown and Sobsey, 2010). Therefore, the affordability and ubiquity of PET bottles must be carefully weighed by SODIS researchers and implementers against its UVB-blocking properties. Further research will be useful in elucidating the health implications of these trade-offs.

## 2.6. Conclusions

Overall, the results of this work indicate that alternative container materials and additives can dramatically increase the level of disinfection achieved with SODIS. The enhanced inactivation of MS2 coliphage, which is resistant to wavelengths > 320 nm, can likely be extrapolated to other UVA-resistant viruses, which may not experience much inactivation during conventional SODIS. The enhanced inactivation of bacteria may be particularly relevant if waterborne bacterial pathogens in contaminated waters resemble wastewater-derived *E. coli* and *E. faecalis* bacteria in their greater resistance to wavelengths > 320 nm relative to laboratory-cultured cells.

## 2.7. Acknowledgements

This work was supported by a grant from the Blum Center for Developing Economies at U.C. Berkeley and an NSF Graduate Fellowship to MBF.

Special thanks to the many individuals whose assistance in the laboratory, field, and conceptual aspects of this work made this study possible. Thanks to Fermin Reygadas, the UMSS CASA team, including Lic. Ana Maria Romero, Ing. Alvaro Mercado, Fernando Arias Meneses, Cecilia Decker Franco, Alexandro Canaza Jorges, Wilber Hinojosa Delgadillo, and Don Emilio; The Fundacion SODIS team, including Michael Schulte, Elsa Sanchez, Alberto Castro, Matthias Saladin, and Maria Luisa Chavez. Thanks also to the many other students, NGO staff and field workers, and research personnel who assisted in this study.

# 3. Sunlight Action Spectra for Inactivation of MS2 and PRD1 Bacteriophage in Clear Water

## 3.1. Chapter Summary

Sunlight action spectra were measured in clear water for two bacteriophage: PRD1, a double-stranded DNA virus, and MS2, a single-stranded RNA virus. Viruses were diluted into phosphate buffered saline (20 mM PBS, pH 7.5) and exposed for 22 h to simulated sunlight either directly or through one of six glass filters with 50% cutoff wavelengths ranging from 280 - 350 nm. The biological response assayed was virus survival as measured using the double agar layer plaque method. Both UVA (320 - 400 nm) and UVB (280 - 320 nm) light were found to contribute to PRD1 inactivation, while only UVB inactivated MS2. A computational model was developed for interpreting these action spectra with 3-nm resolution. Using these methods, we provide detailed estimates of the sensitivity of MS2 and PRD1 to photoinactivation from 285 - 345 nm. The resulting sensitivity coefficients can be combined with solar spectra to estimate inactivation rates in clear water under different sunlight conditions. This approach will be useful for modeling the inactivation of viruses and other microorganisms in sunlit natural and engineered systems.

## 3.2. Introduction

The germicidal properties of natural sunlight and artificial light on animal viruses (Hollaender and Oliphant, 1944), plant viruses (Hollaender and Duggar, 1936), bacterial viruses (bacteriophage) (Gates, 1934), bacteria (Gates, 1934), and fungi (Hollaender and Emmons, 1941b) are longstanding research topics. The biological response (i.e. persistence, inactivation, mutation) of an organism to ultraviolet (UV) light exposure over a range of wavelengths can be described by a photoaction spectrum (Gates, 1934). The earliest action spectra were obtained primarily in order to characterize the chemical and biological structures of microorganisms (Powell and Setlow, 1956); researchers first determined that genes were composed of nucleic acids when action spectra for mutations in corn pollen, fungi, and viruses matched nucleic acid absorbance spectra (Hollaender and Emmons, 1941a; Rivers and Gates, 1928; Stadler and Uber, 1942). Because one of the absorption maxima of DNA occurs near 260 nm (Jagger, 1985b) and because of the technical limitations of the light sources traditionally used, most action spectra studies have only utilized wavelengths spanning a portion of the UVC region (190-280 nm).

Understanding the role of sunlight in inactivating viruses and other microorganisms requires characterizing the effects of the different solar wavelengths that reach the surface of the earth, especially in the UVB (280 - 320 nm) and UVA (320 - 400 nm) regions. While action spectra for the loss of culturability of many organisms closely correspond to the absorption spectra of their genetic material in the UVC region, photoaction spectra for sunlight inactivation in the UVB and UVA regions may be quite different (Coohill, 1991; Jagger, 1985b) because longer wavelengths may damage organisms through a variety of mechanisms including protein damage (Eischeid et al., 2009; Wigginton et al., 2010) and reactions with endogenous and exogenous sensitizers to form potentially harmful reactive

oxygen species (Kohn and Nelson, 2007a). Few studies have produced UVB and UVA action spectra for viruses (Peak and Peak, 1978; Rontó et al., 1992; Tyrrell, 1978b). In addition, out of all the previous studies of sunlight inactivation of viruses, only those of Sinton and colleagues (Sinton et al., 2002a; Sinton et al., 1999) measured and reported the spectrum of the sunlight, which is critical information for interpreting results.

In this study we developed action spectra for one DNA and one RNA virus in clear water (no exogenous sensitizers) using polychromatic simulated sunlight. We modeled the viruses' response to sunlight to develop coefficients for estimating the sensitivity of each virus to wavelengths over the 280-496 nm range with 3-nm resolution. These spectral sensitivity coefficients can be combined with measured or predicted sunlight intensity spectra to estimate inactivation rates under different sunlight conditions. Ongoing experiments aim to validate this approach.

## 3.3. Materials and Methods

### 3.3.1. Viruses

MS2, a single stranded 3.6-kbp RNA bacteriophage, and PRD1, a double stranded 15-kbp DNA bacteriophage, were propagated in *E. coli* $F_{amp}$ (ATCC # 700891) and in *Salmonella typhimurium* LT2 (ATCC # 19585), respectively, by broth enrichment (USEPA, 2001). Bacteriophage and hosts were kindly provided by Prof. Mark Sobsey (University of North Carolina).

Bacteriophage enrichments were centrifuged at 4,000 x *g* for 10 min to remove cellular debris, 0.22-μm filtered, then precipitated in 8% polyethylene glycol - 0.3 M NaCl (wt/vol, PEG 6000) overnight at 4°C. The following day samples were centrifuged at 23,000 x *g* for 30 min, and virus pellets were resuspended in phosphate buffered saline [PBS; 20 mM total phosphate (mono + dibasic) and 10 mM NaCl, pH 7.5], and the upper phase was filtered through a 0.22 μm filter. MS2 was chloroform extracted (1:3 vol/vol) and centrifuged for 4,000 x *g* for 10 min prior to 0.22 μm filtration, while PRD1 was not because its lipids would be disrupted. Virus stocks were stored at -80 °C for use in UV experiments. Previous experience suggests that these methods adequately remove broth photosensitizers capable of contributing to indirect inactivation of the phage.

Bacteriophage plaque assays were performed using the double agar layer (DAL) method (Adams, 1959b) to titer stocks and to enumerate viruses after exposure to UV light. DAL was performed with 100-μL virus inocula, and a modified Luria Burtani (LB) molten agar (0.75% wt/vol) and bottom agar (1.5% wt/vol). Modified LB agar includes the following ingredients: Bacto Agar (0.75% or 1.5% wt/vol, BD, Sparks, MD), 10 g/L Bacto Tryptone (BD), 0.137 M NaCl, 1 g/L yeast (EMD Chemicals, Darmstadt, Germany), 0.0055 M dextrose (EMD Chemicals), 0.002 M Calcium Chloride (Fisher). DAL plates were incubated at 36 °C for 18 h and enumerated as PFU/mL.

### 3.3.2. Solar Simulator

Samples were irradiated using an ozone-free 1000 W Xe arc lamp housed in an Oriel solar simulator (Oriel model # 91194-1000, Newport Co., Irvine, CA) that projected an 8 × 8 in. beam of collimated light. An Oriel AM 1.5:G:A "global" filter and an atmospheric attenuation filter (Oriel part # 81017, Newport Co.) were used to simulate a solar spectrum (Figure 3.1 A, no filter). Solar simulator spectra (with both the global and atmospheric attenuation filters in place) were measured using portable UV-visible spectroradiometers (RPS 200 and RPS 380, International Light, Peabody, MA).

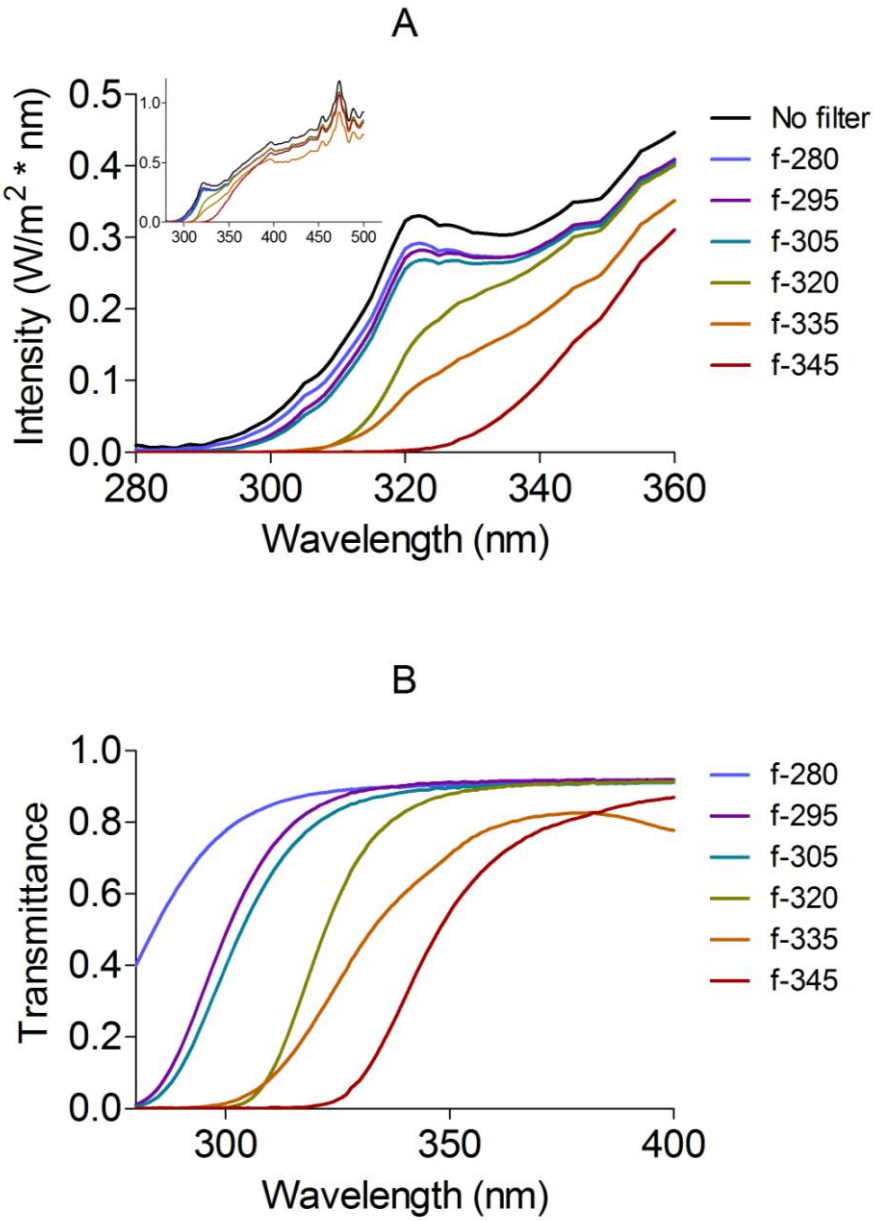


Figure 3.1 A) Intensity of sunlight with and without filters used in action spectra experiments. B) Transmittance spectra of optical filters used in this study. Filter names indicate the approximate 50% cutoff wavelength (in nm) of each filter.

### 3.3.3. Action spectrum experimental design

Purified MS2 and PRD1 were diluted together to titers of $10^6$ PFU/mL in 100 mL phosphate buffered saline (PBS, 20 mM, pH 7.5) in 55 × 100 mm black-painted glass beakers ("reactors"). Samples were stirred magnetically and maintained at 20 °C in a water bath with a recirculating chiller (Thermo Electron). Sample beakers were i) left uncovered; ii) covered with 2 × 2 in. square glass optical cutoff filters [glass filters: Schott WG280 ("f-280"), Schott WG295 ("f-295"), Schott WG305 ("f-305"), Schott WG320 ("f-320"), Schott KG5 ("f-335"), and Kopp 9345 ("f-345")]; or iii) covered with aluminum foil for dark controls and exposed to simulated sunlight for 22 h. Sub-samples were removed at 0, 2, 4, 6, 8, 12, 22 h and immediately frozen at -80 °C. Experiments were performed in triplicate over three consecutive days (each condition was tested in one reactor each day). The measured biological response to sunlight was loss of culturability (ability to form plaques), which was quantified as described above.

Glass filters had 50% transmittance values at wavelengths ranging from 280 nm to 350 nm (Figure 3.1 B). Filter transmittance spectra were recorded on a Perkin Elmer Lambda 14 UV-visible spectrophotometer (Waltham, MA). Solar simulator output over the course of the experiments was constant at 277 W/m$^2$ summed over 280 to 700 nm.

### 3.3.4. Model Development

#### 3.3.4.1. Intensity Spectra

Each of the seven reactors was covered with a different filter (or none), and thus delivered a different light spectrum. The transmittance of each filter multiplied by the solar simulator irradiance at each wavelength is shown in Figure 3.1 A (the raw irradiance data are used for the no filter condition). These spectra represent the intensity to which organisms in the different reactors were exposed and were used as inputs for the numerical model.

#### 3.3.4.2. Inactivation Curves

Virus inactivation was modeled using pseudo first-order kinetics (see below); inactivation rate constants ($k^i_j$) were calculated as the negative slope of the linear regression lines (ln ($N/N_o$) vs time) for each combination of virus (i) and reactor (j).

#### 3.3.4.3. Inactivation Model

Inactivation rate constants were modeled using Equation 1:

$$k^i{}_j = \int_0^\infty \left[ I_j(\lambda) * P^i(\lambda) \right] d\lambda \qquad (1)$$

Where $I_j(\lambda)$ is the spectral irradiance of light (in W/m$^2$*nm) delivered to reactor j and $P^i(\lambda)$ is the spectral sensitivity coefficient, or the relative contribution (in m$^2$/W*h) of photons at wavelength $\lambda$ to the inactivation rate of organism i. Because measurements revealed that the solution absorbed less than 1% of light at all wavelengths of interest, the assumption $I(\lambda) = I_0(\lambda)$ could be made.

To simplify calculations, spectra were discretized into 3-nm bins. Thus, $I_{j,w}(\lambda)$ is the irradiance of light (in $W/m^2$) entering reactor j integrated over a 3-nm wavelength range centered at $\lambda$, and $P^i_w(\lambda)$ is the spectral sensitivity coefficient, or the relative contribution (in $m^2/W*h$) of photons in this range to the inactivation rate of organism i. Equation 1 thus becomes:

$$k^i_j = \sum_{\lambda_{Lower}}^{\lambda_{Upper}} \left[ I_{j,w}(\lambda) * P^i_w(\lambda) * \Delta\lambda \right] \qquad (2)$$

3.3.4.4. Computational Model

A computational model was developed in MATLAB (The MathWorks, Natick, MA) to characterize action spectra by calculating the spectral sensitivity coefficients $P^i_w(\lambda)$ that best fit the measured inactivation rate constants $k^i_j$ (which represented the mean of triplicate inactivation trials) for each virus (i) in each of the seven reactors (j).

To prepare data for the model, solar spectra were adjusted for the absorbance of each glass filter, and a 7 x 73 matrix ($I_{wj}$) was constructed representing the irradiance of light (integrated over 3 nm bins) reaching each of the 7 reactors in the 280 – 496 nm wavelength range. A 7 x 1 vector ($k^i_j$) was constructed containing as its elements the inactivation rate constants for each reactor.

The model first aggregated the irradiance data from 73 to 7 bins, each spanning a wavelength range of 31 nm. This yielded $I^1_{wj}$, a 7 x 7 matrix, to be used for the first iteration, described below. We also generated a 7 x 1 vector of randomly chosen initial guesses $p^0_w$ from a log-normal distribution bounded by the reasonable values 0 – 2 $m^2/W*h$. We then used a constrained nonlinear multivariable optimization function (fmincon, MATLAB Optimization Toolbox version 4.2) to attempt to determine the sensitivity coefficients $p^1_w$ that best satisfied Equation 2 by minimizing the sum of the squared differences between the measured and calculated $k^i_j$ values. The active-set (medium-scale) algorithm within fmincon was used to iteratively change the elements of $p^1_w$, constraining them to remain within the same bounds as $p^0_w$. While this initial system of 7 unknown coefficients $p^1_w$ and 7 equations $k^i_j = I^1_{jw}p^1_w$ could be solved analytically, doing so yielded non-physical (negative) $p^1_w$, so constrained optimization was used instead. We next reduced the wavelength bin size to 30 nm, adding an $8^{th}$ bin (of slightly different size), and linearly interpolating an $8^{th}$ P value into $p^1_w$ to yield an 8 x 1 vector, $p^1_w*$. Equation 1 was then resolved in a best-fit sense using fmincon with initial guesses $p^1_w*$ to obtain $p^2_w$. This process was repeated until a vector of 73 sensitivity values ($p^{31}_w = P^i_w$), corresponding to a wavelength bin size of 3 nm, was obtained in the final iteration. Since this is a severely under-constrained problem (73 unknowns and 7 equations) returning as its output a local minimum of error rather than a unique solution, a variety of different solutions $P^i_w$ were found as the initial guess $p^0_w$ was varied. Therefore, the model was run 1000 times for each virus, using a different set of randomly generated initial guesses each time, and the results were analyzed to obtain a single best-fit set of sensitivity coefficients $[P^i_w(\lambda_w)]$ vs. central bin wavelength for each organism.

Specifically, error values were calculated as the sum of the squared differences between the calculated $k^i_j$ values and measured k values over all reactors j for the given organism i. From the model, the single best fit iteration with the smallest error value was selected and used to obtain mean values of spectral sensitivity coefficients $[P^i_w(\lambda_w)]$ for each reactor/filter set. These results were then double-smoothed by 5-nm boxcar averaging to produce plots of $P(\lambda)$ vs. $\lambda$. Smoothing was introduced to eliminate small discontinuities in the spectral sensitivity coefficients over 3-nm intervals. A single "best fit" datum was used rather than converged statistics (mean and standard deviation) because this spectral sensitivity curve was closest to the optimal solution to our under-determined (but constrained) system of equations; in other words, our Monte-Carlo approach finds many local minima of error, not necessarily the global minimum. The complete MATLAB code for this computational model, as well as the sensitivity analysis and backtesting procedures, is presented in Appendix 1.

#### 3.3.4.5. Sensitivity Analysis

Several methods were employed to characterize the sensitivity of the model output to initial conditions. Mean ($m^i_j$) and standard deviation ($s^i_j$) values were calculated for each of the $k^i_j$ values obtained from triplicate inactivation experiments. For each $k^i_j$, alternative $k^i_j$* values were randomly chosen from within the range $m^i_j$ +/- $s^i_j$ so as to have a sample population mean ($\mu^i_j$) and standard deviation ($\sigma^i_j$), based on $m^i_j$ and $s^i_j$. These alternative $k^i_j$* values were used in the above computational model to generate alternative spectral sensitivity coefficients $[P^i_w(\lambda_w)^*]$ for each wavelength, which were then double-smoothed. This process was iterated 100 times, with different $k^i_j$* values (as well as different initial $P^i_w$* values) randomly selected each time. Within each iteration, log-normally-distributed, randomly generated initial values were used for 10 replicate model runs and errors were calculated as above with the single lowest-error result being selected from each iteration of 10 runs. Median values and median absolute deviations for the set of 100 iterations were then plotted to indicate the degree of variation within the sample population. The use of these nonparametric statistics, as opposed to mean and standard deviation values, was justified based on the lack of evidence for a normal distribution of $[P^i_w(\lambda_w)^*]$ outputs.

#### 3.3.4.6. Back-Testing

The computational approach was back-tested by generating 31 hypothetical sets of spectral sensitivity coefficients, each with a single peak centered at 250, 260, 270,…,550 nm. These hypothetical values were then used to calculate $k^i_j$ values using Equation 1. These $k^i_j$ values were inserted into the computational model, which was solved 100 times using random initial values for $P^i_w$. The resulting "best fit datum" set of spectral sensitivity coefficients was compared to the hypothetical initial values to give an indication of the computational model's useful working range with the given filter set and sunlight spectrum. The errors obtained for these fits were plotted as a function of peak center wavelength. The relative standard deviations of light spectrum intensities across the 7 filter conditions were also plotted in the same figure, since increased variation in light conditions was expected to contribute to improved model resolution. Additionally, a 3-peak back-test was also conducted to determine whether multiple peaks

disproportionately confounded the computational model. The effects of varying the distance between peaks and the location of the three-peak ensemble were studied. Finally, a backtest was conducted using a monotonically-decreasing curve to assess the performance of the model in the absence of any input peaks.

#### 3.3.4.7. Photodamage Spectra

The spectral sensitivity coefficients calculated using the above model were multiplied by the irradiance values from the unfiltered simulated solar spectrum in order to demonstrate the relative contributions of different wavelengths of light to inactivation under typical sunlight conditions. These irradiance-weighted spectral sensitivity coefficients are referred to below as "photodamage coefficients" ($D^i(\lambda) = I_0(\lambda)*P^i(\lambda)$) for convenience.

#### 3.3.4.8. Literature Review

Virus action spectra were reviewed from nearly twenty publications since 1934. Two papers (Sinton et al., 2002a; Sinton et al., 1999) reported enough data to make direct comparisons with our work, and their data were captured using Graph Grabber software (http://www.quintessa.org/FreeSoftware/GraphGrabber/) and converted to inactivation rate constants (k) with units of $m^2/MJ$.

### 3.3.5. Statistical Tests

Statistical tests were performed using MATLAB and Prism (GraphPad Software, La Jolla, CA). ANOVA and Tukey's post-test were used to compare virus inactivation rate constants within a single virus type, and two-tailed t-tests were used to compare between PRD1 and MS2 rate constants within filter treatments.

## 3.4. Results

### 3.4.1. Linear Regression of MS2 and PRD1

Virus inactivation roughly followed first-order kinetics for each filter condition (Figure 3.2). Within each virus type, there were significant differences among inactivation rate constants for the seven different filter conditions ($p<0.0001$, ANOVA). However, Tukey's post-test showed that MS2 inactivation rate constants for dark controls were not significantly different from k values for samples irradiated in reactors with f-320, f-335, or f-345 filters (Table 3.1, Figure 3.2). All other filters produced MS2 inactivation rate constants significantly different from the dark control ($p<0.05$) and, as expected, filters transmitting increasing amounts of UVB light produced successively (and significantly) faster MS2 inactivation rates (Table 3.1).

Table 3.1 Linear regression coefficients for MS2 and PRD1 for each of eight sunlight exposure conditions.

| Filter | MS2 (n=3) | | | | PRD1 (n=3) | | |
|---|---|---|---|---|---|---|---|
| | Sig Dif [a] | $k_{obs}$ ($h^{-1}$) ± st dev | $R^2$ ± st dev | | Sig Dif | $k_{obs}$ ($h^{-1}$) ± st dev | $R^2$ ± st dev |
| No filter | A | 0.148 ± 0.004 | 0.985 ± 0.005 | | A | 0.475 ± 0.043 | 0.986 ± 0.013 |
| f-280[b] | B | 0.107 ± 0.009 | 0.986 ± 0.011 | | B | 0.407 ± 0.007 | 0.996 ± 0.001 |
| f-295 | C | 0.076 ± 0.005 | 0.979 ± 0.021 | | B | 0.374 ± 0.041 | 0.992 ± 0.002 |
| f-305 | D | 0.060 ± 0.003 | 0.856 ± 0.121 | | B | 0.338 ± 0.038 | 0.997 ± 0.003 |
| f-320 | E | 0.009 ± 0.004 | 0.489 ± 0.136 | | C | 0.199 ± 0.025 | 0.997 ± 0.002 |
| f-335 | E | 0.013 ± 0.006 | 0.808 ± 0.105 | | C/D[c] | 0.159 ± 0.005 | 0.995 ± 0.003 |
| f-345 | E | 0.005 ± 0.002 | 0.983 ± 0.022 | | D | 0.107 ± 0.008 | 0.983 ± 0.022 |
| Dark | E | 0.003 ± 0.001 | 0.634 ± 0.049 | | E | 0.002 ± 0.005 | 0.429 ± 0.859 |

[a] $p<0.05$

[b] n=2 for f-280 for MS2 and PRD1

[c] PRD1 inactivation with a WG320 filter was similar to the f-335 filter but different than f-345 filter, while the PRD1 inactivation rates with f-335 and f-345 filters were not different from each other.

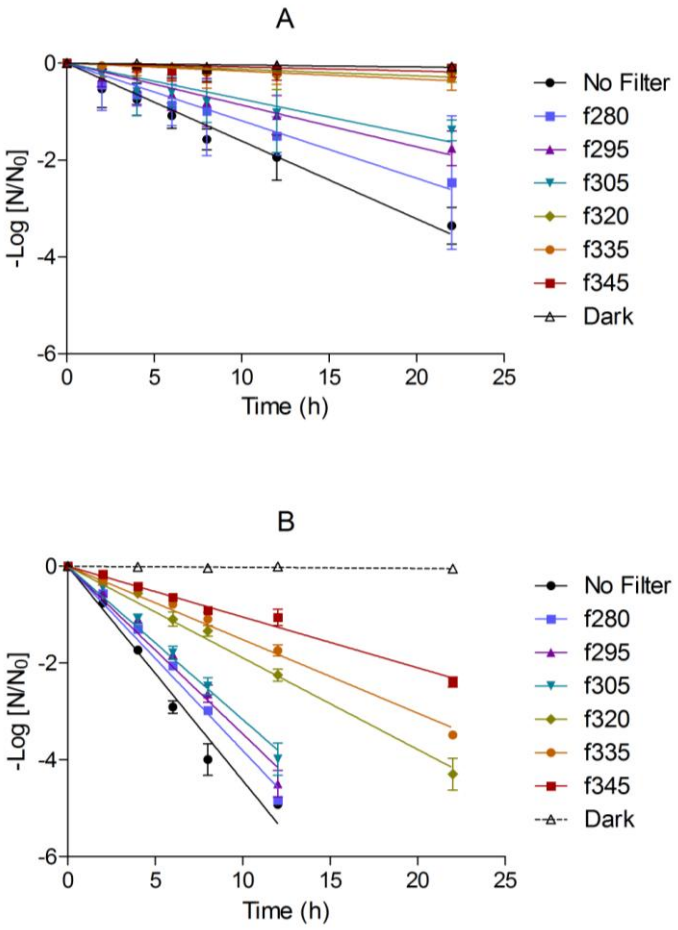


Figure 3.2 Inactivation of bacteriophage exposed to simulated sunlight modified with various cutoff filters: A) MS2 and B) PRD1. Lines indicate linear regressions; error bars indicate the 95% confidence interval of each point.

The rate constant for PRD1 dark controls was significantly different from that for each irradiated PRD1 sample ($p<0.05$) (Table 3.1). No significant difference ($p<0.05$) in PRD1 inactivation rate constants was observed among f-280, f-295, and f-305 filters, although they were each less effective than no filter at inactivating PRD1. Inactivation rates with the f-335 and f-345 filters were not significantly different from each other. MS2 and PRD1 linear regression $R^2$ coefficients were high for most samples and were uniformly high for samples with inactivation rates more than two standard deviations above those of the dark controls (3.1). There was no difference in the inactivation rates of MS2 and PRD1 in the dark controls ($p=0.7474$, two-tailed t-test).

### 3.4.2. Action spectra of MS2 and PRD1

The rate of inactivation for both viruses decreased with increasing 50% cutoff filter wavelengths. PRD1 was inactivated faster than MS2 by simulated sunlight under each filter condition tested ($p<0.05$ for each test, two-tailed t-test) (Figure 3.3 A). For filters with 50% cutoff wavelengths in the UVB range, PRD1 was inactivated three to six times

faster than MS2 (Figure 3.3 A). MS2 was not inactivated when filters with 50% cutoff wavelengths in the UVA range were used, while PRD1 was inactivated.

Values of $k_{obs}$ were normalized relative to full sunlight (i.e., no filter treatment) (Figure 3.3 B), emphasizing the fact that longer wavelengths contributed more to the inactivation of PRD1 than to that of MS2.

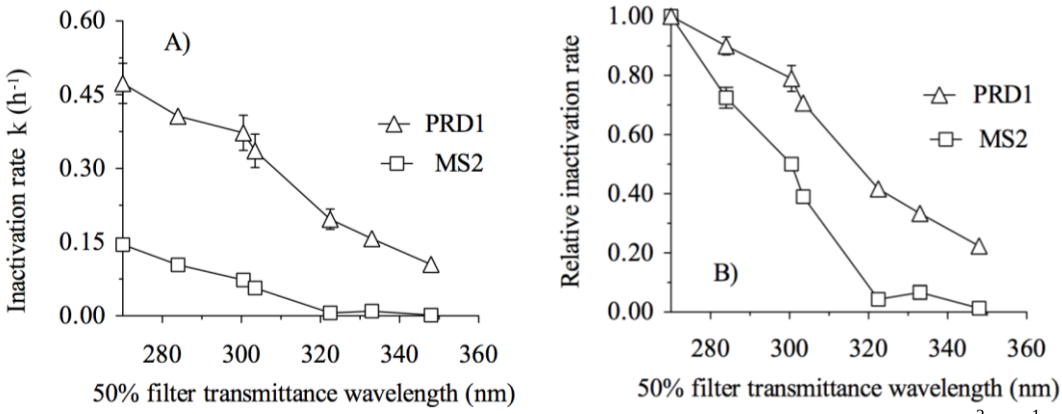


Figure 3.3 Effect of sunlight wavelength on A) MS2 and PRD1 inactivation rate constant k ($m^2$ $MJ^{-1}$) and B) k normalized relative to full sunlight ("no filter"). k's from Table 3.1 were plotted against each of six sunlight filters 50% transmittance values in nm. $k = {}_{sun} - k_{dark}$ and was the mean of n = 3 trials. Full sunlight was represented at 270 nm at our discretion.

### 3.4.3. Comparisons to published action spectra

Normalized $k_{obs}$ values for MS2 and PRD1 were compared with extrapolated normalized $k_{obs}$ values from the literature (Sinton et al., 2002a; Sinton et al., 1999). In our solar simulator, PRD1 had a normalized inactivation rate profile similar to the profiles observed for $F^+$ RNA coliphage (DNA bacteriophage) naturally present in wastewater as extrapolated from the work conducted by Sinton and colleagues in natural sunlight (Sinton et al., 2002a; Sinton et al., 1999)(Figure 3.4 A). Both PRD1 and somatic coliphage were sensitive to wavelengths in the UVA range.

The relative inactivation rate profiles of F+ RNA coliphage, as extrapolated from the work of Sinton and colleagues (Sinton et al., 2002a; Sinton et al., 1999), were similar to each other and both profiles were different from the profile of MS2 (a type of F+ RNA coliphage) observed in our study using simulated sunlight (Figure 3.4 B). UVB wavelengths were alone responsible for the majority of the MS2 inactivation in our work, while Sinton et al.'s findings showed UVA and visible wavelengths were also important to F+ RNA coliphage inactivation.

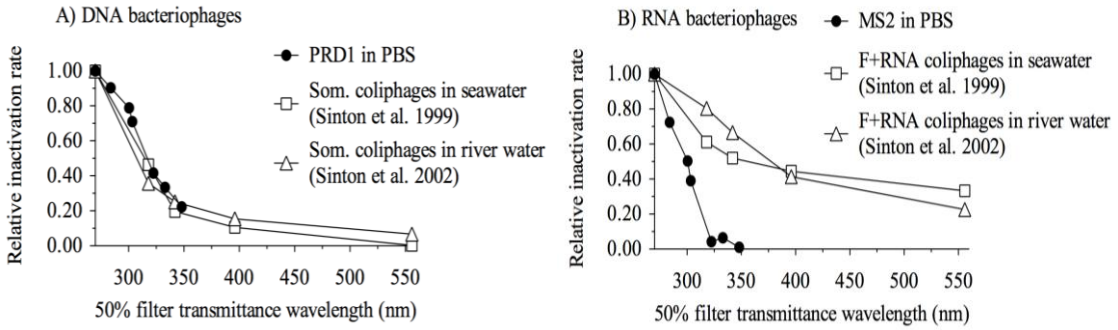


Figure 3.4 Effect of sunlight wavelength on relative inactivation rate k normalized to full sunlight for A) DNA bacteriophage and B) RNA bacteriophage in PBS (circles), seawater (squares), and river water (triangles). $k = k_{sun} - k_{dark}$ and was the mean of n = 3 trials for MS2 and PRD1 (n=2 for f-280), and n=1 F+RNA and somatic coliphage. Inactivation rates for F+RNA and somatic coliphage from Sinton and colleagues (Sinton et al., 2002a; Sinton et al., 1999).

### 3.4.4. Computational model for MS2 and PRD1 inactivation

Spectral sensitivity coefficients for MS2 and PRD1 were determined from the experimentally measured inactivation rate constants using a novel computational model. Both MS2 and PRD1 were more sensitive to sunlight at 280 nm (the shortest wavelength measured) than to other wavelengths, with sensitivity coefficients decreasing to a local minimum around 290 - 295 nm (Table 3.2, Figure 3.5). At longer wavelengths, MS2 and PRD1 had peaks at approximately 305 nm, while PRD1 also exhibited a peak at approximately 350 nm; neither virus was sensitive to visible wavelengths in the PBS solution used for all experiments.

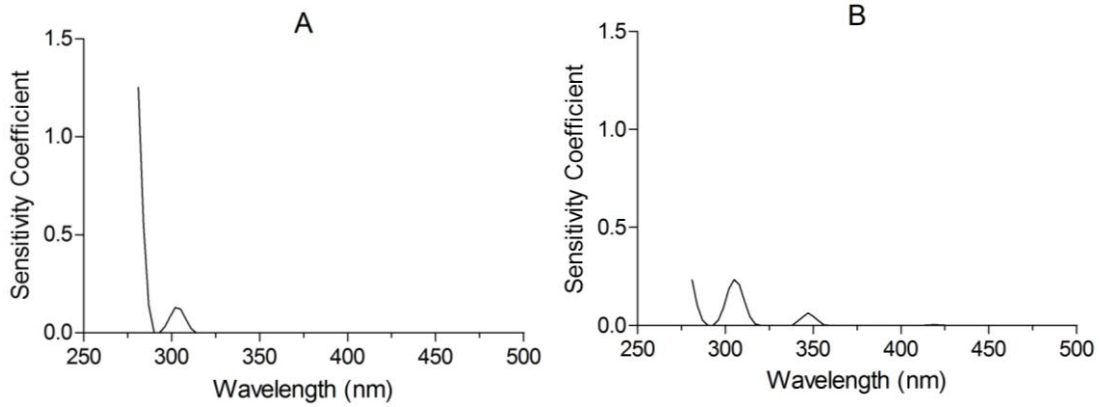


Figure 3.5 Calculated sensitivity coefficients for A) MS2 and B) PRD1 from 280 to 500 nm. Sensitivity coefficients (in $m^2/W*h$) illustrate the contribution of a given irradiance ($W/m^2*nm$) at each wavelength to the observed inactivation rate (1/h). Each figure represents the single best fit model solution.

Table 3.2 Peak wavelengths and integrations for calculated spectral sensitivity coefficients for MS2 and PRD1

| | MS2 | | | | PRD1 | | |
|---|---|---|---|---|---|---|---|
| Peak # | Peak λ | Area | % | Peak # | Peak λ | Area | % |
| 1 | 281 | 3.96 | 74.5 | 1 | 281 | 0.73 | 18 |
| 2 | 302 | 1.36 | 25.5 | 2 | 305 | 2.75 | 67.5 |
| 3 | | | | 3 | 347 | 0.59 | 14.5 |
| Total | | 5.32 | | Total | | 4.07 | |

A sensitivity analysis indicated that the peaks in virus sensitivity below 300 nm and at 305-315 nm were robust to random perturbation, as indicated by the prevalence of nonzero values generated by the analysis in these wavelength regions (Figure 3.6 A, B). The third peak observed for PRD1 at approximately 350 nm was less robust, as an alternate model solution was common, in which the second two peaks were merged into a single peak (Figure 3.6 B). This peak is particularly difficult to verify because the optical cutoff filters used did not provide sufficient resolution at these longer wavelengths (Figure 3.7).

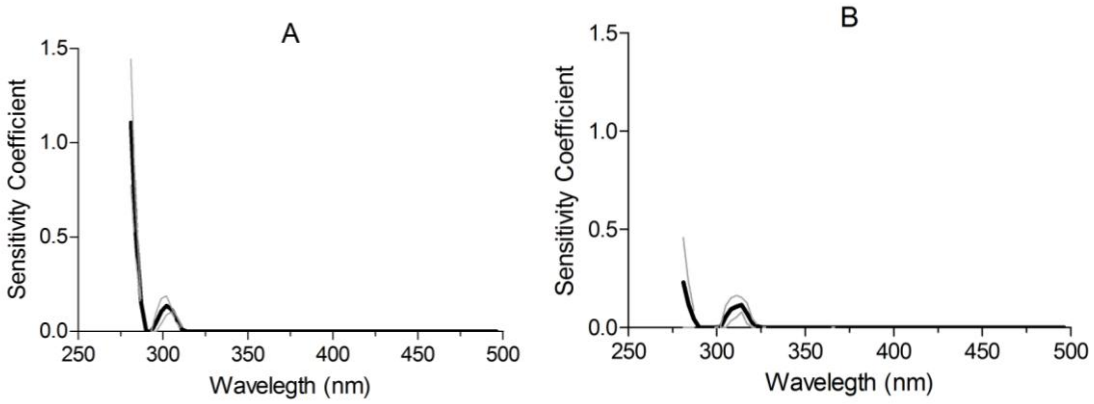


Figure 3.6 Sensitivity analysis for A) MS2 and B) PRD1. Black lines represent median values for recalculated sensitivity coefficients sorted by value at each wavelength, while grey lines represent average absolute deviations.

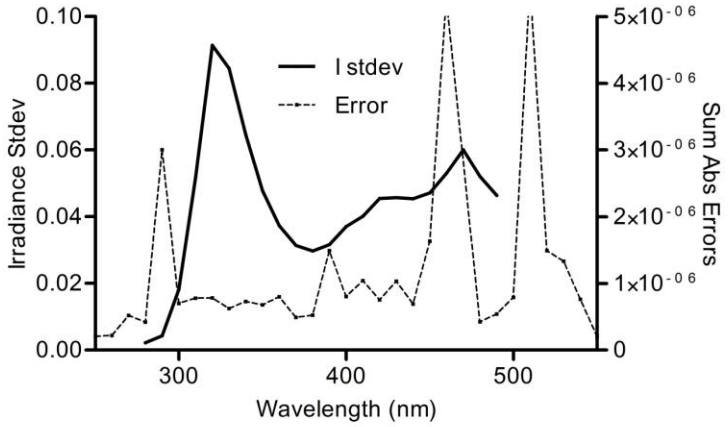


Figure 3.7 Sum of the squared errors for single peak back-testing results as a function of input peak central wavelength (dashed line), displayed on the same horizontal axes as the normalized standard deviation of sunlight intensity values for the seven reactors (solid line). Vertical axis scales were selected for clarity, and the tops of error peaks at 460 and 510 nm are not shown. deviation of sunlight intensity values for the seven reactors (solid line). Vertical axis scales were selected for clarity, and the tops of error peaks at 460 and 510 nm are not shown.

Single-peak back-tests revealed relatively sound model performance at all wavelengths below 450 nm (Figure 3.8), while three-peak back-testing results demonstrated reasonable accuracy from 285 - 345 nm but not outside of that range (Figures 3.9, 3.10). The "no-peak" backtest produced reasonably accurate results over the 280-496 nm range and did not produce significant artifactual peaks (Figure 3.11). It was encouraging that neither the sensitivity analysis nor the back-test validation procedures produced large "false peaks" under the conditions tested, although a small false "daughter" peak occurred next to a larger peak in one 3-peak back-test trial (Figure 3.10 C), and some instances of peaks merging (Figure 3.10 D) or being split in two (Figure 3.10 H) occurred at longer wavelengths (>345 nm).

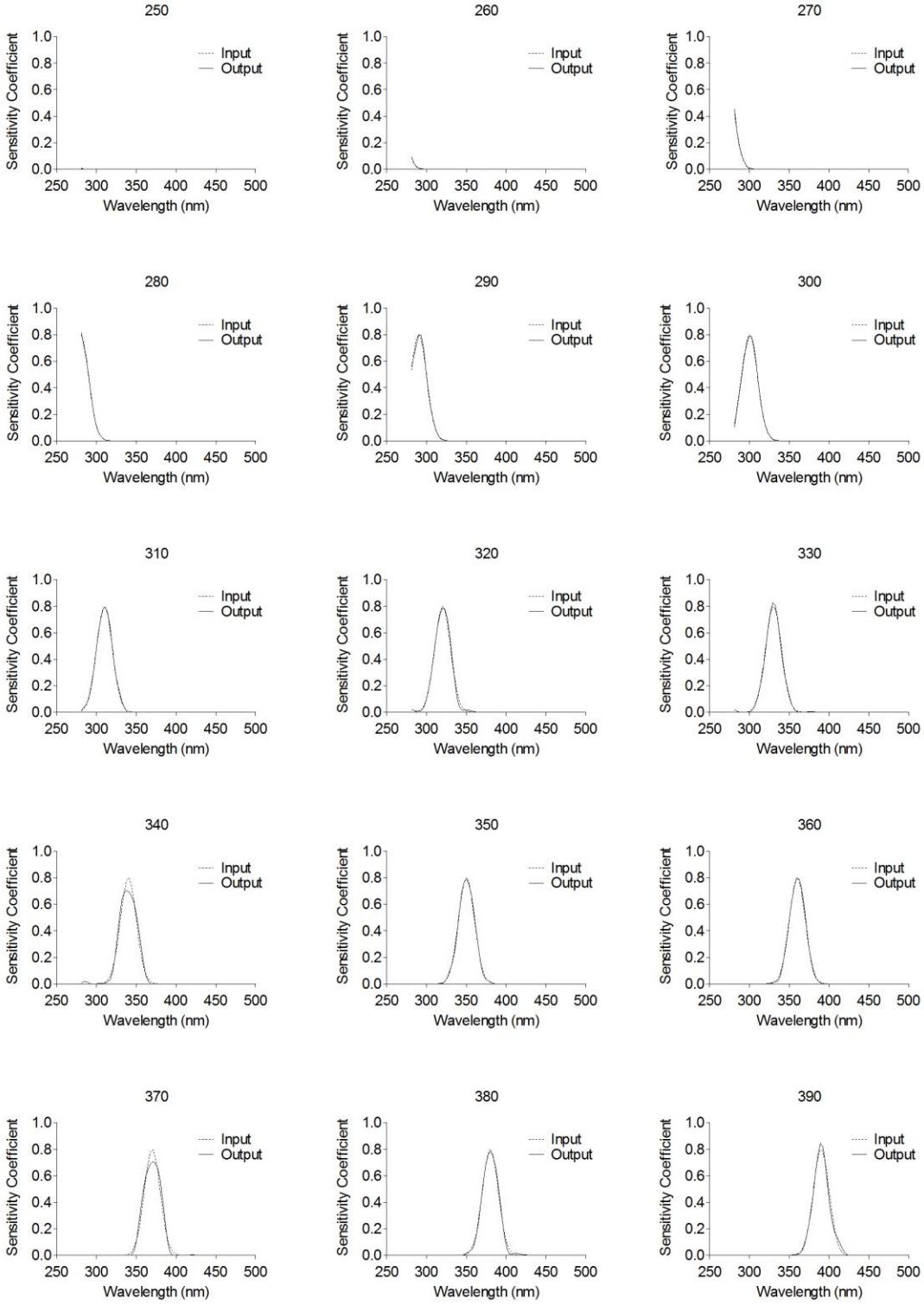
250
260
270
280
290
300
310
320
330
340
350
360
370
380
390
Input
Output
Sensitivity Coefficient
Wavelength (nm)
0.0
0.2
0.4
0.6
0.8
1.0
250
300
350
400
450
500

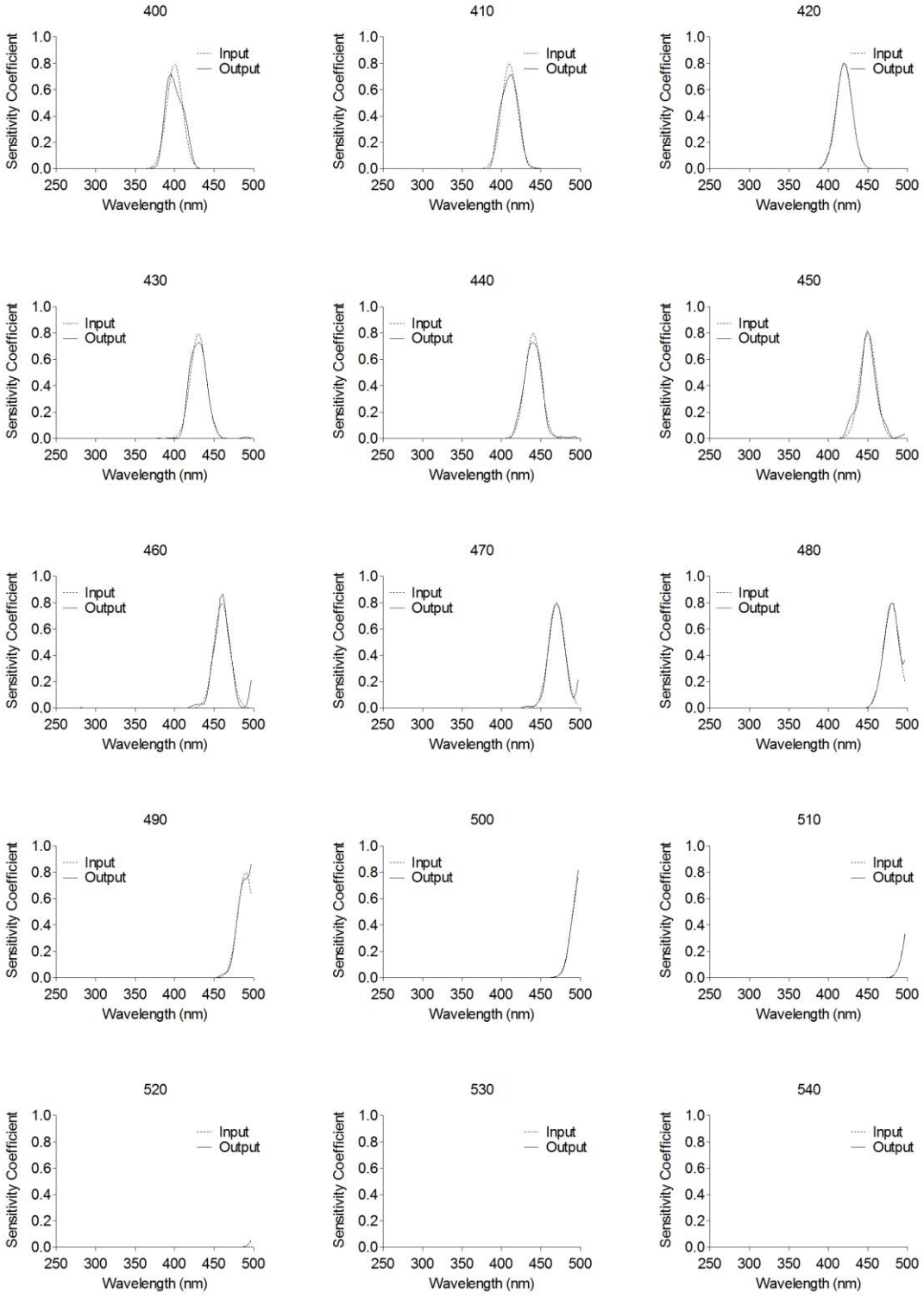


Figure 3.8 Model best-fit result for a one-peak input sample spectrum with a peak wavelength of 250 nm, 260 nm, 270 nm,…,540 nm. Dashed lines represent input values, solid lines represents model outputs.

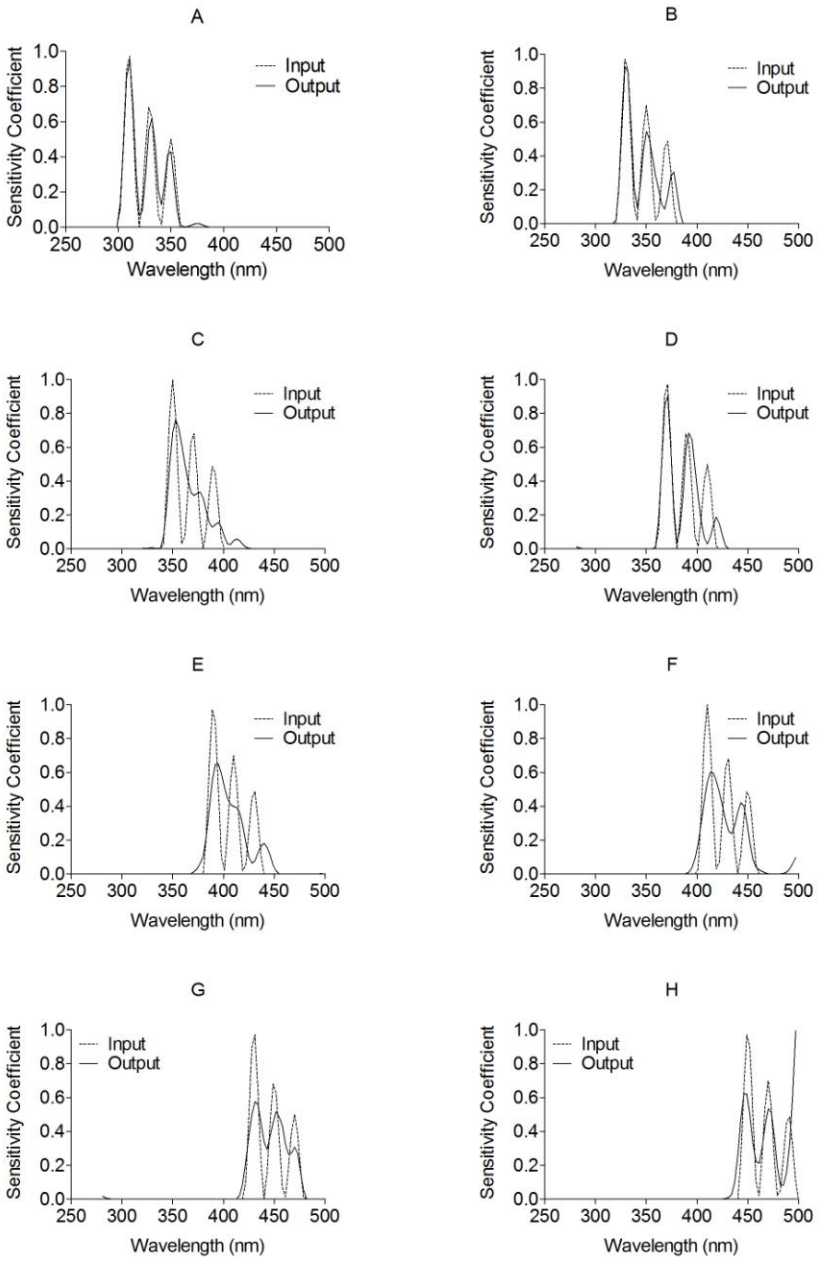


Figure 3.9 Model best-fit result for a three-peak input sample spectrum with an inter-peak distance of 20 nm and a central wavelength for the first peak of A) 310 nm, B) 330 nm, C) 350 nm,…,H) 450 nm. Dashed lines represent input values, solid lines represents model outputs.

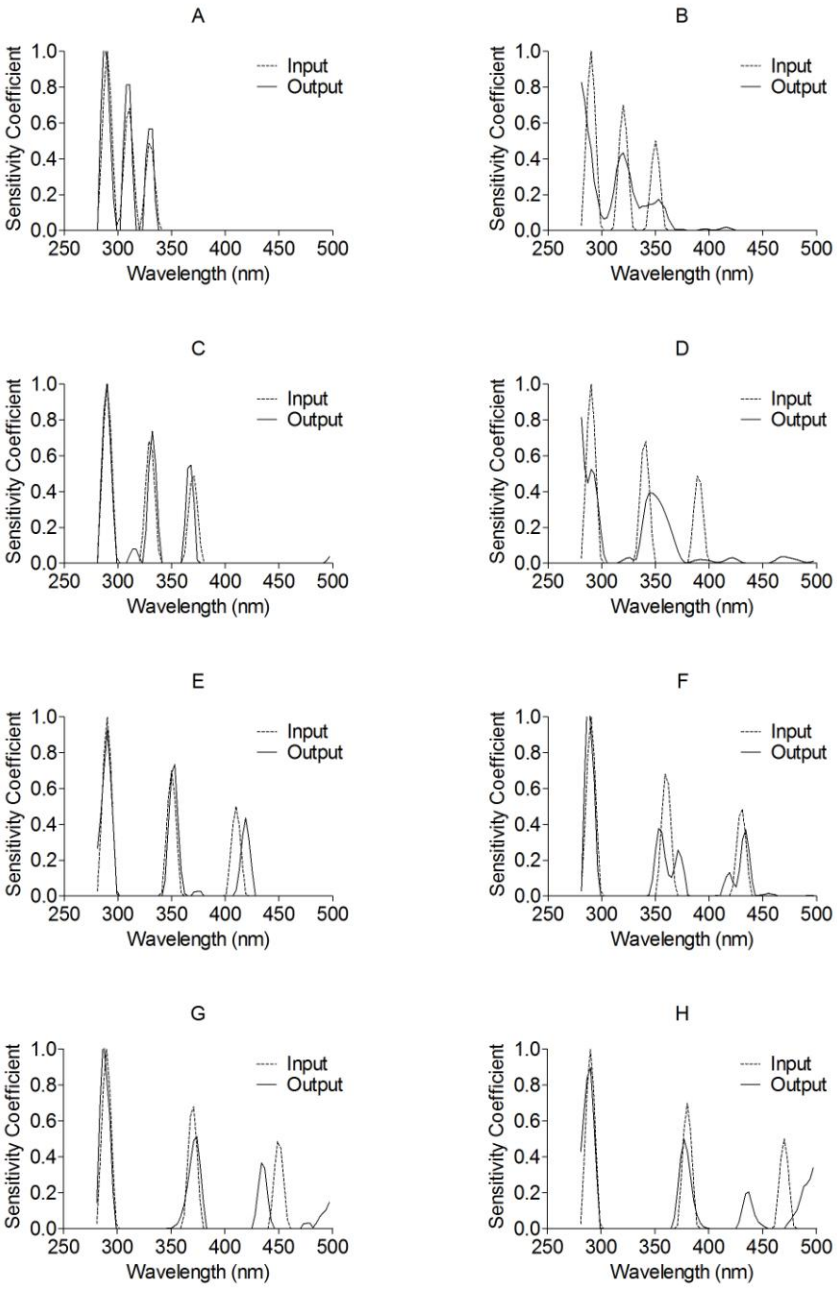


Figure 3.10 Model best-fit result for a three-peak input sample spectrum with a central wavelength for the first peak of 250 nm and an inter-peak distance of A) 20 nm B) 30 nm, C) 40 nm,…,H) 90 nm. Dashed lines represent input values, solid lines represents model outputs.

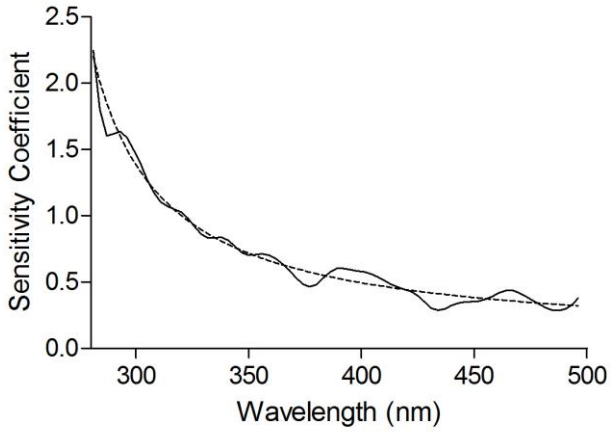


Figure 3.11 Model best-fit result for a monotonic sample spectrum with no peaks described by the equation: y = (1/0.015*(x-250))+0.05. Dashed lines represent input values, solid lines represents model output.

Two additional measures of model robustness, the sum of absolute errors from single peak back-tests and standard deviation of transmittance values among the seven filters were plotted as a function of wavelength (Figure 3.7). Error values were highest above 450 nm with a smaller peak at 290 nm, while transmittance variance was lowest below 300 nm.

Irradiance-weighted photodamage spectra show the relative contributions of different wavelengths of light to inactivation under typical sunlight conditions. From Table 3.3 and Figure 3.12, it can be seen clearly that the sensitivity of PRD1 to longer wavelengths, which are present in much higher intensity in sunlight, results in an overall higher inactivation rate constant compared to MS2. The small peaks in photodamage coefficients observed at 380 nm for MS2 and approximately 420 nm for PRD1 were not found to be significantly different from the baseline in sensitivity analyses, and are estimated to account for less than 5% of inactivation under typical sunlight conditions. Thus, while it is not known whether these peaks are authentic or artifactual, they are likely to negligible for most applications.

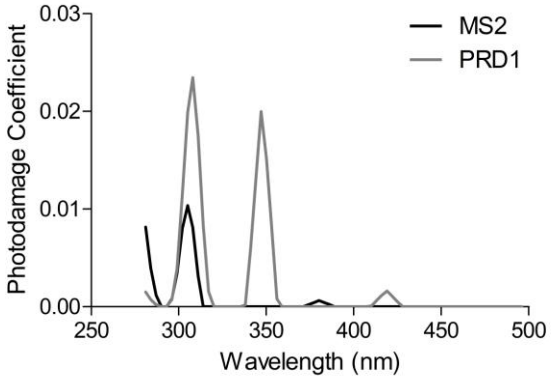


Figure 3.12 Calculated irradiance-weighted spectral sensitivity coefficients (photodamage coefficients: $D^i(\lambda) = I_0(\lambda)*P^i(\lambda)$) for A) MS2 and B) PRD1 from 280 to 500 nm. Photodamage coefficients (in nm/h) illustrate the contribution of a given wavelength of typical simulated sunlight to the observed inactivation rate (in 1/h). Each figure represents the product of the unfiltered simulated solar irradiance spectrum and the lowest error single solution for the spectral sensitivity coefficients P(λ) generated by repeated model runs as presented in Fig. 3. The total area under each curve is equal to the inactivation rate constant measured for that organism under the no filter condition (see Equation 2).

Table 3.3 Peak wavelengths and integrations for irradiance-weighted spectral sensitivity coefficients for MS2 and PRD1.

| | MS2 | | | | PRD1 | | |
|---|---|---|---|---|---|---|---|
| Peak # | Peak λ | Area | % | | Peak λ | Area | % |
| 1 | **281** | **0.03** | **20.5** | | 281 | 0.01 | 1.1 |
| 2 | **305** | **0.10** | **75.2** | | **308** | **0.26** | **55.3** |
| 3 | 380 | 0.01 | 4.3 | | **347** | **0.19** | **40.3** |
| 4 | | | | | 419 | 0.02 | 3.2 |
| Total | | 0.14 | | | | 0.47 | |

## 3.5. Discussion

### 3.5.1. Sensitivity of MS2 and PRD1 to sunlight

PRD1 was found to be more sensitive to sunlight than MS2 for all conditions studied, particularly to UVA light, which had little effect on MS2. The greater sensitivity of PRD1 is consistent with that phage's larger genome, and is in agreement with most previous studies on the inactivation of these viruses (Love et al., 2010; Lytle and Sagripanti, 2005), although Hotze and colleagues (Hotze et al., 2009) found that MS2 was more sensitive than PRD1 to UVA light from a fluorescent UVA source. This discrepancy is puzzling, but may be due to differences in experimental methods and in the output spectra of the light sources used.

### 3.5.2. Model-Derived Sensitivity Spectra

Published virus action spectra are typically characterized by peaks around 260 nm where DNA and RNA maximally absorb UV, followed by a steady decline in virus susceptibility up to approximately 300 nm, where most researchers stopped collecting data (Rauth, 1965). We studied inactivation and sensitivity from 280-500 nm to explore the effects of all likely biocidal sunlight wavelengths on viruses. While the precise mechanisms of inactivation remain unknown, absorption of UVB and UVA photons by nucleic acids and proteins may be a critical step in the inactivation of MS2 and PRD1 in PBS (Chen et al., 2009b; Rauth, 1965). These excited chromophores may undergo direct photolysis or react in aerobic solutions to form reactive oxygen species that damage other targets (Rauth, 1965). A study on the inactivation of MS2 by UVC suggests that nucleic acids may photosensitize damage to proteins(Wigginton et al., 2010); such protein-genome interactions might play a similar role in UVB-mediated damage.

The observation that both MS2 and PRD1 were highly sensitive to the shortest sunlight wavelengths (280 - 290 nm) is consistent with direct or indirect nucleic acid-sensitized damage. By contrast, the sensitivity peaks identified for both bacteriophage in the 305 - 310 nm region (Figure 3.5), while similar to a ~313 nm shoulder in the UV sensitivity of T4 bacteriophage (Tyrrell, 1978b), do not correspond to known peaks for DNA or RNA absorbance or photodamage. These peaks may represent absorbance by and damage to aromatic amino acids (e.g. tryptophan) or other protein components. 254 nm light can damage amino acid residues in the protein capsid of MS2 (Wigginton et al., 2010)and UVB light might produce similar damage, affecting viruses' capsid integrity or their ability to attach to, infect, or replicate within a host. While previous MS2 absorbance spectra did not reveal a peak near 305-310 nm (Johnson et al., 2007), nor did quantum yield data reveal a peak in that range for many viruses of interest (Rauth, 1965), neither approach measured virus inactivation in the 305-310 nm region. However, circular dichroism (CD) spectroscopy (a technique that measures protein folding and stability under stress) showed aromatic amino acid activity at 305 - 310 nm for hepatitis C virus (Kunkel and Watowich, 2004). Thus, spectra for photochemical activity and/or virus inactivation may differ from absorbance spectra (Chen et al., 2009a). Sunlight absorption by and damage to viral nucleic acids and proteins should be measured in parallel with loss of infectivity to further elucidate the mechanisms of inactivation.

### 3.5.3. The Role of Photosensitizers

We attempted to eliminate all sensitizers from our experimental solutions, whereas Sinton et al.'s work was performed in river water or seawater spiked with 2-3% (vol/vol) waste stabilization pond effluent or sewage (Sinton et al., 2002a; Sinton et al., 1999), and thus very likely contained significant concentrations of photosensitizers. Our normalized MS2 inactivation rates were far lower than those of Sinton et al.'s F+ RNA coliphage (a family to which MS2 belongs), particularly at longer wavelengths (Figure 2.4 B). Although biological differences may partly explain the variations in spectral response, a more likely explanation is that photons at longer wavelengths were absorbed by photosensitizers in Sinton et al.'s reactors, producing ROS such as singlet oxygen which subsequently damaged the coliphage (Davies-Colley et al., 1999; Kohn et al., 2007; Kohn and Nelson, 2007a). Interestingly, the normalized inactivation rates of PRD1 in our study

were in good agreement with the rates for somatic coliphage reported by Sinton and colleagues (Figure 3.4 A). This agreement may indicate similar spectral sensitivity of PRD1 and somatic coliphage to sunlight, and may further indicate that exogenous photosensitizers did not play a significant role in the inactivation of the latter variety of DNA phage. It should be noted that somatic coliphage are a diverse group, and variable response to sunlight has been documented in field isolates (Love et al., 2010).

### 3.5.4. Sensitivity Analysis

The results of the sensitivity analysis (Figure 3.6) and model back-testing (Figures 3.7-3.11) suggest that the computational model produced reasonable estimates of virus sensitivity to sunlight over the 285 - 345 nm range, and that the spectral sensitivity peaks observed at wavelengths <300 nm and between 305 - 310 nm are likely to be genuine, although the magnitudes predicted by the model may not be exact. For PRD1, an apparent peak at approximately 350 nm should be interpreted with some caution, as it falls outside the region over which the model could predict with confidence. It cannot be conclusively determined whether PRD1 has two distinct peaks at 305 and 350 nm (as our unperturbed model indicates) or a single, broader peak at slightly longer wavelengths (as the sensitivity analysis suggests). Nonetheless, the inactivation behavior of PRD1 under typical sunlight conditions would be quite similar for both sensitivity spectra.

Future action spectrum experiments with filters providing greater resolution at wavelengths below 285 nm and above 345 nm would increase the power of the current method and its ability to characterize and resolve the sensitivity of viruses over a broader range of sunlight wavelengths. Furthermore, eliminating the atmospheric attenuation filter used in this trial could increase sunlight intensity below 300nm and increase resolution at the shortest UVB wavelengths.

### 3.5.5. Advantages and Limitations of the Study Design and Computational Model

Many action spectra have relied on monochrometers to produce narrow bands of light or simple optical filters to produce sharp cutoffs. When observed biological responses are attributed to the desired spectrum (i.e. the central wavelength of a monochrometer slit or the wavelengths above a filter's nominal cutoff), rather than to the entire spectrum transmitted, significant errors may occur. Furthermore, light sources with discrete emission bands such as mercury vapor lamps may introduce artifacts by delivering unrealistically-high intensities at wavelengths of low organism sensitivity, while delivering little or no intensity at highly biocidal wavelengths. This study used a xenon arc lamp and optical filters to produce polychromatic light that was similar in intensity and spectral properties to natural sunlight. By taking advantage of the gradual cut-offs of optical filters and by modeling inactivation as a function of actual irradiances reaching target organisms, we were able to resolve detailed viral responses to sunlight wavelengths.

However, additional resolution was obtained at the cost of greater uncertainty. Sensitivity coefficients produced by the model are estimates based on optimizations of an under-determined system, rather than direct measurements. This uncertainty could be reduced

by using greater numbers of filters with more diverse transmittance values over the wavelength ranges of interest. Furthermore, higher order terms could be included in future models to address possible synergistic effects between wavelengths. Finally, further work is required to assess the effects of using PBS for inactivation experiments. This buffer contains far more phosphate than natural waters and lacks divalent cations, and may thus affect the speciation of transition metals and the surface charge of microorganisms in photoinactivation trials.

### 3.5.6. Applications of Action Spectra Findings

Measuring the sensitivity of organisms to polychromatic light is critical for modeling sunlight-mediated inactivation in processes including solar water disinfection, wastewater stabilization pond operation, and the fate of pathogens in recreational waters. In clear waters, Equation 2 and the sensitivity coefficients from Figure 3.5 can be used to estimate MS2 and PRD1 inactivation rate constants for any time of day, season, and latitude for which irradiance spectra can be measured or modeled; accounting for light attenuation with depth would further allow the impacts of mixing and stratification on sunlight-mediated inactivation to be explored. Similar approaches are widely applied for estimating the photodegradation rates of chemicals in natural waters based on the quantum yield for the transformation of interest; the sensitivity coefficients for viruses, $P^i(\lambda)$, are analogous to the product of a wavelength-specific quantum yield and the compound's molar extinction coefficient. An important next step is to determine the sensitivity coefficients for enteric viruses of interest. For example, Adenovirus type 2 and Poliovirus type 3 were recently found to be significantly inactivated only in the presence of UVB wavelengths, suggesting that these viruses may have action spectra more similar to that of MS2 than PRD1 (Love et al., 2010).

Further work is required to refine, validate, and apply our experimental approach and computational model. It should be noted that in waters with significant exogenous photosensitizers, additional inactivation mechanisms may occur (Kohn et al., 2007), and Equation 2 does not account for these. Validation under field conditions is also desirable, for example via focused studies similar to those reported by Boehm and colleagues (Boehm et al., 2009a).

## 3.6. Acknowledgements

This work was supported by an NSF CAREER/PECASE award to KN (BES-0239144) and by the U.C. Berkeley Blum Center for Developing Economies.

# 4. Wavelength Dependence of the Inactivation of Laboratory and Wastewater Isolates of *Escherichia coli* by Simulated Sunlight.

## 4.1. Chapter Summary

Sunlight is known to inactivate *E. coli* in a manner dependent on both the intensity and wavelengths of light present. Simulated sunlight closely approximating natural sunlight was used to study the inactivation of three laboratory *E. coli* strains and three *E. coli* strains isolated from wastewater. Both UVB and UVA wavelengths contributed to the inactivation of all strains, which exhibited strong similarities in their inactivation characteristics. Detailed polychromatic sunlight sensitivity spectra are reported and compared to the findings of earlier monochromatic photoaction spectra, as well as the results of low-resolution polychromatic filter studies. Inactivation results for *E. coli* naturally present in diluted raw wastewater are also compared, and show lower sensitivity to UVA than cultured wastewater isolates or laboratory strains. The implications of these findings for understanding and predicting the photoinactivation of *E. coli* in natural and engineered systems, including the solar disinfection of drinking water, are discussed. Mechanistic implications of the results are also addressed.

## 4.2. Introduction

Sunlight has long been known to inactivate microorganisms in water (Acra, 1984; Calkins et al., 1976; Downes, 1877; Wegelin et al., 1994). While the mechanisms by which inactivation occurs are not entirely understood, the sensitivity of a variety of organisms to light of different wavelengths has been studied. So-called photoaction spectra (PASs), which describe the influence of different wavelengths of light on inactivation rates, have been published for several laboratory *E. coli* strains (Peak et al., 1984; Tyrrell, 1980; Webb and Brown, 1979; Webb and Tuveson, 1982), and show strong sensitivity to UVB wavelengths, with UVA sensitivities that are 4-6 orders of magnitude lower (Figure 4.1). Photoaction spectra collected in both the presence and absence of oxygen suggest that *E. coli* sensitivity to UVB wavelengths is largely oxygen-independent, while sensitivity to UVA wavelengths, particularly at 334, 365, and 405 nm, is oxygen-dependent (Webb and Brown, 1979). Although the sources of specific peaks in the UVA sensitivities of *E. coli* strains are not well understood, studies have observed that 365 nm light causes single-strand DNA breakage in bacteria (Tuveson et al., 1983; Tyrrell et al., 1974), while synergistic action has been observed between 365 and 405 nm light (Webb et al., 1982). Such work is significant because it informs mechanistic inquiries into photoinactivation processes.

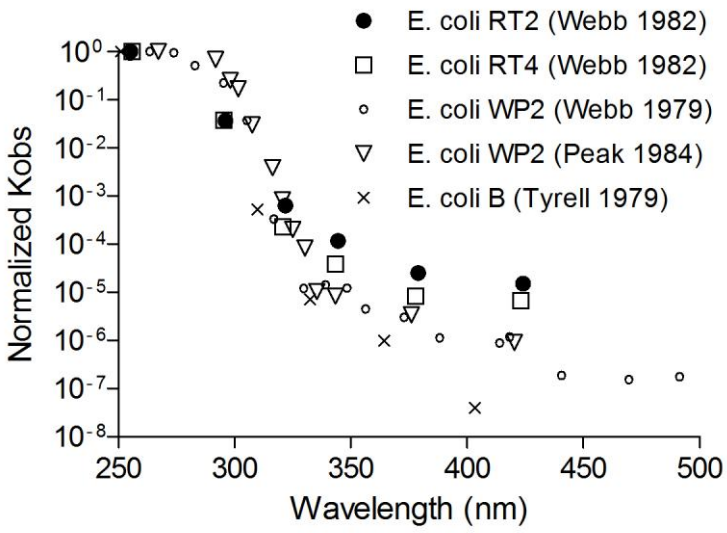


Figure 4.1 Normalized photoaction spectra from several published studies measuring the inactivation of *E. coli* B, WP2, RT2, and RT4 by light from a mercury vapor lamp filtered through a monochrometer. All strains were grown aerobically on rich media.

In addition to the photoaction spectra cited above, which were primarily conducted using light produced by mercury vapor lamps and filtered through monochrometers, a number of studies using polychromatic natural and simulated sunlight with optical cutoff filters have yielded further information about the wavelength sensitivities of *E. coli* and fecal coliforms. Curtis et al. (Curtis et al., 1992) found that *E. coli* 29181 grown on minimal glucose medium (MGM) and irradiated in buffered distilled water was only sensitive to wavelengths up to approximately 430 nm. The authors attributed inactivation to direct DNA damage in the UVB region and photooxidative damage in the UVA and visible regions (Curtis et al., 1992). Similarly, Khaengraeng and Reed (Reed, 2004) found significant, oxygen-dependent sensitivity of laboratory-cultured *E. coli* in distilled water to the UVA region of simulated sunlight. Likewise, Wegelin et al. (Wegelin et al., 1994) found that UVA dominated the inactivation by simulated sunlight of cultured *E. coli* in buffer, followed by violet light, while UVB light had little effect. By contrast, Sinton et al. (Sinton et al., 2002b) found that fecal coliforms in wastewater stabilization pond (WSP) effluent were primarily sensitive to damage by UVB (< 318 nm) wavelengths (attributed to a combination of photooxidative processes and direct DNA damage), but that these organisms remained somewhat sensitive to UVA and visible wavelengths as well. It should be noted that WSP effluent is likely to contain substances that both screen UV light and act as potential exogenous photosensitizers, and these substances may also affect the observed photoaction spectrum.

While these prior studies address the effects of monochromatic and polychromatic light on cultured and wastewater-derived organisms, the gaps in wavelengths measured by monochrometer studies are problematic, while the low resolution of cutoff filter-based methods make mechanistic determinations difficult, as does the variability between different groups' findings. While both monochrometer and filter-based studies shed light on the subject of *E. coli* photoinactivation, more research is needed to understand and

predict the rates at which *E. coli* and other organisms are inactivated in natural and engineered systems. Recently developed computational methods may facilitate higher-resolution interrogation of sunlight inactivation experiments conducted with optical filters.

## 4.3. Materials and Methods

### 4.3.1. Chemicals and Reagents.

All chemicals were reagent-grade and used as received unless stated otherwise.

### 4.3.2. Bacteria.

#### 4.3.2.1. Lab Strains

*E. coli* K12 strain MG1655 was generously provided by Dr. James Imlay at the University of Illinois in Champagne Urbana. *E. coli* K12 29181 (ATCC # 29181, A.K.A. *E. coli* R 483) and *E. coli* $F_{amp}$ (ATCC # 700891) were obtained from ATCC. Upon receipt of frozen stocks of each strain, a sterile LB agar plate was inoculated with the thawed liquid sample and cultured overnight at 37° C. A single colony of each strain was then selected and inoculated into 10 mL of fresh LB broth and incubated overnight at 37° C with shaking, centrifuged at 5000 x g, resuspended in phosphate buffered saline (PBS, pH 7, 50 mM), and mixed with sterile glycerol (50% v/v) before being stored at -80° C as a secondary glycerol stock.

#### 4.3.2.2. Wastewater Organisms

Wastewater samples consisted of primary wastewater effluent collected from the East Bay Municipal Utility District's main wastewater treatment plant with the generous assistance of EBMUD personnel. Briefly, sterile 1 L polypropylene sampling containers containing 10 mg of sodium thiosulfate (to neutralize any traces of chlorine present in the sample) were filled to overflowing with samples of primary effluent collected at the outlet of a single clarifier (#14) using a glass jar mounted on a dip sampler. Multiple batches of wastewater were collected from the same clarifier on separate days, and strains were isolated from these samples. Each of the three isolates used in the study was isolated from a separate batch of wastewater collected on a different day. *E. coli* isolates were collected by spreading several 20 µL aliquots from each batch of wastewater onto LB agar plates supplemented with 0.1% sodium dodecyl sulfate and 0.15 g/L X-glucuronide (LB-SDS-Xgluc, where X-gluc = 5-Bromo-4-chloro-3-indoxyl-beta-D-glucuronide cyclohexylammonium salt). Single colonies which grew with a bluish color (glucuronidase positive) were selected as candidate isolates, of which 30 were initially identified. Liquid cultures and glycerol stocks of all 30 isolates were then prepared according to the procedure described above for preparing secondary glycerol stocks of reference strains. Wastewater isolates were confirmed as either *E. coli* or another species via multiple methods including 16S sequencing (as described in the Supplemental Material Section), biochemical typing (API 20E, bioMerieux, Inc, Hazelwood, MO), and isolation on selective and/or chromogenic media including MTEC and modified MTEC agar, as well as LB-SDS-Xgal (5-bromo-4-chloro-3-indolyl- beta-D-galactopyranoside) agar. All isolates used (Isolates 8, 14, and 36) produced colonies that were consistent in

color and appearance with those expected for *E. coli* on MTEC and modified MTEC agar, and as well as on LB-SDS-Xgluc and LB-SDS-Xgal plates, and yielded API20E profiles that were also consistent with identification as *E. coli* (Table 4.1). Alignments of the 16S sequences amplified from each of the isolates used had >98% sequence similarity with the sequence amplified for *E. coli* strain K-12 MG1655, and a BLAST search of the isolate sequences produced high probability matches with *E. coli*.

For experiments, liquid cultures of all bacterial strains were prepared by inoculating 10 mL of LB broth with a fresh glycerol stock, incubating overnight at 37° C to stationary phase, harvesting by centrifugation at 5000 x g, and resuspending the pellets in phosphate buffered saline (PBS: pH 7, 50 mM) at the desired concentration (typically $10^6$ colony-forming units per mL (CFU/mL).

Table 4.1 API20E Biochemical testing results for *E. coli* MG1655 and the 3 wastewater isolates used in this trial, as well as the reference strain *E. coli* 25922. Tests 1-20 correspond to the following assays: β-galactosidase production (ONPG test), Arginine dihydrolase (ADH), Lysine decarboxylase (LDC), Ornithine decarboxylase (ODC), Citrate utilization (CIT), $H_2S$ production (H2S), Urease production (URE), Deamination of tryptophan or phenylalanine (TDA), Indole production (IND), Acetoin production (VP), Gelatin liquefaction (GEL), Acid from glucose (GLU), Acid from mannitol (MAN), Acid from inositol (INO), Acid from sorbitol (SOR), Acid from rhamnose (RHA), Acid from sucrose (SUC), Acid from melibiose (MEL), Acid from amygdalin (AMY), Acid from arabinose (ARA).

| Test # | 1 | 2 | 3 | 4 | 5 | 6 | 7 | 8 | 9 | 10 | 11 | 12 | 13 | 14 | 15 | 16 | 17 | 18 | 19 | 20 |
|---|---|---|---|---|---|---|---|---|---|---|---|---|---|---|---|---|---|---|---|---|
| Test | ONPG | ADH | LDC | ODC | CIT | H2S | URE | TDA | IND | VP | GEL | GLU | MAN | INO | SOR | RHA | SUC | MEL | AMY | ARA |
| Iso8 | + | - | + | + | - | - | - | - | + | - | - | + | + | - | + | + | - | + | - | + |
| Iso14 | + | - | + | + | - | - | - | - | + | - | - | + | + | - | - | + | - | + | - | + |
| Iso36 | + | - | + | + | - | - | - | - | + | - | - | + | + | - | + | + | - | + | - | + |
| MG1655 | + | - | + | + | - | - | - | - | + | - | - | + | + | - | + | + | - | # | - | + |
| EC 25922 | + | - | + | + | - | - | - | - | + | - | - | + | + | - | + | + | - | + | - | + |

#### 4.3.2.3. Bacterial Enumeration

Unless otherwise indicated, *E. coli* colony-forming units were enumerated using the spread-plate method on LB agar that was supplemented with 0.05% (Wt/V) sodium pyruvate, which was added to scavenge metabolically produced hydrogen peroxide (Khaengraeng and Reed, 2005). Plates were incubated overnight at 37°C prior to enumeration. In the case of wastewater experiments, LB-SDS-X-gluc plates supplemented with 0.05% (Wt/V) sodium pyruvate were used (in order to inhibit Gram positive bacteria and more easily identify *E. coli*) and incubated as described above. Blue colonies growing at 37° C on LB-SDS-X-gluc plates within 24 h were counted as *E. coli*.

#### 4.3.2.4. DNA Extraction and Amplification and Sequencing Procedure

Cells were cultured overnight in LB broth as described above, and cultures were centrifuged and resuspended in PBS. Extraction of genomic DNA was carried out using a MO BIO Ultraclean Soil DNA Isolation Kit (Carlsbad, CA), and DNA extracts were

maintained at -80°C. A portion of the 16S ribosomal DNA of each strain was amplified via PCR as follows. 2.5 µL of extracted DNA was added to 12.5 µL of Amplitaq Gold PCR master mix (Applied Biosystems, Carlsbad, CA), along with 0.050 µL of 0.2 µM forward and 0.083 µL of 0.20 µM reverse primer and 9.87 µL of nuclease-free water. The following primers were used for PCR amplification: 27F: 5'-AGAGTTTGATCCTGGCTCAG-3'. 1492R: 5'-GGTTACCTTGTTACGACTT-3' (Weisburg et al., 1991). PCR conditions were as follows. Amplified sequences were confirmed by gel electrophoresis and quantified using Quant-iT Picogreen ds-DNA reagent (Molecular Probes, Carlsbad, CA). Approximately 25 µg of amplified DNA was added to 13 µL of sterile, nuclease-free distilled water, and the appropriate forward or reverse primer was added to each sample before it was submitted to the UC Berkeley Sequencing Facility. Following sequencing, forward and reverse sequences were reconciled using the Geneious software package (Biomatters Ltd., Auckland, New Zealand), and consensus sequences were submitted to a BLAST search. In each case, the vast majority the top 100 matches (presented below) were *E. coli* strains.

#### 4.3.2.5. Sequence Processing and Alignment Procedure

Forward and reverse sequences were aligned using Geneious Basic 4.6.5 (Biomatters Ltd., Auckland, NZ), and nucleotides that were not identified by the sequencing facility were identified manually wherever possible using the spectra provided by the sequencing facility. The consensus sequences for the forward and reverse transcription products from each strain are presented below. The four strains were also aligned using the same software package, and the aligned sequences and alignment summary statistics are presented below. BLAST Searches of each sequence were conducted using the Basic Local Alignment Search Tool (Blast 2.2.25+ (Zhang et al., 2000)) against all bacteria (1565 genomes) and archaea (83 genomes) in the BLAST database on March 5, 2011, and the top 100 results for each of these searches are presented in Appendix 2.

### 4.3.3. Inactivation Trials

#### 4.3.3.1. Irradiation Conditions

Samples were irradiated using an ozone-free 1000 W Xe arc lamp housed in an Oriel Solar Simulator (Model 91194-1000), which projected an 8 × 8 in. beam of collimated light. Oriel AM 1.5:G:A "global" and AM 1.5:G:C "UV-BC-blocking" filters were used to simulate a solar spectrum (Figure 4.2). Solar simulator spectra were measured using a Stellarnet Black Comet portable UV-VIS spectroradiometer. Samples were maintained at 15° C in a recirculating water bath and irradiated in a reactor array made from 12-well uncoated polystyrene plates with a capacity of 5 mL per well. Specifically, plates were cut and arranged on a sheet of polycarbonate to create nine evenly spaced sets of four wells each, for a total of 36 wells arranged in a 6 x 6 grid. The sets of wells were fitted with small polystyrene angle brackets to hold 2" x 2" optical filters in place over each set of 4 wells. Thus, when irradiated, the array held 8 optical filters, each covering 4 wells, and an additional 4 wells were left uncovered in the center (Figure 4.3).

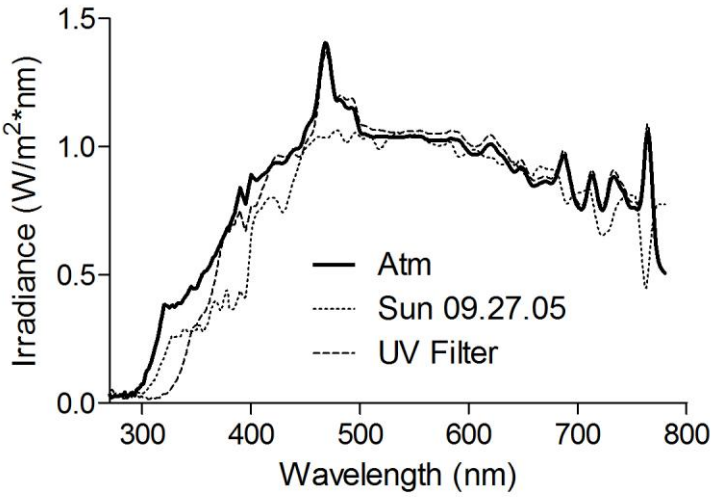


Figure 4.2 Comparison of natural sunlight (Berkeley, California) to the output of an Oriel 91194-1000 solar simulator with a UVBC-blocking or atmospheric filter.

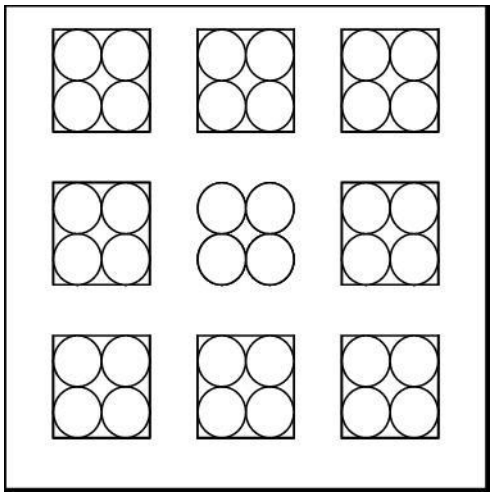

Figure 4.3 Reactor configuration for inactivation experiments.

Laboratory strains and wastewater isolates were grown overnight in LB broth, then centrifuged and resuspended in PBS, while wastewater was allowed to stand for several hours before decanting the supernatant for use in inactivation trials. Concentrated *E. coli* (approx $10^7$ CFU/mL for cultured strains) suspended in PBS were diluted into 200 mL phosphate buffered saline (PBS, pH 7.5) and mixed thoroughly before being pipetted into each of the 5 mL wells ("reactors"). Samples were i) left uncovered; ii) covered with 2"x2" square glass optical cutoff filters [glass filters: Schott WG280 ("f-280"), Schott WG295 ("f-295"), Schott WG305 ("f-305"), Schott WG320 ("f-320"), Schott KG5 ("f-335"), Kopp 9345 ("f-345"), Schott L-39 ("f-390"), and Schott GG455 ("f-455")]; or iii) covered with aluminum foil for dark controls. Reactors were manually stirred at regular intervals and 200 µL aliquots were periodically collected. Aliquots were diluted into PBS and either plated immediately or stored at 4º C and plated within 8 h of collection. Dark controls were kept in the same water bath as the samples. The measured biological

response to sunlight was loss of culturability (decrease in colony forming units), which was quantified using standard plate count techniques as described above. Wastewater samples were diluted 1:10 into sterile PBS for a final volume of 200 mL and used directly as described above (at an approximate *E. coli* concentration of $10^4$ CFU/mL) or spiked with approximately $10^7$ CFU/mL of cultured *E. coli* prior to use as described above. However, a slightly different set of filters was used in wastewater experiments. This filter set included one uncovered condition as well as filters f-280, f-320, f-335, f-345, and two additional 2"x2" square glass optical cutoff filters [glass filters: Kopp 7380 ("f-355") and Hoya L-37 ("f-370")].

Glass filters had 50% transmittance values at wavelengths ranging from 280 nm to 455 nm. Filter transmittance spectra were recorded on a Perkin Elmer Lambda 14 UV-visible spectrophotometer (Waltham, MA). The transmittance of each filter is shown in Figure 4.4 A. These transmittance measurements were also multiplied by the measured simulated sunlight intensity spectrum at each reactor position (although the variation in beam intensity between positions was relatively small) and used as inputs for the numerical model, as they represent the intensity to which organisms in the different reactors were exposed. Solar simulator output over the course of all experiments was relatively constant at 277 $W/m^2$ (200-700 nm). Figure 4.4 B presents the standard deviation of the light intensities reaching each of nine reactors at each wavelength, plotted on the same axes as the intensity spectrum for the unfiltered condition. These data were plotted to give an indication of the wavelength ranges over which the unfiltered simulated sunlight intensity was significantly different from zero and over which the sets of optical filters used provided significantly different filtered sunlight spectra, since both of these conditions were assumed to be necessary to draw meaningful conclusions about the sensitivity of organisms to different wavelengths.

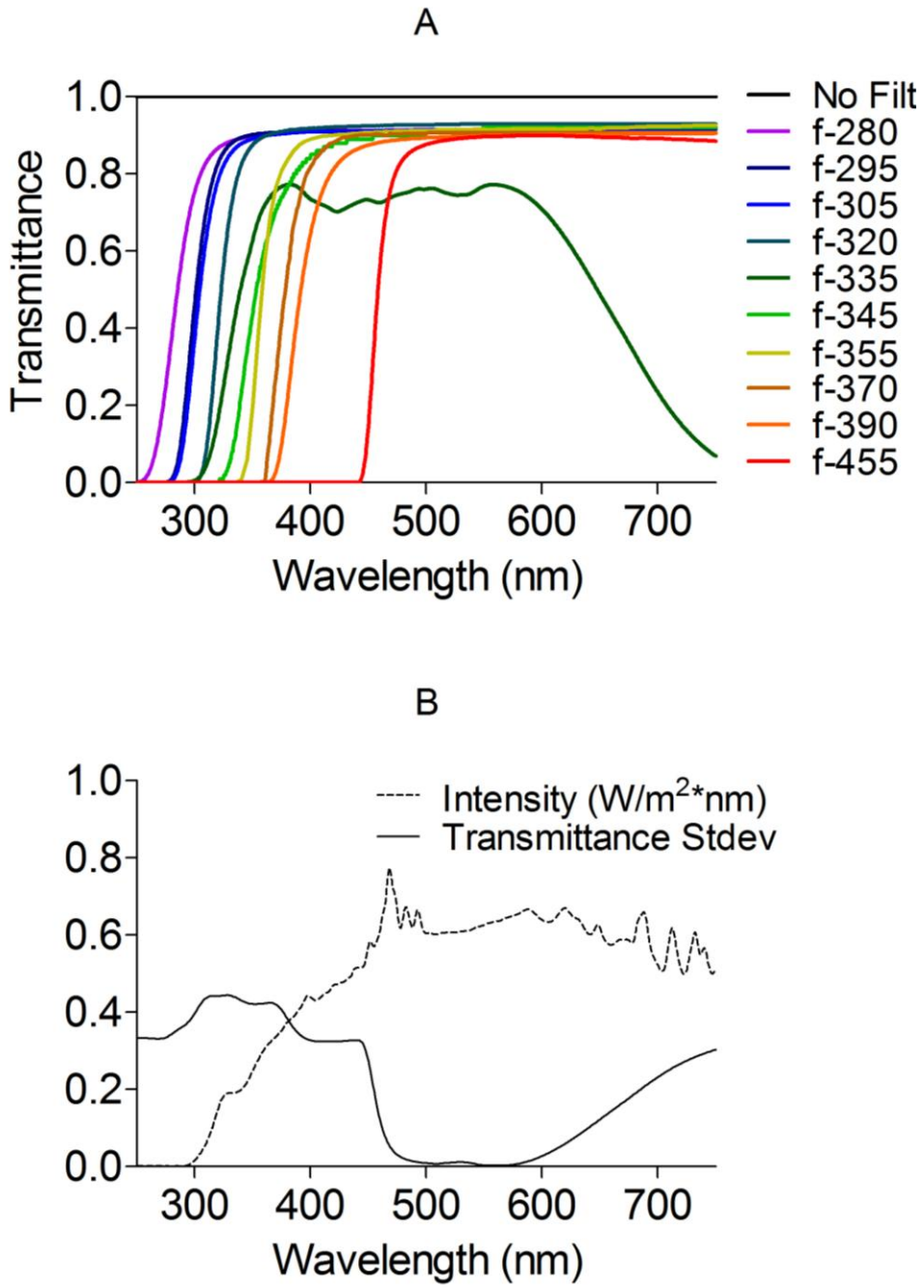


Figure 4.4 A) Transmittance spectra for each of the 2"x2" glass optical filters used in inactivation experiments. B) Unfiltered lamp intensity (Intensity(λ)) and standard deviation of relative filter transmittances (Stdev(λ)) plotted as a function of wavelength. Specifically, if $T^r_i(\lambda)$ is the transmittance of filter i at wavelength λ divided by the maximum transmittance of filter i over the 200-1000 nm range, Stdev(λ) is the standard deviation of the set of $T^r_i(\lambda)$ values for all filters and the no filter condition at wavelength λ.

### 4.3.4. Data Analysis

#### 4.3.4.1. Inactivation Rate Coefficients

Inactivation rate coefficients and shoulder values were determined by performing regressions on plots of ln(concentration [CFU/mL]) vs. time irradiated using a modified form of the equation presented by Wegelin et al (Wegelin et al., 1994) and Harm (Harm, 1980):

$$N = N_0\left[1-\left(1-\exp\left(k_1 * t\right)\right)^{\exp\left(1/k_2\right)}\right] \quad (1)$$

Where $k_1$ and $k_2$ are fitting parameters. Shoulder times were calculated as: $t_s = 1/ k_1 * k_2$ , while $t_{99.9\%}$ values were calculated as the time at which $N/N_0 = 0.001$, based on the $k_1$ and $k_2$ values given by the regression, and were compared to observed values to ensure reasonable agreement. Error margins calculated for modeling parameters and the error bars shown in figures represent the 95% confidence interval unless stated otherwise.

#### 4.3.4.2. Regression Model

Equation 1 was simplified to the case in which exactly 3-log inactivation occurs. In this case, a straight line was forced through the origin and the point ($t = t_{99.9\%}$, $N = 0.001\ N_0$), with a slope of $k_{99.9}$, corresponding to a hypothetical first order rate constant describing the rate at which three log inactivation is reached for the strain of interest. A first-order approximation was used in the interest of operational convenience, because equations capturing the shoulder kinetics typical of *E. coli* inactivation presented too complex a problem to be accurately solved with the current optimization approach. While this metric is clearly not an accurate representation of the inactivation kinetics of *E. coli* by sunlight, it may provide a more easily-applied and less error-prone metric of inactivation efficacy than estimates of the parameters in Equation 1. In this case, $k_{99.9}$ is given by:

$$k_{99.9}{}^{i}{}_{j} = -\ln\left(10^{-3}\right) \Big/ t_{99.9\%}{}^{i}{}_{j} \quad (2)$$

$$k_{99.9}{}^{i}{}_{j} = \int_0^{\infty}\left[I_j(\lambda) * P^i(\lambda)\right] d\lambda \quad (3)$$

Where: $$I(\lambda) = I_0(\lambda) * 10^{-[A(\lambda)]} \quad (4)$$

In the above expressions, $I_j(\lambda)$ is the intensity of light (in $W/m^2$) delivered to the contents of a given reactor j, and $P^i(\lambda)$ is the spectral sensitivity coefficient, or the relative contribution (in $m^2/W*h$) of light energy at wavelength $\lambda$ to the inactivation of organism i, as described by the inactivation rate ($k_{99.9}$). These variables are calculated and discretized as described elsewhere (Fisher et al., Manuscript in Preparation-b). Light intensity data were grouped into 3-nm bins and these were used to calculate the relative

sensitivity of each organism to light in each 3-nm bin over a defined wavelength range ($\lambda_{lower}$ to $\lambda_{upper}$).

Using discretized variables, Equation 3 takes the form:

$$k^{i}{}_{j} = \sum_{\lambda_{Lower}}^{\lambda_{Upper}} \left[ I_{j}(\lambda_{w}) * P^{i}{}_{w}(\lambda_{w}) \right] \Delta\lambda \qquad (5)$$

4.3.4.3. Computational Model

A computational model previously developed (Ibid) in MATLAB (The MathWorks, Natick, MA) to characterize the action spectra of viruses was used to estimate action spectra for the *E. coli* strains studied. This characterization was accomplished by calculating the spectral sensitivity coefficients $P^{i}_{w}(\lambda_{w})$ that best fit the measured inactivation rate constant $k^{i}_{j}$ for each organism (i) in each reactor (j). The model was run and subjected to sensitivity analyses and backtesting as described previously (Ibid).

4.3.4.4. Literature Photoaction Spectra

*E. coli* photoaction spectra were reviewed from numerous publications, of which four reported enough data to make direct comparisons with our work. Data from these studies were captured using Graph Grabber software (http://www.quintessa.org/FreeSoftware/GraphGrabber/) and normalized to unitless sensitivity coefficients in order to plot all data on the same axes. Normalization was done by dividing the sensitivity at each measured wavelength by the sensitivity at the measured wavelength closest to 260 nm. When two points were roughly equidistant from 260 nm, the point with the highest sensitivity was chosen. Normalized sensitivity coefficients were then plotted as a function of wavelength.

4.3.4.5. Photodamage Spectra

Photodamage spectra were calculated by multiplying the photoaction spectrum calculated using the computational model by the mean intensity spectrum for the unfiltered reactors in the trial used to generate that photoaction spectrum. Thus, each photodamage spectrum plots wavelength (nm) as the independent variable, with the dependent variable given by:

$$DMG^{i}(\lambda) = \left[ I_{0}(\lambda) * P^{i}(\lambda) \right] \qquad (6)$$

where $I_0$ is the average intensity for those reactors with no optical filter. For literature photoaction spectra, relative sensitivity coefficients were multiplied by the intensity value measured for the solar simulator used in this study (from the MG1655 inactivation trial) associated with the closest corresponding wavelength. Thus, the area under each photodamage curve is equal to 1/t99.9 (1/h) for the no-filter condition. Literature photodamage spectra were produced by multiplying the normalized sensitivity coefficients described above by the same intensity values measured for the solar simulator used in this study.

## 4.4. Results

### 4.4.1. Characterization of *E. coli* Strains.

*E. coli* strains MG1655, 29181 and $F_{amp}$ are well characterized and were obtained from ATCC. Strain MG1655 and the wastewater isolates were found to exhibit phenotypes characteristic of *E. coli* as demonstrated by biochemical testing (Table 4.1) and the amplified 16S sequences were consistent with identification as *E. coli* (Figure 4.5). Moreover, the genetic distances among isolates suggest that the isolates used were not identical to each other or to *E. coli* MG1655.

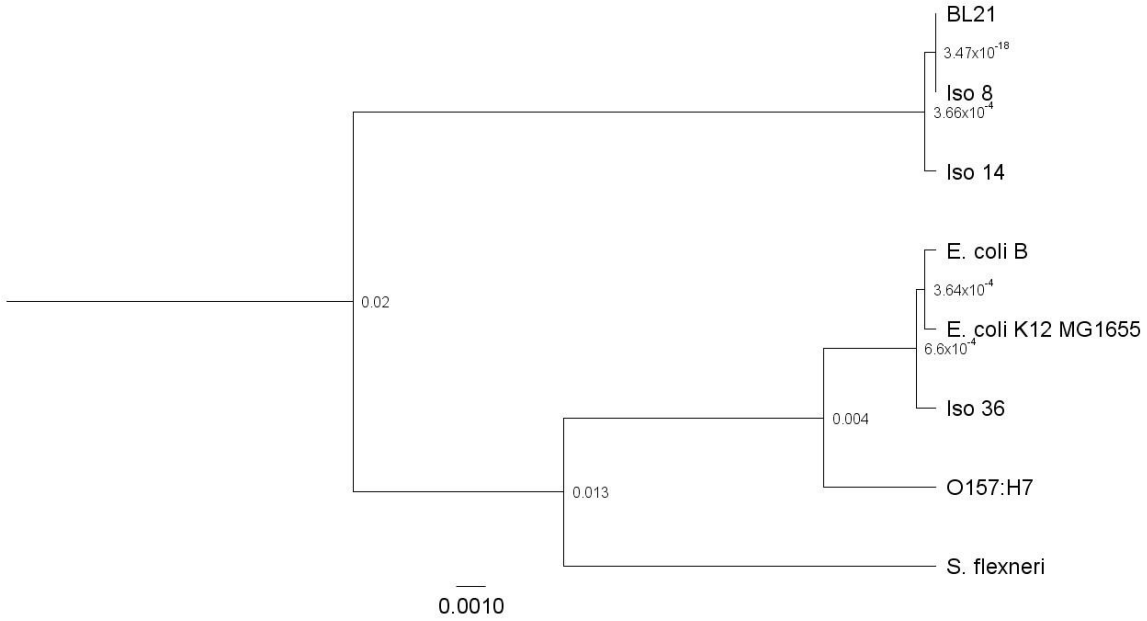


Figure 4.5 Phylogenetic tree for *E. coli* strains used in this work.

### 4.4.2. Inactivation Rates

All *E. coli* strains showed significant sensitivity to both UVA and UVB light, with significant inactivation occurring even when the 390 nm cutoff filter was used (Figure 4.6 A, Figure 4.7, Table 4.2). While inactivation remained measurable for most strains when the 455 nm cutoff filter was used, inactivation rates were quite low, suggesting low sensitivity to all but the very shortest wavelengths of visible light. While the inactivation rates of five of the six strains were quite similar with each filter, *E. coli* 29181 showed dramatically faster inactivation than the other strains under every filter condition (Figure 4.6 A, Figure 4.7, Table 4.2). Moreover, while the rate of inactivation of each strain was slightly different, the relative inactivation rates of all strains for each of the 8 filters used, relative to the no-filter condition, were remarkably similar (Figure 4.6 B).

Table 4.2 Three-log inactivation times for all strains studied with all filters used. Values in parentheses represent 95% confidence intervals.

| Strain | No Filter | f-280 | f-295 | f-305 | f-320 | f-335 | f-345 | f-390 | f-455 |
|---|---|---|---|---|---|---|---|---|---|
| MG 1655 | 5.99 (0.064) | 6.76 (0.467) | 7.37 (0.615) | 7.58 (0.142) | 9.45 (0.198) | 12.6 (0.443) | 16.0 (0.773) | 38.7 (1.461) | 47.7 (15.02) |
| 29181 | 3.37 (0.047) | 3.72 (0.015) | 3.93 (0.103) | 4.14 (0.116) | 5.03 (0.138) | 6.42 (0.181) | 7.27 (0.611) | 13.9 (0.982) | 25.9 (2.423) |
| $F_{amp}$ | 6.67 (0.049) | 7.78 (0.225) | 8.67 (0.194) | 8.43 (0.253) | 10.9 (0.109) | 14.5 (0.668) | 16.7 (1.017) | 32.6 (1.393) | 81.8 (19.14) |
| Iso8 | 7.10 (0.058) | 8.77 (0.512) | 9.15 (0.356) | 8.98 (0.118) | 11.1 (0.093) | 16.3 (1.155) | 19.5 (1.250) | 42.3 (5.074) | 119.0 (86.70) |
| Iso14 | 7.62 (0.155) | 9.39 (0.470) | 10.6 (0.294) | 10.0 (0.446) | 12.0 (0.535) | 19.6 (0.483) | 20.6 (1.743) | 32.8 (0.781) | 105.9 (80.31) |
| Iso36 | 6.10 (0.100) | 6.96 (0.069) | 8.00 (0.142) | 8.26 (0.421) | 10.4 (0.282) | 14.9 (0.910) | 15.8 (1.589) | 32.2 (1.727) | 254. (17.72) |

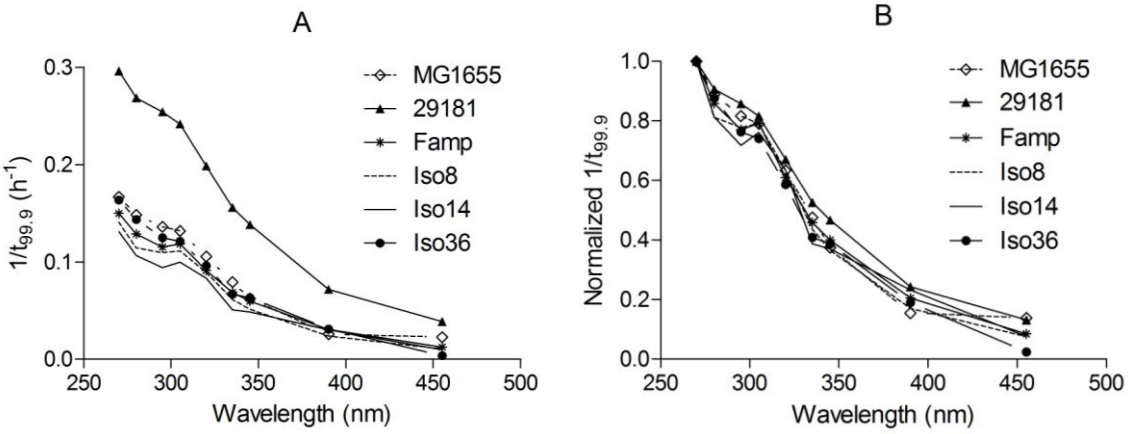


Figure 4.6 Reciprocal three-log inactivation times ($1/t_{99.9}$) vs filter 50% transmittance wavelength for all strains studied with all filters used. Full sunlight was plotted at 270 nm for convenience. A) Absolute inactivation rates (1/h). B) Normalized inactivation rates ($k/k_{270}$).

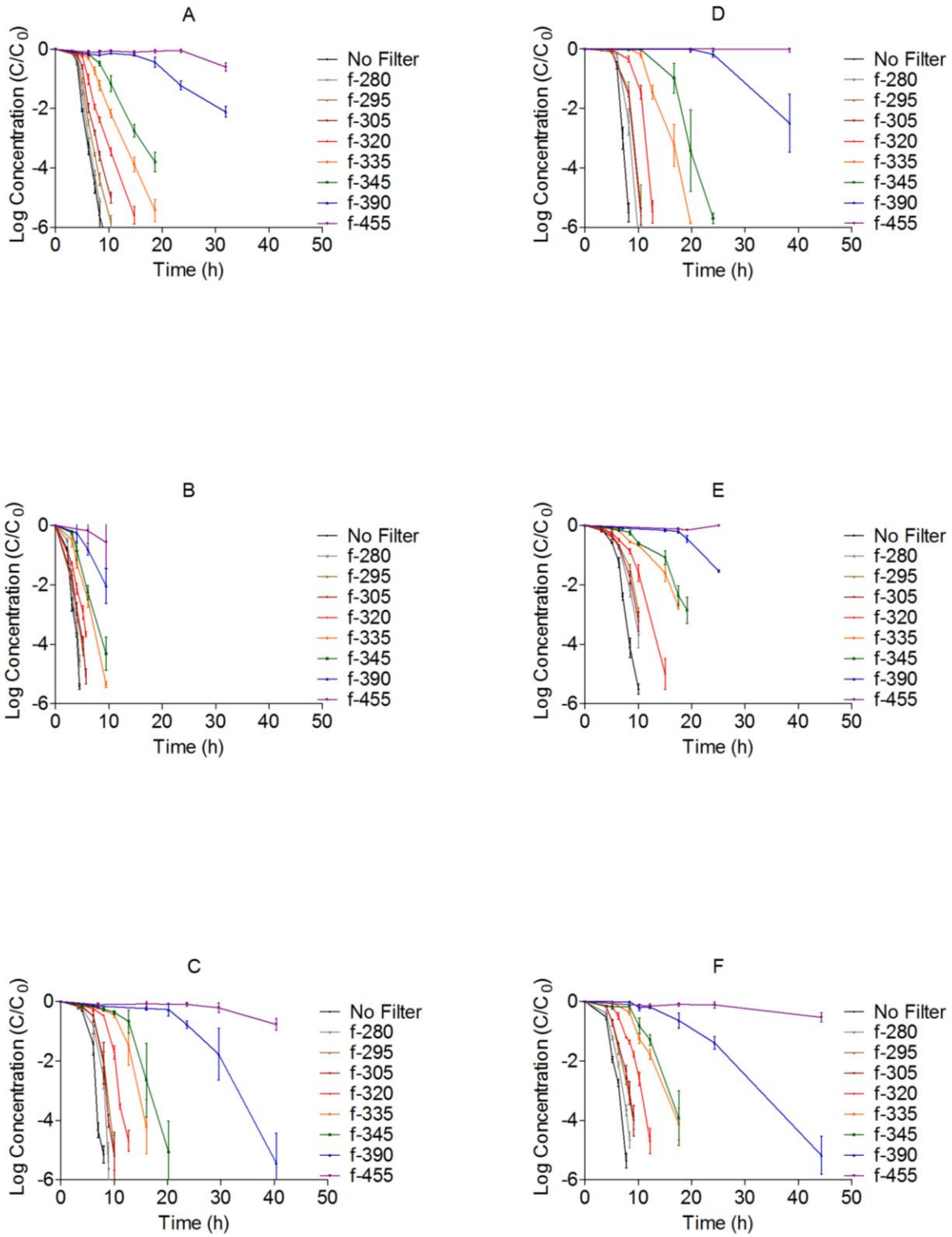


Figure 4.7 Inactivation curves for *E. coli* grown in LB broth and exposed to simulated sunlight with or without optical filters. Inactivation curves: Log concentration vs. time irradiated. Error bars represent 95% confidence intervals. 1) MG1655; 2) Famp; 3) 29181; 4) Iso 8; 5) Iso 14; 6) Iso 36.

Specifically, inactivation appeared to show a bimodal response to increasing cutoff wavelength, with inactivation rates decreasing sharply from the no filter to 280 nm cutoff condition, then more slowly from the f-280 to f-305 condition, followed by a steeper decline from the f-305 to f-335 or f-345 filters, after which the effect of further increasing cutoff wavelength become more gradual (Figures 4.6 A, B). These patterns appear to suggest greater sensitivity to wavelengths < 280 nm and between 305-335/345 nm than to wavelengths in the 280-305 and > 345 nm ranges.

#### 4.4.3. Photoaction spectra of *E. coli* strains.

All *E. coli* strains showed strong sensitivity to UVB light, with maximal sensitivity coefficients at wavelengths at or below 321 nm (Figure 4.8, Table 4.3). All strains also exhibited sensitivity peaks in the UVA region. While the exact locations and intensities of these peaks varied (Table 4.3, Figure 4.8), the tendency was for significant peaks to emerge at approximately 350 and 385 nm. In several cases slight peaks were also observed at approximately 500 nm.

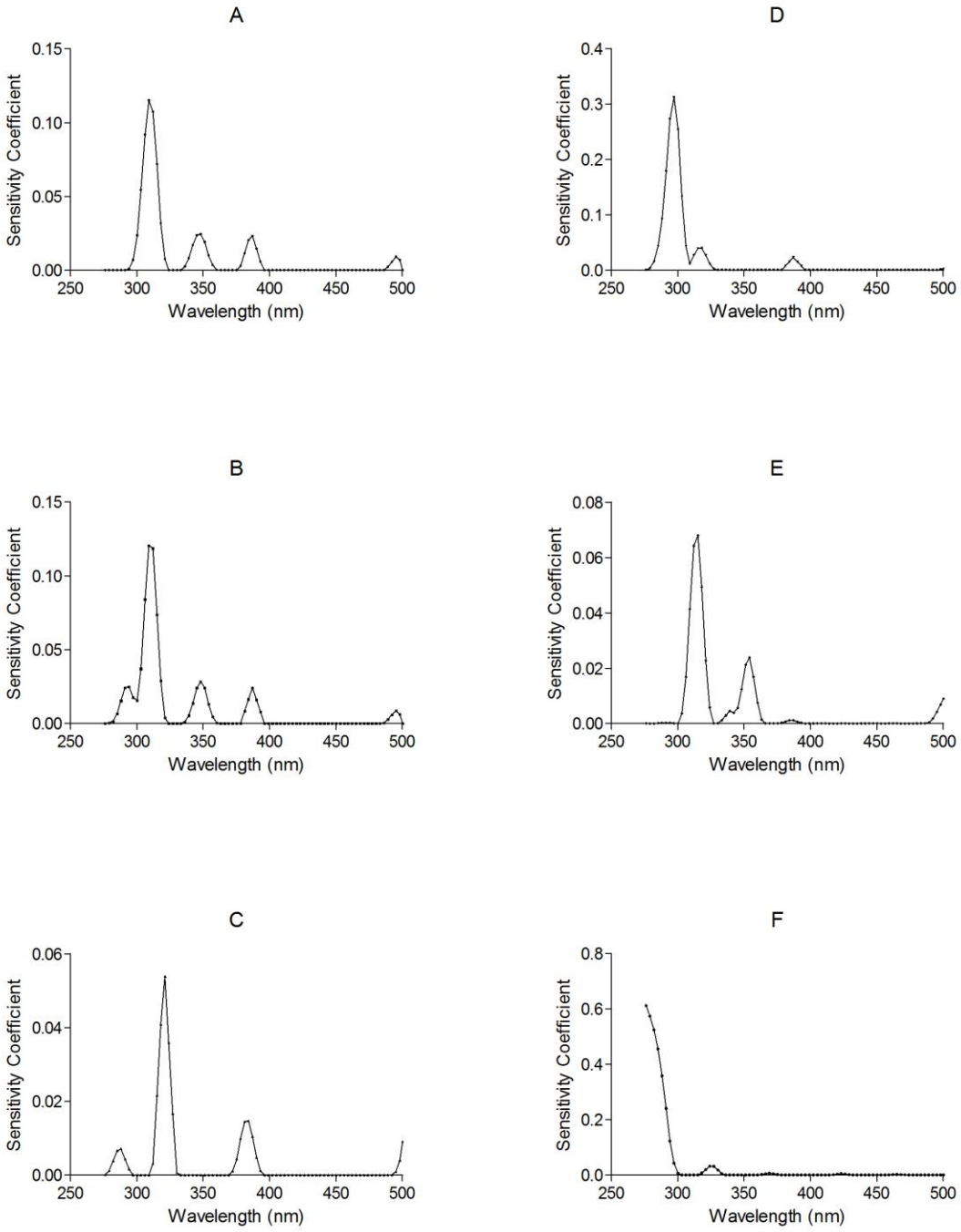


Figure 4.8 Photoaction spectra for *E. coli* grown in LB broth and exposed to simulated sunlight in PBS with or without optical filters. Spectral sensitivity coefficient as a function of wavelength. Error bars represent 95% confidence intervals. 1) MG1655; 2) Famp; 3) 29181; 4) Iso 8; 5) Iso 14; 6) Iso 36.

Table 4.3 Sensitivity coefficient peak wavelengths for all strains studied. Values in parentheses represent the area under each peak in $m^2/W*h$

| Strain | UVB1 280-300 | UVB2 300-320 | UVA1 320-340 | UVA2 340-360 | UVA3 360-380 | UVA4 380-400 | Vis1 400-450 | Vis2 450-500 |
|---|---|---|---|---|---|---|---|---|
| MG 1655 | | 309 (1.54) | | 348 (0.327) | | 387 (0.235) | | 495 (0.0723) |
| 29181 | | 309 (1.721) | | 348 (0.346) | | 387 (0.220) | 444 (0.0002) | 495 (0.0721) |
| $F_{amp}$ | 288 (0.075) | | 321 (0.519) | | | 384 (0.183) | | 500 (0.038) |
| Iso8 | 297 (4.519) | | | | | 387 (0.208) | | 500 (0.012) |
| Iso14 | 291 (0.003) | 315 (0.815) | | 354 (0.303) | | 384 (0.012) | | 500 (0.062) |
| Iso36 | 276 (8.819) | | 324 (0.349) | | 369 (0.061) | | 423 (0.052) | 465 (0.021) |

### 4.4.4. Sensitivity Analysis

The sensitivity analysis showed that the peaks observed at wavelengths > 300 nm were fairly robust, in that they did not generally disappear when the model was perturbed, with the exception of the small peak at approximately 385 nm for Isolate 14 (Figure 4.9). However, in some cases the peaks at wavelengths < 300 nm appeared more sensitive to model perturbation, suggesting that these results were less robust. No additional peaks arose as a result of the sensitivity analyses performed, and merging of peaks was not observed. Thus, the peaks at approximately 310, 350, and 385 nm appeared significant and robust in most cases. While *E. coli* are known to be extremely sensitive to wavelengths below 300 nm (Peak et al., 1984; Tyrrell, 1980; Webb and Brown, 1979; Webb and Tuveson, 1982), estimated sensitivity coefficients at these wavelengths were highly sensitive to perturbation.

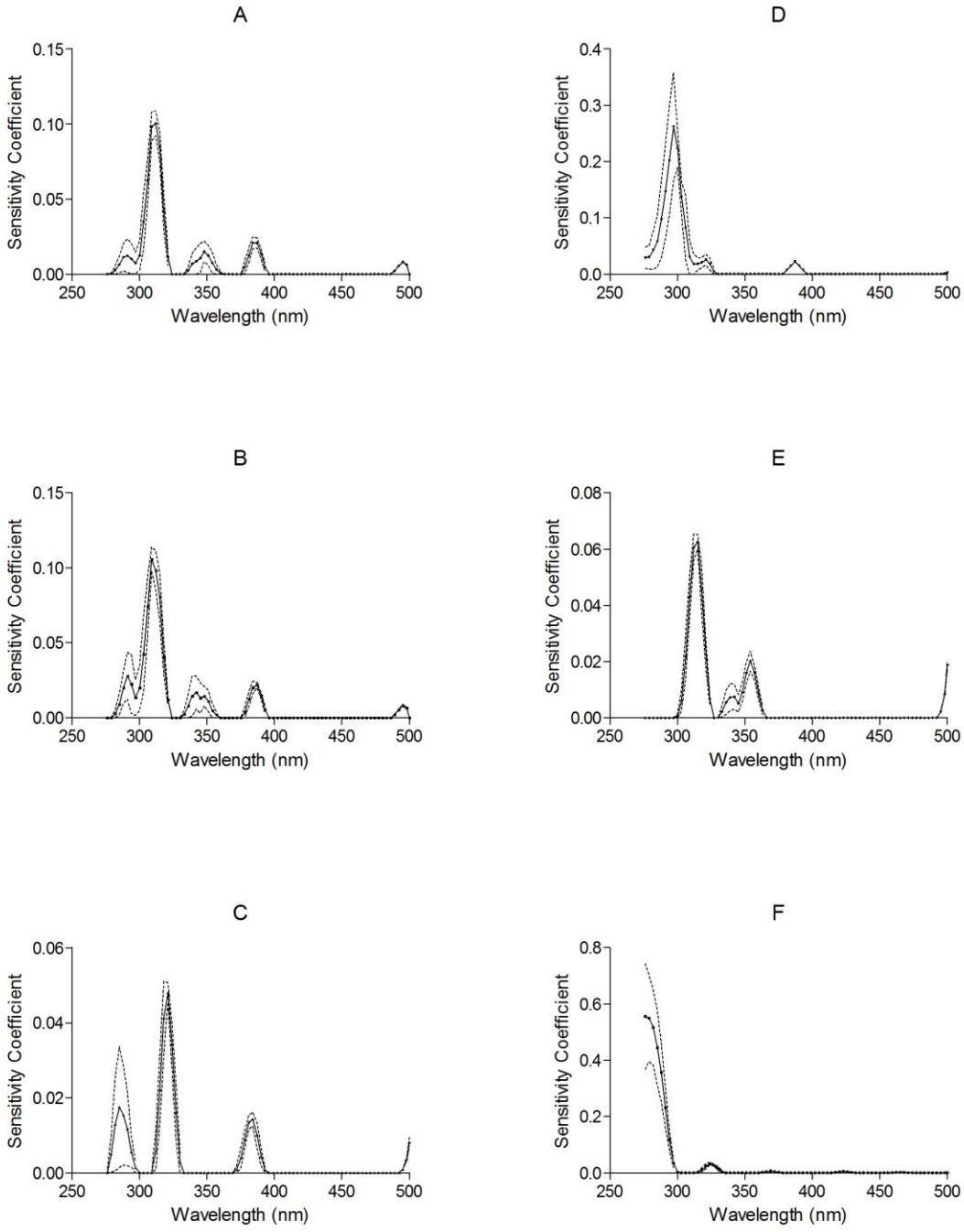


Figure 4.9 Sensitivity analysis for photoaction spectra of *E. coli* grown in LB broth and exposed to simulated sunlight in PBS with or without optical filters. Spectral sensitivity coefficient as a function of wavelength. Error bars (dotted lines) represent 95% confidence intervals. 1) MG1655; 2) Famp; 3) 29181; 4) Iso 8; 5) Iso 14; 6) Iso 36.

### 4.4.5. Backtesting

The backtesting results showed several strengths and weaknesses of the model. The model fit single peaks far better than three-peak ensembles, particularly with small

interpeak distances (Figure 4.10-4.13). Furthermore, the model was more successful at fitting the data between 310-400 nm, than outside that range, possibly due to low intensities of light at shorter wavelengths and lower filter standard deviation (e.g. fewer filters with sufficiently different transmittances) outside of the 310-400 nm range (Figure 4.5 B). An inspection of Figures 4.10-4.12 shows that when the model produces significant errors, these have specific characteristics; one common error is peak-merging, in which three adjacent peaks are replaced by two peaks with centers in between those of the three input peaks (Figure 4.11 350-370 and 400-450). Another common error is the appearance of artifactual "daughter" peaks introduced to "take up the slack" created by merging peaks (e.g. Figure 4.11 340-360) or incorrectly estimating the size of one or more peaks (e.g., Figure 4.11 380, Figure 4.12 60, 80). These daughter peaks appeared to be more common in the UVB1 and UVA2 regions. Where daughter peaks overlapped with parent peaks, the effect was one of apparent "peak splitting," but this did not significantly displace the parent peak. In the case of merged peaks, the new peaks appeared to preserve the "center of mass" of the old groupings, corrected for intensity. The occurrence of "daughter peaks" also coincided with an underestimation of the magnitude, but not the location, of one or more "correct" peaks. Thus, in all cases where the model predicted a large peak, that corresponded to one or more true peaks in that location. Peak merging and peak underestimation appeared to occur more frequently when one or more peaks was outside the 310-400 nm region. Thus, on the basis of these results, it appears that the model does a reasonable job of identifying critical regions of sensitivity over the 310-400 nm range, although performance may deteriorate when multiple peaks are clustered closely together, particularly at the edges of this range (Figures 4.10-4.13). Furthermore, in the no-peak backtest, the model output approximated the input with reasonable accuracy at wavelengths above 300 nm. However, at wavelengths below 300 nm, the data were not reflected in the model output (Figure 4.14).

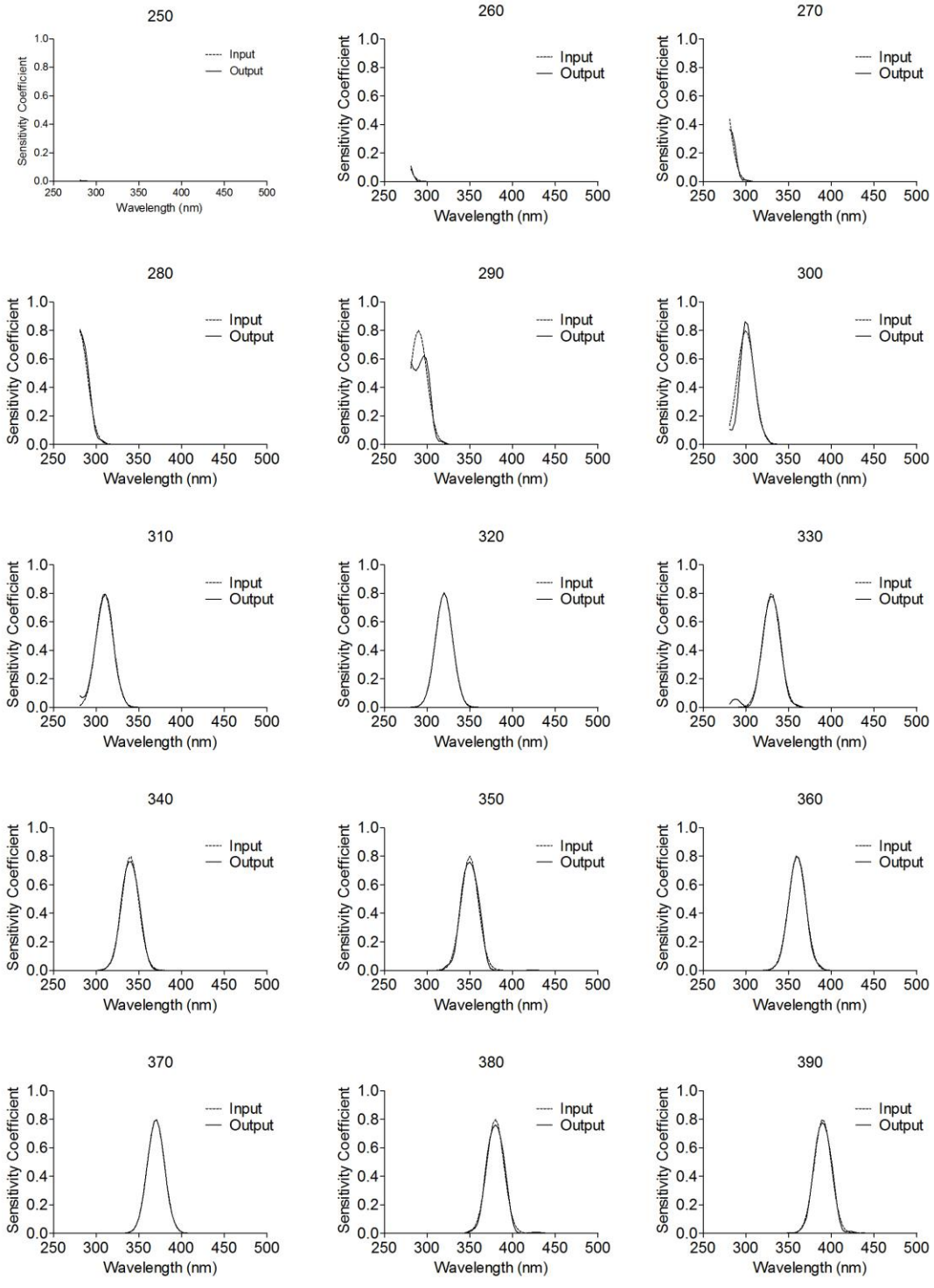
250
260
270
280
290
300
310
320
330
340
350
360
370
380
390
Input
Output
Sensitivity Coefficient
Wavelength (nm)
0.0
0.2
0.4
0.6
0.8
1.0
250
300
350
400
450
500

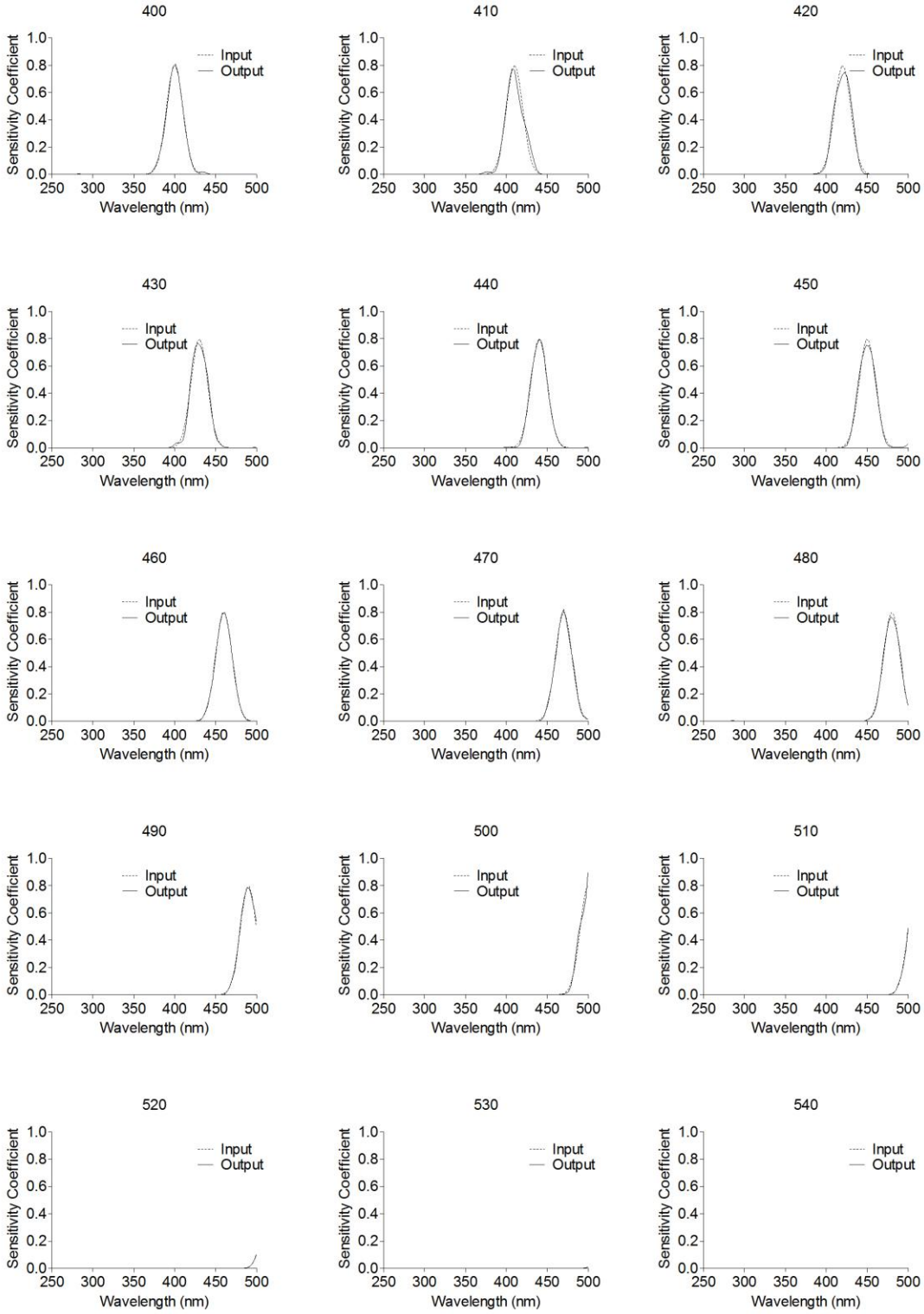


Figure 4.10 Backtesting results for photoaction spectra. Single peak bactest with peaks centered at 250 nm; 260 nm; … 540 nm (Errors are summarized in Figure 4.13 A). Curves represent input dataset (dashed line - - -, corresponding to an arbitrary curve generated by the authors) and model output (solid line —).

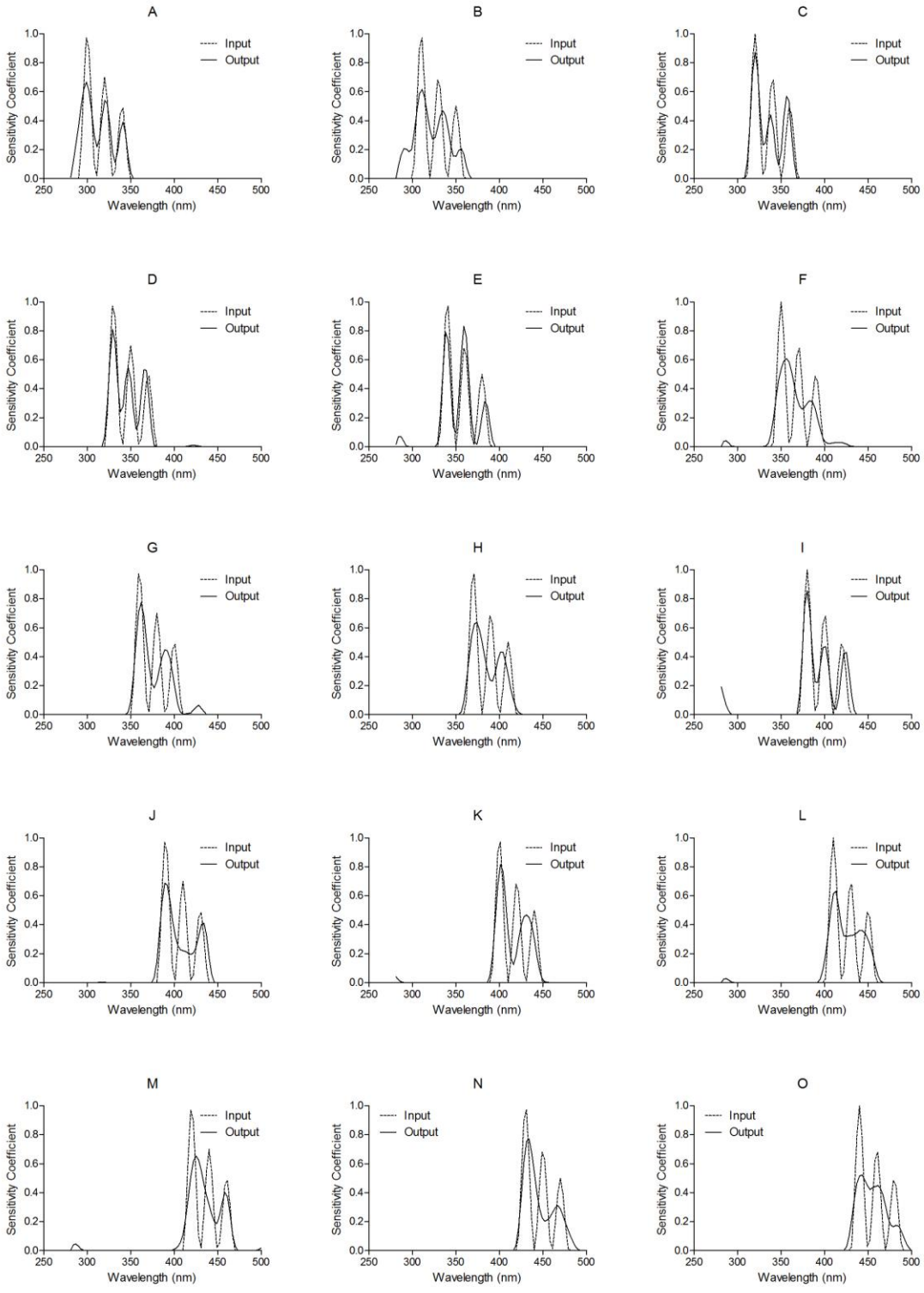
A
B
C
D
E
F
G
H
I
J
K
L
M
N
O
Input
Output
Sensitivity Coefficient
Wavelength (nm)
0.0
0.2
0.4
0.6
0.8
1.0
250
300
350
400
450
500

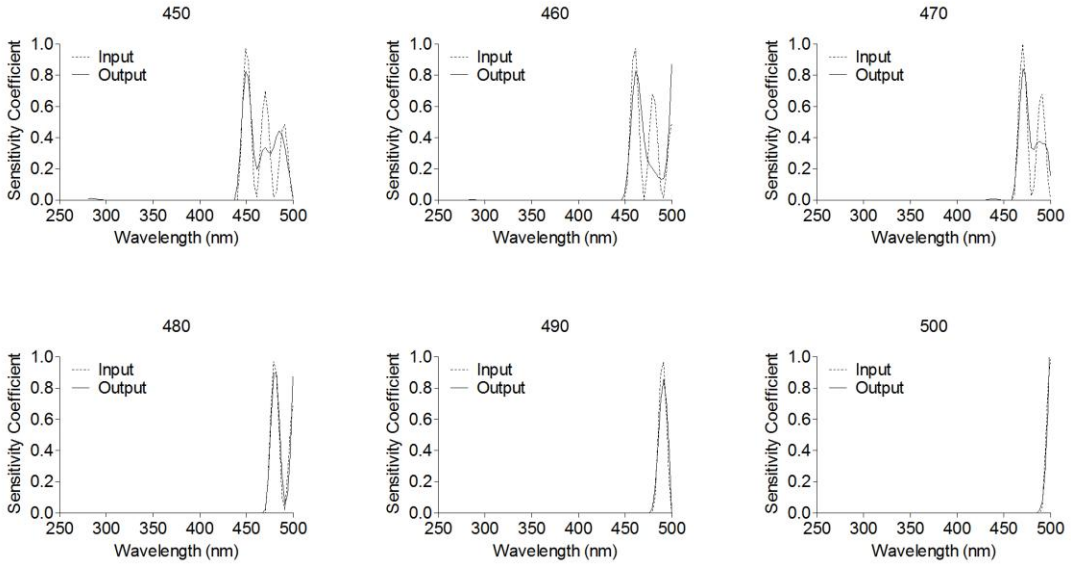


Figure 4.11 Three-peak backtest with 20-nm interpeak distances and variable primary peak location. The first peak in the grouping is centered at A) 300 nm; B) 310 nm; … O) 500 nm. Additional peaks were calculated up to 580 nm but were omitted in the interest of space. Curves represent input dataset (dashed line ---, corresponding to an arbitrary grouping of three curves generated by the authors) and model output (solid line ―).

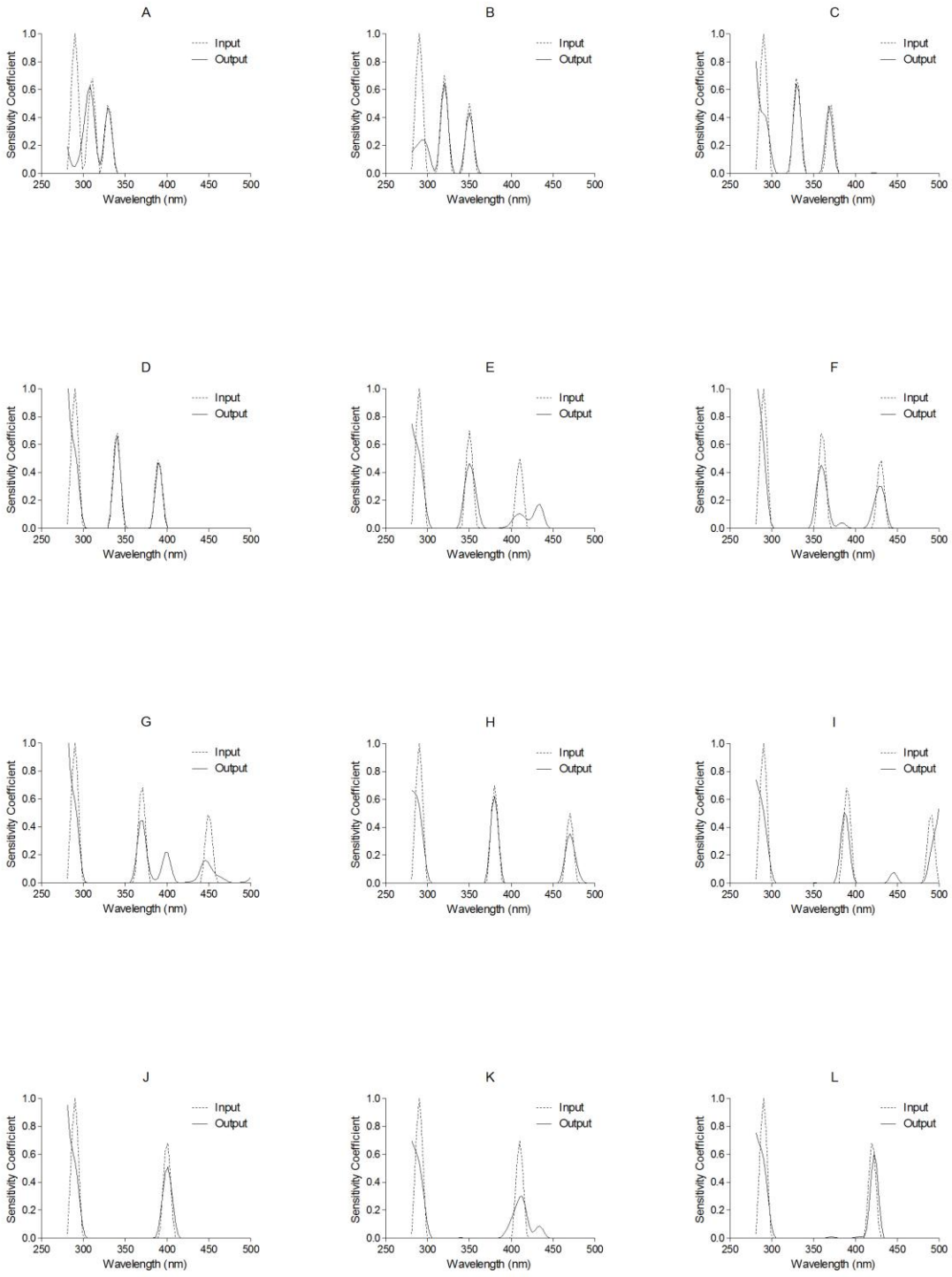


Figure 4.12 Three-peak backtest with variable interpeak distances and a primary peak centered at 290 nm. The groupings have interpeak distances of A) 20 nm; B) 30 nm; … L) 130 nm. Additional groupings were calculated with interpeak distances up to 150 nm but were omitted in the interest of space. Curves represent input dataset (dashed line ---, corresponding to an arbitrary grouping of three curves generated by the authors) and model output (solid line —).

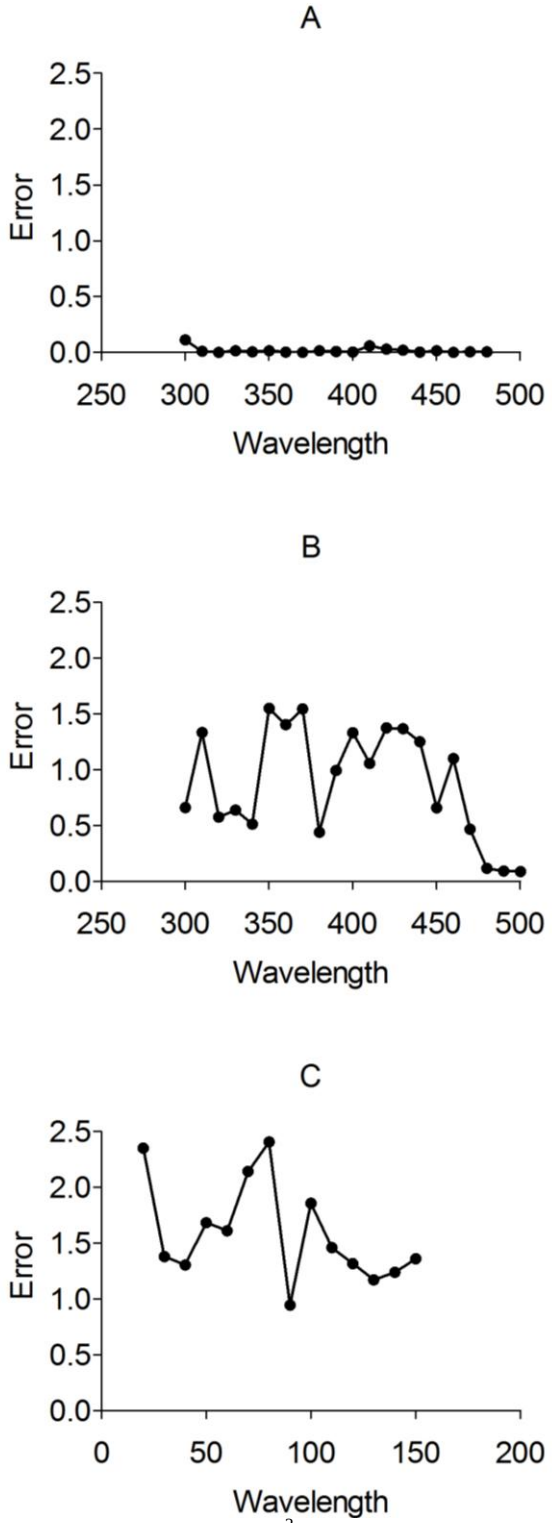


Figure 4.13 A) Sum of squared errors [(input-output)$^2$] vs the central wavelength of a single peak backtest (see Figure 4.10). B) Sum of squared errors vs primary peak central wavelength for a three-peak backtest with 20-nm interpeak distances and variable primary peak location (see Figure 4.11). C) Sum of squared errors vs interpeak distance for a three-peak bactest with variable interpeak distances and a primary peak centered at 290 nm (see Figure 4.12).

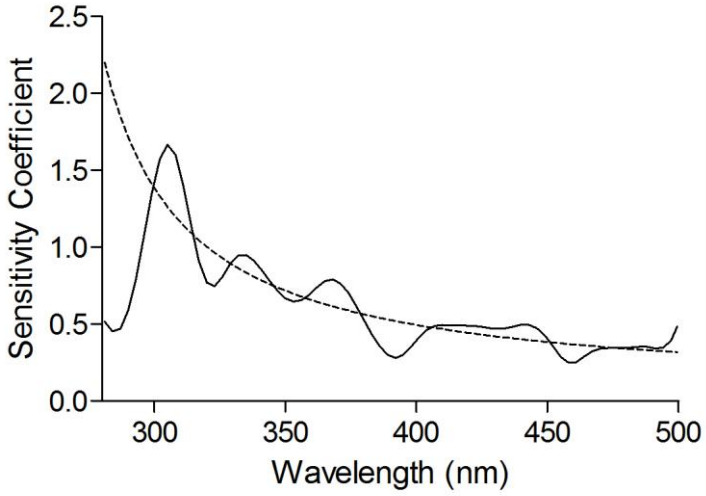


Figure 4.14 Backtest for a monotonic sample spectrum with no peaks described by the equation: y = (1/0.015*(x-250))+0.05. Dashed lines represent input values, solid lines represents model output.

### 4.4.6. Intensity-Weighted Spectral Sensitivity Coefficients

Figure 4.15 shows intensity-weighted plots of spectral sensitivity coefficients as a function of wavelength (photodamage spectra) for the six *E. coli* strains studied. These photodamage spectra were created by multiplying the spectral sensitivity coefficients generated using the computational model by the unfiltered intensity spectra measured in this study. These spectra show moderate damage from UVB and significant damage from UVA wavelengths. These findings are also consistent with Figures 4.6 A and B, in which the greatest slopes are observed in the UVB2 (300-320 nm) region for most strains. However, it should be noted that UVB1 (280-300 nm) and UVB2 intensities were extremely low in this study, and thus the results at these wavelengths are subject to greater uncertainty than those in other regions. It is noteworthy that while substantial photodamage was due to UVA wavelengths, much of this effect was concentrated in the UVA2 (340-360 nm) and UVA4 (380-400 nm) regions, with essentially no damage due to 325-340 nm wavelengths (Table 4.4) and only Isolate 14 showing significant photodamage in the 360-375 nm region.

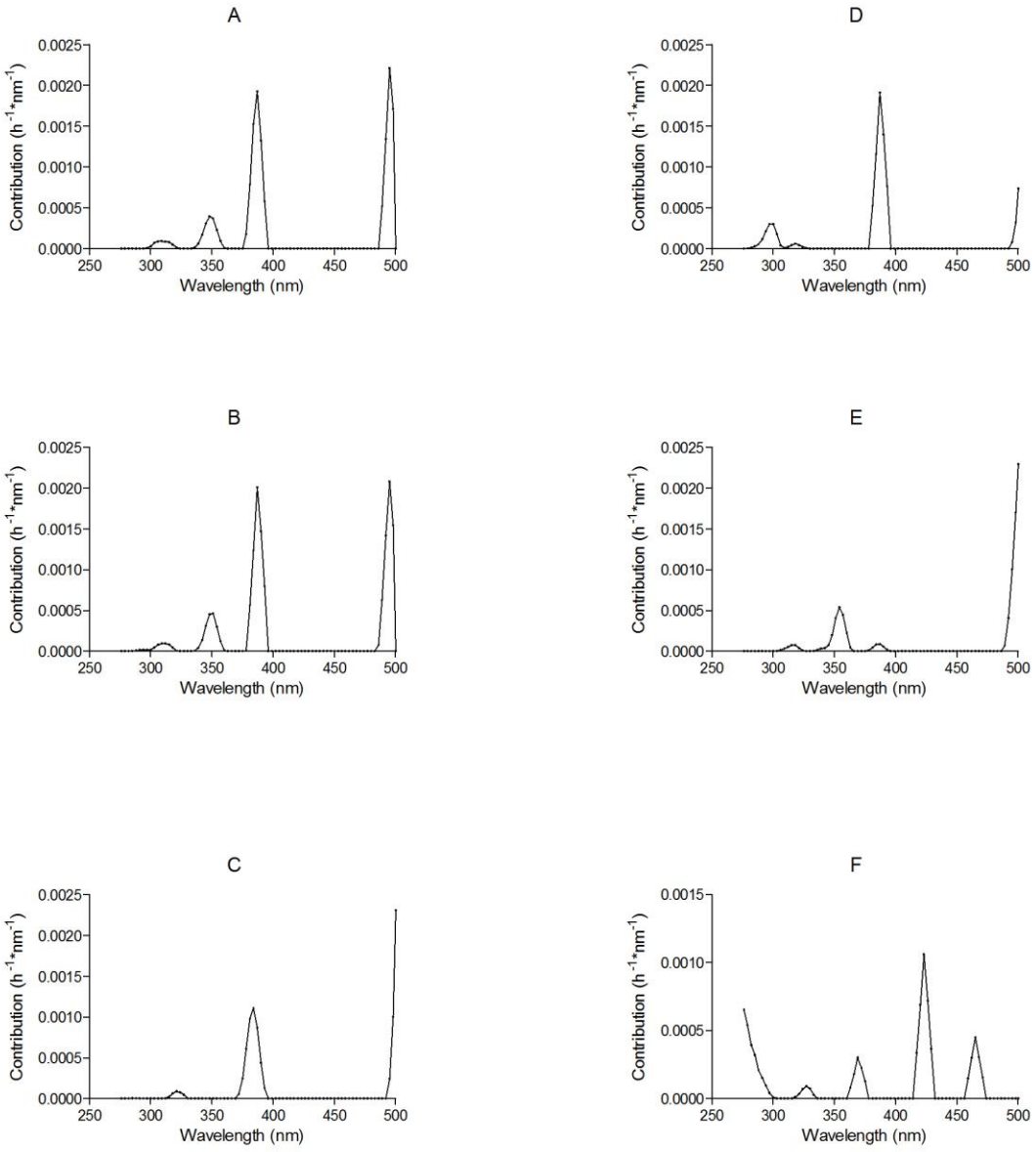


Figure 4.15 Photodamage spectra for *E. coli* grown in LB broth and exposed to simulated sunlight in PBS. A) MG1655. B) 29181; C) Famp; D) Iso 8; E) Iso 14; F) Iso 36.

Table 4.4 Photodamage coefficient peak wavelengths for all strains studied. Values in parentheses represent the fraction of total photodamage under each peak.

| Strain | UVB1 280-300 | UVB2 300-320 | UVA1 320-340 | UVA2 340-360 | UVA3 360-380 | UVA4 380-400 | Vis1 400-450 | Vis2 450-500 |
|---|---|---|---|---|---|---|---|---|
| MG 1655 | | 309 (0.036) | | 348 (0.116) | | 387 (0.443) | | 495 (0.405) |
| 29181 | | 309 (0.038) | | 348 (0.130) | | 387 (0.427) | 444 (0.001) | 495 (0.404) |
| $F_{amp}$ | 288 (0.002) | | 321 (0.039) | | | 384 (0.560) | | 500 (0.399) |
| Iso8 | 297 (0.177) | | | | | 387 (0.700) | | 500 (0.123) |
| Iso14 | 291 (0.0001) | 315 (0.040) | | 354 (0.262) | | 384 (0.040) | | 500 (0.658) |
| Iso36 | 276 (0.296) | | 324 (0.038) | | 369 (0.112) | | 423 (0.389) | 465 (0.166) |

Figure 4.16 shows photodamage spectra calculated from literature photoaction spectra. The points are not connected because data were collected using monochrometers and the intervening wavelengths were not studied. These spectra show significant damage by UVC and UVB to all strains studied. A significant peak in photodamage is observed at approximately 305 nm for E. coli WP2, but no points were recorded at or near this wavelength for the other strains studied. Furthermore, no strains show significant damage from UVA wavelengths. However, the studies by Webb and Tuveson (Webb and Tuveson, 1982) and Webb and Peak (Peak et al., 1984) did not measure points near 350 or 385 nm.

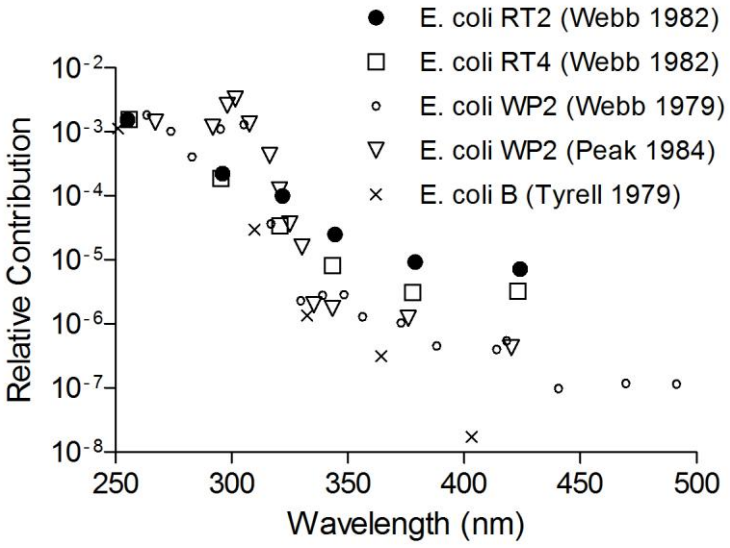


Figure 4.16 Relative sensitivity coefficients from published photoaction spectra for *E. coli* B, WP2, RT2, and RT4 grown aerobically in rich media multiplied by the intensity spectrum measured for the inactivation of *E. coli* MG1655 by simulated sunlight in the current study.

### 4.4.7. Inactivation of Wastewater *E. coli*.

Wastewater studies were carried out in glass beakers, with only one replicate of each filter condition studied. Furthermore, the concentration of *E. coli* CFUs in wastewater samples was far lower than in samples of cultured laboratory bacteria, resulting in inactivation data that span fewer orders of magnitude, and are characterized by a higher signal-to-noise ratio. As a result, it was not possible to create meaningful regression-based photoaction spectra of these data using the computational model. However, an analysis of inactivation rates as a function of filter 50% transmittance cutoff wavelengths still yields useful comparisons to laboratory cultures of lab strains and wastewater isolates. Wastewater *E. coli* were found to be inactivated at similar rates to cultured *E. coli* MG1655 in full simulated sunlight. When filters with 50% transmittance wavelengths at 320 nm and higher were used, however, wastewater *E. coli* were inactivated far more slowly than cultured *E. coli* MG1655 spiked (at 1000x higher concentration) into the same matrix (Figure 4.17).

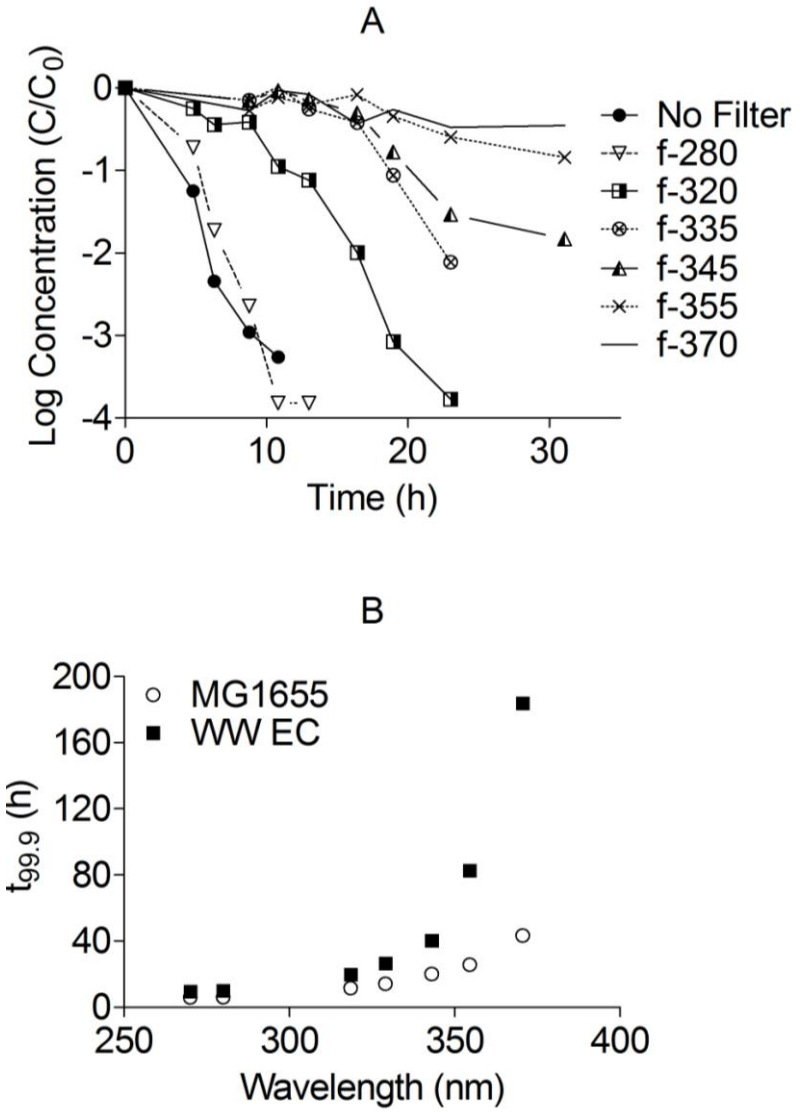


Figure 4.17 Inactivation of wastewater *E. coli* by simulated sunlight. A) Inactivation curves for *E. coli* in diluted wastewater. B) Three-log inactivation times ($t_{99.9}$) vs filter 50% transmittance wavelength for *E. coli* MG1655 and wastewater *E. coli* in diluted wastewater. The no filter condition is plotted at a 50% transmittance wavelength of 270 nm for convenience.

## 4.5. Discussion

### 4.5.1. Inactivation Rates

All strains showed high sensitivity coefficients in the 276-321 nm range relative to longer wavelengths. Most strains also exhibited smaller peaks centered roughly around 350 and 385 nm, with a few exceptions. However, because irradiance values were nearly 0 at the shortest wavelengths studied, apparent differences between strains in the UVB region may be artifactual. The differences in UVA sensitivities may indicate genuine differences in the relative sensitivities of the strains studied to these wavelengths. However, these differences may also reflect the natural variability in experimental data, particularly where inactivation was more rapid (as was the case with *E. coli* 29181), and therefore more difficult to accurately observe. Alternatively, some of these differences may represents artifactual "peak splitting," "peak merging," and/or "peak shifting" phenomena, which can occur with the current model in regions of low filter resolution, particularly where two or more peaks occur in close proximity to each other. Because the UVA peaks occurred in regions of relatively high lamp intensity and filter resolution with relatively low backtesting error, it is unlikely that these UVA peaks are artifactual. However, the exact locations, magnitudes, and numbers of peaks for each strain might have varied somewhat as a consequence of stochastic model variability. Finally, all strains exhibited apparent sensitivity in the Vis2 region, although this may be an artifact of the model's tendency to curve upward at the maximum wavelengths studied. Such an explanation seems particularly likely in light of the slow inactivation rates observed for reactors covered with filter GG455 (Table 4.2, Figure 4.6). The apparent sensitivity peak at approximately 310 nm suggested by model outputs is also consistent with the observations in Table 4.2 and Figure 4.6 that the difference in three-log inactivation times between the f-320 and f-305 conditions is generally greater than between the f-305 and f-280 conditions. Furthermore, these wavelengths coincide with peaks observed in the photoaction spectra of bacteriophage in clear water (Fisher et al., Manuscript in Preparation-b), suggesting that classes of chromophores present in both bacteria and viruses, such as proteins or nucleic acids, may be involved.

However, while almost all the strains studied were highly sensitive to UVB light, the extremely low intensity of light available in this region reduces the importance of shorter wavelengths under natural conditions. Thus, it is necessary to examine photodamage spectra to determine which wavelength ranges will contribute significantly to inactivation of *E. coli* under different conditions. Figure 4.15 shows significant damage from both UVA and UVB wavelengths. Specifically, the results suggest that *E. coli* exposed to polychromatic light appear to be primarily sensitive to UVB, UVA2, and UVA4 wavelengths.

These findings differ from the observations of earlier monochrometer-based studies (Peak et al., 1983; Tyrrell, 1980; Webb and Brown, 1979; Webb and Tuveson, 1982). While the work of Peak et al. and Webb and Brown with *E. coli* WP2 did identify a sensitivity peak at approximately 305 nm, consistent with our current results, all of the above-cited monochometer-based studies found results suggesting negligible importance of UVA

wavelengths under typical sunlight conditions (Figure 4.16). One possible explanation for this discrepancy is that, because different UV wavelengths can act synergistically (Webb et al., 1982), UVA sensitivity may be significantly underestimated by monochromatic studies. Admittedly, such effects could also interfere with polychromatic studies employing optical filters, and it is possible that some of the inactivation attributed to UVA light in the present study is actually due to synergistic interactions of these wavelengths with longer or shorter wavelengths of light. Such errors could be minimized in future work by the use of an adequate number of filters with both long-pass and short-pass cutoffs at a variety of wavelengths, and by introducing algorithms designed to account for synergistic effects between wavelengths. Another possibility is that, since this study found high sensitivity to 350 and 385 nm light for many strains, while prior studies using monochrometers and medium pressure mercury vapor lamps chiefly examined 328, 334, 365, and 405 nm emission peaks, the sensitivity peaks in the UVA2 and UVA4 regions may have been missed in part or in whole by some prior groups.

Another potential source of discrepancies between our findings and results from the literature may be the way in which earlier monochromatic studies were conducted. Because inactivation of *E. coli* by longer wavelengths is characterized by a much longer shoulder period than inactivation by UVB wavelengths (Figure 4.7), it may be that some monochrometer-based studies focusing primarily on the effects of UVB did not deliver sufficient doses of light at UVA wavelengths to reach the end of the shoulder period, and thus under-reported sensitivities at these wavelengths by orders of magnitude. Admittedly, this source of error may have affected the inactivation of some *E. coli* strains screened by the f-455 filter in the current study as well (e.g. Figure 4.7, D, E). However, because most of the strains studied underwent less than one log inactivation after more than 24 h of continuous exposure to wavelengths > 455 nm, the applied significance of these wavelengths under typical field conditions is likely to be minimal.

The findings of the current study, that UVA light (as well as UVB) is important for *E. coli* inactivation under natural sunlight conditions, are in agreement with the observations of Curtis (Curtis et al., 1992), Wegelin (Wegelin et al., 1994) and Khaengraeng and Reed (Reed, 2004), all of whom observed that in the presence of polychromatic light, *E. coli* can be quite sensitive to UVA. While the value of monochrometer-based photoaction spectra collected by previous groups remains unquestioned, further investigation may reveal that the results of such studies should be applied cautiously to situations involving polychromatic sunlight and photooxidative stress.

### 4.5.2. Mechanistic Implications.

The finding that many of the *E. coli* strains studied in this work have maxima in their sensitivity coefficients in the UVB region and at 350 and 385 nm raises questions regarding potential chromophores that might be active in these regions. Proteins may be important chromophores for sensitizing inactivation at ~310 nm, and have been previously observed to sensitize nucleic acid damage to viruses exposed to UV light (Pecson et al., 2009). Potential candidate chromophores capable of absorbing light at 350 nm include NADH and NADPH ($\lambda_{max}$ = ~260, 340 nm), which have been found to contribute to in-vitro DNA photodamage via a mechanism involving hydrogen peroxide

and transition metals (Ito et al., 2007) and to photosensitize the production of the reactive species superoxide (Cunningham et al., 1985a). Additional potential candidates for chromophores absorbing light at 350 and/or 385 nm include riboflavin and flavin mononucleotide ($\lambda_{max}$ = ~275, 350-360, ~450 nm), which photosensitize the production of the reactive species singlet oxygen from ground state molecular oxygen (Baier et al., 2006b), as well as the reduction of oxygen to superoxide radical anion (Cunningham et al., 1985a). Mutants deficient in riboflavin synthesis have been found to be resistant to near-UV light (Lloyd et al., 1990), a finding consistent with the role of riboflavin and/or flavoproteins as potential endogenous photosensitizers. Finally, the nucleic acids 4-thiouridine ($\lambda_{max}$ ~335 nm) can also absorb light at wavelengths up to 350 nm, and has been identified as a potentially important chromophore in photochemical damage to tRNA *in-vivo* (Kramer and Ames, 1987) and the photoproduction of superoxide *in-vitro* (Cunningham et al., 1985a). Quantum yields for superoxide photoproduction from Cunningham et al., (Cunningham et al., 1985a) are multiplied by the intensities characteristic of the simulated solar spectrum used in this study in Table 4.5. While the absorption maxima of the above molecules may not match exactly with observed peaks, these maxima can shift depending upon the conditions and surrounding species to which the chromophores are exposed.

Table 4.5 Superoxide radical anion production rates (molecules superoxide/molecule sensitizer*s) for different cellular metabolites (NADH, NADPH, riboflavin, 2-thiouracil and 4-thiouridine) when exposed to simulated sunlight (Cunningham et al., 1985a), multiplied by the simulated sunlight spectrum used in the MG1655 inactivation trial in this study.

| Wavelength (nm) | Photons/s | NADH | NADPH | Riboflavin | S2Ura | S4U |
|---|---|---|---|---|---|---|
| 290 | 2.24E+15 | 8.98E+07 | 4.71E+08 | 2.00E+07 | 9.45E+06 | 1.01E+07 |
| 334 | 3.20E+17 | 2.18E+09 | 2.82E+09 | 3.52E+08 | 1.47E+09 | 1.02E+09 |
| 365 | 5.90E+17 | 1.00E+09 | 2.42E+09 | 1.00E+09 | 2.18E+08 | 3.89E+06 |
| 405 | 8.77E+17 | 2.63E+09 | 2.10E+09 | 4.73E+08 | 2.89E+08 | 1.58E+09 |

Finally, a number of porphyrins and porphyrin-containing bacterial cytochromes absorb light in the UVA4/Vis 1 region (Yamanaka, 1992), and porphyrin-deficient *E. coli* mutants have been found to be resistant to near-UV light (Tuveson and Sammartano, 1986a), while *E. coli* overexpressing cloned cytochromes were sensitized to inactivation by near-UV light (Sammartano and Tuveson, 1987). These findings in the literature suggest that cytochromes may be potential intracellular sensitizers as well. However, numerous other potential sensitizers exist, and further work will be required to identify which sensitizers may correspond to the different UVA sensitivity peaks observed in the current work and other studies.

One interesting implication of the possibility that cellular constituents such as NADH/NADPH, riboflavin/flavoproteins and/or cytochromes may be involved in photoinactivation is that these macromolecules and cofactors are widely conserved among gram-negative and gram-positive bacteria, as well as Eukaryotes and members of other kingdoms. Thus, similar wavelength ranges may be important to understanding photochemical damage across a broad range of microorganisms.

### 4.5.3. Similarities and Differences in Inactivation Rates

The striking similarities between inactivation profiles for the different organisms (Figure 4.6 B) suggest that, under similar growth conditions, many *E. coli* strains may have similar responses to near-UV light, despite any genetic differences (Figure 4.5). Furthermore, the finding that *E. coli* present in wastewater were less sensitive to UVA wavelengths than were cultured laboratory strains (Figure 4.17) is consistent with literature studies using wastewater-derived *E. coli* and fecal coliforms, which found low sensitivity to UVA as compared to UVB light (Davies-Colley et al., 1997; Sinton et al., 2002b), while studies using cultured laboratory strains often found high sensitivity to UVA (Reed, 2004; Wegelin et al., 1994). It is interesting to note that Sinton et al. and Davies-Colley et al. (Davies-Colley et al., 1997; Sinton et al., 2002b) observed low UVA sensitivity of wastewater-derived bacteria even in the presence of WSP water containing natural chromophores that might have contributed to inactivation at longer wavelengths (Kadir, 2010).

It is possible that a minority of strains have sunlight-resistant genotypes, and that these strains become enriched in sunlight-exposed wastewater as the sensitive strains die off, so that a wastewater sample containing large numbers of strains would be far more resistant than three randomly selected isolates. The small number of isolates used in this study is not sufficient to draw far-reaching conclusions about this possibility, and further work will be needed. However, the possibility that differences between inactivation rates for laboratory and wastewater-derived organisms may largely be due to factors other than genetic differences should also be explored.

Non-genetic factors such as particle association or bacterial growth conditions may contribute to the lower sensitivity of wastewater (WW) *E. coli* to UVA, relative to cultured laboratory strains. While wastewater particles may be protected from sunlight by particle association, it seems unlikely that such associations would preferentially protect cells from UVA but not UVB wavelengths. Thus, enmeshment of cells in particles, while potentially important, is unlikely to explain the differences between WW and cultured cells observed in this study (Figure 4.17).

By contrast, the possibility that levels of endogenous photosensitizers present in *E. coli* cells vary substantially with environmental and growth conditions is of great interest. Because wastewater *E. coli* grow in the mammalian gut under relatively anaerobic conditions where iron and other nutrients may be in limited supply (Freter et al., 1983; Payne and Finkelstein, 1978), a number of physiological differences from lab organisms might arise. Other groups have reported that lower specific growth rates correspond to reduced sensitivity to simulated sunlight (Berney et al., 2006d). In addition, specific growth rate influences the production levels of various proteins (Pedersen et al., 1978), and the biosynthesis rates of flavins and other metabolites keep pace with protein synthesis (Wilson and Pardee, 1962). It would be interesting to ascertain whether the slower bacterial growth rates (Freter et al., 1983) and the scarcity of iron (Payne and Finkelstein, 1978) in the mammalian gut affect the UVA sensitivity of *E. coli*. This possibility is particularly intriguing in light of the finding that iron is important in the

UVA sensitivity of human cells (Tyrrell et al., 2000), in part due to the photochemistry of heme-containing respiratory proteins. If such factors also differentiate wastewater and laboratory-cultured *E. coli* in their sensitivities to sunlight, then the utility of the latter as a mechanistic model for the photoinactivation of enteric pathogens in the environment may be significantly curtailed.

#### 4.5.4. Predictive Power of Polychromatic Studies Plus Computational Analysis

Early studies described the wavelength dependence of *E. coli* inactivation in both the presence and absence of oxygen. However, many of these studies have utilized only a single laboratory strain of *E. coli*, and/or used light sources with spectra that may not adequately approximate natural sunlight. Furthermore, monochrometer-based studies utilize only one narrow wavelength range at a time to probe organisms of interest, neglecting potential effects of missing wavelengths and polychromatic light while subjecting cells to unnaturally high intensities at the irradiated wavelengths. By contrast, studies using optical filters have previously been unable to yield high degrees of wavelength resolution, since cutoffs by these filters are rarely sharp. Thus, it is difficult to determine, *ab initio*, what fraction of the inactivation observed in the presence of such a filter is due to light transmitted above its nominal cutoff wavelength, as compared to the small amount of potentially more biologically-active light transmitted below the cutoff wavelength (Figure 4.4).

Computational methods can help researchers address these issues. While experiments using full-spectrum simulated sunlight with a handful of filters are logistically simple to perform, accurate measurements of the precise spectrum of light reaching each reactor make it possible to account for and even take advantage of the non-ideal cutoff behavior of commonly-used optical filters. This approach is of great value in attempting to use laboratory results to predict inactivation rates of organisms under different sunlight conditions or in the presence or absence of natural or artificial "optical filters," such as plastic containers or overlying water columns. Natural sunlight presents greater challenges than do solar simulators, since intensity spectra are constantly changing, and a given day's sunlight conditions cannot easily be reproduced, but the inclusion of representative and/or time-averaged spectra could nonetheless enhance the comparability and reproducibility of future studies.

#### 4.5.5. Implications for Solar Disinfection

The use of sunlight to disinfect drinking water is a well established point-of-use treatment method, and is currently being promoted on a global scale. Understanding the wavelength dependence of *E. coli* inactivation has three implications for solar drinking water disinfection, or SODIS. First, the finding that both UVA and UVB are significant for photoinactivation is relevant when considering the materials used for drinking water disinfection. While UVB can contribute significantly to sunlight inactivation of cultured *E. coli* strains, the most common type of SODIS containers are PET bottles, which block most UVB light. To the extent that bacterial pathogens of interest resemble wastewater *E. coli* in their sensitivity to UVB wavelengths, the limitations of PET may be an important consideration for future applications. Alternative materials have been explored, and bottles made from more UVB-transparent materials such as polypropylene copolymer

have been found to significantly accelerate the inactivation of laboratory cultures and wastewater-derived *E. coli* and *Enterococci* (Fisher et al., Manuscript in Progress). It is worth noting, however, that the ubiquitous presence of PET bottles in many developing country settings may make them an extremely low-cost and practical option, and this must be weighed against any technical limitations.

The apparently lower sensitivity of wastewater *E. coli*, as compared to laboratory strains, to simulated sunlight in the UVA range is of interest. Typically, cultured strains are used to measure the performance of solar disinfection in laboratory and field trials (Boyle et al., 2008; Wegelin et al., 1994). However, if the relative sensitivities of laboratory-cultured and wastewater-derived bacteria are significantly different, conventionally grown, laboratory-cultured *E. coli* may not prove to be the best indicator organisms for the study of SODIS. Further work to understand the apparent differences in inactivation behavior between laboratory and wastewater *E. coli* may also be needed.

Finally, while pathogenic bacteria are of great concern vis-à-vis point-of-use drinking water disinfection, prokaryotic pathogens such as protozoan cysts, amoebae, and helminth eggs also present substantial health risks in developing countries. It will be of interest to observe whether the wavelength dependence of sunlight inactivation of these organisms resembles the inactivation of *E. coli*. To the extent that cellular metabolites such as flavins, NADH/NADPH, and cytochromes may be involved as sensitizers, they may also play a role in the photoinactivation of these parasites.

#### 4.5.6. Limitations of the Current Approach

The loss of infectivity/culturability of microorganisms can be a complicated process, and the concept of a "sensitivity coefficient" may become less useful where factors such as cellular defenses and repair mechanisms, radical scavengers, antioxidants, and non-catalytic photosensitizers become important. However, we hypothesize that there may exist a range of conditions for which the concept of spectral sensitivity coefficients is useful for understanding and predicting sunlight inactivation rates. Within this range, $P^i(\lambda)$ can be thought of as analogous to the product of absorbance and quantum yield values in the photolysis literature [$P^i(\lambda) \sim A_i(\lambda)*\phi_i(\lambda)$], in that it can be used to calculate the rate of the process of interest when irradiance conditions are known or can be modeled. Thus, the approach and results presented here may facilitate the prediction of *E. coli* inactivation rates, and the influence of such factors as water depth and clarity (i.e. transmittance spectrum), seasonal variations in sunlight intensity, and light screening by various container materials on these rates.

## 4.6. Conclusion

Overall, the results of this work suggest that many *E. coli* strains may have similar responses to different wavelengths of UV and visible light. In particular, the sensitivity of the strains studied to both UVA and UVB wavelengths suggests that earlier monochrometer-based photoaction spectra cannot be directly applied to photoinactivation by sunlight. However, the finding that wastewater *E. coli* appeared to be less sensitive to UVA than lab strains may explain the large differences in *E. coli* inactivation rates

reported for natural and simulated sunlight inactivation studies in the literature, and has implications for the relevance of laboratory-cultured bacteria as indicators for fecal contamination.

The current method appears to produce useful results for predicting and modeling the inactivation of *E. coli* in transparent water samples free of high concentrations of sensitizing chromophores. Future work should turn to identifying the intracellular constituents responsible for sensitizing *E. coli* to the wavelengths of light observed to drive inactivation in this study.

## 5. Evidence for the Roles of Iron, Hydrogen Peroxide, and Superoxide in the Inactivation of *Escherichia coli* by Simulated Sunlight.

### 5.1. Chapter Summary

Sunlight inactivation of *E. coli* has previously been shown to accelerate in the presence of oxygen, exogenously-added hydrogen peroxide, and bioavailable forms of iron. In this study, mutants unable to effectively scavenge hydrogen peroxide or superoxide were found to be sensitized to simulated sunlight, while cells grown under low-iron conditions were protected. Furthermore, prior exposure to simulated sunlight was found to sensitize cells to subsequent hydrogen peroxide exposure in the dark, but this effect was attenuated for cells grown with low iron. Mutants deficient in recombination DNA repair were sensitized to simulated sunlight, but growth in the presence of iron chelators reduced the degree of sensitization conferred by this mutation. These findings suggest that hydrogen peroxide, superoxide, and intracellular iron all participate in the photoinactivation of *E. coli*, and further suggest that the inactivation rate of enteric bacteria in the environment may be strongly dependent on iron availability.

### 5.2. Introduction

Sunlight inactivates a range of microorganisms in water (Acra, 1984; Downes, 1877; Eisenstark, 1971; Luckiesh, 1946; Wegelin et al., 1994), but the mechanisms by which inactivation occurs are not well understood. While DNA lesions resulting from the direct absorption of sunlight in the UVB region (280-320 nm) can be an important mechanism for photobiological damage (Sinha and Hader, 2002), oxygen also plays a critical role in photoinactivation (Reed, 1997), particularly at wavelengths longer than 313 nm (Webb and Brown, 1979). The oxygen-dependent component of this inactivation is believed to be due to photooxidative damage rather than direct DNA absorption (Ibid). For the purpose of this discussion, photooxidative damage may be defined as a photochemical process that begins with the absorption of light by a chromophore and results in the formation of reactive species that ultimately inactivate an organism. While important photooxidative processes may arise from the excitation of exogenous chromophores in bulk solution or sorbed onto the surfaces of organisms, this study specifically examines processes involving endogenous sensitizers. In this case, endogenous sensitizers are defined as those chromophores originating within the organisms of interest, although some endogenous sensitizers may leak out into solution as inactivation proceeds.

Reactive oxygen species (ROS) such as hydroxyl radical, superoxide radical anion, hydrogen peroxide, and singlet oxygen are believed to play important roles in photooxidative damage, and both peroxyl radicals and reactive nitrogen species (RNS) have also been proposed as reactive intermediates (Halliwell, 1999). The oxygen dependence of *E. coli* photoinactivation is generally attributed to the toxic effects of photochemically-produced ROS (Reed, 1997). More specifically, Kadir (Kadir, 2010) found that the singlet oxygen quencher histidine reduced the rate of bacterial inactivation by simulated sunlight, while Gourmelon et al. (Gourmelon et al., 1994) found that the

hydroxyl radical scavenger thiourea protected irradiated *E. coli* from inactivation, suggesting that these species may be involved in photooxidative damage. However, because hydroxyl radical is a nonspecific oxidant that reacts at diffusion limited rates with adjacent molecules, it is surprising that the addition of exogenous "scavengers" could sufficiently outcompete endogenous HO• sinks to significantly reduce the effects of this radical species *in-vivo*.

*E. coli* photoinactivation rates likewise decreased in the presence of hydrogen peroxide scavengers (Curtis et al., 1992; Curtis, 1994; Gourmelon et al., 1994; Sammartano and Tuveson, 1984) and increased in the presence of added $H_2O_2$ (Fisher et al., 2008; Hartman and Eisenstark, 1978; Keenan, 2001; Sciacca et al., 2010). While *E. coli* mutants lacking *katF*, a gene required for producing the catalase protein HPII, have been found to be more sensitive to near-UV radiation (Sammartano et al., 1986), this sensitivity has been attributed to other functions of *katF*, and not to a reduction in catalase activity (Eisenstark, 1989; Sak et al., 1989). Mutants lacking other catalase genes were not found to be sensitized to near-UV light (Eisenstark and Perrot, 1987), and researchers have more recently demonstrated that alkyl hydroperoxide reductase (Ahp), and not catalase, is the most important scavenger of intracellular hydrogen peroxide in *E. coli* growing in the dark, as this enzyme eliminates the low intracellular concentrations of hydrogen peroxide typically present in aerobic cells faster than catalases (Seaver and Imlay, 2001b). Thus, differences in enzyme kinetics may explain why catalase mutants are not strongly sensitized to near-UV light, despite the demonstrated importance of hydrogen peroxide in *E. coli* photoinactivation. Because $H_2O_2$ is itself fairly unreactive toward biomolecules, and in light of the evidence that added $H_2O_2$ and enterobactin-bound iron can accelerate photoinactivation (Hoerter et al., 1996), it has been suggested that an intracellular Fenton-like mechanism might be important in *E. coli* photoinactivation (Hoerter et al., 1996).

$$Fe^{2+} + H_2O_2 \rightarrow Fe^{3+} + OH^- + HO\bullet \qquad (1)$$

$$Fe^{3+} + Red \rightarrow Fe^{2+} + Ox \qquad (2)$$

The Fenton reaction is the ferrous iron-dependent decomposition of hydrogen peroxide (Equations 1, 2). Intracellular Fe(II) may be either free, sorbed to proteins, nucleic acids, and lipids (Imlay, 2003; Rush et al., 1990), or incorporated into protein moieties such as porphyrins (Tuveson and Sammartano, 1986a) or iron-sulfur clusters (Fridovich, 1998; Imlay, 2003). Bound iron is capable of being released from enzyme cofactors such as iron-sulfur clusters by ROS such as superoxide (Imlay, 2003). Superoxide, in turn, can be produced by the adventitious reduction of molecular oxygen by reduced flavins in the electron transport chain (Ibid). Moreover, superoxide and singlet oxygen can be produced by the photoexcitation of flavins, as well as of other cellular components such as NADH and NADPH (Cunningham et al., 1985b; Cunningham et al., 1985c). Thus, there are ample opportunities for free intracellular iron to participate in reactions inside cells exposed to light and oxygen. When superoxide generated either as a result of aerobic metabolism (Seaver and Imlay, 2001a) or from the photoexcitation of endogenous sensitizers undergoes dismutation reactions within the cell, hydrogen peroxide is

produced. This reaction (Equations 3, 4) is generally catalyzed by the enzyme superoxide dismutase (which utilizes Cu-Zn, Fe, or Mn cofactors [denoted by M below]), although free transition metals may also catalyze this reaction (Halliwell, 1999).

$$M^{(n+1)+}\text{-SOD} + O_2\bullet^- \rightarrow O_2 + M^{(n)+}\text{-SOD} \quad (3)$$

$$M^{(n)+}\text{-SOD} + O_2\bullet^- + 2\ H^+ \rightarrow H_2O_2 + M^{(n+1)+}\text{-SOD} \quad (4)$$

When intracellular iron and hydrogen peroxide react, the resulting hydroxyl radical has the potential to oxidize DNA, cell membranes, and proteins, making Fenton chemistry a source of oxidative stress and inactivation (Halliwell, 1999). It is probably not crucial to determine whether the highly active nonspecific oxidant produced by the Fenton reaction at circum-neutral pH is HO• or, as some groups have proposed, an Fe (IV) species such as $(FeO)^{2+}$ (Fridovich, 1998; Hug and Leupin, 2003; Sharpe et al., 2003). In either case, Fenton's reaction has been shown to be the mechanism by which added $H_2O_2$ reacts with intracellular iron to inactivate *E. coli* in the dark, since its toxic effects were abolished by the addition of membrane-permeable iron chelators (Imlay et al., 1988b; Imlay, 2003), and this reaction has also been implicated in *E. coli* inactivation by near UV light (290-400 nm; no added $H_2O_2$) (Hoerter et al., 1996). Similar reactions have also been shown to occur in the presence of copper ions in the dark (Halliwell, 1999; Sagripanti and Kraemer, 1989).

However, much remains unknown about the intracellular photochemical reactions that participate in the inactivation of *E. coli* by natural and simulated sunlight. Groups have proposed that intracellular photoFenton reactions may damage DNA (Hoerter et al., 1996), while others have suggested that mechanisms involving the *E. coli* electron transport chain may cause damage to membranes (Berney et al., 2006c; Bosshard et al., 2010; Moss and Smith, 1981). Protein damage has also been observed in UVA- irradiated cells (Hoerter et al., 2005a). It is probable that some combination of any or all of these mechanisms may be involved, depending upon the organism and its environment. The finding that the *E. coli* electron transport chain is a key target in photoinactivation (Bosshard et al., 2010) is of particular interest, since this group of transmembrane proteins is rich in potential photosensitizers such as flavins and porphyrins, as well as superoxide-labile iron-sulfur clusters (Imlay, 2006) and other moieties capable of participating in photooxidative reactions.

In this work, the effects of low-iron growth conditions as well as mutations eliminating ROS-scavenging and DNA repair enzymes on the rate at which laboratory-cultured *E. coli* were inactivated by exposure to simulated sunlight were studied to determine whether these effects were consistent with an intracellular Fenton mechanism of photoinactivation. We further examined the effects of prior sunlight exposure on the sensitivity of cells to hydrogen peroxide, both for cells grown normally and under low-iron conditions, to determine whether these effects were consistent with a possible role of sunlight in increasing free intracellular iron concentrations.

## 5.3. Materials and Methods

### 5.3.1. Chemicals and Reagents

All chemicals were reagent-grade and used as received unless stated otherwise. Unstabilized hydrogen peroxide (30%) was obtained from Fluka Chemie AG, CH-9470 Buchs.

### 5.3.2. Bacteria

*E. coli* K12 strains MG1655, LC106, JI367, JI370, KCI416 and LEM17 were generously provided by Dr. James Imlay at the University of Illinois in Champagne Urbana. MG1655 is a wild-type K12 strain. JI367 is unable to produce catalases E and G ($kat^-$), JI370 lacks alkyl hydoperoxide reductase ($Ahp^-$), while LC106 lacks peroxidase and is unable to produce catalases E and G ($kat^-$, $Ahp^-$), and KCI416 lacks the superoxide dismutases *sodA* and *sodB* ($sod^-$). Finally, strain LEM17 lacks the recombination DNA repair protein RecA ($recA^-$).

Strains were stored as glycerol stocks at -80° C and were maintained for shorter periods by continuous culture on Luria-Bertani (LB) agar plates, supplemented with the antibiotics kanamycin or tetracycline as needed to maintain and select the desired cells. Unless otherwise indicated, liquid cultures were prepared fresh daily in LB broth, incubated at 37° C to stationary phase, harvested by centrifugation, and resuspended in phosphate buffered saline (PBS: pH 7, 0.1 M) at the desired concentration (typically $10^6$ colony-forming units (CFU)/mL). In iron limitation experiments, cells were grown either in LB broth with added iron chelators (1 mM desferrioxamine mesylate or 100 μM bipyridine) or in minimal essential medium with Earle's Balanced Salts (MEM/EBSS NEAA Modified: HyClone, Logan, Utah). Cells were also grown in the presence of 1 mM of the copper and iron chelator, bathocuproine. In the case of chelators added to rich media, it should be noted that these ligands had the potential to limit metal ion uptake both by chelating metals in the growth medium and by entering cells and chelating intracellular iron and/or copper. In the case of growth on minimal essential medium (no added chelators), Fe/Cu limitation was due to the absence of all but trace amounts of iron (and copper) in the growth medium. Following centrifugation, all bacteria were allowed to acclimate in PBS for 1 h prior to irradiation.

### 5.3.3. Bacterial Enumeration

Unless otherwise indicated, *E. coli* colony-forming units were enumerated using the spread-plate method on LB agar supplemented with 0.05% (w/v) sodium pyruvate to scavenge metabolically produced hydrogen peroxide (incubation at 37°C). In the case of trials in which cells were exposed to added hydrogen peroxide, sodium pyruvate (0.5%) was also added to aliquots before they were diluted and plated in order to quench any residual $H_2O_2$.

### 5.3.4. Inactivation Trials

Samples were irradiated using an ozone-free 1000 W Xe arc lamp housed in an Oriel Solar Simulator (Model 91194-1000), which projected an 8 × 8 inch beam of collimated light. An Oriel AM 1.5:G:A "global" filter with either an AM 1.5:G:C "UV-BC-

blocking" filter or an Oriel model 81017 atmospheric attenuation filter was used to simulate a solar spectrum (Figure 4.2). The global and atmospheric filters were used in all trials except mutant inactivation studies, chelator studies, and enzyme inactivation trials, for which the UVBC blocking filter was used because the presence of UVB light masked differences between inactivation rates of the various conditions. Solar simulator spectra were measured using a Stellarnet BLK-C-SR (StellarNet, Inc. Tampa, Florida) and International Light RPS 200 and RPS 380 (International Light Technologies, Peabody, Massachusetts) portable UV-VIS spectroradiometers. It should be noted that gradual changes in intensity over the life of each lamp and between lamps resulted in differences in baseline inactivation rates between experiments performed at different times. Typical total doses of light delivered to reactors were calculated from comparisons of measurements over the course of multiple experiments and were approximately 300 $W/m^2$ (200-700 nm) and 30 $W/m^2$ (UVA) (Table 5.1). Thus, for comparison to studies measuring fluence, exposure times in hours should be multiplied by approximately 1.1 (for 200-700 nm) and 0.11 (for UVA) to obtain fluence rates in $MJ/m^2$.

Table 5.1 Calculated maximum, minimum, and typical irradiances and typical fluence rates for experiments conducted using the atmospheric or UVBC-blocking filter. Irradiances are in $W/m^2$. Fluence rates are in $MJ/m^2*h$. UVA, UVB, and visible wavelength ranges are defined as in the Terms and Abbreviations section above.

| | Atmospheric Filter | | | | UVBC-Blocking Filter | | | |
|---|---|---|---|---|---|---|---|---|
| Wavelength Range | Min ($W/m^2$) | Max ($W/m^2$) | Typical ($W/m^2$) | Typical Fluence Rate ($MJ/m^2*h$) | Min ($W/m^2$) | Max ($W/m^2$) | Typical ($W/m^2$) | Typical Fluence Rate ($MJ/m^2*h$) |
| UVB | 2.1 | 4.4 | 2.1 | 0.008 | 0.0 | 0.0 | 0 | 0 |
| UVA | 27.6 | 48.6 | 37 | 0.133 | 21.5 | 36.5 | 29 | 0.104 |
| Visible | 219.5 | 324.1 | 275 | 0.990 | 195.4 | 324.1 | 275 | 0.990 |
| Total | 253.0 | 367.9 | 314 | 1.130 | 216.8 | 358.2 | 307 | 1.105 |

Samples were maintained at 20° C in a recirculating water bath and continuously stirred in 55 × 100 mm black-painted glass beakers on a stir plate. The beakers were kept uncovered and irradiated from above. In $H_2O_2$ sensitization experiments, cells were irradiated in 12-well polystyrene plates with a well capacity of 5 mL and were manually stirred at regular intervals while being cooled in a 20° C recirculating water bath before being incubated with 100 μM $H_2O_2$ at 4°C. In all trials, samples consisted of *E. coli* cells (~$10^6$ CFU/mL) suspended in PBS unless otherwise indicated.

In all experiments, aliquots were removed at regular intervals and plated immediately. One aliquot was removed from each reactor prior to irradiation, wrapped in foil, and kept as a dark control in the same water bath as the samples before being plated as described above at the completion of each experiment.

### 5.3.5. Inactivation Rate Coefficients

Inactivation coefficients and shoulder values were determined by performing regressions on plots of ln(concentration [CFU/mL]) vs. time irradiated using the equation presented by Wegelin et al (Wegelin et al., 1994) and Harm (Harm, 1980):

$$N = N_0[1 - (1 - \exp(kt))^m] \quad (5)$$

Where k and m are fitting parameters. Shoulder times were calculated as: $t_s = (\ln(m))/k$, while $t_{99.9\%}$ values were calculated as the time at which $N/N_0 = 0.001$, based on the k and m values given by the regression, and were compared to observed values to ensure reasonable agreement. First order approximations were also used in comparing the results of certain trials. In these trials, slopes, confidence intervals, and $R^2$ values were calculated using the analysis toolpak in Microsoft Excel® (Microsoft Corporation, Redmond, WA). Error margins calculated for modeling parameters, and the error bars shown in figures represent the 95% confidence interval unless stated otherwise.

### 5.3.6. Analytical Methods

Hydrogen peroxide was analyzed colorimetrically using the method of Bader et al. (Bader et al., 1988) as modified by Voelker and Sulzberger (Voelker and Sulzberger, 1996), which relies on horseradish peroxidase to catalyze the oxidation of N,N-diethyl-p-phenylene diamine (DPD) by $H_2O_2$ to a colored product. Samples were quantified based on their absorbance at 552 nm, measured on a UV-Vis spectrophotometer with a 1-cm pathlength using a molar extinction coefficient of 22,000 $M^{-1}cm^{-1}$. Our detection limit was 500 nM with a linear range of 500 nM to 50 µM. Concentrations above 50 µM were diluted to within this range prior to measurement.

Catalase and MG1655 cell activity was measured as the initial scavenging rate of 25 µM hydrogen peroxide by a fixed concentration of enzyme/cells, where peroxide concentration was measured as described above.

## 5.4. Results

### 5.4.1. Inactivation of catalase, peroxidase, and superoxide dismutase mutants

*E. coli* mutants unable to produce certain ROS-scavenging enzymes were found to be more sensitive to simulated sunlight than wild-type cells. The mutant strain JI370, which lacks alkyl hydroperoxidase ($Ahp^-$), and LC106, which lacks peroxidase and cannot produce catalases E and G ($kat^-$, $Ahp^-$), were found to be more sensitive to simulated sunlight than wild-type cells (Figure 1). Likewise, a mutant unable to express the superoxide dismutase genes *sodA* and *sodB* (KCI416, $sod^-$) was considerably more sensitive to photoinactivation than wild type *E. coli* cells (Figure 5.1). However, JI367, which cannot produce catalases E and G ($kat^-$), was not inactivated at a rate significantly different from that of wild-type *E. coli*.

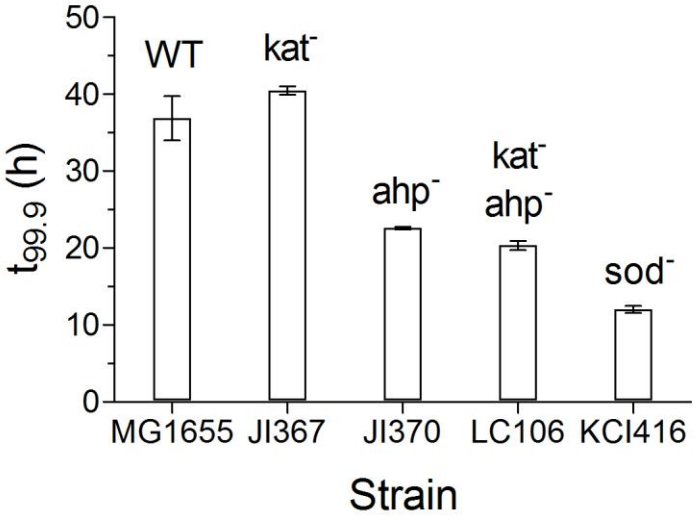


Figure 5.1 Three-log inactivation times for E. coli mutants exposed to simulated sunlight using a UVBC-blocking filter. Values represent the means of three trials, and error bars represent 95% confidence intervals.

### 5.4.2. Effect of growth under iron-limiting conditions

*E. coli* K12 MG1655 cells grown on minimal essential medium (MEM) were found to be more resistant to simulated sunlight than cells grown on the same medium with 50 μM added $FeCl_2$ (Figure 5.2). Cells cultured under both conditions appeared to experience a similar two-hour shoulder period of little or no inactivation, following which the rates of inactivation were significantly different.

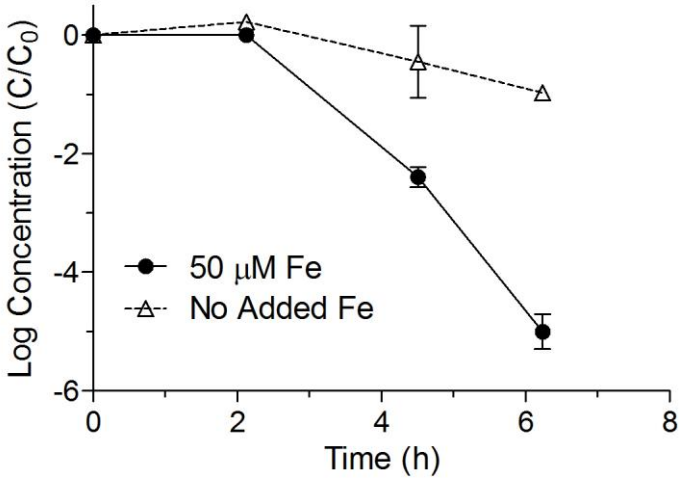


Figure 5.2 Inactivation curves for *E. coli* K12 MG1655 grown in minimal medium with or without 50 μM $FeCl_3$ and exposed to simulated sunlight in uncovered reactors. Error bars represent 95% confidence intervals.

### 5.4.3. Effect of growth in the presence of iron chelators

Growth of *E. coli* K12 MG1655 in LB broth containing 100 and 1000 μM of the iron chelators bipyridine and desferrioxamine (DFO), respectively, significantly reduced the rate at which these cells were inactivated by simulated sunlight (Figure 5.3). Specifically, while cells grown under all conditions appeared to experience a three-hour shoulder period, the subsequent rate of inactivation was highest for *E. coli* MG1655 grown without additives, and decreased for cells grown in the presence of DFO and bipyridine. Growth in the presence of the copper and iron chelator bathocuproine (1000 μM) appeared to reduce inactivation rates slightly as well. These experiments were repeated multiple times with similar results.

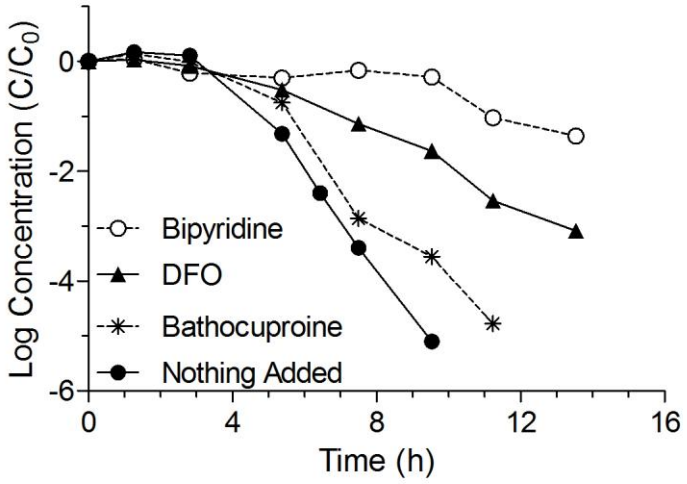


Figure 5.3 Inactivation curves for *E. coli* K12 MG1655 grown in LB broth with or without 1000 μM bathocuproine, 1000 μM desferrioxamine, or 100 μM bipyridine added to the culture medium, and exposed to simulated sunlight using a UVBC-blocking filter.

### 5.4.4. Effect of growth in the presence of iron chelators on a recA mutant

The *E. coli* mutant LEM17, which is deficient in recombination DNA repair (RecA-), was found to be far more sensitive to simulated sunlight than wild-type cells. Furthermore, the linear inactivation rate of this strain ($1.09 \pm 0.20\ h^{-1}$) was significantly reduced (to $0.31 \pm 0.13\ h^{-1}$) by growth in LB broth in the presence of 100 μM DFO prior to irradiation in PBS (Figure 5.4, Table 5.2). This experiment was repeated multiple times with similar results. While LEM 17 grew poorly in air, as described by the original authors, the addition of desferrioxamine to the culture medium appeared to enhance the growth of aerobic liquid cultures.

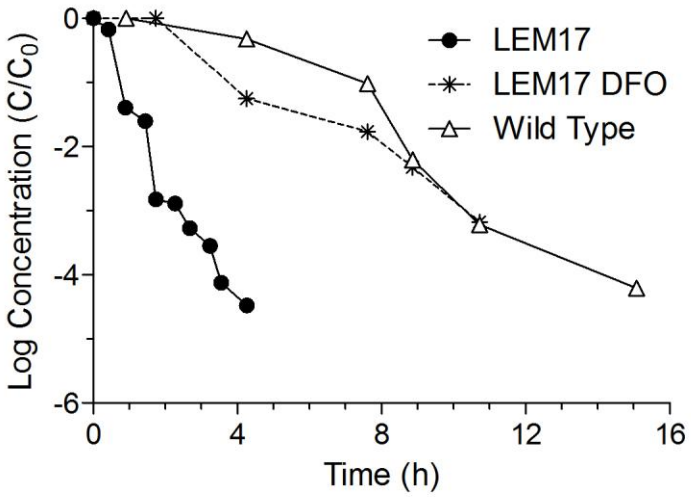


Figure 5.4 Inactivation curves for *E. coli* K12 MG1655 and the recA mutant *E. coli* K12 LEM17 grown in LB broth with or without 1000 μM desferrioxamine added to the culture medium, and exposed to simulated sunlight using a UVBC-blocking filter.

Table 5.2 Comparison of inactivation curve slopes for *E. coli* K12 MG1655 grown without desferrioxamine and *E. coli* LEM 17 grown with or without 100 μM DFO. Values in parentheses represent 95% confidence intervals. Slopes significantly different from the wild-type nothing-added condition are denoted with an asterisk (*).

| Condition | Slope (95% CI) | $R^2$ |
|---|---|---|
| LEM 17 | 1.09* (0.20) | 0.95 |
| LEM 17 DFO | 0.31 (0.13 ) | 0.97 |
| MG 1655 | 0.28 (0.09 ) | 0.91 |

### 5.4.5. Effect of Prior Irradiation on Sensitivity to Hydrogen Peroxide

*E. coli* MG1655 cells which had been exposed to one or two hours of simulated sunlight were found to be more sensitive to incubation with 100 μM $H_2O_2$ at 4° C than were cells that had been held in the dark (Figure 5.5; log reductions at each time point were significantly different at the 95% confidence level for the 2 h condition, and all but one time point for the 1 h condition). Moreover, the cells receiving two hours' exposure also appeared to be more sensitive than those exposed for one hour, although the differences were not significant (Figure 5.5). It should be noted that the concentration of hydrogen peroxide added (100 μM) is about three orders of magnitude greater than typical concentrations inside respiring *E. coli* cells, and would be expected to increase intracellular concentrations to well above levels capable of causing damage, even after accounting for the effects of $H_2O_2$-scavenging enzymes (Seaver and Imlay, 2001a). Thus, the more pronounced effect of $H_2O_2$ on pre-irradiated cells is likely due to an enhancement by prior irradiation of conditions that are already capable of inducing oxidative stress.

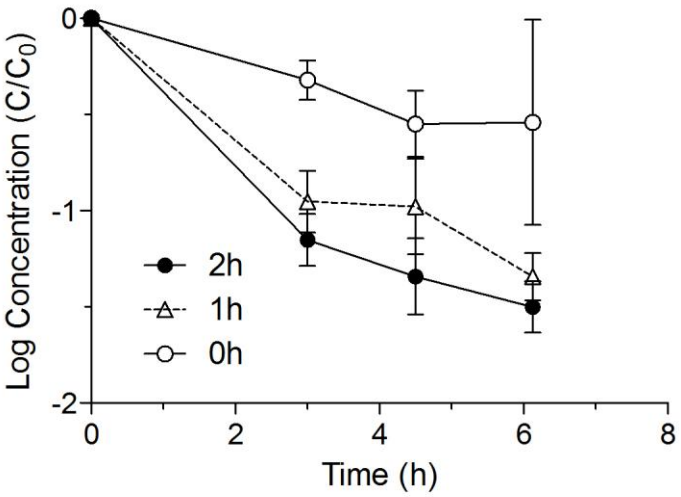


Figure 5.5 Dark inactivation curves for *E. coli* K12 MG1655 incubated in PBS with 100 μM $H_2O_2$ following exposure for 0, 1, or 2 h to simulated sunlight using a UVBC-blocking filter.

### 5.4.6. Effect of Iron Status and Prior Irradiation on Sensitivity to Hydrogen Peroxide

*E. coli* MG1655 cells that were grown under low-iron conditions before exposure to two hours of simulated sunlight were found to be significantly less sensitive to incubation with 100 μM $H_2O_2$ at 4° C than were cells which had been incubated in media with 50 μM added $FeCl_2$. (Figure 5.6).

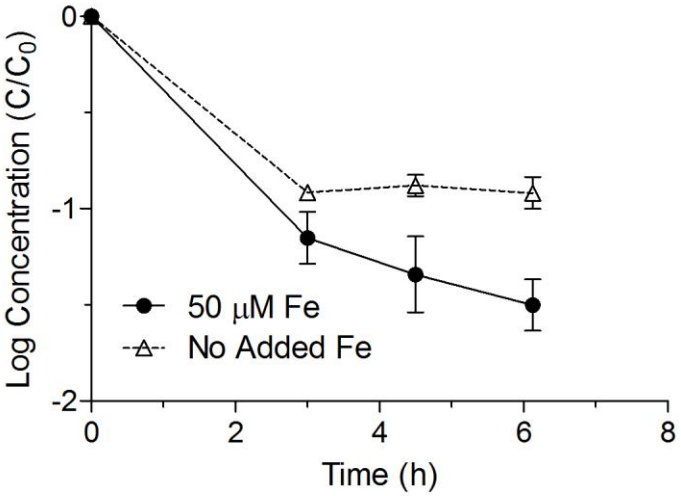


Figure 5.6 Dark inactivation curves for *E. coli* K12 MG1655 grown in minimal medium with or without 50 μM $FeCl_3$, then incubated in PBS with 100 μM $H_2O_2$ following exposure for 0, 1, or 2 h to simulated sunlight using a UVBC-blocking filter.

## 5.5. Discussion

### 5.5.1. Importance of Iron

The fact that iron plays an important role in *E. coli* photoinactivation has been previously demonstrated by Hoerter et al. (Hoerter et al., 1996), who found that exogenously added iron-loaded (but not Al-loaded) enterobactin (a siderophore used by *E. coli* to acquire iron from its environment) accelerated *E. coli* photoinactivation. In addition, Hoerter and colleagues observed that deltafur mutants lacking a key gene that regulates iron uptake and other functions were sensitized to UVA light (Hoerter et al., 2005b). The current work builds upon these and other prior studies by demonstrating that not only do excess iron and iron-regulation mutations have a sensitizing effect, but that low-iron growth conditions have a protective effect on wild-type *E. coli* as well. This distinction is significant in that it illustrates that iron and/or iron-containing species limit photoinactivation rates at physiological levels in laboratory-grown *E. coli*.

### 5.5.2. Importance of Hydrogen Peroxide

The observation that catalase-deficient mutants are not inactivated more rapidly than wild-type cells is not surprising given the findings of Seaver and Imlay (Seaver and Imlay, 2001b) that peroxidase is primarily responsible for scavenging intracellular $H_2O_2$ in respiring *E. coli* (in the dark), while catalase is important primarily for scavenging exogenous hydrogen peroxide. These findings are also consistent with the work of Eisenstark and Perrot (Eisenstark and Perrot, 1987), who found that *E. coli* katE and katG mutants were not sensitized to NUV light from a mercury vapor source. Thus, it seems reasonable to conclude that peroxidase mutants are more sensitive to light because intracellular hydrogen peroxide plays an important role in photoinactivation of these strains. However, the finding that cells lacking Ahp are inactivated more rapidly does not necessarily mean that $H_2O_2$ is involved in sunlight damage in wild-type strains under environmental conditions.

Hydrogen peroxide is known to damage DNA in the dark, both via a Fenton mechanism (Imlay et al., 1988b) and by other iron-independent pathways (Asad and Leitao, 1991), and can also damage cell membranes and proteins (Halliwell, 1999). A review by Imlay suggests that hydrogen peroxide may attack DNA at appreciable levels under typical environmental and growth conditions (Imlay, 2003), and Petersen et al. report that $H_2O_2$ plays a significant role in UVA damage to human keratinocytes (Petersen et al., 2000). Thus, while it seems highly plausible that $H_2O_2$ may likewise participate in photoinactivation of wild-type *E. coli*, further work is needed to understand its role under environmental conditions.

### 5.5.3. Importance of Superoxide

The finding that superoxide dismutase-deficient cells are also sensitized to simulated sunlight is consistent with the observations of Knowles and Eisenstark (Knowles and Eisenstark, 1994) that SOD-deficient *E. coli* strains were more sensitive to inactivation by NUV light from a mercury vapor source. Furthermore, several potential photosensitizers have been identified in *E. coli*, including iron-containing porphyrins within the respiratory chain (Tuveson and Sammartano, 1986a), as well as

NADH/NADPH, riboflavin and other flavins, which are all known to photosensitize the production of superoxide (Cunningham et al., 1985b; Cunningham et al., 1985c). The observation that SOD mutants appear to be considerably more sensitive to simulated sunlight than peroxidase mutants in this study suggests that superoxide's involvement may not be limited to its role as a $H_2O_2$ precursor. Since superoxide is known to liberate iron from iron-sulfur clusters in the dark, and since these clusters are among the most abundant and widely conserved types of enzymatic cofactors (Imlay, 2003; 2006), this may be one important means by which $O_2\bullet^-$ participates in the photoinactivation process. This observation also highlights the added value of comparing different mutants within a single set of experiments, where irradiation and culture conditions can be held constant. While previous studies have examined the inactivation of *E. coli* lacking catalase (Eisenstark and Perrot, 1987) or superoxide dismutase (Knowles and Eisenstark, 1994) by NUV light from mercury vapor sources, to our knowledge this is the first study to compare the inactivation of catalase, peroxidase, and SOD mutants by polychromatic simulated sunlight. The use of polychromatic simulated sunlight is significant because it exposes cells to all environmentally-relevant wavelengths at realistic intensities, rather than selected wavelengths at intensities that may be much higher than those found in natural sunlight.

One likely site for superoxide-mediated reactions to occur is the bacterial electron transport chain (ETC). The ETC is a structure in which "wires" of adjacent Fe-S clusters transport electrons between physically-separated redox couples, many of which contain potential superoxide photosensitizers such as flavins and porphyrins (Imlay, 2006). Without functional Fe-S clusters, NAD(P)H oxidation would be decoupled from proton efflux pumps, and cells would be unable to sustain their membrane potentials or produce ATP via respiration. Bosshard and colleagues found that the *E. coli* electron transport chain (ETC) is a key target of sunlight, which damages NADH dehydrogenase [EC 1.6.5.3], succinate dehydrogenase [EC 1.3.99.1], and L-lactate dehydrogenase [E.C. 1.1.2.3], and disrupts ATP production (Bosshard et al., 2010). Given that the first two target enzymes identified by Bosshard et al. contain multiple Fe-S cofactors, it seems plausible that damage to one or both of these targets might be due to production of superoxide by photosensitizers within the ETC, and might precipitate a cascade of intracellular Fe release and photoFenton damage to a wide variety of cell constituents. Furthermore, L-lactate dehydrogenase contains both porphyrin and flavin cofactors, and thus might be directly damaged by sunlight and/or might sensitize damage to NADH- and succinate dehydrogenases. Such a mechanism of ETC disruption would be consistent with the findings of Berney et al., who observed that sunlight resulted in loss of membrane potential and ATP depletion, among other forms of cellular photodamage (Berney et al., 2006c). It should be noted that, while sunlight inactivation generally occurs in aerobic environments, facultative anaerobes such as *E. coli* might still be able to metabolize in the absence of a functioning ETC. However, it may be the case that oxidative stress produced by the combination of sunlight, oxygen, and the remnants of a damaged ETC proves highly toxic to cells, especially those attempting to repair cellular damage in the face of diminished metabolic capacity.

### 5.5.4. Interactions of Iron with Hydrogen Peroxide

The observation that one or two hours' exposure to simulated sunlight sensitized *E. coli* to exogenously-added $H_2O_2$ is consistent with a mechanism in which the synergy of light and hydrogen peroxide is potentiated by physical or chemical changes occurring within the cell. Such changes might include i) increasing the cell's permeability to $H_2O_2$, ii) reducing its endogenous peroxide-scavenging capacity, iii) increasing the availability of iron or another species capable of reacting with $H_2O_2$ to produce toxic products, or iv) directly or indirectly reducing a key species in a toxic redox reaction such as Fe(III).

The first option (i) seems unlikely, since cell membranes are known to be permeable to hydrogen peroxide under normal conditions (Seaver and Imlay, 2001a). However, it is possible that light further increases the cell's already significant $H_2O_2$ permeability. The second option (ii) seems plausible, since catalase is known to be inactivated by near-UV light (Zigman et al., 1976). However, it was observed that while bovine liver catalase was rapidly inactivated by simulated sunlight (with a UVBC-blocking filter), the ability of whole *E. coli* MG1655 cells to scavenge exogenously-added hydrogen peroxide decreased much more slowly (Figure 5.7). These findings suggest that while photoinactivation of ROS scavengers may be important, these enzymes may not be inactivated by simulated sunlight at rates high enough to explain the rapid increase in sensitivity to $H_2O_2$ observed under the conditions of this study. However, it should be noted that the use of the UVBC-blocking filter in enzyme inactivation trials may have reduced the importance of this mode of photobiological damage.

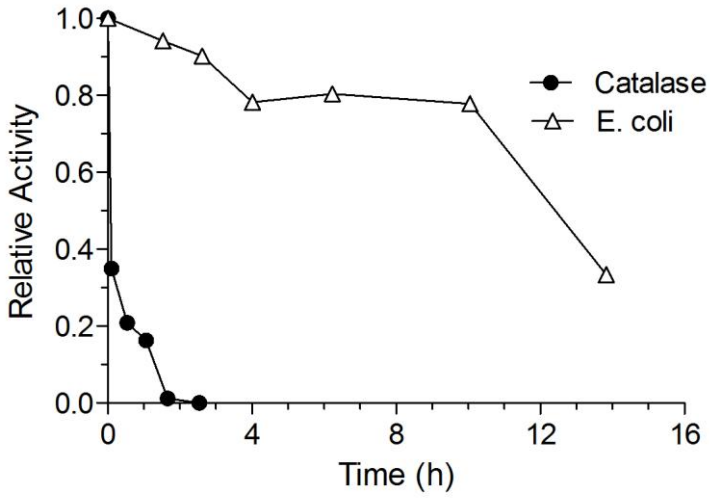


Figure 5.7 Change in log relative activity Vs. time irradiated for bovine liver catalase, *E. coli* MG1655 cells. Catalase and MG1655 cell activities were measured as hydrogen peroxide scavenging rates. All experiments were performed using a UVBC-blocking filter.

The third possibility (iii), that light increases available intracellular iron concentrations, seems consistent with our findings that *E. coli* grown in iron-limiting media or in the presence of iron chelators is inactivated by light more slowly than when grown in unamended iron-rich broth. This observation connects the involvement of iron and

hydrogen peroxide, and suggests that intracellular iron may participate in the mechanism by which light sensitizes cells to $H_2O_2$. While Hoerter et al. (Hoerter et al., 1996) showed that excess iron sensitized cells to $H_2O_2$, and Imlay and Linn found that metal chelators protected cells from $H_2O_2$ in the dark (Imlay and Linn, 1988), our results show that even the concentrations of iron present in unamended (laboratory-grown) cells were relevant to hydrogen peroxide-mediated killing by simulated sunlight, and that reducing these iron concentrations had a protective effect.

Finally, the fourth possibility, that light plays a role in the redox cycling of intracellular iron, is also consistent with the observations supporting hypothesis iii. Specifically, sunlight is known to photoreduce complexed transition metals and drive Fenton photochemistry in natural waters (White et al., 2003) and engineered systems (Zapata et al., 2009), and likely does the same within living cells. The effects of photoreducing intracellular iron in the presence of $H_2O_2$ would likely be analogous to those of releasing additional intracellular Fe under those conditions. Specifically, more iron and more reduced iron would both increase the rate at which Fenton chemistry damages cells.

#### 5.5.5. Iron and DNA Damage

While an abundant and biochemically versatile species such as iron could participate in cellular damage in numerous ways, the dramatic reduction in the sensitivity of RecA mutants to simulated sunlight after growth in LB broth containing the iron chelator DFO suggests that DNA damage may be one of the ways in which iron potentiates photoinactivation. This finding is consistent with other groups' prior observations that iron is an important participant in DNA damage in the dark (Imlay, 2003). However, as in the case of the other mutant experiments, it cannot be conclusively determined that the same processes are similarly important in wild-type cells.

#### 5.5.6. Role of Growth Conditions

Bacterial growth rate and conditions may also have implications for photoinactivation. Studies have found that sunlight inactivation rates for *E. coli* are dependent on growth rate, with slower-growing cells being more resistant to light (Berney et al., 2006b). Specific growth rate influences the rate of protein production (Pedersen et al., 1978), which in turn affects the rate of biosynthesis of potential photosensitizers such as riboflavin and other flavins (Wilson and Pardee, 1962). Thus, changes in growth rate may affect the levels of both photosensitizers and intermediate targets such as proteins containing iron-sulfur clusters. The rate of production of Fe-S clusters is further likely to depend on the availability of iron during cell growth (McHugh et al., 2003). Finally, oxygen concentrations may affect the types and levels of Fe-S clusters and redox couples present in the ETC. Since many bacterial pathogens of concern are derived from human and mammalian guts, where specific growth rates (Freter et al., 1983), iron levels (Payne and Finkelstein, 1978), and oxygen concentrations may all be low, understanding potential connections between these factors and rates of intracellular photochemical processes may be important for predicting and enhancing the rate of bacterial photoinactivation in solar disinfection and in natural environmental processes.

### 5.5.7. Role of Repair Mechanisms

Ample evidence exists that exposure to sunlight in the presence of oxygen can result in damage to proteins, membranes, and DNA in bacteria. While this damage can ultimately inactivate bacteria, it occurs in the context of multiple repair and protective mechanisms designed to minimize oxidative stress and damage. The extent to which Fenton-active transition metals such as iron, hydrogen peroxide, and superoxide are available to participate in photooxidative processes is greatly influenced by these protective mechanisms. In the case of *E. coli*, iron availability is tightly regulated by the *Fur* gene and by metal binding proteins such as bacterioferritin and ferritin (Touati, 2000), DPS (a DNA binding protein isolated from starved cells), and others (Halliwell, 1999). Furthermore, Fe-S clusters sequester significant amounts of iron. At the same time, superoxide levels are maintained at a minimum by the activity of superoxide dismutases (Imlay, 2006), while hydrogen peroxide concentrations are minimized by HPI, HPII, and Ahp (Halliwell, 1999; Seaver and Imlay, 2001b). DNA damage is repaired as it occurs by a number of DNA repair enzymes including uvrA, RecA, photoreactivating enzyme (PRE) (Harm, 1980), DNA Polymerase I, and others (Witkin, 1976). Finally, damaged membranes and proteins can be replaced via standard anabolic cellular metabolism. However, while all these mechanisms can protect cells under low levels of oxidative stress, they can potentially be overwhelmed during intense episodes of photooxidation. Metal chelators such as bacterioferritin contain heme groups (Hantke, 2001), and these may potentially be sensitive to light, while Fe-S clusters can be inactivated by superoxide, releasing iron (Imlay, 2003; 2006). Hydrogen peroxide-scavenging enzymes may be damaged by exposure to sunlight (Figure 5.7), while the metabolic processes that maintain these enzymes, as well as much of the machinery involved in repairing DNA damage and replacing damaged proteins, is dependent on the cell's metabolic activity and transmembrane potential. Since these last functions have been shown to be inhibited by sunlight, it is reasonable to assume that a photooxidative cascade of sufficient magnitude can overwhelm most, if not all, of a cell's defense mechanisms.

### 5.5.8. Applied significance

It has been observed that *E. coli* derived from wastewater (Fisher et al., Manuscript in Preparation-a) and wastewater-impacted creeks (Fisher et al., 2008) are more resistant to sunlight than laboratory cultured organisms. Furthermore, *E. coli* grown under iron-limiting conditions (such as those that may arise in the gut) are known to switch off the synthesis of Fe-S containing ETC enzymes in general (Imlay, 2006) and NADH dehydrogenase and succinate dehydrogenase in particular (Masse and Gottesman, 2002). Because these enzymes have been implicated as key participants in photooxidative damage (Bosshard et al., 2010), this regulatory strategy may prove to be one of the factors contributing to the reduced sensitivity of iron-starved laboratory cultures and wastewater-derived cells to sunlight. Additional research will be necessary to explore this possible connection and, if it is found to be an important one, determine whether superoxide-driven redox mechanisms are involved.

## 5.6. Conclusions

Taken together, these results suggest that iron status strongly affects the pathways by which sunlight and exogenous hydrogen peroxide damage *E. coli*. Furthermore, evidence

from mutant strains supports the involvement of hydrogen peroxide and superoxide in photoinactivation, and the involvement of iron in photooxidative DNA damage, although these results are not necessarily generalizable to wild-type cells. Continuing to elucidate the mechanisms of intracellular photooxidative stress in *E. coli* and other organisms may help us better understand the ways in which sunlight inactivates both laboratory cultures and bacteria present in natural and engineered systems.


### 5.7. Acknowledgements

This work was supported by the Blum Center for Developing Economies, an NSF Graduate Research Fellowship to MBF, and an NSF CAREER/PECASE award to KLN (CBET-0239144). Thanks to Dr. Jim Imlay (UIUC) and to the CGRS facility at Yale University for generously providing strains and instructions on their culture and use.


## 6. Conclusions and Future Directions

It is hoped that this work will be of interest to applied researchers and practitioners in the fields of water and wastewater treatment as well as to groups interested in the mechanisms by which sunlight and oxygen damage microorganisms. Furthermore, it is hoped that the analytical innovations used in these investigations may prove helpful to other researcher groups. Finally, further work is proposed to apply the results of these studies to microbial photoinactivation processes in a range of settings.

### 6.1. Applied Significance

#### 6.1.1. *E. coli* grown on Rich Media are More Susceptible than Fecal Microorganisms to Inactivation by Sunlight

The increased sensitivity of *E. coli* grown on rich media to solar UVA radiation makes laboratory-cultures of that species a poor tool for evaluating solar photoinactivation processes. Specifically, the slower inactivation of wastewater bacteria and MS2 bacteriophage under all conditions tested in our Chapter 2 studies imply that spikes of laboratory-grown *E. coli* should not be used as a disinfection process indicator unless a clear relationship can be established between the inactivation of this indicator and the destruction of more recalcitrant pathogens. At present, the absence of detectable laboratory-cultured bacteria cannot be considered an indication that viruses or fecal bacteria have been inactivated, particularly at temperatures below 45° C and in materials that exclude UVB wavelengths. The finding that wastewater organisms are more resistant to disinfection than laboratory strains is not novel. However, the observation that this trend is reproducible and wavelength-dependent (Chapter 4), and that wastewater isolates were more sensitive to UVA when grown on rich media, while laboratory organisms became more resistant to sunlight when grown on minimal media (Chapter 5) may be novel. The observation that the protective effect of minimal media was abolished by the addition of iron suggests further avenues for research. Future studies may investigate whether bacteria grown on minimal media provide sufficiently conservative process indicators for the photoinactivation of fecal organisms.

### 6.1.2. Optical Properties of Containers

While it has long been known that UVB wavelengths are highly germicidal, the current work suggests that the longest UVB and shortest UVA wavelengths are of such importance to solar disinfection that slight shifts in the optical properties of materials can significantly affect their suitability for solar water treatment (Chapters 2-4). The finding that organisms in polypropylene copolymer bottles were inactivated twice as rapidly as in PET, despite the lower UVA transmittance of the former material (Chapter 2), suggests that subtle differences in container thickness and plasticizer concentrations may also have important effects, even within a given class of polymers. Furthermore, because of the relatively high cost of acrylics, plexiglass, and fluoropolymers, the identification of inexpensive polymers that are more scratch-resistant and UVB-transparent than PPCO will be of great interest. Flexible containers with excellent optical transparency (i.e. SODIS bags) are currently being deployed by research groups, and their microbiological performance is likely to be impressive if they prove to be acceptable to users and survivable in the field.

### 6.1.3. Simple Additives Can Accelerate the Sunlight Inactivation of Bacteria and Viruses

The finding that low-cost peroxide-generating additives were able to accelerate sunlight inactivation (Chapter 2) has a variety of potential applications. Oxidant combinations that are stable in solid form, have inoffensive taste and odor profiles, and are unlikely to form disinfection byproducts of concern are of interest in sunlit and dark applications. Furthermore, the catalytic use of copper ions provides a residual with the potential to reduce recontamination events. Naturally, the possibility that oxidants which are noxious to bacteria and viruses are not entirely harmless to humans must be seriously investigated. Although peroxide, copper, and ascorbate are each generally regarded as safe at the concentrations in question, their combined properties may be different. One potential application of such systems might be in reducing the energy consumption of small-to-medium scale UV water treatment facilities, particularly if these compounds can be shown to accelerate the inactivation of dsDNA viruses such as Adenovirus, which are among the most UV-resistant waterborne pathogens of concern.

## 6.2. Mechanistic Implications

### 6.2.1. Wavelength Dependence of Photoinactivation

While both UVA and UVB wavelengths have long been known to affect microorganisms, this work offers a more in-depth look at the interplay between various wavelengths of polychromatic light as they damage and destroy bacteria and viruses. The results imply the existence of significant local maxima and minima in sunlight sensitivity at a variety of wavelengths (Chapters 3 and 4). The methods used in this work are not yet sufficiently refined to allow us to assert with great confidence that these maxima and minima are all genuine and that their location and magnitude are as described; this will be the subject of further work on polychromatic photoinactivation. However, if maxima do exist in the UVA/B spectrum, these wavelengths may offer clues both to the mechanisms of microbial damage and repair and to new and more energy-efficient ways to exploit these characteristics in water and wastewater treatment as well as in clinical settings.

From a mechanistic perspective, the possibility of sensitivity minima is intriguing as well. While our computational model predicted sensitivity values near zero for some organisms at some UVA wavelengths, this is highly unlikely in practice. It remains to be seen whether, in the presence of polychromatic light, each additional photon at one wavelength is indeed orders of magnitude more toxic than a photon at shorter, nearby wavelengths, or whether this prediction represents an artifact to be corrected in future applications of polychromatic action spectrometry.

#### 6.2.2. Monochromatic Photoaction Spectra Underestimate the UVA Sensitivity of *E. coli* Grown on Rich Media

While current polychromatic methods may overestimate the effects of UVA (Chapters 3 and 4), it seems likely that early photoaction spectra dramatically underestimated the importance of UVA relative to UVB in bacterial inactivation. Thus, there may be qualitative differences between the action of light from mercury lamps on cells and the effects of natural sunlight exposure. Understanding those differences may expand our knowledge of photobiological processes, place prior investigations in a richer theoretical context, and alert researchers to the caveats of using monochromatic light sources for photobiological research in the future.

#### 6.2.3. Involvement of Iron and Hydrogen Peroxide in *E. coli* Photoinactivation

The evidence that iron and Fenton chemistry play an important role in oxidative and photooxidative stress has been overwhelming for decades. However, the finding that sunlight sensitizes *E. coli* to inactivation by hydrogen peroxide in the dark, and that the degree of this sensitization depends on iron supplementation during growth (Chapter 5) is a novel observation. This observation provides further evidence that some of the changes sunlight causes in *E. coli* require both iron and hydrogen peroxide to induce lethality. The release of intracellular iron from FeS clusters and/or the disruption of SOD activity are two conceivable explanations for these observations, although by no means the only two. Simple experiments should be able to eliminate one or both of these hypotheses in future investigations, shedding further light on the question of how exactly sunlight "ramps up" oxidative Fenton damage to aerobic organisms.

### 6.3. Methods: Polychromatic Action Spectra

Polychromatic optical filter sets coupled with computation models may provide new ways to study the transformation of chemicals and microorganisms by sunlight in the laboratory and the natural environment. To the extent that polychromatic photobiological processes differ from monochromatic ones, there may be applications for a tool that allows researchers to probe wavelengths of interest without eliminating light in other regions. If increasing the intensity of light in the UVB range, maximizing the variety of filter transmittances at wavelengths of interest, and expanding the computational model to address higher-order effects can eliminate much of the uncertainty in this approach, polychromatic action spectra may provide useful insights into a range of photochemical and photobiological topics.

## 6.4. Future Directions

### 6.4.1. SODIS

The findings of this work present opportunities and challenges for SODIS implementation. PET is inexpensive and ubiquitous, and the observation that it is far from an optimal material for solar disinfection opens the door to a suite of new problems. However, there is increasing evidence that adherence, not efficacy, may be the biggest challenge for SODIS implementation (Chapter 1). Thus, an expansion of SODIS beyond PET bottles may open new opportunities for sustained adoption of alternative disinfection options. Specifically, the development of purpose-build SODIS containers that are optimized for convenience, efficacy, and aesthetics is one active area of research. In addition, the finding that ceramic and granular media filters enjoy high adherence rates and effectively remove eukaryotic pathogens, but not necessarily viruses and bacteria, may provide opportunities for synergies with SODIS processes using UVB-transparent materials.

### 6.4.2. Beyond SODIS

The findings of this work may also be relevant to wastewater treatment and processes in natural waters. There may be multiple settings in which it is desirable to disinfect waters that have already undergone some form of treatment, but contain too much dissolved organic matter for effective chlorination and remain too turbid for cost-effective UVC treatment. The ability of solar UVA/B wavelengths to penetrate to greater depths than UVC in water, even if only by a few cm, may be of use in such contexts, particularly given the reasonable price of sunlight. Furthermore, the finding that the addition of peroxide, copper, and/or ascorbate can enhance the inactivation of bacteria and virus indicators in dilute wastewater is of additional interest. The addition of copper or iron and peroxide to primary wastewater effluent may be one way to enhance the photoinactivation of organisms in ponds receiving such waters. While Fenton-based advanced oxidation processes have been known for decades, their application to wastewater treatment in developing country settings may be more novel.

Furthermore, the dual findings of the importance of iron status and the predictive power of polychromatic action spectra offer exciting possibilities for exploring the fate and transport of microorganisms in environmental systems. Specifically, the ability to measure organism-specific sensitivity spectra, calculate sunlight spectra for a given place and time, and subsequently predict the inactivation rate of an organism of interest is a powerful tool. Correcting for the effects of growth conditions in the laboratory may greatly extend the validity of that tool for predicting the behavior of fecal organisms. In waters where the concentrations and influence of dissolved exogenous chromophores are either known or negligible, it should be possible to begin to model the survival and transport of pathogens in surface waters with increased accuracy, and to validate these predictions with direct measurements. Such models might be useful for topics ranging from anticipating beach closures and modeling riparian contamination to comparing the influence of light, transport, predation, and settling on the survival of organisms in lakes, ponds, and wetlands.

It has been interesting, in the course of this work, to observe how many aspects of photooxidative stress in the environment have been brilliantly addressed in the 1970's and 80's, and yet how much remains to be discovered. That two of our planet's most abundant elements and their interactions with its primary source of energy should still contain so many mysteries is both exciting and inspiring.

## 7. Appendix 1: MATLAB Code for Computational Model

The MATLAB code used for the computational model is presented below. This code calculates spectral sensitivity coefficients based on intensity measurements and observed inactivation rates (k values) for inactivation trials, as well as code for conducting sensitivity analysis and backtesting procedures.

### 7.1. Wrapper for Coefficient Approximation

```
clear all
%%%%%%%%%%%%%% settings  %%%%%%%%%%%%%%%%%%%%%%%%%%%%%%%%
runtype = 'backtest';
% options are:
% 'backtest' (artificial P spectra)
% 'normal' (use mean k values)
% 'sens' (sensitivity analysis with varying k values)

%output descriptions:
%backtest: rows of csv are wavelength bin centers, actual P,
calculated P
%normal:  rows of csv are wavelength bin centers, calculated P
%sens:  rows of csv are wavelength bin centers, median P, MAD P

n_guesses = 100;  %number of randomly generated initial guesses for
P to try
%if Parallel Toolbox installed, set equal to number of CPU cores

finalbinsize = 1;  %width of highest resolution, final bin (nm)
LB = 0;  %lower bound for P
UB = 2.5;  %upper bound for P
span = 3;  %smooth intensity data and P spectra *twice* using a
moving
%average of this span (1 for no smoothing)

sens_trials = 3;  %number of randomly generated realizations of k to
try
%when runtype = 'sens'
numstds = 1;  %number of standard deviations to choose random k
values
%within when runtype = 'sens'

lambdamin = 280;  %defines lower end of wavelength range of interest
(nm)
lambdamax = 496;  %defines upper end of wavelength range of interest
(nm)

%settings for fmincon
tolfun = 1E-4;
maxiter = 15000;
maxevals = 1E6;

%settings for plots
```

```
numfontsize = 14;
labelfontsize = 16;
ymax = 1;

output_folder = '/home/fsc/Desktop/UV_inact_model/output/';

%%%%%%%%  input folders and files %%%%%%%%%%%%%%%%%%%%%%%%%
%folder with intensity data:

intensity_folder = '/home/fsc/Desktop/UV_inact_model/virus_input/';
  %  intensity_folder =
'/home/fsc/Desktop/UV_inact_model/ecoli_input/';

%%%%%%%%%%%%%%% backtest %%%%%%%%%%%%%%%%%%%%%%%%%%%%%%%%%%%%%%%%%%%%%
%specify folders with backtest data files (known P spectra)
%format is csv, row 1 = wavelength, row 2 = P values
%size = 2 rows X number_of_wavelengths cols
%individual files are automatically read

backtest_folders = {...

'/home/fsc/Desktop/UV_inact_model/virus_backtest_data/monotonic/',..
.

'/home/fsc/Desktop/UV_inact_model/virus_backtest_data/multipeak/3pea
k_spreading/',...

'/home/fsc/Desktop/UV_inact_model/virus_backtest_data/multipeak/3pea
k_translation/',...

'/home/fsc/Desktop/UV_inact_model/virus_backtest_data/singlepeak/'
    };

%                 backtest_folders = {...
%
'/home/fsc/Desktop/UV_inact_model/ecoli_backtest_data/monotonic/'...
%
'/home/fsc/Desktop/UV_inact_model/ecoli_backtest_data/multipeak/3pea
k_spreading/',...
%
'/home/fsc/Desktop/UV_inact_model/ecoli_backtest_data/multipeak/3pea
k_translation/',...
%
'/home/fsc/Desktop/UV_inact_model/ecoli_backtest_data/singlepeak/'
%                     };



%specify file with intensity data that will be used with backtest P
spectra to
%generate k values
%format is csv, row 1 = wavelength, row 2:N+1 = intensity
%values for each of N experiments
```

```
%size = number_of_experiments+1 rows X number_of_wavelengths cols

 % intensity_file = 'Intensity_Vals_EC_MG1655_D.csv';
intensity_file = 'Intensity_MS2data.csv';

%%%%%%%%%%   normal or sens
%%%%%%%%%%%%%%%%%%%%%%%%%%%%%%%%%%%%%%%%%%%%%%

%list of csv files with intensity data
%format is csv, row 1 = wavelength, row 2:N+1 = intensity
%values for each of N experiments
%size = number_of_experiments+1 rows X number_of_wavelengths cols

intensity_files = {...
    'Intensity_MS2data.csv',...
    'Intensity_PRD1data.csv'...
    };
%
%                   intensity_files = {...
%                  'Intensity_Vals_EC_MG1655_D.csv',...
%                   'Intensity_Vals_EC_29181_D.csv'...
%                   'Intensity_Vals_EC_Iso_8_D.csv'...
%                   'Intensity_Vals_EC_Iso_14_D.csv'...
%                   'Intensity_Vals_EC_Iso_36_D.csv'...
%                   'Intensity_Vals_EC_FAMP_D.csv'...
%                   };

%folder with input files containing k values
%values
inputfile_folder = '/home/fsc/Desktop/UV_inact_model/virus_input/';
% inputfile_folder =
'/home/fsc/Desktop/UV_inact_model/ecoli_input/';

%list of csv files with k values for each experiment
%be sure order matches order of intensity_files!

%col 1 = mean k values for the replicates each experiment
%col 2 = standard deviations of k throughout replicates of each
experiment
%size = number_of_experiments rows X 2 cols

inputfiles = {...
    'Fit_MS2 mean sdev.csv',...
    'Fit_PRD1 mean sdev.csv'...
    };

%                             inputfiles = {...
%                  'Fit_Vals_EC_MG1655_D.csv',...
%                   'Fit_Vals_EC_29181_D.csv'...
%                   'Fit_Vals_Iso8_D.csv'...
%                   'Fit_Vals_Iso14_D.csv'...
%                   'Fit_Vals_Iso36_D.csv'...
%                   'Fit_Vals_EC_FAMP_D.csv'...
```

```
%                   };

%%%%%%%%%%%%%%%%%%%%%%%%%%%%%%%%%%%%%%%%%%%%%%%%%%%%%%%%%%%%%%%%%%%%%%%%%%%%
%%%
%run model

collect_filenames;  %generates list of input files
par_init;  %check for Parallel Toolbox and start workers if present
inputfile_loop;  %loop code over all input files
```

### 7.2. Script for Collecting Filenames

```
inputfilelist = {};
outputnamelist = {};

if strcmp(runtype,'backtest')

    %generate master list of backtest data files to run with
    for folder = backtest_folders

        temp = dir([folder{1},'*.csv']);
        filenames = {temp.name}';
        clear fullpaths
        for i = 1:length(filenames)
            fullpaths{i,1} = [folder{1},filenames{i}];
        end
        inputfilelist = [inputfilelist; fullpaths]; %append
filenames in each folder to master list
        clear temp
        for i = 1:length(filenames)
            temp{i,1} = [intensity_file(1:end-
4),'_',filenames{i}(1:end-4)];  %generate prefixes for outputfiles
in this folder
        end
        outputnamelist = [outputnamelist; temp];  %append output
prefixes to master list
    end

elseif strcmp(runtype,'normal') || strcmp(runtype,'sens')

    clear outputnamelist
    for i = 1:length(inputfiles)
        outputnamelist{i,1} = inputfiles{i}(1:end-4);
        inputfilelist{i,1} = [inputfile_folder,inputfiles{i}];
    end

end
```

### 7.3. Script for Initiating Parallel Processing

```
if is_partoolbox_installed()
    if matlabpool('size') == 0
```

```
        matlabpool  %open parallel workers
    end

    spmd
        warning('off','optim:fmincon:SwitchingToMediumScale')
    end

else
    warning('off','optim:fmincon:SwitchingToMediumScale')
end
```

### 7.4. Function for Determining Whether Parallel Processing Toolbox Is Installed

```
function havepar = is_partoolbox_installed()

temp = ver;
toolboxes = {temp.Name};

havepar = ismember('Parallel Computing Toolbox',toolboxes);
```

### 7.5. Input File Loop

```
inputi = 0;
for inputfile = inputfilelist'
    inputi = inputi+1;

%%%%%%%%%%%%%%  read intensity data %%%%%%%%%%%%%%%%%%%%%%%%%%%%%%%%

    if strcmp(runtype,'backtest')

        data = csvread([intensity_folder,intensity_file]);
        I_lambda = data(1,:);  %wavelengths
        data = data(2:end,:); %remove row of wavelengths, leaving
intensities
        I = data(:,(I_lambda >= lambdamin & I_lambda <= lambdamax));
%light intensity data

    elseif strcmp(runtype,'normal') || strcmp(runtype,'sens')

        data = csvread([intensity_folder,intensity_files{inputi}]);
        I_lambda = data(1,:);
        data = data(2:end,:); %remove row of wavelengths, leaving
intensities
        I = data(:,(I_lambda >= lambdamin & I_lambda <= lambdamax));
%light intensity data

    end

    for i = 1:size(I,1)
        I(i,:) = dsmooth(I(i,:),span);  %smooth intensity data
    end
```

```
    %%%%%%%%%%%%%%  read or generate k values
%%%%%%%%%%%%%%%%%%%%%%%%%%%%

    if strcmp(runtype,'normal') || strcmp(runtype,'sens')

        data = csvread([inputfilelist{inputi}]);
        k = data(:,1);
        k_std = data(:,2);

    elseif strcmp(runtype,'backtest')
        data = csvread([inputfilelist{inputi}]);
        data_lambda = data(1,:);  %wavelengths
        data = data(2,:); %remove row of wavelengths, leaving P
        Pknown = data((data_lambda >= lambdamin & data_lambda <=
lambdamax));
        k = I*Pknown';

    end

    %%%%%%%% loop for sampled k values if runtype = sens
%%%%%%%%%%%%%%%%

    if strcmp(runtype,'sens')
        Pall =
NaN(sens_trials,n_guesses,ceil(size(I,2)/finalbinsize));
%initialize results array
        sens_loop;  %calls guess_loop inside

      %%%%%%%%%%%%%%%% loop for initial guesses of P spectra
%%%%%%%%%%

    elseif strcmp(runtype,'normal') || strcmp(runtype,'backtest')
        k_in = k;
        P = NaN(n_guesses,ceil(size(I,2)/finalbinsize));
%initialize results array
        guess_loop;

    end

%%%%%%%%%%%%%%%%%%%%%%%%%%%%%%%%%%%%%%%%%%%%%%%%%%%%%%%%%%%%%%%%%%%%%%%%%%%%%%%
%%%
    postprocess;  %saves csv output files and plots to output_folder

end
```

### 7.6. Sensitivity Analysis Loop

```
clear k_ins errorall

for s = 1:sens_trials
    disp(['On sens trial ',num2str(s),' of ',num2str(sens_trials)])

    k_in = sens_sampler(k,k_std,numstds);
```

```
    k_ins{s} = k_in;  %store sampled k values for possible post
processing

    P = NaN(n_guesses,ceil(size(I,2)/finalbinsize));  %initialize
results array
    guess_loop;  %loop over different initial guesses and find best-
fit P

    Pall(s,:,:) = P;  %store all solutions for this sens iteration
    errorall(s,:) = error;  %store all errors for this sens
iteration

end
```

### 7.7. Sensitivity analysis sampling function

```
function [sampledk] = sens_sampler(k,k_std,numstds)

lowerbnds = k-k_std*numstds;
upperbnds = k+k_std*numstds;

sampledk = normrnd(k,k_std);  %choose random k values from a normal
distribution

while any(sampledk <= lowerbnds | sampledk >= upperbnds)  %if any
sampled values lie beyond imposed bounds, sample again until all
bounds are satisfied
    sampledk = normrnd(k,k_std);
end
```

### 7.8. Guess Loop for Coefficient Approximation

```
clear error

lambdafinal = [];

parfor guesscount = 1:n_guesses  %loop over different initial
guesses in parallel

    disp(['On guesscount ',num2str(guesscount),' of
',num2str(n_guesses)])

    uniform_dist = rand(1,size(I,2))*(UB - LB) + LB;  %uniformly
distributed random values between LB and UB
    powfacts = rand(1,size(I,2))*(0 - -10 ) + -10;  %uniformly
distributed random values between -10 and 0
    p0 = uniform_dist.*10.^powfacts;  %lognormally distributed
values from LB to UB

    initialbinsize = round(size(I,2)/size(I,1));  %make number of
initial bins = number of experiments
```

```
    binsizes = initialbinsize:-1:finalbinsize;  %wavelengths per bin
for each iteration

    n_bins = ceil(size(I,2) ./ binsizes);  %number of bins for each
iteration

    bini = 0;  %counter for loop over bins

    binnedI = cell(1,length(binsizes));
    avglambda = cell(1,length(binsizes));
    binnedp0 = cell(1,length(binsizes));
    lb = cell(1,length(binsizes));
    ub = cell(1,length(binsizes));
    p = cell(1,length(binsizes));

    for binsize = binsizes %iterate optimization from coarse to fine
resolution
        bini = bini+1;

        start = 1;  %initialize starting wavelength of first bin to
1st index
        last = binsize;  %last wavelength for first bin

        for i = 1:n_bins(bini)  %generate aggregrated intensity data

            if i == n_bins(bini)  %for last bin, set final
wavelength to account for binsize not evenly dividing number of
wavelengths
                last = size(I,2);
            end

            binnedI{bini}(:,i) = sum(I(:,start:last),2);  %aggregate
intensity data
            avglambda{bini}(i) = mean(I_lambda(start:last));
%calculate wavelength values at bin centers

            if bini == 1
                binnedp0{bini}(i) = mean(p0(start:last));  %for
first iteration, use initial guesses from loaded data
            end

            start = start+binsize;  %increment starting wavelength
for next bin
            last = last + binsize;  %increment ending wavelength for
next bin

        end

        if bini > 1  %for all iterations after first, interpolate
initial guesses from previous iteration into new bins

            binnedp0{bini} = interp1(avglambda{bini-
1}(:),binnedp0{bini-1}(:),avglambda{bini}(:),'linear','extrap');
```

```
        end

        lb{bini} = repmat(LB,n_bins(bini),1);  %lower bounds for
sensitivity coeffs are zero
        ub{bini} = repmat(UB,n_bins(bini),1);

        fmin = @(p)objective_fun(p,binnedI{bini},k_in,span);
%anonymous function to handle constants (intensity, k) with respect
to optimization

        try
            [p{bini}] =
fmincon(fmin,binnedp0{bini}(:),[],[],[],[],lb{bini},ub{bini}(:),[],o
ptimset('Display','notify','MaxFunEvals',maxevals,'tolfun',tolfun,'m
axiter',maxiter));
        catch %in case NaN or Inf are generated during optimization
            p{bini} = NaN(size(binnedp0{bini}));
        end

        if bini > 1
            binnedp0{bini-1} = p{bini}; %use this solution for
initial guess to next refined solution
        end

    end

    if span > 1
        P(guesscount,:) = dsmooth(p{end},span); %save most resolved
solution  %must smooth fmincon output since smoothing is done
internally
        error(guesscount) =
objective_fun(p{end},binnedI{bini},k_in,span);  %must recalc error
based on smoothed P
    else
        P(guesscount,:) = p{end}; %save most resolved solution
        error(guesscount) =
objective_fun(p{end},binnedI{bini},k_in,span);  %must recalc error
based on smoothed P
    end

    lambdafinal(guesscount,:) = avglambda{end}; %save most resolved
wavelength vector

    p = []; binnedp0 = [];  %reset temporary variables

end

lambdafinal = lambdafinal(1,:);
```

### 7.9. Script for Loading User-Supplied Inactivation Rate Constant Values

```
inputi = 0;
```

```
for inputfile = inputfilelist'
    inputi = inputi+1;

%%%%%%%%%%%%%%  read intensity data %%%%%%%%%%%%%%%%%%%%%%%%%%%%%%%%

    if strcmp(runtype,'backtest')

        data = csvread([intensity_folder,intensity_file]);
        I_lambda = data(1,:);  %wavelengths
        data = data(2:end,:); %remove row of wavelengths, leaving
intensities
        I = data(:,(I_lambda >= lambdamin & I_lambda <= lambdamax));
%light intensity data

    elseif strcmp(runtype,'normal') || strcmp(runtype,'sens')

        data = csvread([intensity_folder,intensity_files{inputi}]);
        I_lambda = data(1,:);
        data = data(2:end,:); %remove row of wavelengths, leaving
intensities
        I = data(:,(I_lambda >= lambdamin & I_lambda <= lambdamax));
%light intensity data

    end

    for i = 1:size(I,1)
        I(i,:) = dsmooth(I(i,:),span);  %smooth intensity data
    end

    %%%%%%%%%%%%%  read or generate k values
%%%%%%%%%%%%%%%%%%%%%%%%%

    if strcmp(runtype,'normal') || strcmp(runtype,'sens')

        data = csvread([inputfilelist{inputi}]);
        k = data(:,1);
        k_std = data(:,2);

    elseif strcmp(runtype,'backtest')
        data = csvread([inputfilelist{inputi}]);
        data_lambda = data(1,:);  %wavelengths
        data = data(2,:); %remove row of wavelengths, leaving P
        Pknown = data((data_lambda >= lambdamin & data_lambda <=
lambdamax));
        k = I*Pknown';

    end

    %%%%%%%% loop for sampled k values if runtype = sens
%%%%%%%%%%%%%%

    if strcmp(runtype,'sens')
```

```
        Pall =
NaN(sens_trials,n_guesses,ceil(size(I,2)/finalbinsize));
%initialize results array
        sens_loop;  %calls guess_loop inside

      %%%%%%%%%%%%%%%% loop for initial guesses of P spectra
%%%%%%%%%%

    elseif strcmp(runtype,'normal') || strcmp(runtype,'backtest')
        k_in = k;
        P = NaN(n_guesses,ceil(size(I,2)/finalbinsize));
%initialize results array
        guess_loop;

    end

%%%%%%%%%%%%%%%%%%%%%%%%%%%%%%%%%%%%%%%%%%%%%%%%%%%%%%%%%%%%%%%%%%%%%%%%%%%
%%%
    postprocess;  %saves csv output files and plots to output_folder

end
```

### 7.10. Objective Function for Optimization

```
function [M] = objective_fun(P,I,k_meas,span)

if size(I,2) ~= size(P,1)
    P = P';  %make sure P is a column vector
end

if span > 1
    P = dsmooth(P,span);
end

k_calc = I*P;  %calculated rate constants based on current guess for
sensivity coeffs

M = sum(    sqrt((k_meas-k_calc).^2) );  %sum of squared errors to
be minimized
```

### 7.11. Double-Smoothing Procedure

```
function [smoothed] = dsmooth(x,n)

smoothed = smooth(smooth(x,n),n);
```

### 7.12. Postprocessing Script

```
if ~exist(output_folder)
    mkdir(output_folder)
end
```

```
%fix errors for runs that failed entirely
if strcmp(runtype,'normal') || strcmp(runtype,'backtest')
    error(isnan(error)) = Inf;
elseif strcmp(runtype,'sens')
    errorall(isnan(errorall)) = Inf;
end

%sort solutions by error between actual and computed k
if strcmp(runtype,'normal') || strcmp(runtype,'backtest')

    [ ~ , inds] = sort(error);
    sortedP = P(inds,:);
    bestP = sortedP(1,:);

elseif strcmp(runtype,'sens')

    clear bestPall
    [ ~ , inds] = sort(errorall,2);
    for i = 1:size(Pall,1)  %sens count
        sortedPall = squeeze(Pall(i,inds(i,:),:));
        bestPall(i,:) = squeeze(sortedPall(1,:));
    end
    medians = median(bestPall,1);
    mads = mad(bestPall,1,1);

end

if strcmp(runtype,'backtest')

    Pinterp =
interp1(lambdamin:lambdamax,Pknown,lambdafinal,'linear','extrap');

csvwrite([output_folder,outputnamelist{inputi},'_backtest_output.csv
'],[lambdafinal; Pinterp; bestP]);

    plot(lambdafinal,bestP,'-')
    hold on
    plot(lambdafinal,Pinterp,'--')
    set(gca,'fontsize',numfontsize)
    xlabel('wavelength (nm)','fontsize',labelfontsize)
    ylabel('sensitivity coefficient','fontsize',labelfontsize)
    ylim([0 ymax])
    grid on
    print(gcf,'-
dpdf',[output_folder,outputnamelist{inputi},'_backtest_output.pdf'])
    close

save([output_folder,outputnamelist{inputi},'_backtest_matlabdump.mat
']);

elseif strcmp(runtype,'normal')
```

```
csvwrite([output_folder,outputnamelist{inputi},'_normal_output.csv']
,[lambdafinal;bestP]);

    plot(lambdafinal,bestP,'-')
    set(gca,'fontsize',numfontsize)
    xlabel('wavelength (nm)','fontsize',labelfontsize)
    ylabel('sensitivity coefficient','fontsize',labelfontsize)
    ylim([0 ymax])
    grid on
    print(gcf,'-
dpdf',[output_folder,outputnamelist{inputi},'_normal_output.pdf'])
    close

save([output_folder,outputnamelist{inputi},'_normal_matlabdump.mat']
);

elseif strcmp(runtype,'sens')


csvwrite([output_folder,outputnamelist{inputi},'_sens_output.csv'],[
lambdafinal;medians; mads]);

    shadedErrorBar(lambdafinal,medians,[mads;mads]);
    set(gca,'fontsize',numfontsize)
    xlabel('wavelength (nm)','fontsize',labelfontsize)
    ylabel('sensitivity coefficient','fontsize',labelfontsize)
    ylim([0 ymax])
    grid on

    print(gcf,'-
dpdf',[output_folder,outputnamelist{inputi},'_sens_output.pdf'])
    close

save([output_folder,outputnamelist{inputi},'_sens_matlabdump.mat']);

end
```

### 7.13. Function for Creating Shaded Error Bars

```
function H=shadedErrorBar(x,y,errBar,lineProps,transparent)
% function H=shadedErrorBar(x,y,errBar,lineProps,transparent)
%
% Purpose
% Makes a 2-d line plot with a pretty shaded error bar made
% using patch. Error bar color is chosen automatically.
%
% Inputs
% x - vector of x values [optional, can be left empty]
% y - vector of y values or a matrix of n observations by m cases
%     where m has length(x);
% errBar - if a vector we draw symmetric errorbars. If it has a
%          size of [2,length(x)] then we draw asymmetric error bars
```

```
%          with row 1 being the upper bar and row 2 being the lower
%          bar. ** alternatively ** errBar can be a cellArray of
%          two function handles. The first defines which statistic
%          the line should be and the second defines the error
%          bar.
% lineProps - [optional,'-k' by default] defines the properties of
%             the data line. e.g.:
%             'or-', or {'-or','markerfacecolor',[1,0.2,0.2]}
% transparent - [optional, 0 by default] if ==1 the shaded error
%               bar is made transparent, which forces the renderer
%               to be openGl. However, if this is saved as .eps the
%               resulting file will contain a raster not a vector
%               image.
%
% Outputs
% H - a structure of handles to the generated plot objects.
%
%
% Examples
% y=randn(30,80); x=1:size(y,2);
% shadedErrorBar(x,mean(y,1),std(y),'g');
% shadedErrorBar(x,y,{@median,@std},{'r-o','markerfacecolor','r'});
% shadedErrorBar([],y,{@median,@std},{'r-o','markerfacecolor','r'});
%
% Overlay two transparent lines
% y=randn(30,80)*10; x=(1:size(y,2))-40;
% shadedErrorBar(x,y,{@mean,@std},'-r',1);
% hold on
% y=ones(30,1)*x; y=y+0.06*y.^2+randn(size(y))*10;
% shadedErrorBar(x,y,{@mean,@std},'-b',1);
% hold off
%
%
% Rob Campbell - November 2009

%%%%%%%%%%%%%%%%%%%%%%%%%%%%%%%%%%%%%%%%%%%%%%%%%%%%%%%%%%%%%%%%%%%%%%%
% Error checking
error(nargchk(3,5,nargin))

%Process y using function handles if needed to make the error bar
%dynamically
if iscell(errBar) && ~isvector(y)
    fun1=errBar{1};
    fun2=errBar{2};
    errBar=fun2(y);
    y=fun1(y);
elseif ~iscell(errBar) && isvector(y)
    y=y(:)';
else
    error('2nd and 3rd input arguments are not compatible')
end

if isempty(x)
```

```
    x=1:length(y);
else
    x=x(:)';
end

if length(x) ~= length(y)
    error('inputs x and y are not of equal lengths')
end

%If only one error bar is specified then we will mirror it, turning
it into
%both upper and lower bars.
if length(errBar)==length(errBar(:))
    errBar=repmat(errBar(:)',2,1);
else
    f=find(size(errBar)==2);
    if isempty(f), error('errBar has the wrong size'), end
    if f==2, errBar=errBar'; end
end

if length(x) ~= length(errBar)
    error('inputs x and y must have the same length as errBar')
end

%Set default options
defaultProps={'-k'};
if nargin<4 || isempty(lineProps)
    lineProps=defaultProps;
end
if ~iscell(lineProps)
    lineProps={lineProps};
end

if nargin<5 || ~isnumeric(transparent)
    transparent=0;
end

%%%%%%%%%%%%%%%%%%%%%%%%%%%%%%%%%%%%%%%%%%%%%%%%%%%%%%%%%%%%%%%%%%%%
% Plot the main line. We plot this first in order to extract the RGB
values
% for the line colour. I am not aware of a function that does this.
H.mainLine=plot(x,y,lineProps{:});


% Work out the color of the shaded region and associated lines
% Using alpha requires the render to be openGL and so you can't
% save a vector image. On the other hand, you need alpha if you're
% overlaying lines. We therefore provide the option of choosing
alpha
% or a de-saturated solid colour for the patch surface.

col=get(H.mainLine,'color');
edgeColor=col+(1-col)*0.55;
```

```
patchSaturation=0.15; %How de-saturated or transparent to make the
patch
if transparent
    faceAlpha=patchSaturation;
    patchColor=col;
    set(gcf,'renderer','openGL')
else
    faceAlpha=1;
    patchColor=col+(1-col)*(1-patchSaturation);
    set(gcf,'renderer','painters')
end

%Calculate the y values at which we will place the error bars
uE=y+errBar(1,:);
lE=y-errBar(2,:);

%Add the error-bar plot elements
holdStatus=ishold;
if ~holdStatus, hold on,  end

%Make the cordinats for the patch
yP=[lE,fliplr(uE)];
xP=[x,fliplr(x)];

%remove any nans otherwise patch won't work
xP(isnan(yP))=[];
yP(isnan(yP))=[];

H.patch=patch(xP,yP,1,'facecolor',patchColor,...
              'edgecolor','none',...
              'facealpha',faceAlpha);

%Make nice edges around the patch.
H.edge(1)=plot(x,lE,'-','color',edgeColor);
H.edge(2)=plot(x,uE,'-','color',edgeColor);

%The main line is now covered by the patch object and was plotted
first to
%extract the RGB value of the main plot line. I am not aware of an
easy way
%to change the order of plot elements on the graph so we'll just
remove it
%and put it back (yuk!)
delete(H.mainLine)
H.mainLine=plot(x,y,lineProps{:});


if ~holdStatus, hold off, end
```

# 8. Appendix 2: DNA Sequences and Alignments for *E. coli* Strains

## 8.1. Sequences

### 8.1.1. *E. coli* MG1655 (1375 bp)

GCTGACGAGTGGCGGACGGGTGAGTAATGTCTGGGAAACTGCCTGATGGAGGGGGATAACTACTGGAAACG
GTAGCTAATACCGCATAACGTCGCAAGACCAAAGAGGGGGACCTTCGGGCCTCTTGCCATCGGATGTGCCC
AGATGGGATTAGCTAGTAGGTGGGGTAACGGCTCACCTAGGCGACGATCCCTAGCTGGTCTGAGAGGATGA
CCAGCCACACTGGAACTGAGACACGGTCCAGACTCCTACGGGAGGCAGCAGTGGGGAATATTGCACAATGG
GCGCAAGCCTGATGCAGCCATGCCGCGTGTATGAAGAAGGCCTTCGGGTTGTAAAGTACTTTCAGCGGGGA
GGAAGGGAGTAAAGTTAATACCTTTGCTCATTGACGTTACCCGCAGAAGAAGCACCGGCTAACTCCGTGCC
AGCAGCCGCGGTAATACGGAGGGTGCAAGCGTTAATCGGAATTACTGGGCGTAAAGCGCACGCAGGCGGTT
TGTTAAGTCAGATGTGAAATCCCCGGGCTCAACCTGGGAACTGCATCTGATACTGGCAAGCTTGAGTCTCG
TAGAGGGGGGTAGAATTCCAGGTGTAGCGGTGAAATGCGTAGAGATCTGGAGGAATACCGGTGGCGAAGGC
GGCCCCCTGGACGAAGACTGACGCTCAGGTGCGAAAGCGTGGGGAGCAAACAGGATTAGATACCCTGGTAG
TCCACGCCGTAAACGATGTCGACTTGGAGGTTGTGCCCTTGAGGCGTGGCTTCCGGAGCTAACGCGTTAAG
TCGACCGCCTGGGGAGTACGGCCGCAAGGTTAAAACTCAAATGAATTGACGGGGGCCCGCACAAGCGGTGG
AGCATGTGGTTTAATTCGATGCAACGCGAAGAACCTTACCTGGTCTTGACATCCACGGAAGTTTTCAGAGA
TGAGAATGTGCCTTCGGGAACCGTGAGACAGGTGCTGCATGGCTGTCGTCAGCTCGTGTTGTGAAATGTTG
GGTTAAGTCCCGCAACGAGCGCAACCCTTATCCTTTGTTGCCAGCGGTCCGGCCGGGAACTCAAAGGAGAC
TGCCAGTGATAAACTGGAGGAAGGTGGGGATGACGTCAAGTCATCATGGCCCTTACGACCAGGGCTACACA
CGTGCTACAATGGCGCATACAAAGAGAAGCGACCTCGCGAGAGCAAGCGGACCTCATAAAGTGCGTCGTAG
TCCGGATTGGAGTCTGCAACTCGACTCCATGAAGTCGGAATCGCTAGTAATCGTGGATCAGAATGCCACGG
TGAATACGTTCCCGGGCCTTGTACACACCGCCCGTCACACCATGGGAGTGGGTTGCAAAAGAAGTAGGTAG
CTTAACCTTCGGGAGGGCGCTACCAC

### 8.1.2. Isolate 8 (1408 bp)

AGTCGAACGGTAACAGGAAGCAGCTTGCTGCTTCGCTGACGAGTGGCGGACGGGTGAGTAATGTCTGGGAA
ACTGCCTGATGGAGGGGGATAACTACTGGAAACGGTAGCTAATACCGCATAACGTCGCAAGACCAAAGAGG
GGGACCTTCGGGCCTCTTGCCATCGGATGTGCCCAGATGGGATTAGCTAGTAGGTGGGGTAACGGCTCACC
TAGGCGACGATCCCTAGCTGGTCTGAGAGGATGACCAGCCACACTGGAACTGAGACACGGTCCAGACTCCT
ACGGGAGGCAGCAGTGGGGAATATTGCACAATGGGCGCAAGCCTGATGCAGCCATGCCGCGTGTATGAAGA
AGGCCTTCGGGTTGTAAAGTACTTTCAGCGGGGAGGAAGGGAGTAAAGTTAATACCTTTGCTCATTGACGT
TACCCGCAGAAGAAGCACCGGCTAACTCCGTGCCAGCAGCCGCGGTAATACGGAGGGTGCAAGCGTTAATC
GGAATTACTGGGCGTAAAGCGCACGCAGGCGGTTTGTTAAGTCAGATGTGAAATCCCCGGGCTCAACCTGG
GAACTGCATCTGATACTGGCAAGCTTGAGTCTCGTAGAGGGGGGTAGAATTCCAGGTGTAGCGGTGAAATG
CGTAGAGATCTGGAGGAATACCGGTGGCGAAGGCGGCCCCCTGGACGAAGACTGACGCTCAGGTGCGAAAG
CGTGGGGAGCAAACAGGATTAGATACCCTGGTAGTCCACGCCGTAAACGATGTCGACTTGGAGGTTGTGCC
CTTGAGGCGTGGCTTCCGGAGCTAACGCGTTAAGTCGACCGCCTGGGGAGTACGGCCGCAAGGTTAAAACT
CAAATGAATTGACGGGGGCCCGCACAAGCGGTGGAGCATGTGGTTTAATTCGATGCAACGCGAAGAACCTT
ACCTGGTCTTGACATCCACAGAACTTTCCAGAGATGGATTGGTGCCTTCGGGAACTGTGAGACAGGTGCTG
CATGGCTGTCGTCAGCTCGTGTTGTGAAATGTTGGGTTAAGTCCCGCAACGAGCGCAACCCTTATCCTTTG
TTGCCAGCGGTCCGGCCGGGAACTCAAAGGAGACTGCCAGTGATAAACTGGAGGAAGGTGGGGATGACGTC
AAGTCATCATGGCCCTTACGACCAGGGCTACACACGTGCTACAATGGCGCATACAAAGAGAAGCGACCTCG
CGAGAGCAAGCGGACCTCATAAAGTGCGTCGTAGTCCGGATTGGAGTCTGCAACTCGACTCCATGAAGTCG
GAATCGCTAGTAATCGTGGATCAGAATGCCACGGTGAATACGTTCCCGGGCCTTGTACACACCGCCCGTCA
CACCATGGGAGTGGGTTGCAAAAGAAGTAGGTAGCTTAACCTTCGGGAGGGCGCTACCA

### 8.1.3. Isolate 14 (1380 bp)

CTTTGCTGACGAGTGGCGGACGGGTGAGTAATGTCTGGGAAACTGCCTGATGGAGGGGGATAACTACTGGA
AACGGTAGCTAATACCGCATAACGTCGCAAGACCAAAGAGGGGGACCTTCGGGCCTCTTGCCATCGGATGT
GCCCAGATGGGATTAGCTAGTAGGTGGGGTAACGGCTCACCTAGGCGACGATCCCTAGCTGGTCTGAGAGG
ATGACCAGCCACACTGGAACTGAGACACGGTCCAGACTCCTACGGGAGGCAGCAGTGGGGAATATTGCACA
ATGGGCGCAAGCCTGATGCAGCCATGCCGCGTGTATGAAGAAGGCCTTCGGGTTGTAAAGTACTTTCAGCG
GGGAGGAAGGGAGTAAAGTTAATACCTTTGCTCATTGACGTTACCCGCAGAAGAAGCACCGGNCTAANTCC
GTGCCAGCAGCCGCGGTAATACGGAGGGTGCAAGCGTTAATCGGAATTACTGGGCGTAAAGCGCACGCAGG
CGGTTTGTTAAGTCAGATGTGAAATCCCCGGGCTCAACCTGGGAACTGCATCTGATACTGGCAAGCTTGAG
TCTCGTAGAGGGGGGTAGAATTCCAGGTGTAGCGGTGAAATGCGTAGAGATCTGGAGGAATACCGGTGGCG
AAGGCGGCCCCCTGGACGAAGACTGACGCTCAGGTGCGAAAGCGTGGGGAGCAAACAGGATTAGATACCCT
GGTAGTCCACGCCGTAAACGATGTCGACTTGGAGGTTGTGCCCTTGAGGCGTGGCTTCCGGAGCTAACGCG
TTAAGTCGACCGCCTGGGGAGTACGGCCGCAAGGTTAAAACTCAAATGAATTGACGGGGGCCCGCACAAGC
GGTGGAGCATGTGGTTTAATTCGATGCAACGCGAAGAACCTTACCTGGTCTTGACATCCACAGAANTTTNC
AGAGATGNNNNNGTGCCTTCGGGAACNGTGAGACAGGTGCTGCATGGCTGTCGTCAGCTCGTGTTGTGAAA
TGTTGGGTTAAGTCCCGCAACGAGCGCAACCCTTATCCTTTGTTGCCAGCGGTCCGGCCGGGAACTCAAAG
GAGACTGCCAGTGATAAACTGGAGGAAGGTGGGGATGACGTCAAGTCATCATGGCCCTTACGACCAGGGCT
ACACACGTGCTACAATGGCGCATACAAAGAGAAGCGACCTCGCGAGAGCAAGCGGACCTCATAAAGTGCGT
CGTAGTCCGGATTGGAGTCTGCAACTCGACTCCATGAAGTCGGAATCGCTAGTAATCGTGGATCAGAATGC
CACGGTGAATACGTTCCCGGGCCTTGTACACACCGCCCGTCACACCATGGGAGTGGGTTGCAAAAGAAGTA
GGTAGCTTAACCTTCGGGAGGGCGCTACCAC

### 8.1.4. Isolate 36 (1139 bp)

ATACCGCATAACGTCGCAAGACCAAAGAGGGGGACCTTAGGGCCTCTTGCCATCGGATGTGCCCAGATGGG
ATTAGCTAGTAGGTGGGGTACGGCTCACCTAGGCGACGATCCCTAGCTGGTCTGNGAGGATGACCGCCACA
CTGGAACTGAGACACGGTCCAGACTCCTACGGGAGGCAGCAGTGGGGAATATTGCACAATGGGCCAAGCCT
GATGCAGCCATGCCGCGTGTATGAAGAGGCCTTCGGGTTGTAAAGTACTTTCAGCGGGGAGGAAGGGAGTA
AAGTTAATACCTTTGCTCATTGACGTTACCCGCAGAAGAAGCACCGGCTAACTCCGTGCCAGCAGCCGCGG
TAATACGGAGGGTGCAAGCGTTAATCGGAATTACTGGGCGTAAAGCGCACGCAGGCGGTTTGTTAAGTCAG
ATGTGAAATCCCCGGGCTCAACCTGGGAACTGCATCTGATACTGGCAAGCTTGAGTCTCGTAGAGGGGGGT
AGAATTCCAGGTGTAGCGGTGAAATGCGTAGAGATCTGGAGGAATACCGGTGGCGAAGGCGGCCCCCTGGA
CGAAGACTGACGCTCAGGTGCGAAAGCGTGGGGAGCAAACAGGATTAGATACCCTGGTAGTCCACGCCGTA
AACGATGTCGACTTGGAGGTTGTGCCCTTGAGGCGTGGCTTCCGGAGCTAACGCGTTAAGTCGACCGCCTG
GGGAGTACGGCCGCAAGGTTAAAACTCAAATGAATTGACGGGGGCCCGCACAAGCGGTGGAGCATGTGGTT
TAATTCGATGCAACGCGAAGAACCTTACCTGGTCTTGACATCCACGGAAGTTTTCAGAGATGAGAATGTGC
CTTCGGGAACCGTGAGACAGGTGCTGCATGGCTGTCGTCAGCTCGTGTTGTGAAATGTTGGGTTAAGTCCC
GCAACGAGCGCAACCCTTATCCTTTGTTGCCAGCGGTCCGGCCGGGAACTCAAAGGAGACTGCCAGTGATA
AACTGGAGGAAGGTGGGGATGACGTCAAGTCATCATGGCCCTTACGACCAGGGCTACACACGTGCTACAAT
GGCGCATACAAAGAGAAGCGACCTCGCGAGAGCAAGCGGACCTCATAAAGTGCGTCGTAGTCCGGATTGGA
GTC

## 8.2. Alignments

### 8.2.1. Alignment of all Four Sequenced Strains

```
          1         10         20         30         40         50         60
          |         |          |          |          |          |          |
MG1655    ----------------------------------GCTGACGAGTGGCGGACGGGTGAGTA
Iso 8     AGTCGAACGGTAACAGGAAGCAGCTTGCTGCTTCGCTGACGAGTGGCGGACGGGTGAGTA
Iso 14    -------------------------------CTTTGCTGACGAGTGGCGGACGGGTGAGTA
Iso 36    ------------------------------------------------------------

MG1655    ATGTCTGGGAAACTGCCTGATGGAGGGGGATAACTACTGGAAACGGTAGCTAATACCGCA
Iso 8     ATGTCTGGGAAACTGCCTGATGGAGGGGGATAACTACTGGAAACGGTAGCTAATACCGCA
Iso 14    ATGTCTGGGAAACTGCCTGATGGAGGGGGATAACTACTGGAAACGGTAGCTAATACCGCA
Iso 36    ----------------------------------------------------ATACCGCA

MG1655    TAACGTCGCAAGACCAAAGAGGGGGACCTTCGGGCCTCTTGCCATCGGATGTGCCCAGAT
Iso 8     TAACGTCGCAAGACCAAAGAGGGGGACCTTCGGGCCTCTTGCCATCGGATGTGCCCAGAT
Iso 14    TAACGTCGCAAGACCAAAGAGGGGGACCTTCGGGCCTCTTGCCATCGGATGTGCCCAGAT
Iso 36    TAACGTCGCAAGACCAAAGAGGGGGACCTTAGGGCCTCTTGCCATCGGATGTGCCCAGAT

MG1655    GGGATTAGCTAGTAGGTGGGGTAACGGCTCACCTAGGCGACGATCCCTAGCTGGTCTGAG
Iso 8     GGGATTAGCTAGTAGGTGGGGTAACGGCTCACCTAGGCGACGATCCCTAGCTGGTCTGAG
Iso 14    GGGATTAGCTAGTAGGTGGGGTAACGGCTCACCTAGGCGACGATCCCTAGCTGGTCTGAG
Iso 36    GGGATTAGCTAGTAGGTGGGGT-ACGGCTCACCTAGGCGACGATCCCTAGCTGGTCTGNG

MG1655    AGGATGACCAGCCACACTGGAACTGAGACACGGTCCAGACTCCTACGGGAGGCAGCAGTG
Iso 8     AGGATGACCAGCCACACTGGAACTGAGACACGGTCCAGACTCCTACGGGAGGCAGCAGTG
Iso 14    AGGATGACCAGCCACACTGGAACTGAGACACGGTCCAGACTCCTACGGGAGGCAGCAGTG
Iso 36    AGGATGACC-GCCACACTGGAACTGAGACACGGTCCAGACTCCTACGGGAGGCAGCAGTG

MG1655    GGGAATATTGCACAATGGGCGCAAGCCTGATGCAGCCATGCCGCGTGTATGAAGAAGGCC
Iso 8     GGGAATATTGCACAATGGGCGCAAGCCTGATGCAGCCATGCCGCGTGTATGAAGAAGGCC
Iso 14    GGGAATATTGCACAATGGGCGCAAGCCTGATGCAGCCATGCCGCGTGTATGAAGAAGGCC
Iso 36    GGGAATATTGCACAATGGGC-CAAGCCTGATGCAGCCATGCCGCGTGTATGAAGA-GGCC

MG1655    TTCGGGTTGTAAAGTACTTTCAGCGGGGAGGAAGGGAGTAAAGTTAATACCTTTGCTCAT
Iso 8     TTCGGGTTGTAAAGTACTTTCAGCGGGGAGGAAGGGAGTAAAGTTAATACCTTTGCTCAT
Iso 14    TTCGGGTTGTAAAGTACTTTCAGCGGGGAGGAAGGGAGTAAAGTTAATACCTTTGCTCAT
Iso 36    TTCGGGTTGTAAAGTACTTTCAGCGGGGAGGAAGGGAGTAAAGTTAATACCTTTGCTCAT

MG1655    TGACGTTACCCGCAGAAGAAGCACCGG-CTAACTCCGTGCCAGCAGCCGCGGTAATACGG
Iso 8     TGACGTTACCCGCAGAAGAAGCACCGG-CTAACTCCGTGCCAGCAGCCGCGGTAATACGG
Iso 14    TGACGTTACCCGCAGAAGAAGCACCGGNCTAANTCCGTGCCAGCAGCCGCGGTAATACGG
Iso 36    TGACGTTACCCGCAGAAGAAGCACCGG-CTAACTCCGTGCCAGCAGCCGCGGTAATACGG

MG1655    AGGGTGCAAGCGTTAATCGGAATTACTGGGCGTAAAGCGCACGCAGGCGGTTTGTTAAGT
Iso 8     AGGGTGCAAGCGTTAATCGGAATTACTGGGCGTAAAGCGCACGCAGGCGGTTTGTTAAGT
Iso 14    AGGGTGCAAGCGTTAATCGGAATTACTGGGCGTAAAGCGCACGCAGGCGGTTTGTTAAGT
Iso 36    AGGGTGCAAGCGTTAATCGGAATTACTGGGCGTAAAGCGCACGCAGGCGGTTTGTTAAGT

MG1655    CAGATGTGAAATCCCCGGGCTCAACCTGGGAACTGCATCTGATACTGGCAAGCTTGAGTC
Iso 8     CAGATGTGAAATCCCCGGGCTCAACCTGGGAACTGCATCTGATACTGGCAAGCTTGAGTC
Iso 14    CAGATGTGAAATCCCCGGGCTCAACCTGGGAACTGCATCTGATACTGGCAAGCTTGAGTC
Iso 36    CAGATGTGAAATCCCCGGGCTCAACCTGGGAACTGCATCTGATACTGGCAAGCTTGAGTC
```

```
MG1655  TCGTAGAGGGGGGTAGAATTCCAGGTGTAGCGGTGAAATGCGTAGAGATCTGGAGGAATA
Iso 8   TCGTAGAGGGGGGTAGAATTCCAGGTGTAGCGGTGAAATGCGTAGAGATCTGGAGGAATA
Iso 14  TCGTAGAGGGGGGTAGAATTCCAGGTGTAGCGGTGAAATGCGTAGAGATCTGGAGGAATA
Iso 36  TCGTAGAGGGGGGTAGAATTCCAGGTGTAGCGGTGAAATGCGTAGAGATCTGGAGGAATA

MG1655  CCGGTGGCGAAGGCGGCCCCCTGGACGAAGACTGACGCTCAGGTGCGAAAGCGTGGGGAG
Iso 8   CCGGTGGCGAAGGCGGCCCCCTGGACGAAGACTGACGCTCAGGTGCGAAAGCGTGGGGAG
Iso 14  CCGGTGGCGAAGGCGGCCCCCTGGACGAAGACTGACGCTCAGGTGCGAAAGCGTGGGGAG
Iso 36  CCGGTGGCGAAGGCGGCCCCCTGGACGAAGACTGACGCTCAGGTGCGAAAGCGTGGGGAG

MG1655  CAAACAGGATTAGATACCCTGGTAGTCCACGCCGTAAACGATGTCGACTTGGAGGTTGTG
Iso 8   CAAACAGGATTAGATACCCTGGTAGTCCACGCCGTAAACGATGTCGACTTGGAGGTTGTG
Iso 14  CAAACAGGATTAGATACCCTGGTAGTCCACGCCGTAAACGATGTCGACTTGGAGGTTGTG
Iso 36  CAAACAGGATTAGATACCCTGGTAGTCCACGCCGTAAACGATGTCGACTTGGAGGTTGTG

MG1655  CCCTTGAGGCGTGGCTTCCGGAGCTAACGCGTTAAGTCGACCGCCTGGGGAGTACGGCCG
Iso 8   CCCTTGAGGCGTGGCTTCCGGAGCTAACGCGTTAAGTCGACCGCCTGGGGAGTACGGCCG
Iso 14  CCCTTGAGGCGTGGCTTCCGGAGCTAACGCGTTAAGTCGACCGCCTGGGGAGTACGGCCG
Iso 36  CCCTTGAGGCGTGGCTTCCGGAGCTAACGCGTTAAGTCGACCGCCTGGGGAGTACGGCCG

MG1655  CAAGGTTAAAACTCAAATGAATTGACGGGGGCCCGCACAAGCGGTGGAGCATGTGGTTTA
Iso 8   CAAGGTTAAAACTCAAATGAATTGACGGGGGCCCGCACAAGCGGTGGAGCATGTGGTTTA
Iso 14  CAAGGTTAAAACTCAAATGAATTGACGGGGGCCCGCACAAGCGGTGGAGCATGTGGTTTA
Iso 36  CAAGGTTAAAACTCAAATGAATTGACGGGGGCCCGCACAAGCGGTGGAGCATGTGGTTTA

MG1655  ATTCGATGCAACGCGAAGAACCTTACCTGGTCTTGACATCCACGGAAGTTTTCAGAGATG
Iso 8   ATTCGATGCAACGCGAAGAACCTTACCTGGTCTTGACATCCACAGAACTTTCCAGAGATG
Iso 14  ATTCGATGCAACGCGAAGAACCTTACCTGGTCTTGACATCCACAGAANTTTNCAGAGATG
Iso 36  ATTCGATGCAACGCGAAGAACCTTACCTGGTCTTGACATCCACGGAAGTTTTCAGAGATG

MG1655  AGAATGTGCCTTCGGGAACCGTGAGACAGGTGCTGCATGGCTGTCGTCAGCTCGTGTTGT
Iso 8   GATTGGTGCCTTCGGGAACTGTGAGACAGGTGCTGCATGGCTGTCGTCAGCTCGTGTTGT
Iso 14  NNNNNGTGCCTTCGGGAACNGTGAGACAGGTGCTGCATGGCTGTCGTCAGCTCGTGTTGT
Iso 36  AGAATGTGCCTTCGGGAACCGTGAGACAGGTGCTGCATGGCTGTCGTCAGCTCGTGTTGT

MG1655  GAAATGTTGGGTTAAGTCCCGCAACGAGCGCAACCCTTATCCTTTGTTGCCAGCGGTCCG
Iso 8   GAAATGTTGGGTTAAGTCCCGCAACGAGCGCAACCCTTATCCTTTGTTGCCAGCGGTCCG
Iso 14  GAAATGTTGGGTTAAGTCCCGCAACGAGCGCAACCCTTATCCTTTGTTGCCAGCGGTCCG
Iso 36  GAAATGTTGGGTTAAGTCCCGCAACGAGCGCAACCCTTATCCTTTGTTGCCAGCGGTCCG

MG1655  GCCGGGAACTCAAAGGAGACTGCCAGTGATAAACTGGAGGAAGGTGGGGATGACGTCAAG
Iso 8   GCCGGGAACTCAAAGGAGACTGCCAGTGATAAACTGGAGGAAGGTGGGGATGACGTCAAG
Iso 14  GCCGGGAACTCAAAGGAGACTGCCAGTGATAAACTGGAGGAAGGTGGGGATGACGTCAAG
Iso 36  GCCGGGAACTCAAAGGAGACTGCCAGTGATAAACTGGAGGAAGGTGGGGATGACGTCAAG

MG1655  TCATCATGGCCCTTACGACCAGGGCTACACACGTGCTACAATGGCGCATACAAAGAGAAG
Iso 8   TCATCATGGCCCTTACGACCAGGGCTACACACGTGCTACAATGGCGCATACAAAGAGAAG
Iso 14  TCATCATGGCCCTTACGACCAGGGCTACACACGTGCTACAATGGCGCATACAAAGAGAAG
Iso 36  TCATCATGGCCCTTACGACCAGGGCTACACACGTGCTACAATGGCGCATACAAAGAGAAG

MG1655  CGACCTCGCGAGAGCAAGCGGACCTCATAAAGTGCGTCGTAGTCCGGATTGGAGTCTGCA
Iso 8   CGACCTCGCGAGAGCAAGCGGACCTCATAAAGTGCGTCGTAGTCCGGATTGGAGTCTGCA
Iso 14  CGACCTCGCGAGAGCAAGCGGACCTCATAAAGTGCGTCGTAGTCCGGATTGGAGTCTGCA
Iso 36  CGACCTCGCGAGAGCAAGCGGACCTCATAAAGTGCGTCGTAGTCCGGATTGGAGTC----
```

```
MG1655  ACTCGACTCCATGAAGTCGGAATCGCTAGTAATCGTGGATCAGAATGCCACGGTGAATAC
Iso 8   ACTCGACTCCATGAAGTCGGAATCGCTAGTAATCGTGGATCAGAATGCCACGGTGAATAC
Iso 14  ACTCGACTCCATGAAGTCGGAATCGCTAGTAATCGTGGATCAGAATGCCACGGTGAATAC
Iso 36  ------------------------------------------------------------

MG1655  GTTCCCGGGCCTTGTACACACCGCCCGTCACACCATGGGAGTGGGTTGCAAAAGAAGTAG
Iso 8   GTTCCCGGGCCTTGTACACACCGCCCGTCACACCATGGGAGTGGGTTGCAAAAGAAGTAG
Iso 14  GTTCCCGGGCCTTGTACACACCGCCCGTCACACCATGGGAGTGGGTTGCAAAAGAAGTAG
Iso 36  ------------------------------------------------------------

MG1655  GTAGCTTAACCTTCGGGAGGGCGCTACCAC
Iso 8   GTAGCTTAACCTTCGGGAGGGCGCTACCA-
Iso 14  GTAGCTTAACCTTCGGGAGGGCGCTACCAC
Iso 36  -----------------------------
```

### 8.2.2. Alignment Statistics for all Four Sequences

Length: 1410
Pairwise % Identity: 99.2%
Identical Sites: 1127 (79.9%)

### 8.2.3. BLAST Search Results for all Four Sequences

#### 8.2.3.1. *E. coli* MG1655

| Hit No. | Hit Description | Hit Accession | HSP Score | HSP Identity |
|---|---|---|---|---|
| 1 | Escherichia coli EC4100B ECL.Contig132_1, whole genome shotgun sequence | AERU01000014 | 1372 | 1375 |
| 2 | Escherichia coli EC4100B ECL.Contig121_1, whole genome shotgun sequence | AERU01000035 | 1372 | 1375 |
| 3 | Escherichia coli O157:H7 str. EC1212 ECD.Contig131_1, whole genome shotgun sequence | AERQ01000020 | 1372 | 1375 |
| 4 | Escherichia coli 3431 gec3431.assembly.64, whole genome shotgun sequence | ADUM01000088 | 1372 | 1375 |
| 5 | Escherichia coli 3431 gec3431.assembly.65, whole genome shotgun sequence | ADUM01000089 | 1372 | 1375 |
| 6 | Escherichia coli TW14425 TW14425_c19, whole genome shotgun sequence | AELE01000019 | 1372 | 1375 |
| 7 | Escherichia coli MS 145-7 E_coliMS145-7-1.0.1_Cont31.1, whole genome shotgun sequence | ADWS01000032 | 1372 | 1375 |
| 8 | Escherichia coli MS 115-1 E_coli115-1-1.0_Cont12.1, whole genome shotgun sequence | ADTL01000003 | 1372 | 1375 |
| 9 | Escherichia coli FVEC1412 cont1.110, whole genome shotgun sequence | ACXI01000110 | 1372 | 1375 |
| 10 | Escherichia coli TA271 cont1.142, whole genome shotgun sequence | ADAZ01000142 | 1372 | 1375 |
| 11 | Escherichia coli H736 cont1.89, whole genome shotgun sequence | ADAU01000089 | 1372 | 1375 |
| 12 | Escherichia coli M605 cont1.94, whole genome shotgun sequence | ADAV01000094 | 1372 | 1375 |
| 13 | Escherichia coli TA143 cont1.141, whole genome shotgun sequence | ADAY01000141 | 1372 | 1375 |
| 14 | Escherichia sp. 1_1_43 cont1.33, whole genome shotgun sequence | ACID01000033 | 1372 | 1375 |
| 15 | Escherichia coli O157:H7 str. EC4042 gcontig_1113125281292, whole genome shotgun sequence | ABHM02000001 | 1372 | 1375 |
| 16 | Escherichia coli O157:H7 str. EC4045 gcontig_1113126024325, whole genome shotgun sequence | ABHL02000001 | 1372 | 1375 |
| 17 | Escherichia coli O157:H7 str. EC4206 gcontig_1113126024111, whole genome shotgun sequence | ABHK02000001 | 1372 | 1375 |
| 18 | Escherichia coli E110019 gcontig_1112495928714, whole genome shotgun sequence | AAJW02000003 | 1372 | 1375 |
| 19 | Escherichia coli E110019 gcontig_1112495928756, whole genome shotgun sequence | AAJW02000004 | 1372 | 1375 |
| 20 | Escherichia coli E110019 gcontig_1112495928844, whole genome shotgun sequence | AAJW02000060 | 1372 | 1375 |
| 21 | Escherichia coli 53638 gcontig_1105238512145, whole genome shotgun sequence | AAKB02000001 | 1372 | 1375 |
| 22 | Escherichia coli O157:H7 str. EC4196 gcontig_1105416507183, whole genome shotgun sequence | ABHO01000004 | 1372 | 1375 |
| 23 | Escherichia coli O157:H7 str. TW14359, complete genome | NC_013008 | 1372 | 1375 |
| 24 | Escherichia coli BW2952, complete genome | NC_012759 | 1372 | 1375 |
| 25 | Escherichia coli UMN026, complete genome | NC_011751 | 1372 | 1375 |
| 26 | Escherichia coli S88, complete genome | NC_011742 | 1369 | 1374 |
| 27 | Escherichia coli IAI1, complete genome | NC_011741 | 1372 | 1375 |
| 28 | Escherichia fergusonii ATCC 35469, complete genome | NC_011740 | 1372 | 1375 |
| 29 | Escherichia coli O127:H6 str. E2348/69, complete genome | NC_011601 | 1372 | 1375 |
| 30 | Escherichia coli SE11 chromosome, complete genome | NC_011415 | 1372 | 1375 |
| 31 | Escherichia coli O157:H7 str. EC4115, complete genome | NC_011353 | 1372 | 1375 |

| | | | | |
|---|---|---|---|---|
| 32 | Escherichia coli str. K-12 substr. DH10B, complete genome | NC_010473 | 1372 | 1375 |
| 33 | Escherichia coli ATCC 8739, complete genome | NC_010468 | 1372 | 1375 |
| 34 | Escherichia coli UTI89 chromosome, complete genome | NC_007946 | 1372 | 1375 |
| 35 | Escherichia coli str. K-12 substr. W3110 chromosome, complete genome | AC_000091 | 1372 | 1375 |
| 36 | Escherichia coli str. K-12 substr. MG1655 chromosome, complete genome | NC_000913 | 1372 | 1375 |
| 37 | Escherichia coli RN587/1 RN587.assembly.32, whole genome shotgun sequence | ADUS01000025 | 1369 | 1374 |
| 38 | Escherichia coli RN587/1 RN587.assembly.36, whole genome shotgun sequence | ADUS01000029 | 1369 | 1374 |
| 39 | Escherichia coli 1357 OK1357.assembly.173, whole genome shotgun sequence | ADUR01000081 | 1369 | 1374 |
| 40 | Escherichia coli LT-68 gecLT68.assembly.37, whole genome shotgun sequence | ADUP01000030 | 1369 | 1374 |
| 41 | Escherichia coli LT-68 gecLT68.assembly.39, whole genome shotgun sequence | ADUP01000032 | 1369 | 1374 |
| 42 | Escherichia coli LT-68 gecLT68.assembly.40, whole genome shotgun sequence | ADUP01000034 | 1369 | 1374 |
| 43 | Shigella sonnei 53G gss53G.assembly.144, whole genome shotgun sequence | ADUU01000047 | 1369 | 1374 |
| 44 | Escherichia coli WV_060327, whole genome shotgun sequence | AERT01000002 | 1369 | 1374 |
| 45 | Escherichia coli WV_060327, whole genome shotgun sequence | AERT01000016 | 1369 | 1374 |
| 46 | Shigella boydii ATCC 9905 SGB.Contig113_1, whole genome shotgun sequence | AERN01000056 | 1369 | 1374 |
| 47 | Escherichia coli 3431 gec3431.assembly.47, whole genome shotgun sequence | ADUM01000069 | 1369 | 1374 |
| 48 | Shigella flexneri 2a str. 2457T gss2457T.assembly.65, whole genome shotgun sequence | ADUV01000061 | 1369 | 1374 |
| 49 | Escherichia coli 2362-75 gec2362.assembly.47, whole genome shotgun sequence | ADUL01000041 | 1369 | 1374 |
| 50 | Escherichia coli 2362-75 gec2362.assembly.55, whole genome shotgun sequence | ADUL01000050 | 1369 | 1374 |
| 51 | Escherichia coli 1827-70 gec1827.assembly.31, whole genome shotgun sequence | ADUK01000024 | 1369 | 1374 |
| 52 | Escherichia coli MS 153-1 E_coli153-1-1.0_Cont20.1, whole genome shotgun sequence | ADTX01000014 | 1369 | 1374 |
| 53 | Escherichia coli TA206 cont1.157, whole genome shotgun sequence | ADAX01000157 | 1369 | 1374 |
| 54 | Escherichia coli 83972 contig00152, whole genome shotgun sequence | ACGN01000123 | 1369 | 1374 |
| 55 | Shigella dysenteriae 1012 gcontig_1112603762653, whole genome shotgun sequence | AAMJ02000006 | 1369 | 1374 |
| 56 | Escherichia coli E110019 gcontig_1112495928854, whole genome shotgun sequence | AAJW02000005 | 1369 | 1374 |
| 57 | Escherichia coli F11 gcontig_1112495917000, whole genome shotgun sequence | AAJU02000010 | 1369 | 1374 |
| 58 | Escherichia coli O157:H7 str. EC508 gcontig_1108341391741, whole genome shotgun sequence | ABHW01000042 | 1369 | 1374 |
| 59 | Escherichia coli O157:H7 str. EC4076 gcontig_1105762734293, whole genome shotgun sequence | ABHQ01000001 | 1369 | 1374 |
| 60 | Escherichia coli O111:H- str. 11128, complete genome | NC_013364 | 1369 | 1374 |
| 61 | Escherichia coli O26:H11 str. 11368, complete genome | NC_013361 | 1369 | 1374 |
| 62 | Escherichia coli B str. REL606 chromosome, complete genome | NC_012967 | 1369 | 1374 |
| 63 | Escherichia coli BL21-Gold(DE3)pLysS AG chromosome, complete genome | NC_012947 | 1369 | 1374 |
| 64 | Escherichia coli ED1a chromosome, complete genome | NC_011745 | 1369 | 1374 |
| 65 | Escherichia coli E24377A, complete genome | NC_009801 | 1369 | 1374 |
| 66 | Escherichia coli APEC O1, complete genome | NC_008563 | 1369 | 1374 |

| | | | | |
|---|---|---|---|---|
| 67 | Shigella flexneri 5 str. 8401, complete genome | NC_008258 | 1369 | 1374 |
| 68 | Escherichia coli 536, complete genome | NC_008253 | 1369 | 1374 |
| 69 | Shigella boydii Sb227, complete genome | NC_007613 | 1369 | 1374 |
| 70 | Shigella sonnei Ss046, complete genome | NC_007384 | 1369 | 1374 |
| 71 | Escherichia coli O157:H7 str. EDL933 chromosome, complete genome | NC_002655 | 1369 | 1374 |
| 72 | Escherichia coli O157:H7 str. Sakai, complete genome | NC_002695 | 1369 | 1374 |
| 73 | Shigella flexneri 2a str. 301, complete genome | NC_004337 | 1369 | 1374 |
| 74 | Shigella boydii ATCC 9905 SGB.Contig115_1, whole genome shotgun sequence | AERN01000004 | 1367 | 1374 |
| 75 | Escherichia coli 2362-75 gec2362.assembly.61, whole genome shotgun sequence | ADUL01000057 | 1367 | 1374 |
| 76 | Escherichia coli 2362-75 gec2362.assembly.74, whole genome shotgun sequence | ADUL01000071 | 1367 | 1374 |
| 77 | Escherichia coli 2362-75 gec2362.assembly.83, whole genome shotgun sequence | ADUL01000081 | 1367 | 1374 |
| 78 | Escherichia coli F11 gcontig_1112495918566, whole genome shotgun sequence | AAJU02000050 | 1367 | 1374 |
| 79 | Escherichia coli CFT073, complete genome | NC_004431 | 1367 | 1373 |
| 80 | Escherichia coli RN587/1 RN587.assembly.30, whole genome shotgun sequence | ADUS01000023 | 1366 | 1374 |
| 81 | Escherichia coli 1180 OK1180.assembly.81, whole genome shotgun sequence | ADUQ01000078 | 1366 | 1373 |
| 82 | Shigella flexneri 2a str. 2457T gss2457T.assembly.51, whole genome shotgun sequence | ADUV01000046 | 1366 | 1373 |
| 83 | Shigella flexneri 2a str. 2457T gss2457T.assembly.58, whole genome shotgun sequence | ADUV01000053 | 1366 | 1373 |
| 84 | Escherichia coli NC101 contig6, whole genome shotgun sequence | AEFA01000022 | 1366 | 1373 |
| 85 | Escherichia coli F11 gcontig_1112495914622, whole genome shotgun sequence | AAJU02000017 | 1366 | 1373 |
| 86 | Escherichia coli F11 gcontig_1112495919726, whole genome shotgun sequence | AAJU02000035 | 1366 | 1373 |
| 87 | Escherichia coli O157:H7 str. EC4486 gcontig_1106603634670, whole genome shotgun sequence | ABHS01000045 | 1366 | 1374 |
| 88 | Escherichia coli O55:H7 str. CB9615 chromosome, complete genome | NC_013941 | 1366 | 1373 |
| 89 | Escherichia coli SMS-3-5, complete genome | NC_010498 | 1366 | 1373 |
| 90 | Shigella flexneri 2a str. 2457T, complete genome | NC_004741 | 1366 | 1373 |
| 91 | Escherichia coli EPECa14 EPECa14.assembly.156, whole genome shotgun sequence | ADUN01000062 | 1364 | 1374 |
| 92 | Escherichia coli 1357 OK1357.assembly.168, whole genome shotgun sequence | ADUR01000075 | 1363 | 1372 |
| 93 | Escherichia coli LT-68 gecLT68.assembly.36, whole genome shotgun sequence | ADUP01000029 | 1363 | 1372 |
| 94 | Escherichia coli LT-68 gecLT68.assembly.38, whole genome shotgun sequence | ADUP01000031 | 1363 | 1372 |
| 95 | Shigella flexneri 2a str. 2457T gss2457T.assembly.50, whole genome shotgun sequence | ADUV01000045 | 1363 | 1372 |
| 96 | Shigella flexneri 2a str. 2457T gss2457T.assembly.55, whole genome shotgun sequence | ADUV01000050 | 1363 | 1372 |
| 97 | Shigella flexneri 2a str. 2457T gss2457T.assembly.69, whole genome shotgun sequence | ADUV01000065 | 1363 | 1372 |
| 98 | Escherichia coli 2362-75 gec2362.assembly.56, whole genome shotgun sequence | ADUL01000051 | 1363 | 1372 |
| 99 | Escherichia coli TW10828 TW10828_c1, whole genome shotgun sequence | AELC01000001 | 1363 | 1372 |
| 100 | Escherichia coli TW10828 TW10828_c31, whole genome shotgun sequence | AELC01000031 | 1363 | 1372 |

### 8.2.3.2. Isolate 8

| Hit No. | Hit def | Hit accession | HSP Score | HSP Identity |
|---|---|---|---|---|
| 1 | Escherichia coli TW14425 TW14425_c28, whole genome shotgun sequence | AELE01000028 | 1405 | 1408 |
| 2 | Escherichia coli TW11681 TW11681_c6, whole genome shotgun sequence | AELD01000006 | 1405 | 1408 |
| 3 | Escherichia coli TW11681 TW11681_c33, whole genome shotgun sequence | AELD01000033 | 1405 | 1408 |
| 4 | Escherichia coli TW11681 TW11681_lrc1077, whole genome shotgun sequence | AELD01000130 | 1405 | 1408 |
| 5 | Escherichia coli 1827-70 gec1827.assembly.32, whole genome shotgun sequence | ADUK01000025 | 1405 | 1408 |
| 6 | Escherichia coli 1827-70 gec1827.assembly.35, whole genome shotgun sequence | ADUK01000028 | 1405 | 1408 |
| 7 | Escherichia coli MS 85-1 E_coliMS85-1-1.0.1_Cont119.1, whole genome shotgun sequence | ADWQ01000120 | 1405 | 1408 |
| 8 | Escherichia coli E22 gcontig_1112495660814, whole genome shotgun sequence | AAJV02000013 | 1405 | 1408 |
| 9 | Escherichia coli 53638 gcontig_1105238512145, whole genome shotgun sequence | AAKB02000001 | 1405 | 1408 |
| 10 | Escherichia coli O103:H2 str. 12009, complete genome | NC_013353 | 1405 | 1408 |
| 11 | Escherichia coli B str. REL606 chromosome, complete genome | NC_012967 | 1405 | 1408 |
| 12 | Escherichia coli BL21-Gold(DE3)pLysS AG chromosome, complete genome | NC_012947 | 1405 | 1408 |
| 13 | Escherichia coli ATCC 8739, complete genome | NC_010468 | 1405 | 1408 |
| 14 | Escherichia coli E22 gcontig_1112495647308, whole genome shotgun sequence | AAJV02000007 | 1403 | 1408 |
| 15 | Escherichia coli E128010 gecE128010.assembly.191, whole genome shotgun sequence | ADUO01000101 | 1402 | 1407 |
| 16 | Escherichia coli TW11681 TW11681_c9, whole genome shotgun sequence | AELD01000009 | 1402 | 1407 |
| 17 | Escherichia coli TW11681 TW11681_c25, whole genome shotgun sequence | AELD01000025 | 1402 | 1407 |
| 18 | Escherichia coli 1827-70 gec1827.assembly.31, whole genome shotgun sequence | ADUK01000024 | 1402 | 1407 |
| 19 | Escherichia coli MS 124-1 E_coliMS124-1-1.0.1_Cont14.1, whole genome shotgun sequence | ADWT01000015 | 1402 | 1407 |
| 20 | Escherichia coli IAI39 chromosome, complete genome | NC_011750 | 1402 | 1407 |
| 21 | Escherichia coli HS, complete genome | NC_009800 | 1402 | 1407 |
| 22 | Escherichia coli B354 cont1.60, whole genome shotgun sequence | ACXG01000060 | 1400 | 1407 |
| 23 | Escherichia coli E128010 gecE128010.assembly.120, whole genome shotgun sequence | ADUO01000023 | 1399 | 1406 |
| 24 | Escherichia coli TW14425 TW14425_c7, whole genome shotgun sequence | AELE01000007 | 1399 | 1406 |
| 25 | Escherichia coli TW14425 TW14425_c33, whole genome shotgun sequence | AELE01000033 | 1399 | 1406 |
| 26 | Escherichia coli TW14425 TW14425_c1523, whole genome shotgun sequence | AELE01000133 | 1399 | 1406 |
| 27 | Escherichia coli TW11681 TW11681_c53, whole genome shotgun sequence | AELD01000053 | 1399 | 1406 |
| 28 | Escherichia coli TW10598 TW10598_hyb_c7, whole genome shotgun sequence | AELA01000007 | 1399 | 1406 |
| 29 | Escherichia coli TW10598 TW10598_hyb_c34472, whole genome shotgun sequence | AELA01000276 | 1399 | 1406 |
| 30 | Escherichia coli TA280 cont1.126, whole genome shotgun sequence | ADBA01000126 | 1399 | 1406 |
| 31 | Escherichia coli E22 gcontig_1112495657964, whole genome shotgun sequence | AAJV02000011 | 1399 | 1406 |
| 32 | Escherichia coli E22 gcontig_1112495657890, whole genome shotgun sequence | AAJV02000053 | 1399 | 1406 |

| | | | | |
|---|---|---|---|---|
| 33 | Escherichia coli SE11 chromosome, complete genome | NC_011415 | 1399 | 1406 |
| 34 | Escherichia coli SMS-3-5, complete genome | NC_010498 | 1399 | 1406 |
| 35 | Shigella sonnei Ss046, complete genome | NC_007384 | 1399 | 1406 |
| 36 | Escherichia coli RN587/1 RN587.assembly.31, whole genome shotgun sequence | ADUS01000024 | 1396 | 1405 |
| 37 | Escherichia coli 1180 OK1180.assembly.78, whole genome shotgun sequence | ADUQ01000074 | 1396 | 1405 |
| 38 | Escherichia coli 1180 OK1180.assembly.85, whole genome shotgun sequence | ADUQ01000082 | 1396 | 1405 |
| 39 | Escherichia coli LT-68 gecLT68.assembly.35, whole genome shotgun sequence | ADUP01000028 | 1396 | 1405 |
| 40 | Escherichia coli E128010 gecE128010.assembly.197, whole genome shotgun sequence | ADUO01000107 | 1396 | 1405 |
| 41 | Escherichia coli 3431 gec3431.assembly.76, whole genome shotgun sequence | ADUM01000101 | 1396 | 1405 |
| 42 | Escherichia coli 1827-70 gec1827.assembly.24, whole genome shotgun sequence | ADUK01000016 | 1396 | 1405 |
| 43 | Escherichia coli B185 cont1.79, whole genome shotgun sequence | ACXF01000079 | 1396 | 1405 |
| 44 | Escherichia coli M718 cont1.141, whole genome shotgun sequence | ADAW01000141 | 1396 | 1405 |
| 45 | Escherichia coli O157:H7 str. TW14588 gcontig_1117790713610, whole genome shotgun sequence | ABKY02000001 | 1396 | 1405 |
| 46 | Escherichia coli O157:H7 str. EC4042 gcontig_1113125281292, whole genome shotgun sequence | ABHM02000001 | 1396 | 1405 |
| 47 | Escherichia coli O157:H7 str. EC4045 gcontig_1113126024325, whole genome shotgun sequence | ABHL02000001 | 1396 | 1405 |
| 48 | Escherichia coli E22 gcontig_1112495647362, whole genome shotgun sequence | AAJV02000012 | 1396 | 1405 |
| 49 | Escherichia coli O157:H7 str. EC4024 gcontig_1109799301388, whole genome shotgun sequence | ABJT01000130 | 1396 | 1405 |
| 50 | Escherichia coli O157:H7 str. EC4401 gcontig_1107724394665, whole genome shotgun sequence | ABHR01000045 | 1396 | 1405 |
| 51 | Escherichia coli O157:H7 str. EC4076 gcontig_1105762734371, whole genome shotgun sequence | ABHQ01000030 | 1396 | 1405 |
| 52 | Escherichia coli O157:H7 str. EC4113 gcontig_1105762725347, whole genome shotgun sequence | ABHP01000070 | 1396 | 1405 |
| 53 | Escherichia coli O157:H7 str. EC4113 gcontig_1105762730945, whole genome shotgun sequence | ABHP01000150 | 1396 | 1405 |
| 54 | Escherichia coli O157:H7 str. EC4196 gcontig_1105416507815, whole genome shotgun sequence | ABHO01000016 | 1396 | 1405 |
| 55 | Escherichia coli O55:H7 str. CB9615 chromosome, complete genome | NC_013941 | 1396 | 1405 |
| 56 | Escherichia coli O111:H- str. 11128, complete genome | NC_013364 | 1396 | 1405 |
| 57 | Escherichia coli O157:H7 str. TW14359, complete genome | NC_013008 | 1396 | 1405 |
| 58 | Escherichia coli UMN026, complete genome | NC_011751 | 1396 | 1405 |
| 59 | Escherichia coli IAI1, complete genome | NC_011741 | 1396 | 1405 |
| 60 | Escherichia coli O157:H7 str. EC4115, complete genome | NC_011353 | 1396 | 1405 |
| 61 | Escherichia coli O157:H7 str. Sakai, complete genome | NC_002695 | 1396 | 1405 |
| 62 | Escherichia coli TW10828 TW10828_c10, whole genome shotgun sequence | AELC01000010 | 1394 | 1405 |
| 63 | Escherichia coli FVEC1302 cont1.16, whole genome shotgun sequence | ACXH01000016 | 1394 | 1405 |
| 64 | Escherichia coli 1357 OK1357.assembly.140, whole genome shotgun sequence | ADUR01000045 | 1393 | 1404 |
| 65 | Escherichia coli 1180 OK1180.assembly.79, whole genome shotgun sequence | ADUQ01000075 | 1393 | 1404 |
| 66 | Escherichia coli O157:H7 str. EC1212 ECD.Contig132_1, whole genome shotgun sequence | AERQ01000011 | 1393 | 1404 |
| 67 | Escherichia coli TW14425 TW14425_c31, whole genome shotgun sequence | AELE01000031 | 1393 | 1404 |

| | | | | |
|---|---|---|---|---|
| 68 | Escherichia coli H591 cont1.156, whole genome shotgun sequence | ADBB01000156 | 1393 | 1406 |
| 69 | Escherichia coli O157:H7 str. FRIK2000 MBRI2000contig00335, whole genome shotgun sequence | ACXO01000167 | 1393 | 1404 |
| 70 | Escherichia coli O157:H7 str. EC4206 gcontig_1113126024111, whole genome shotgun sequence | ABHK02000001 | 1393 | 1404 |
| 71 | Escherichia coli O157:H7 str. EC508 gcontig_1108341390915, whole genome shotgun sequence | ABHW01000020 | 1393 | 1404 |
| 72 | Escherichia coli O157:H7 str. EC508 gcontig_1108341394631, whole genome shotgun sequence | ABHW01000162 | 1393 | 1404 |
| 73 | Escherichia coli O157:H7 str. EC869 gcontig_1106613681604, whole genome shotgun sequence | ABHU01000003 | 1393 | 1404 |
| 74 | Escherichia coli O157:H7 str. EC869 gcontig_1106613680316, whole genome shotgun sequence | ABHU01000005 | 1393 | 1404 |
| 75 | Escherichia coli O157:H7 str. EC869 gcontig_1106613679308, whole genome shotgun sequence | ABHU01000090 | 1393 | 1404 |
| 76 | Escherichia coli O157:H7 str. EC4501 gcontig_1106627451009, whole genome shotgun sequence | ABHT01000017 | 1393 | 1404 |
| 77 | Escherichia coli O157:H7 str. EC4501 gcontig_1106627450941, whole genome shotgun sequence | ABHT01000060 | 1393 | 1404 |
| 78 | Escherichia coli O157:H7 str. EC4486 gcontig_1106603635210, whole genome shotgun sequence | ABHS01000097 | 1393 | 1404 |
| 79 | Escherichia coli O157:H7 str. EC4076 gcontig_1105762734291, whole genome shotgun sequence | ABHQ01000005 | 1393 | 1404 |
| 80 | Escherichia coli O157:H7 str. EC4076 gcontig_1105762734269, whole genome shotgun sequence | ABHQ01000006 | 1393 | 1404 |
| 81 | Escherichia coli O157:H7 str. EC4076 gcontig_1105762734255, whole genome shotgun sequence | ABHQ01000079 | 1393 | 1404 |
| 82 | Escherichia coli O157:H7 str. EC4113 gcontig_1105762723171, whole genome shotgun sequence | ABHP01000024 | 1393 | 1404 |
| 83 | Escherichia coli O157:H7 str. EC4196 gcontig_1105416508497, whole genome shotgun sequence | ABHO01000053 | 1393 | 1404 |
| 84 | Escherichia coli BW2952, complete genome | NC_012759 | 1393 | 1404 |
| 85 | Escherichia coli 55989, complete genome | NC_011748 | 1393 | 1404 |
| 86 | Escherichia coli str. K-12 substr. DH10B, complete genome | NC_010473 | 1393 | 1404 |
| 87 | Escherichia coli E24377A, complete genome | NC_009801 | 1393 | 1404 |
| 88 | Escherichia coli str. K-12 substr. W3110 chromosome, complete genome | AC_000091 | 1393 | 1404 |
| 89 | Escherichia coli O157:H7 str. EDL933 chromosome, complete genome | NC_002655 | 1393 | 1404 |
| 90 | Escherichia coli str. K-12 substr. MG1655 chromosome, complete genome | NC_000913 | 1393 | 1404 |
| 91 | Escherichia coli RN587/1 RN587.assembly.30, whole genome shotgun sequence | ADUS01000023 | 1391 | 1404 |
| 92 | Escherichia coli E128010 gecE128010.assembly.196, whole genome shotgun sequence | ADUO01000106 | 1391 | 1404 |
| 93 | Shigella sonnei 53G gss53G.assembly.142, whole genome shotgun sequence | ADUU01000045 | 1390 | 1404 |
| 94 | Escherichia coli TW10722 TW10722_c9, whole genome shotgun sequence | AELB01000009 | 1390 | 1403 |
| 95 | Escherichia coli TW10722 TW10722_c17, whole genome shotgun sequence | AELB01000017 | 1390 | 1403 |
| 96 | Escherichia coli TW10722 TW10722_c42, whole genome shotgun sequence | AELB01000042 | 1390 | 1403 |
| 97 | Escherichia coli MS 79-10 E_coliMS79-10-1.0.1_Cont35.1, whole genome shotgun sequence | ADWR01000036 | 1390 | 1403 |
| 98 | Escherichia coli O26:H11 str. 11368, complete genome | NC_013361 | 1390 | 1403 |
| 99 | Escherichia coli TW10722 TW10722_c704, whole genome shotgun sequence | AELB01000337 | 1388 | 1402 |
| 100 | Escherichia coli 101-1 gcontig_1112603664959, whole genome shotgun sequence | AAMK02000047 | 1387 | 1401 |

### 8.2.3.3. Isolate 14

| Hit No. | Hit def | Hit accession | HSP score | HSP identity |
|---|---|---|---|---|
| 1 | Escherichia coli E128010 gecE128010.assembly.197, whole genome shotgun sequence | ADUO01000107 | 1356 | 1370 |
| 2 | Escherichia coli 3431 gec3431.assembly.76, whole genome shotgun sequence | ADUM01000101 | 1356 | 1370 |
| 3 | Escherichia coli 1827-70 gec1827.assembly.31, whole genome shotgun sequence | ADUK01000024 | 1356 | 1370 |
| 4 | Escherichia coli B185 cont1.79, whole genome shotgun sequence | ACXF01000079 | 1356 | 1370 |
| 5 | Escherichia coli TA280 cont1.126, whole genome shotgun sequence | ADBA01000126 | 1356 | 1370 |
| 6 | Escherichia coli M718 cont1.141, whole genome shotgun sequence | ADAW01000141 | 1356 | 1370 |
| 7 | Escherichia coli O157:H7 str. TW14588 gcontig_1117790713610, whole genome shotgun sequence | ABKY02000001 | 1356 | 1370 |
| 8 | Escherichia coli O157:H7 str. EC4042 gcontig_1113125281292, whole genome shotgun sequence | ABHM02000001 | 1356 | 1370 |
| 9 | Escherichia coli O157:H7 str. EC4045 gcontig_1113126024325, whole genome shotgun sequence | ABHL02000001 | 1353 | 1369 |
| 10 | Escherichia coli E22 gcontig_1112495647362, whole genome shotgun sequence | AAJV02000012 | 1356 | 1370 |
| 11 | Escherichia coli 53638 gcontig_1105238512145, whole genome shotgun sequence | AAKB02000001 | 1356 | 1370 |
| 12 | Escherichia coli O157:H7 str. EC4024 gcontig_1109799301388, whole genome shotgun sequence | ABJT01000130 | 1356 | 1370 |
| 13 | Escherichia coli O157:H7 str. EC4401 gcontig_1107724394665, whole genome shotgun sequence | ABHR01000045 | 1356 | 1370 |
| 14 | Escherichia coli O157:H7 str. EC4076 gcontig_1105762734371, whole genome shotgun sequence | ABHQ01000030 | 1356 | 1370 |
| 15 | Escherichia coli O157:H7 str. EC4113 gcontig_1105762725347, whole genome shotgun sequence | ABHP01000070 | 1356 | 1370 |
| 16 | Escherichia coli O157:H7 str. EC4113 gcontig_1105762730945, whole genome shotgun sequence | ABHP01000150 | 1356 | 1370 |
| 17 | Escherichia coli O157:H7 str. EC4196 gcontig_1105416507815, whole genome shotgun sequence | ABHO01000016 | 1356 | 1370 |
| 18 | Escherichia coli O55:H7 str. CB9615 chromosome, complete genome | NC_013941 | 1356 | 1370 |
| 19 | Escherichia coli O157:H7 str. TW14359, complete genome | NC_013008 | 1356 | 1370 |
| 20 | Escherichia coli IAI39 chromosome, complete genome | NC_011750 | 1356 | 1370 |
| 21 | Escherichia coli IAI1, complete genome | NC_011741 | 1356 | 1370 |
| 22 | Escherichia coli SE11 chromosome, complete genome | NC_011415 | 1356 | 1370 |
| 23 | Escherichia coli O157:H7 str. EC4115, complete genome | NC_011353 | 1356 | 1370 |
| 24 | Escherichia coli SMS-3-5, complete genome | NC_010498 | 1356 | 1370 |
| 25 | Escherichia coli ATCC 8739, complete genome | NC_010468 | 1356 | 1370 |
| 26 | Escherichia coli O157:H7 str. Sakai, complete genome | NC_002695 | 1356 | 1370 |
| 27 | Escherichia coli 1357 OK1357.assembly.140, whole genome shotgun sequence | ADUR01000045 | 1353 | 1369 |
| 28 | Escherichia coli EC4100B ECL.Contig132_1, whole genome shotgun sequence | AERU01000014 | 1353 | 1369 |
| 29 | Escherichia coli EC4100B ECL.Contig121_1, whole genome shotgun sequence | AERU01000035 | 1353 | 1369 |
| 30 | Escherichia coli O157:H7 str. EC1212 ECD.Contig132_1, whole genome shotgun sequence | AERQ01000011 | 1353 | 1369 |
| 31 | Escherichia coli O157:H7 str. EC1212 ECD.Contig131_1, whole genome shotgun sequence | AERQ01000020 | 1353 | 1369 |
| 32 | Escherichia coli 3431 gec3431.assembly.64, whole genome shotgun sequence | ADUM01000088 | 1353 | 1369 |
| 33 | Escherichia coli 3431 gec3431.assembly.65, whole genome shotgun sequence | ADUM01000089 | 1353 | 1369 |

| | | | | |
|---|---|---|---|---|
| 34 | Escherichia coli TW14425 TW14425_c28, whole genome shotgun sequence | AELE01000028 | 1353 | 1369 |
| 35 | Escherichia coli TW14425 TW14425_c31, whole genome shotgun sequence | AELE01000031 | 1353 | 1369 |
| 36 | Escherichia coli TW11681 TW11681_c6, whole genome shotgun sequence | AELD01000006 | 1353 | 1369 |
| 37 | Escherichia coli TW11681 TW11681_c33, whole genome shotgun sequence | AELD01000033 | 1353 | 1369 |
| 38 | Escherichia coli TW11681 TW11681_lrc1077, whole genome shotgun sequence | AELD01000130 | 1353 | 1369 |
| 39 | Escherichia coli 1827-70 gec1827.assembly.32, whole genome shotgun sequence | ADUK01000025 | 1353 | 1369 |
| 40 | Escherichia coli 1827-70 gec1827.assembly.35, whole genome shotgun sequence | ADUK01000028 | 1353 | 1369 |
| 41 | Escherichia coli MS 85-1 E_coliMS85-1-1.0.1_Cont119.1, whole genome shotgun sequence | ADWQ01000120 | 1353 | 1369 |
| 42 | Escherichia coli B354 cont1.60, whole genome shotgun sequence | ACXG01000060 | 1353 | 1370 |
| 43 | Escherichia coli FVEC1302 cont1.16, whole genome shotgun sequence | ACXH01000016 | 1353 | 1370 |
| 44 | Escherichia coli FVEC1412 cont1.110, whole genome shotgun sequence | ACXI01000110 | 1353 | 1369 |
| 45 | Escherichia coli M605 cont1.94, whole genome shotgun sequence | ADAV01000094 | 1353 | 1369 |
| 46 | Escherichia coli O157:H7 str. FRIK2000 MBRI2000contig00335, whole genome shotgun sequence | ACXO01000167 | 1353 | 1369 |
| 47 | Escherichia coli O157:H7 str. EC4206 gcontig_1113126024111, whole genome shotgun sequence | ABHK02000001 | 1353 | 1369 |
| 48 | Escherichia coli E22 gcontig_1112495660814, whole genome shotgun sequence | AAJV02000013 | 1353 | 1369 |
| 49 | Escherichia coli O157:H7 str. EC508 gcontig_1108341390915, whole genome shotgun sequence | ABHW01000020 | 1353 | 1369 |
| 50 | Escherichia coli O157:H7 str. EC508 gcontig_1108341394631, whole genome shotgun sequence | ABHW01000162 | 1353 | 1369 |
| 51 | Escherichia coli O157:H7 str. EC869 gcontig_1106613681604, whole genome shotgun sequence | ABHU01000003 | 1353 | 1369 |
| 52 | Escherichia coli O157:H7 str. EC869 gcontig_1106613680316, whole genome shotgun sequence | ABHU01000005 | 1353 | 1369 |
| 53 | Escherichia coli O157:H7 str. EC869 gcontig_1106613679308, whole genome shotgun sequence | ABHU01000090 | 1353 | 1369 |
| 54 | Escherichia coli O157:H7 str. EC4501 gcontig_1106627451009, whole genome shotgun sequence | ABHT01000017 | 1353 | 1369 |
| 55 | Escherichia coli O157:H7 str. EC4501 gcontig_1106627450941, whole genome shotgun sequence | ABHT01000060 | 1353 | 1369 |
| 56 | Escherichia coli O157:H7 str. EC4501 gcontig_1106627441712, whole genome shotgun sequence | ABHT01000072 | 1353 | 1369 |
| 57 | Escherichia coli O157:H7 str. EC4486 gcontig_1106603635210, whole genome shotgun sequence | ABHS01000097 | 1353 | 1369 |
| 58 | Escherichia coli O157:H7 str. EC4076 gcontig_1105762734291, whole genome shotgun sequence | ABHQ01000005 | 1353 | 1369 |
| 59 | Escherichia coli O157:H7 str. EC4076 gcontig_1105762734269, whole genome shotgun sequence | ABHQ01000006 | 1353 | 1369 |
| 60 | Escherichia coli O157:H7 str. EC4076 gcontig_1105762734255, whole genome shotgun sequence | ABHQ01000079 | 1353 | 1369 |
| 61 | Escherichia coli O157:H7 str. EC4113 gcontig_1105762723171, whole genome shotgun sequence | ABHP01000024 | 1353 | 1369 |
| 62 | Escherichia coli O157:H7 str. EC4196 gcontig_1105416507183, whole genome shotgun sequence | ABHO01000004 | 1353 | 1369 |
| 63 | Escherichia coli O103:H2 str. 12009, complete genome | NC_013353 | 1353 | 1369 |
| 64 | Escherichia coli B str. REL606 chromosome, complete genome | NC_012967 | 1353 | 1369 |
| 65 | Escherichia coli BL21-Gold(DE3)pLysS AG chromosome, complete genome | NC_012947 | 1353 | 1369 |
| 66 | Escherichia coli BW2952, complete genome | NC_012759 | 1353 | 1369 |
| 67 | Escherichia coli UMN026, complete genome | NC_011751 | 1353 | 1369 |
| 68 | Escherichia coli S88, complete genome | NC_011742 | 1353 | 1369 |

| | | | | |
|---|---|---|---|---|
| 69 | Escherichia coli O127:H6 str. E2348/69, complete genome | NC_011601 | 1353 | 1369 |
| 70 | Escherichia coli str. K-12 substr. DH10B, complete genome | NC_010473 | 1353 | 1369 |
| 71 | Escherichia coli E24377A, complete genome | NC_009801 | 1353 | 1369 |
| 72 | Escherichia coli HS, complete genome | NC_009800 | 1353 | 1369 |
| 73 | Escherichia coli UTI89 chromosome, complete genome | NC_007946 | 1353 | 1369 |
| 74 | Escherichia coli str. K-12 substr. W3110 chromosome, complete genome | AC_000091 | 1353 | 1369 |
| 75 | Escherichia coli O157:H7 str. EDL933 chromosome, complete genome | NC_002655 | 1353 | 1369 |
| 76 | Escherichia coli str. K-12 substr. MG1655 chromosome, complete genome | NC_000913 | 1353 | 1369 |
| 77 | Escherichia coli E128010 gecE128010.assembly.191, whole genome shotgun sequence | ADUO01000101 | 1352 | 1369 |
| 78 | Escherichia coli TW14425 TW14425_c7, whole genome shotgun sequence | AELE01000007 | 1352 | 1369 |
| 79 | Escherichia coli TW14425 TW14425_c33, whole genome shotgun sequence | AELE01000033 | 1352 | 1369 |
| 80 | Escherichia coli TW14425 TW14425_c1523, whole genome shotgun sequence | AELE01000133 | 1352 | 1369 |
| 81 | Escherichia coli TW11681 TW11681_c53, whole genome shotgun sequence | AELD01000053 | 1352 | 1369 |
| 82 | Escherichia coli TW10598 TW10598_hyb_c34472, whole genome shotgun sequence | AELA01000276 | 1352 | 1369 |
| 83 | Escherichia coli MS 69-1 E_coli69-1-1.0_Cont86.1, whole genome shotgun sequence | ADTP01000052 | 1352 | 1366 |
| 84 | Escherichia coli E22 gcontig_1112495657964, whole genome shotgun sequence | AAJV02000011 | 1352 | 1369 |
| 85 | Escherichia coli E22 gcontig_1112495657890, whole genome shotgun sequence | AAJV02000053 | 1352 | 1369 |
| 86 | Escherichia coli O157:H7 str. EC4196 gcontig_1105416508497, whole genome shotgun sequence | ABHO01000053 | 1352 | 1369 |
| 87 | Shigella sonnei Ss046, complete genome | NC_007384 | 1352 | 1369 |
| 88 | Escherichia coli 1357 OK1357.assembly.173, whole genome shotgun sequence | ADUR01000081 | 1350 | 1368 |
| 89 | Escherichia coli 1180 OK1180.assembly.81, whole genome shotgun sequence | ADUQ01000078 | 1350 | 1368 |
| 90 | Escherichia coli E128010 gecE128010.assembly.196, whole genome shotgun sequence | ADUO01000106 | 1350 | 1369 |
| 91 | Escherichia coli WV_060327, whole genome shotgun sequence | AERT01000002 | 1350 | 1368 |
| 92 | Escherichia coli WV_060327, whole genome shotgun sequence | AERT01000016 | 1350 | 1368 |
| 93 | Shigella boydii ATCC 9905 SGB.Contig113_1, whole genome shotgun sequence | AERN01000056 | 1350 | 1368 |
| 94 | Escherichia coli TW14425 TW14425_c19, whole genome shotgun sequence | AELE01000019 | 1350 | 1368 |
| 95 | Escherichia coli TW11681 TW11681_c9, whole genome shotgun sequence | AELD01000009 | 1350 | 1364 |
| 96 | Escherichia coli TA271 cont1.142, whole genome shotgun sequence | ADAZ01000142 | 1350 | 1369 |
| 97 | Escherichia coli H736 cont1.89, whole genome shotgun sequence | ADAU01000089 | 1350 | 1369 |
| 98 | Escherichia coli TA206 cont1.157, whole genome shotgun sequence | ADAX01000157 | 1350 | 1368 |
| 99 | Escherichia coli O111:H- str. 11128, complete genome | NC_013364 | 1350 | 1368 |
| 100 | Escherichia coli O26:H11 str. 11368, complete genome | NC_013361 | 1350 | 1368 |

### 8.2.3.4. Isolate 36

| Hit No. | Hit Def | Hit Accession | HSP score | HSP Identity |
|---|---|---|---|---|
| 1 | Escherichia coli 2362-75 gec2362.assembly.55, whole genome shotgun sequence | ADUL01000050 | 1127 | 1138 |
| 2 | Escherichia coli 2362-75 gec2362.assembly.74, whole genome shotgun sequence | ADUL01000071 | 1127 | 1138 |
| 3 | Escherichia coli 2362-75 gec2362.assembly.83, whole genome shotgun sequence | ADUL01000081 | 1127 | 1138 |
| 4 | Escherichia coli B str. REL606 chromosome, complete genome | NC_012967 | 1127 | 1138 |
| 5 | Escherichia coli BL21-Gold(DE3)pLysS AG chromosome, complete genome | NC_012947 | 1127 | 1138 |
| 6 | Escherichia coli S88, complete genome | NC_011742 | 1127 | 1138 |
| 7 | Escherichia coli APEC O1, complete genome | NC_008563 | 1127 | 1138 |
| 8 | Escherichia coli UTI89 chromosome, complete genome | NC_007946 | 1127 | 1138 |
| 9 | Escherichia coli LT-68 gecLT68.assembly.37, whole genome shotgun sequence | ADUP01000030 | 1124 | 1137 |
| 10 | Escherichia coli LT-68 gecLT68.assembly.39, whole genome shotgun sequence | ADUP01000032 | 1124 | 1137 |
| 11 | Escherichia coli EC4100B ECL.Contig132_1, whole genome shotgun sequence | AERU01000014 | 1124 | 1137 |
| 12 | Escherichia coli EC4100B ECL.Contig121_1, whole genome shotgun sequence | AERU01000035 | 1124 | 1137 |
| 13 | Escherichia coli O157:H7 str. EC1212 ECD.Contig131_1, whole genome shotgun sequence | AERQ01000020 | 1124 | 1137 |
| 14 | Escherichia coli 3431 gec3431.assembly.64, whole genome shotgun sequence | ADUM01000088 | 1124 | 1137 |
| 15 | Escherichia coli 3431 gec3431.assembly.65, whole genome shotgun sequence | ADUM01000089 | 1124 | 1137 |
| 16 | Escherichia coli TW14425 TW14425_c19, whole genome shotgun sequence | AELE01000019 | 1124 | 1137 |
| 17 | Escherichia coli NC101 contig6, whole genome shotgun sequence | AEFA01000022 | 1124 | 1137 |
| 18 | Escherichia coli MS 145-7 E_coliMS145-7-1.0.1_Cont31.1, whole genome shotgun sequence | ADWS01000032 | 1124 | 1137 |
| 19 | Escherichia coli MS 115-1 E_coli115-1-1.0_Cont12.1, whole genome shotgun sequence | ADTL01000003 | 1124 | 1137 |
| 20 | Escherichia coli FVEC1412 cont1.110, whole genome shotgun sequence | ACXI01000110 | 1124 | 1137 |
| 21 | Escherichia coli TA271 cont1.142, whole genome shotgun sequence | ADAZ01000142 | 1124 | 1137 |
| 22 | Escherichia coli H736 cont1.89, whole genome shotgun sequence | ADAU01000089 | 1124 | 1137 |
| 23 | Escherichia coli M605 cont1.94, whole genome shotgun sequence | ADAV01000094 | 1124 | 1137 |
| 24 | Escherichia coli TA206 cont1.157, whole genome shotgun sequence | ADAX01000157 | 1124 | 1137 |
| 25 | Escherichia coli TA143 cont1.141, whole genome shotgun sequence | ADAY01000141 | 1124 | 1137 |
| 26 | Escherichia sp. 1_1_43 cont1.33, whole genome shotgun sequence | ACID01000033 | 1124 | 1137 |
| 27 | Escherichia coli O157:H7 str. EC4042 gcontig_1113125281292, whole genome shotgun sequence | ABHM02000001 | 1124 | 1137 |
| 28 | Escherichia coli O157:H7 str. EC4045 gcontig_1113126024325, whole genome shotgun sequence | ABHL02000001 | 1124 | 1137 |
| 29 | Escherichia coli O157:H7 str. EC4206 gcontig_1113126024111, whole genome shotgun sequence | ABHK02000001 | 1124 | 1137 |
| 30 | Escherichia coli E110019 gcontig_1112495928714, whole genome shotgun sequence | AAJW02000003 | 1124 | 1137 |
| 31 | Escherichia coli E110019 gcontig_1112495928756, whole genome shotgun sequence | AAJW02000004 | 1124 | 1137 |
| 32 | Escherichia coli E110019 gcontig_1112495928844, whole genome shotgun sequence | AAJW02000060 | 1124 | 1137 |

| | | | | |
|---|---|---|---|---|
| 33 | Escherichia coli 53638 gcontig_1105238512145, whole genome shotgun sequence | AAKB02000001 | 1124 | 1137 |
| 34 | Escherichia coli O157:H7 str. EC4076 gcontig_1105762734293, whole genome shotgun sequence | ABHQ01000001 | 1124 | 1137 |
| 35 | Escherichia coli O157:H7 str. EC4196 gcontig_1105416507183, whole genome shotgun sequence | ABHO01000004 | 1124 | 1137 |
| 36 | Escherichia coli O55:H7 str. CB9615 chromosome, complete genome | NC_013941 | 1124 | 1137 |
| 37 | Escherichia coli O157:H7 str. TW14359, complete genome | NC_013008 | 1124 | 1137 |
| 38 | Escherichia coli BW2952, complete genome | NC_012759 | 1124 | 1137 |
| 39 | Escherichia coli UMN026, complete genome | NC_011751 | 1124 | 1137 |
| 40 | Escherichia coli IAI1, complete genome | NC_011741 | 1124 | 1137 |
| 41 | Escherichia fergusonii ATCC 35469, complete genome | NC_011740 | 1124 | 1137 |
| 42 | Escherichia coli O127:H6 str. E2348/69, complete genome | NC_011601 | 1124 | 1137 |
| 43 | Escherichia coli SE11 chromosome, complete genome | NC_011415 | 1124 | 1137 |
| 44 | Escherichia coli O157:H7 str. EC4115, complete genome | NC_011353 | 1124 | 1137 |
| 45 | Escherichia coli str. K-12 substr. DH10B, complete genome | NC_010473 | 1124 | 1137 |
| 46 | Escherichia coli ATCC 8739, complete genome | NC_010468 | 1124 | 1137 |
| 47 | Escherichia coli str. K-12 substr. W3110 chromosome, complete genome | AC_000091 | 1124 | 1137 |
| 48 | Escherichia coli O157:H7 str. EDL933 chromosome, complete genome | NC_002655 | 1124 | 1137 |
| 49 | Escherichia coli str. K-12 substr. MG1655 chromosome, complete genome | NC_000913 | 1121 | 1136 |
| 50 | Escherichia coli O157:H7 str. Sakai, complete genome | NC_002695 | 1124 | 1137 |
| 51 | Escherichia coli 1357 OK1357.assembly.173, whole genome shotgun sequence | ADUR01000081 | 1121 | 1136 |
| 52 | Shigella sonnei 53G gss53G.assembly.144, whole genome shotgun sequence | ADUU01000047 | 1121 | 1136 |
| 53 | Escherichia coli EPECa14 EPECa14.assembly.156, whole genome shotgun sequence | ADUN01000062 | 1121 | 1137 |
| 54 | Escherichia coli WV_060327, whole genome shotgun sequence | AERT01000002 | 1121 | 1136 |
| 55 | Escherichia coli WV 060327, whole genome shotgun sequence | AERT01000016 | 1121 | 1136 |
| 56 | Shigella boydii ATCC 9905 SGB.Contig113_1, whole genome shotgun sequence | AERN01000056 | 1121 | 1136 |
| 57 | Shigella flexneri 2a str. 2457T gss2457T.assembly.65, whole genome shotgun sequence | ADUV01000061 | 1121 | 1136 |
| 58 | Escherichia coli 2362-75 gec2362.assembly.47, whole genome shotgun sequence | ADUL01000041 | 1121 | 1136 |
| 59 | Escherichia coli 1827-70 gec1827.assembly.31, whole genome shotgun sequence | ADUK01000024 | 1121 | 1136 |
| 60 | Escherichia coli MS 16-3 E_coli16-3-1.0_Cont70.1, whole genome shotgun sequence | ADUA01000035 | 1121 | 1136 |
| 61 | Escherichia coli MS 153-1 E_coli153-1-1.0_Cont20.1, whole genome shotgun sequence | ADTX01000014 | 1121 | 1136 |
| 62 | Escherichia coli 83972 contig00152, whole genome shotgun sequence | ACGN01000123 | 1121 | 1136 |
| 63 | Shigella dysenteriae 1012 gcontig_1112603762653, whole genome shotgun sequence | AAMJ02000006 | 1121 | 1136 |
| 64 | Escherichia coli F11 gcontig_1112495917000, whole genome shotgun sequence | AAJU02000010 | 1121 | 1136 |
| 65 | Escherichia coli O157:H7 str. EC508 gcontig_1108341391741, whole genome shotgun sequence | ABHW01000042 | 1121 | 1136 |
| 66 | Escherichia coli O111:H- str. 11128, complete genome | NC_013364 | 1121 | 1136 |
| 67 | Escherichia coli O26:H11 str. 11368, complete genome | NC_013361 | 1121 | 1136 |
| 68 | Escherichia coli ED1a chromosome, complete genome | NC_011745 | 1121 | 1136 |

| | | | | |
|---|---|---|---|---|
| 69 | Escherichia coli E24377A, complete genome | NC_009801 | 1121 | 1136 |
| 70 | Shigella flexneri 5 str. 8401, complete genome | NC_008258 | 1121 | 1136 |
| 71 | Escherichia coli 536, complete genome | NC_008253 | 1121 | 1136 |
| 72 | Shigella boydii Sb227, complete genome | NC_007613 | 1121 | 1136 |
| 73 | Shigella sonnei Ss046, complete genome | NC_007384 | 1121 | 1136 |
| 74 | Escherichia coli CFT073, complete genome | NC_004431 | 1121 | 1136 |
| 75 | Shigella flexneri 2a str. 301, complete genome | NC_004337 | 1121 | 1136 |
| 76 | Escherichia coli RN587/1 RN587.assembly.32, whole genome shotgun sequence | ADUS01000025 | 1120 | 1136 |
| 77 | Escherichia coli RN587/1 RN587.assembly.36, whole genome shotgun sequence | ADUS01000029 | 1120 | 1136 |
| 78 | Escherichia coli LT-68 gecLT68.assembly.40, whole genome shotgun sequence | ADUP01000034 | 1120 | 1136 |
| 79 | Escherichia coli 3431 gec3431.assembly.47, whole genome shotgun sequence | ADUM01000069 | 1120 | 1136 |
| 80 | Escherichia coli E110019 gcontig_1112495928854, whole genome shotgun sequence | AAJW02000005 | 1120 | 1136 |
| 81 | Escherichia coli RN587/1 RN587.assembly.30, whole genome shotgun sequence | ADUS01000023 | 1118 | 1136 |
| 82 | Escherichia coli 1180 OK1180.assembly.81, whole genome shotgun sequence | ADUQ01000078 | 1118 | 1135 |
| 83 | Shigella boydii ATCC 9905 SGB.Contig115_1, whole genome shotgun sequence | AERN01000004 | 1118 | 1136 |
| 84 | Shigella flexneri 2a str. 2457T gss2457T.assembly.51, whole genome shotgun sequence | ADUV01000046 | 1118 | 1135 |
| 85 | Shigella flexneri 2a str. 2457T gss2457T.assembly.58, whole genome shotgun sequence | ADUV01000053 | 1118 | 1135 |
| 86 | Escherichia coli 2362-75 gec2362.assembly.61, whole genome shotgun sequence | ADUL01000057 | 1118 | 1136 |
| 87 | Escherichia coli MS 57-2 E_coli57-2-1.0_Cont8.1, whole genome shotgun sequence | ADUG01000003 | 1118 | 1135 |
| 88 | Escherichia coli F11 gcontig_1112495914622, whole genome shotgun sequence | AAJU02000017 | 1118 | 1135 |
| 89 | Escherichia coli F11 gcontig_1112495919726, whole genome shotgun sequence | AAJU02000035 | 1118 | 1135 |
| 90 | Escherichia coli F11 gcontig_1112495918566, whole genome shotgun sequence | AAJU02000050 | 1118 | 1136 |
| 91 | Escherichia coli O157:H7 str. EC4486 gcontig_1106603634670, whole genome shotgun sequence | ABHS01000045 | 1118 | 1136 |
| 92 | Escherichia coli SMS-3-5, complete genome | NC_010498 | 1118 | 1135 |
| 93 | Shigella flexneri 2a str. 2457T, complete genome | NC_004741 | 1118 | 1135 |
| 94 | Escherichia coli MS 107-1 E_coliMS107-1-1.0.1_Cont68.1, whole genome shotgun sequence | ADWV01000069 | 1117 | 1135 |
| 95 | Escherichia coli RN587/1 RN587.assembly.28, whole genome shotgun sequence | ADUS01000020 | 1115 | 1134 |
| 96 | Escherichia coli 1357 OK1357.assembly.168, whole genome shotgun sequence | ADUR01000075 | 1115 | 1134 |
| 97 | Escherichia coli LT-68 gecLT68.assembly.36, whole genome shotgun sequence | ADUP01000029 | 1115 | 1134 |
| 98 | Shigella flexneri 2a str. 2457T gss2457T.assembly.50, whole genome shotgun sequence | ADUV01000045 | 1115 | 1134 |
| 99 | Shigella flexneri 2a str. 2457T gss2457T.assembly.55, whole genome shotgun sequence | ADUV01000050 | 1115 | 1134 |
| 100 | Shigella flexneri 2a str. 2457T gss2457T.assembly.69, whole genome shotgun sequence | ADUV01000065 | 1115 | 1134 |

## References


Acra, A., Karahagopian, Y., Raffoul, Z. and Dajani, R. (1980) Disinfection of oral rehydration solutions by sunlight. *Lancet* 2(8206), 1257-1258.

Acra, A.R., Z.; Karahagopian, Y. (1984) Solar Disinfection of Drinking Water and Oral Rehydration Solutions., UNICEF, Beirut.

Acra, S.A. and Demerrell, D. (2001) Solar disinfection of small quantities of water in plastic bags. *Gastroenterology* 120(5), A40-A40.

Adams, M.H. (1959a) Bacteriophages, Interscience Publishers,Inc., N.Y.

Adams, M.H. (1959b) Bacteriophages, Interscience Publishers, New York.

Ahmad, S.I. (1981) Synergistic action of near ultraviolet radiation and hydrogen peroxide on the killing of coliphage T7: possible role of superoxide radical. *Photobiochemistry and Photobiophysics* 2(3), 173-180.

Akaike, T., Sato, K., Ijiri, S., Miyamoto, Y., Kohno, M., Ando, M. and Maeda, H. (1992) Bactericidal activity of alkyl peroxyl radicals generated by heme-iron-catalyzed decomposition of organic peroxides. *Archives of Biochemistry and Biophysics* 294(1), 55-63.

Aldsworth, T.G., Sharman, R.L. and Dodd, C.E.R. (1999) Bacterial suicide through stress. *Cellular and Molecular Life Sciences* 56(5), 378-383.

Alegra, A.E., Ferrer, A., Santiago, G., Sepulveda, E. and Flores, W. (1999) Photochemistry of water-soluble quinones. Production of the hydroxyl radical, singlet oxygen and the superoxide ion. *Journal of Photochemistry and Photobiology A: Chemistry* 127, 57-65.

Altherr, A.-M. (2004) E-mail Correspondence. Lukacs, H.A. (ed), Geneva, Switzerland.

Ananthaswamy, H.N. and Eisenstark, A. (1976) Near-UV-induced breaks in phage DNA: sensitization by hydrogen peroxide (a tryptophan photoproduct). *Photochem Photobiol* 24(5), 439-442.

Ananthaswamy, H.N. and Eisenstark, A. (1977) Repair of hydrogen peroxide-induced single-strand breaks in Escherichia coli deoxyribonucleic acid. *Journal of Bacteriology* 130(1), 187-191.

Arifeen, S., Black, R.E., Antelman, G., Baqui, A., Caulfield, L. and Becker, S. (2001) Exclusive Breastfeeding Reduces Acute Respiratory Infection and Diarrhea Deaths Among Infants in Dhaka Slums. *Pediatrics* 108(4), e67-.

Arnold, B.F. and Colford, J.M., JR (2007) Treating Water with Chlorine at Point-of-Use to Improve Water Quality and Reduce Child Diarrhea in Developing Countries: A Systematic Review and Meta-Analysis. *Am J Trop Med Hyg* 76(2), 354-364.

Asad, N.R. and Leitao, A.C. (1991) Effects of metal ion chelators on DNA strand breaks and inactivation produced by hydrogen peroxide in Escherichia coli: detection of iron-independent lesions. *Journal of Bacteriology* 173(8), 2562-2568.

Bader, H., Sturzenegger, V. and Hoigne, J. (1988) Photometric Method for the Determination of Low Concentrations of Hydrogen Peroxide by the Peroxidase Catalyzed Oxidation of N,N-Diethyl-P-Phenylenediamine (DPD). *Water Research* 22(9), 1109-1115.

Baier, J., Maisch, T., Maier, M., Engel, E., Landthaler, M. and Baumler, W. (2006a) Singlet Oxygen Generation by UVA Light Exposure of Endogenous Photosensitizers, Biophysical Society.

Baier, J., Maisch, T., Maier, M., Engel, E., Landthaler, M. and Baumler, W. (2006b) Singlet oxygen generation by UVA light exposure of endogenous photosensitizers. *Biophys J* 91(4), 1452-1459.

Baker, M.N.T., M. (1981) The Quest for Pure Water: The History of the Twentieth Century, AWWA.

Barstow, C.K. (2010) Development of an Ultraviolet Point-of-Use Device For Household Water Disinfection, University of Colorado at Boulder

Beckman, J.S., Beckman, T.W., Chen, J., Marshall, P.A. and Freeman, B.A. (1990) Apparent hydroxyl radical production by peroxynitrite: implications for endothelial injury from nitric oxide and superoxide. *Proceedings of the National Academy of Sciences of the United States of America* 87(4), 1620-1624.

Berney, M., Weilenmann, H.-U. and Egli, T. (2006a) Gene expression of Escherichia coli in continuous culture during adaptation to artificial sunlight. *Environmental Microbiology* 8(9), 1635-1647.

Berney, M., Weilenmann, H.-U., Ihssen, J., Bassin, C. and Egli, T. (2006b) Specific Growth Rate Determines the Sensitivity of Escherichia coli to Thermal, UVA, and Solar Disinfection. *Appl. Environ. Microbiol.* 72(4), 2586-2593.

Berney, M., Weilenmann, H.U. and Egli, T. (2006c) Flow-cytometric study of vital cellular functions in Escherichia coli during solar disinfection (SODIS). *Microbiology* 152(Pt 6), 1719-1729.

Berney, M., Weilenmann, H.U., Ihssen, J., Bassin, C. and Egli, T. (2006d) Specific growth rate determines the sensitivity of Escherichia coli to thermal, UVA, and solar disinfection. *Appl Environ Microbiol* 72(4), 2586-2593.

Berney, M., Weilenmann, H.U., Simonetti, A. and Egli, T. (2006e) Efficacy of solar disinfection of Escherichia coli, Shigella flexneri, Salmonella Typhimurium and Vibrio cholerae. *J Appl Microbiol* 101(4), 828-836.

Besaratinia, A., Kim, S.-i., Bates, S.E. and Pfeifer, G.P. (2007) Riboflavin activated by ultraviolet A1 irradiation induces oxidative DNA damage-mediated mutations inhibited by vitamin C. *Proceedings of the National Academy of Sciences* 104(14), 5953-5958.

Blanco-Galvez, J., Fernandez-Ibanez, P. and Malato-Rodriguez, S. (2007) Solar Photocatalytic Detoxification and Disinfection of Water: Recent Overview. *Journal of Solar Energy Engineering* 129(1), 4-15.

Blough, N.V.Z., R.G. (1995) Active Oxygen in Chemistry. V. Foote, G., and Liebman (ed), Kluwer Academic Publishers, Dordrecht.

Boehm, A.B., Yamahara, K.M., Love, D.C., Peterson, B.M., McNeill, K. and Nelson, K.L. (2009a) Covariation and photoinactivation of traditional and novel indicator organisms and human viruses at a sewage-impacted marine beach. *Environ. Sci. Technol.* 43(21), 8046-8052.

Boehm, A.B., Yamahara, K.M., Love, D.C., Peterson, B.M., McNeill, K. and Nelson, K.L. (2009b) Covariation and Photoinactivation of Traditional and Novel Indicator Organisms and Human Viruses at a Sewage-Impacted Marine Beach. *Environmental Science & Technology* 43(21), 8046.

Bosshard, F., Berney, M., Scheifele, M., Weilenmann, H.U. and Egli, T. (2009) Solar disinfection (SODIS) and subsequent dark storage of Salmonella typhimurium and Shigella flexneri monitored by flow cytometry. *Microbiology* 155(Pt 4), 1310-1317.

Bosshard, F., Bucheli, M., Meur, Y. and Egli, T. (2010) The respiratory chain is the cell's Achilles' heel during UVA inactivation in Escherichia coli. *Microbiology* 156(Pt 7), 2006-2015.

Boyle, M., Sichel, C., Fernandez-Ibanez, P., Arias-Quiroz, G.B., Iriarte-Puna, M., Mercado, A., Ubomba-Jaswa, E. and McGuigan, K.G. (2008) Bactericidal effect of solar water disinfection under real sunlight conditions. *Appl Environ Microbiol* 74(10), 2997-3001.

Brown, J. and Sobsey, M.D. (2010) Manuscript in Preparation: Evaluating household water treatment options: health-based targets and performance specifications, WHO.

Brownell, S.A., Chakrabarti, A.R., Kaser, F.M., Connelly, L.G., Peletz, R.L., Reygadas, F., Lang, M.J., Kammen, D.M. and Nelson, K.L. (2008) Assessment of a low-cost, point-of-use, ultraviolet water disinfection technology. *J Water Health* 6(1), 53-65.

Brumaghim, J.L., Li, Y., Henle, E. and Linn, S. (2003) Effects of hydrogen peroxide upon nicotinamide nucleotide metabolism in Escherichia coli - Changes in enzyme levels and nicotinamide nucleotide pools and studies of the oxidation of NAD(P)H by Fe(III). *Journal of Biological Chemistry* 278(43), 42495-42504.

Cairncross, S. (2003) Editorial: Water supply and sanitation: some misconceptions. *Tropical Medicine & International Health* 8(3), 193-195.

Calkins, J., Buckles, J.D. and Moeller, J.R. (1976) Role of Solar Ultraviolet-Radiation in Natural-Water Purification. *Photochemistry and Photobiology* 24(1), 49-57.

CDC (2000) Safe Water Systems for the Developing World: A Handbook for Implementing Household-Based Water Treatment and Safe Storage Projects, Centers for Disease Control and Prevention

Chen, R.Z., Craik, S.A. and Bolton, J.R. (2009a) Comparison of the action spectra and relative DNA absorbance spectra of microorganisms: Information important for the determination of germicidal fluence (UV dose) in an ultraviolet disinfection of water. *Water Research* 43(20), 5087-5096.

Chen, R.Z., Craik, S.A. and Bolton, J.R. (2009b) Comparison of the action spectra and relative DNA absorption spectra of microorganisms: Information important for the determination of germicidal fluence (UV dose) in an ultraviolet disinfection of water. *Water Research* 43, 5087-5096.

Chiancone, E., Ceci, P., Ilari, A., Ribacchi, F. and Stefanini, S. (2004) Iron and proteins for iron storage and detoxification. *BioMetals* 17(3), 197-202.

Clark, R.N. (1956) The purification of water on a small scale. *Bulletin of the World Health Organization* 14(4), 820-826.

Clasen, T., Haller, L., Walker, D., Bartram, J. and Cairncross, S. (2007a) Cost-effectiveness of water quality interventions for preventing diarrhoeal disease in developing countries. *J Water Health* 5(4), 599-608.

Clasen, T., Schmidt, W.-P., Rabie, T., Roberts, I. and Cairncross, S. (2007b) Interventions to improve water quality for preventing diarrhoea: systematic review and meta-analysis. *BMJ* 334(7597), 782.

Clasen, T., Naranjo, J., Frauchiger, D. and Gerba, C. (2009) Laboratory Assessment of a Gravity-Fed Ultrafiltration Water Treatment Device Designed for Household Use in Low-Income Settings. *Am J Trop Med Hyg* 80(5), 819-823.

Clasen, T.F., Thao, D.H., Boisson, S. and Shipin, O. (2008) Microbiological Effectiveness and Cost of Boiling to Disinfect Drinking Water in Rural Vietnam. *Environmental Science & Technology* 42(12), 4255-4260.

Conroy, R.M., Elmore Meegan, M., Joyce, T., McGuigan, K.G. and Barnes, J. (1996) Solar disinfection of drinking water and diarrhoea in Maasai children: A controlled field trial. *Lancet* 348(9043), 1695-1697.

Conroy, R.M., Meegan, M.E., Joyce, T., McGuigan, K. and Barnes, J. (1999) Solar disinfection of water reduces diarrhoeal disease: an update. *Archives of Disease in Childhood* 81(4), 337-338.

Conroy, R.M., Meegan, M.E., Joyce, T., McGuigan, K. and Barnes, J. (2001) Solar disinfection of drinking water protects against cholera in children under 6 years of age. *Archives of Disease in Childhood* 85(4), 293-295.

Coohill, T. (1991) Action spectra again? *Photochem Photobiol* 54(5), 859-870.

Cooper, W.J., Zika, R.G., Petasne, R.G. and Plane, J.M.C. (1988) Photochemical formation of H2O2 in natural waters exposed to sunlight. *Journal Name: Environ. Sci. Technol.; (United States); Journal Volume: 22:10*, Medium: X; Size: Pages: 1156-1160.

Craggs, J., Kirk, S.H. and Ahmad, S.I. (1994) Synergistic action of near-UV and phenylalanine, tyrosine or tryptophan on the inactivation of phage T7: Role of superoxide radicals and hydrogen peroxide. *Journal of Photochemistry and Photobiology B: Biology* 24(2), 123-128.

CSTEE (2001) Hydrogen Peroxide Human Health Effects, European Comission Directorate-General Health and Consumer Protection, Brussels, Belgium.

Cunningham, M., Krinsky, N., Giovanazzi, S. and Peak, M. (1985a) Superoxide anion is generated from cellular metabolites by solar radiation and its components. . *J Free Radic Biol Med.* 1(5-6), 381-385.

Cunningham, M.L., Johnson, J.S., Giovanazzi, S.M. and Peak, M.J. (1985b) Photosensitized Production Of Superoxide Anion By Monochromatic (290-405 nm) Ultraviolet Irradiation Of NADH And NADPH Coenzymes. *Photochemistry And Photobiology* 42(2), 125-128.

Cunningham, M.L., Krinsky, N.I., Giovanazzi, S.M. and Peak, M.J. (1985c) Superoxide anion is generated from cellular metabolites by solar radiation and its components. *Journal of Free Radicals in Biology & Medicine* 1(5-6), 381.

Curtis, T.P., Mara, D.D. and Silva, S.A. (1992) Influence of pH, Oxygen, and Humic Substances on Ability of Sunlight to Damage Fecal Coliforms in Waste Stabilization Pond Water. *Applied and Environmental Microbiology* 58(4), 1335-1343.

Curtis, T.P.M., D.D. (1994) The Effects of Sunlight on Mechanisms for the Die-off of Faecal Coliform Bacteria in Waste Stabilization Ponds, University of Leeds, Leeds, U.K.

Davies-Colley, R.J., Donnison, A.M. and Speed, D.J. (1997) Sunlight wavelengths inactivating faecal indicator microorganisms in waste stabilisation ponds. *Water Science and Technology* 35(11-12), 219-225.

Davies-Colley, R.J., Donnison, A.M., Speed, D.J., Ross, C.M. and Nagels, J.W. (1999) Inactivation of faecal indicator microorganisms in waste stabilisation ponds: Interactions of environmental factors with sunlight. *Water Research* 33(5), 1220-1230.

Davies-Colley, R.J., Craggs, R.J., Park, J. and Nagels, J.W. (2005) Optical characteristics of waste stabilization ponds: recommendations for monitoring. *Water Sci Technol* 51(12), 153-161.

Davies, C.M. and Evison, L.M. (1991) Sunlight and the Survival of Enteric Bacteria in Natural-Waters. *Journal of Applied Bacteriology* 70(3), 265-274.

Davies, C.M., Roser, D.J., Feitz, A.J. and Ashbolt, N.J. (2009) Solar radiation disinfection of drinking water at temperate latitudes: inactivation rates for an optimised reactor configuration. *Water Res* 43(3), 643-652.

Dejung, S.F., I.; Almanza, G.; Jarro, R.;, Navarro, L.A., G.; Urquieta, E.; Torrico, A.;, Fenandez, W.I., M.; Birrer, C.; and Stahel, W.A.W., M. (2007) Effect of solar water disinfection (SODIS) on model microorganisms under improved and field SODIS conditions. *Journal of Water Supply: Research and Technology—AQUA* 56(4), 245-256.

Deller, S., Mascher, F., Platzer, S., Reinthaler, F.F. and Marth, E. (2006) Effect of solar radiation on survival of indicator bacteria in bathing waters. *Cent Eur J Public Health* 14(3), 133-137.

Demple, B., Johnson, A. and Fung, D. (1986) Exonuclease III and endonuclease IV remove 3' blocks from DNA synthesis primers in H2O2-damaged Escherichia coli. *Proceedings of the National Academy of Sciences of the United States of America* 83(20), 7731-7735.

Dodd, C.E.R., Sharman, R.L., Bloomfield, S.F., Booth, I.R. and Stewart, G.S.A.B. (1997) Inimical processes: Bacterial self-destruction and sub-lethal injury. *Trends in Food Science & Technology* 8(7), 238-241.

Downes, A.B., T. P. (1877) Researches on the Effect of Light upon Bacteria and other Organisms. *Proceedings of the Royal Society of London* 26, 488-500.

Draper, W.M. and Crosby, D.G. (1983) The photochemical generation of hydrogen peroxide in natural waters. *Archives of Environmental Contamination and Toxicology* 12(1), 121-126.

Drescher, A.C., Greene, D.M. and Gadgil, A.J. (2001) Cryptosporidium Inactivation by Low-Pressure UV in a Water Disinfection Device. *Journal of Environmental Health* 64(3), 31.

Du Preez, M., McGuigan, K.G. and Conroy, R.M. (2010) Solar Disinfection of Drinking Water In the Prevention of Dysentery in South African Children Aged under 5 Years: The Role of Participant Motivation. *Environmental Science & Technology* 44(22), 8744–8749.

Duffy, E.F., Al Touati, F., Kehoe, S.C., McLoughlin, O.A., Gill, L.W., Gernjak, W., Oller, I., Maldonado, M.I., Malato, S., Cassidy, J., Reed, R.H. and McGuigan, K.G. (2004) A novel TiO2-assisted solar photocatalytic batch-process disinfection reactor for the treatment of biological and chemical contaminants in domestic drinking water in developing countries. *Solar Energy* 77(5), 649-655.

E Ubomba-Jaswa, M.A.R.B., K G McGuigan (2008) Inactivation of enteropathogenic E. coli by solar disinfection
(SODIS) under simulated sunlight conditions. *Journal of Physics: Conference Series* 101.

Easterbrook, P.J., Gopalan, R., Berlin, J.A. and Matthews, D.R. (1991) Publication bias in clinical research. *The Lancet* 337(8746), 867-872.

EAWAG/SANDEC (2011) SODIS Solar Water Disinfection, SANDEC (Water & Sanitation in Developing Countries) at EAWAG (Swiss Federal Institute for Environmental Science and Technology), Dübendorf, Switzerland.

Eischeid, A.C., Meyer, J.N. and Linden, K.G. (2009) UV Disinfection of Adenoviruses: Molecular Indications of DNA Damage Efficiency. *Appl. Environ. Microbiol.* 75(1), 23-28.

Eisenberg, J.N.S., Scott, J.C. and Porco, T. (2007) Integrating Disease Control Strategies: Balancing Water Sanitation and Hygiene Interventions to Reduce Diarrheal Disease Burden. *Am J Public Health* 97(5), 846-852.

Eisenstark, A. (1971) Mutagenic and lethal effects of visible and near-ultraviolet light on bacterial cells. *Adv Genet* 16, 167-198.

Eisenstark, A., Buzard, R.L. and Hartman, P.S. (1986) Inactivation of phage by near-ultraviolet radiation and hydrogen peroxide. *Photochem Photobiol* 44(5), 603-606.

Eisenstark, A. (1987) Mutagenic and lethal effects of near-ultraviolet radiation (290-400 nm) on bacteria and phage. *Environmental and Molecular Mutagenesis* 10(3), 317-337.

Eisenstark, A. and Perrot, G. (1987) Catalase has only a minor role in protection against near-ultraviolet radiation damage in bacteria. *Mol Gen Genet* 207(1), 68-72.

Eisenstark, A. (1989) Bacterial genes involved in response to near-ultraviolet radiation. *Adv Genet* 26, 99-147.

Eisenstark, A., John G. Scandalios, T.R.F.W. and John, G.S. (1989) Advances in Genetics, pp. 99-147, Academic Press.

Favre, A., Hajnsdorf, E., Thiam, K. and Caldeira de Araujo, A. (1985) Mutagenesis and growth delay induced in Escherichia coli by near-ultraviolet radiations. *Biochimie* 67(3-4), 335-342.

Fisher, M.B., Keenan, C.R., Nelson, K.L. and Voelker, B.M. (2008) Speeding up solar disinfection (SODIS): effects of hydrogen peroxide, temperature, pH, and copper plus ascorbate on the photoinactivation of E. coli. *J Water Health* 6(1), 35-51.

Fisher, M.B., Iriarte, M. and Nelson, K.L. (Manuscript in Preparation-a) Speeding up SODIS in the field: Additives and UVB-transparent containers accelerate the sunlight inactivation of MS2 bacteriophage and indicator bacteria from Bolivian wastewater and laboratory sources.

Fisher, M.B., Love, D.C., Schuech, R. and Nelson, K.L. (Manuscript in Preparation-b) Sunlight action spectra for inactivation of MS2 and PRD1 bacteriophage in clear water.

Fisher, M.B., Iriarte, M. and Nelson, K.L. (Manuscript in Progress) Solar disinfection (SODIS) of *E. coli, Enterococcus*, and MS2 phage: effects of additives and alternative container materials.

Frederick, J.E. and Erlick, C. (1997) The Attenuation of Sunlight by High-Latitude Clouds: Spectral Dependence and Its Physical Mechanisms. *Journal of the Atmospheric Sciences* 54(24), 2813-2819.

Freter, R., Brickner, H., Fekete, J., Vickerman, M.M. and Carey, K.E. (1983) Survival and Implantation of Escherichia coli in the Intestinal Tract. *Infect. Immun.* 39(2), 686-703.

Fridovich, I. (1998) Oxygen toxicity: A radical explanation. *Journal of Experimental Biology* 201(8), 1203-1209.

Gates, F. (1934) Results of irradiating Staphylococcus aureus bacteriophage with monochromatic ultraviolet light *J Exp Med* 60(2), 179-188.

Gerba, C.P., Gramos, D.M. and Nwachuku, N. (2002) Comparative inactivation of enteroviruses and adenovirus 2 by UV light. *Appl Environ Microbiol* 68(10), 5167-5169.

Goldstein, S., Meyerstein, D. and Czapski, G. (1993) The Fenton reagents. *Free Radical Biology and Medicine* 15(4), 435-445.

Gomez-Couso, H., Fontan-Sainz, M., Sichel, C., Fernandez-Ibanez, P. and Ares-Mazas, E. (2009) Efficacy of the solar water disinfection method in turbid waters experimentally contaminated with Cryptosporidium parvum oocysts under real field conditions. *Trop Med Int Health* 14(6), 620-627.

Gómez-Couso, H., Fontán-Saínz, M., Sichel, C., Fernández-Ibáñez, P. and Ares-Mazás, E. (2009) Efficacy of the solar water disinfection method in turbid waters experimentally contaminated with Cryptosporidium parvum oocysts under real field conditions. *Tropical Medicine & International Health* 14(6), 620-627.

Gort, A.S. and Imlay, J.A. (1998) Balance between Endogenous Superoxide Stress and Antioxidant Defenses. *J. Bacteriol.* 180(6), 1402-1410.

Gourmelon, M., Cillard, J. and Pommepuy, M. (1994) Visible Light Damage to Escherichia Coli in Seawater - Oxidative Stress Hypothesis. *Journal of Applied Bacteriology* 77(1), 105-112.

Grimm, B. (2003) Solar Bottles for our Health. Report of the SODIS Dissemination Project Phase II: April 2003-March 2004, JDA International, Inc., Kokand, Uzbekistan.

Gueymard, C.A. (1995) SMARTS, A Simple Model of the Atmospheric Radiative Transfer of Sunshine: Algorithms and Performance Assessment. , Florida Solar Energy Center, Cocoa, FL.

Gurung, P., Grimm, B. and Autenrieth, M. (2009) Disseminating the SODIS method: Which approach is most effective? *Waterlines* 28, 130-143.

Halliwell, B.G., J.M.C. (1999) Free Radicals in Biology and Medicine, Oxford University Press, Oxford, U.K.

Hantke, K. (2001) Iron and metal regulation in bacteria. *Current Opinion in Microbiology* 4(2), 172.

Hardina, C.M. and Fujioka, R.S. (1991) Soil: The environmental source of Escherichia coli and enterococci in Hawaii's streams. *Environmental Toxicology and Water Quality* 6(2), 185.

Harm, W. (1980) IUPAB Biophysics Series. F.F. Hutchinson, W.M., Lorin J. (ed), Cambridge University Press, London.

Hartman, P.S. and Eisenstark, A. (1978) Synergistic killing of Escherichia coli by near-UV radiation and hydrogen peroxide: distinction between recA-repairable and recA-nonrepairable damage. *J. Bacteriol.* 133(2), 769-774.

Hartman, P.S., Eisenstark, A. and Pauw, P.G. (1979) Inactivation of phage T7 by near-ultraviolet radiation plus hydrogen peroxide: DNA-protein crosslinks prevent DNA injection. *Proc Natl Acad Sci U S A* 76(7), 3228-3232.

Hartman, P.S. and Eisenstark, A. (1980) Killing of Escherichia coli K-12 by near-ultraviolet radiation in the presence of hydrogen peroxide: role of double-strand DNA breaks in absence of recombinational repair. *Mutat Res* 72(1), 31-42.

Heaselgrave, W., Patel, N., Kilvington, S., Kehoe, S.C. and McGuigan, K.G. (2006) Solar disinfection of poliovirus and Acanthamoeba polyphaga cysts in water - a laboratory study using simulated sunlight. *Lett Appl Microbiol* 43(2), 125-130.

Heaselgrave, W.P., N. ; Kilvington, S.; Kehoe, S.C. and McGuigan, K.G. (2006) Solar disinfection of poliovirus and Acanthamoeba polyphaga cysts in water – a laboratory study using simulated sunlight. *Lett Appl Microbiol* 43, 125-130.

Helmann, J.D., Wu, M.F.W., Gaballa, A., Kobel, P.A., Morshedi, M.M., Fawcett, P. and Paddon, C. (2003) The Global Transcriptional Response of Bacillus subtilis to Peroxide Stress Is Coordinated by Three Transcription Factors. *J. Bacteriol.* 185(1), 243-253.

Henle, E.S. and Linn, S. (1997) Formation, prevention, and repair of DNA damage by iron/hydrogen peroxide. *J Biol Chem* 272(31), 19095-19098.

Heri, S., Moser, S. and Mosler, H.J. (2005) Determinants of the diffusion of SODIS: A quantitative field study in Bolivia (Summary Report), EAWAG, Duebendorf, Switzerland.

Heri, S. and Mosler, H.J. (2008) Factors affecting the diffusion of solar water disinfection: a field study in Bolivia. *Health Educ Behav* 35(4), 541-560.

Hiser, A.F., Murphy, J.L., Casanova, L.M. and Sobsey, M.D. (2009) Efficacy of One Drop Metal Ion Disinfectant for Inactivation of Indicator and Pathogenic Microorganisms. *Proceedings of the Water Environment Federation* 2009, 184-194.

Hoerter, J., Eisenstark, A. and Touati, D. (1989) Mutations by near-ultraviolet radiation in Escherichia coli strains lacking superoxide dismutase. *Mutation Research/Fundamental and Molecular Mechanisms of Mutagenesis* 215(2), 161.

Hoerter, J., Pierce, A., Troupe, C., Epperson, J. and Eisenstark, A. (1996) Role of enterobactin and intracellular iron in cell lethality during near-UV irradiation in Escherichia coli. *Photochemistry and Photobiology* 64(3), 537-541.

Hoerter, J.D., Arnold, A.A., Kuczynska, D.A., Shibuya, A., Ward, C.S., Sauer, M.G., Gizachew, A., Hotchkiss, T.M., Fleming, T.J. and Johnson, S. (2005a) Effects of sublethal UVA irradiation on activity levels of oxidative defense enzymes and protein oxidation in Escherichia coli. *J Photochem Photobiol B* 81(3), 171-180.

Hoerter, J.D., Arnold, A.A., Ward, C.S., Sauer, M., Johnson, S., Fleming, T. and Eisenstark, A. (2005b) Reduced hydroperoxidase (HPI and HPII) activity in the Deltafur mutant contributes to increased sensitivity to UVA radiation in Escherichia coli. *J Photochem Photobiol B* 79(2), 151-157.

Hollaender, A. and Duggar, B.M. (1936) Irradiation of Plant Viruses and of Microörganisms with Monochromatic Light: III. Resistance of the Virus of Typical Tobacco Mosaic and Escherichia Coli to Radiation from lambda 3000 to lambda 2250 A. *PNAS* 22(1), 19-24.

Hollaender, A. and Emmons, C. (1941a) Wavelength dependence of mutation production in ultraviolet with special emphasis on fungi. *Cold Spring Harbor Symposia on Quantitative Biology* 9, 179-186.

Hollaender, A. and Emmons, C.W. (1941b) Wavelength Dependence of Mutation Production in the Ultraviolet with Special Emphasis on Fungi. *Cold Spring Harbor Symposia on Quantitative Biology* 9, 179-186.

Hollaender, A. (1943) Effect of long ultraviolet and short visible radiation (3500 to 4900A) on escherichia coli. *Journal of Bacteriology* 46(6), 531-541.

Hollaender, A. and Oliphant, J. (1944) The inactivating effect of monochromatic ultraviolet radiation on influenza virus. *J Bacteriol* 48(4), 447-454.

Hotze, E.M., Badireddy, A.R., Chellam, S. and Wiesner, M.R. (2009) Mechanisms of bacteriophage inactivation via singlet oxygen generation in UV illuminated fullerol suspensions. *Environ. Sci. Technol.* 43(17), 6639-6645.

Hug, S.J. and Leupin, O. (2003) Iron-catalyzed oxidation of arsenic(III) by oxygen and by hydrogen peroxide: pH-dependent formation of oxidants in the Fenton reaction. *Environ Sci Technol* 37(12), 2734-2742.

Hunter, P.R. (2009) Household water treatment in developing countries: comparing different intervention types using meta-regression. *Environ Sci Technol* 43(23), 8991-8997.

Huo, A., Xu, B., Chowdhury, M.A., Islam, M.S., Montilla, R. and Colwell, R.R. (1996) A simple filtration method to remove plankton-associated Vibrio cholerae in raw water supplies in developing countries. *Appl. Environ. Microbiol.* 62(7), 2508-2512.

Ilari, A., Ceci, P., Ferrari, D., Rossi, G.L. and Chiancone, E. (2002) Iron Incorporation into Escherichia coli Dps Gives Rise to a Ferritin-like Microcrystalline Core. *Journal of Biological Chemistry* 277(40), 37619-37623.

Imlay, J.A. and Linn, S. (1987) Mutagenesis and Stress Responses Induced in Escherichia-Coli by Hydrogen-Peroxide. *Journal of Bacteriology* 169(7), 2967-2976.

Imlay, J.A., Chin, S.M. and Linn, S. (1988a) Toxic DNA Damage by Hydrogen-Peroxide through the Fenton Reaction Invivo and Invitro. *Science* 240(4852), 640-642.

Imlay, J.A., Chin, S.M. and Linn, S. (1988b) Toxic DNA damage by hydrogen peroxide through the Fenton reaction in vivo and in vitro. *Science* 240(4852), 640-642.

Imlay, J.A. and Linn, S. (1988) DNA damage and oxygen radical toxicity. *Science* 240(4857), 1302-1309.

Imlay, J.A. (2002) How oxygen damages microbes: oxygen tolerance and obligate anaerobiosis. *Adv Microb Physiol* 46, 111-153.

Imlay, J.A. (2003) Pathways of oxidative damage. *Annual Review of Microbiology* 57, 395-418.

Imlay, J.A. (2006) Iron-sulphur clusters and the problem with oxygen. *Mol Microbiol* 59(4), 1073-1082.

Ishii, S., Ksoll, W.B., Hicks, R.E. and Sadowsky, M.J. (2006) Presence and Growth of Naturalized Escherichia coli in Temperate Soils from Lake Superior Watersheds. *Appl. Environ. Microbiol.* 72(1), 612-621.

Ishii, S., Hansen, D.L., Hicks, R.E. and Sadowsky, M.J. (2007) Beach Sand and Sediments are Temporal Sinks and Sources of Escherichia coli in Lake Superior. *Environmental Science & Technology* 41(7), 2203.

Ito, K., Hiraku, Y. and Kawanishi, S. (2007) Photosensitized DNA damage induced by NADH: Site specificity and mechanism. *Free Radical Research* 41(4), 461-468.

Jacobson, F.S., Morgan, R.W., Christman, M.F. and Ames, B.N. (1989) An Alkyl Hydroperoxide Reductase from Salmonella-Typhimurium Involved in the Defense of DNA against Oxidative Damage - Purification and Properties. *Journal of Biological Chemistry* 264(3), 1488-1496.

Jaegger, J. (1985) Solar-UV actions on Living Cells, Praeger, New York, NY.

Jagger, J. (1967) Introduction to research in ultra-violet photobiology, Prentice-Hall, Englewood Cliffs, NJ.

Jagger, J. (1981) Near-UV Radiation Effects on Microorganisms. *Photochemistry and Photobiology* 34(6), 761-768.

Jagger, J. (1985a) Solar-UV actions on Living Cells, Praeger, New York, NY.

Jagger, J. (1985b) Solar-UV actions on living cells.

Ji, M.F. and Wood, W. (2007) Purchase and Consumption Habits: Not Necessarily What You Intend, pp. 261-276.

Johnson, H.R., Hooker, J.M., Francis, M.B. and Clark, D.S. (2007) Solubilization and stabilization of bacteriophage MS2 in organic solvents. *Biotechnol Bioeng* 97(2), 224-234.

Kadir, K. (2010) Sunlight-Mediated Inactivation Mechanisms of Enteroccocus faecalis and Escherichia coli in Waste Stabilization Ponds, University of California, Berkeley.

Keenan, C.R. (2001) The Effect of Additional Hydrogen Peroxide on Solar Water Disinfection, Massachusetts Institute of Technology, Cambridge MA, USA.

Kehoe, S.C., Joyce, T.M., Ibrahim, P., Gillespie, J.B., Shahar, R.A. and McGuigan, K.G. (2001) Effect of agitation, turbidity, aluminium foil reflectors and container volume on the inactivation efficiency of batch-process solar disinfectors. *Water Research* 35(4), 1061-1065.

Kehoe, S.C., Barer, M.R., Devlin, L.O. and McGuigan, K.G. (2004) Batch process solar disinfection is an efficient means of disinfecting drinking water contaminated with Shigella dysenteriae type I. *Letters in Applied Microbiology* 38(5), 410-414.

Khaengraeng, R. and Reed, R.H. (2005) Oxygen and photoinactivation of *Escherichia coli* in UVA and sunlight. *Journal of Applied Microbiology* 99(1), 39-50.

Kim, C.S. and Jung, J. (1992) Iron-Sulfur Centers as Endogenous Blue Light Sensitizers in Cells: A Study With an Artificial non-Heme Iron Protein, pp. 63-68, Blackwell Publishing Ltd.

Kim, S.Y., Kwon, O.J. and Park, J.W. (2001) Inactivation of catalase and superoxide dismutase by singlet oxygen derived from photoactivated dye. *Biochimie* 83(5), 437-444.

King, B.J., Hoefel, D., Daminato, D.P., Fanok, S. and Monis, P.T. (2008) Solar UV reduces *Cryptosporidium parvum* oocyst infectivity in environmental waters. *Journal of Applied Microbiology* 104(5), 1311-1323.

Knowles, R.L. and Eisenstark, A. (1994) Near-ultraviolet mutagenesis in superoxide dismutase-deficient strains of Escherichia coli. *Environ Health Perspect* 102(1), 88-94.

Kochevar, I.E. (1990) UV-Induced Protein Alterations and Lipid Oxidation in Erythrocyte Membranes, pp. 795-800, Blackwell Publishing Ltd.

Kohn, T., Grandbois, M., McNeill, K. and Nelson, K.L. (2007) Association with natural organic matter enhances the sunlight-mediated inactivation of MS2 coliphage by singlet oxygen. *Environmental Science & Technology* 41(13), 4626-4632.

Kohn, T. and Nelson, K.L. (2007a) Sunlight-mediated inactivation of MS2 coliphage via exogenous singlet oxygen produced by sensitizers in natural waters. *Environ. Sci. Technol.* 41(1), 192-197.

Kohn, T. and Nelson, K.L. (2007b) Sunlight-mediated inactivation of MS2 coliphage via exogenous singlet oxygen produced by sensitizers in natural waters. *Environmental Science & Technology* 41(1), 192-197.

Kraemer, S.M. and Mosler, H.J. (2010) Persuasion factors influencing the decision to use sustainable household water treatment. *Int J Environ Health Res* 20(1), 61-79.

Kramer, G.F. and Ames, B.N. (1987) Oxidative Mechanisms of Toxicity of Low-Intensity near-UV Light in Salmonella-Typhimurium. *Journal of Bacteriology* 169(5), 2259-2266.

Kramer, G.F., Baker, J.C. and Ames, B.N. (1988) Near-UV stress in Salmonella typhimurium: 4-thiouridine in tRNA, ppGpp, and ApppGpp as components of an adaptive response. *J. Bacteriol.* 170(5), 2344-2351.

Kunkel, M. and Watowich, S.J. (2004) Biophysical characterization of hepatitis C virus core protein: implications for interactions within the virus and host. *FEBS Lett* 557(1-3), 174-180.

Lloyd, R.E., Rinkenberger, J.L., Hug, B.A. and Tuveson, R.W. (1990) Growing Escherichia-Coli Mutants Deficient in Riboflavin Biosynthesis with Nonlimiting Riboflavin Results in Sensitization to Inactivation by Broad-Spectrum near-Ultraviolet Light (320-400 Nm). *Photochemistry and Photobiology* 52(4), 897-901.

Lonnen, J., Kilvington, S., Kehoe, S.C., Al-Touati, F. and McGuigan, K.G. (2005) Solar and photocatalytic disinfection of protozoan, fungal and bacterial microbes in drinking water. *Water Research* 39(5), 877-883.

Love, D.C., Silverman, A.C. and Nelson, K.L. (2010) Human Virus and Bacteriophage Inactivation in Clear Water by Simulated Sunlight Compared to Bacteriophage Inactivation at a Southern California Beach. *Environmental Science & Technology* 44(18), 6965-6970.

Luckiesh, M. (1946) Applications of germicidal, erythemal and infrared energy, D. Van Nostrand, New York, New York.

Lukacs, H.A. (2001) From Design To Implementation: Innovative Slow Sand Filtration For Use in Developing Countries, Massachusetts Institute of Technology, Cambridge, MA USA.

Lytle, C.D. and Sagripanti, J.L. (2005) Predicted inactivation of viruses of relevance to biodefense by solar radiation. *J Virol* 79(22), 14244-14252.

Madigan, M.T.M., J.M.; Parker, J. (2002) Brock Biology of Microorganisms, Pearson Education, Inc., Upper Saddle River, NJ.

Makareyeva, E., Makedonov, Y. and Lozovskaya, E. (1997) Photosensitization and photoprotection properties of nicotinic acid derivatives. *Russian Chemical Bulletin* 46(5), 902-905.

Malato, S., Blanco, J., Alarcón, D.C., Maldonado, M.I., Fernández-Ibáñez, P. and Gernjak, W. (2007) Photocatalytic decontamination and disinfection of water with solar collectors. *Catalysis Today* 122(1-2), 137-149.

Mani, S.K., Kanjur, R., Bright Singh, I.S. and Reed, R.H. (2006) Comparative effectiveness of solar disinfection using small-scale batch reactors with reflective, absorptive and transmissive rear surfaces. *Water Research* 40(4), 721.

Masse, E. and Gottesman, S. (2002) A small RNA regulates the expression of genes involved in iron metabolism in Escherichia coli. *Proc Natl Acad Sci U S A* 99(7), 4620-4625.

Mathers, C., Stevens, G. and Mascarenhas, M. (2009) Global health risks: mortality and burden of disease attributable to selected major risks, World Health Organization.

Mausezahl, D., Christen, A., Pacheco, G.D., Tellez, F.A., Iriarte, M., Zapata, M.E., Cevallos, M., Hattendorf, J., Cattaneo, M.D., Arnold, B., Smith, T.A. and Colford, J.M., Jr. (2009) Solar Drinking Water Disinfection (SODIS) to Reduce Childhood Diarrhoea in Rural Bolivia: A Cluster-Randomized, Controlled Trial. *PLoS Med* 6(8), e1000125.

McCormick, J.P., Fischer, J.R., Pachlatko, J.P. and Eisenstark, A. (1976) Characterization of a cell-lethal product from the photooxidation of tryptophan: hydrogen peroxide. *Science* 191(4226), 468-469.

McCormick, J.P. and Thomason, T. (1978) Near-Ultraviolet Photooxidation of Tryptophan - Proof of Formation of Superoxide Ion. *Journal of the American Chemical Society* 100(1), 312-313.

McGuigan, K.G., Joyce, T.M., Conroy, R.M., Gillespie, J.B. and Elmore-Meegan, M. (1998) Solar disinfection of drinking water contained in transparent plastic bottles:

characterizing the bacterial inactivation process. *Journal of Applied Microbiology* 84(6), 1138-1148.

McGuigan, K.G., Mendez-Hermida, F., Castro-Hermida, J.A., Ares-Mazas, E., Kehoe, S.C., Boyle, M., Sichel, C., Fernandez-Ibanez, P., Meyer, B.P., Ramalingham, S. and Meyer, E.A. (2006) Batch solar disinfection inactivates oocysts of Cryptosporidium parvum and cysts of Giardia muris in drinking water. *J Appl Microbiol* 101(2), 453-463.

McHugh, J.P., Rodriguez-Quinones, F., Abdul-Tehrani, H., Svistunenko, D.A., Poole, R.K., Cooper, C.E. and Andrews, S.C. (2003) Global iron-dependent gene regulation in Escherichia coli. A new mechanism for iron homeostasis. *J Biol Chem* 278(32), 29478-29486.

McLaughlin, L.A., Levy, K., Beck, N.K., Shin, G.A., Meschke, J.S. and Eisenberg, J.N. (2009) An observational study on the effectiveness of point-of-use chlorination. *J Environ Health* 71(8), 48-53.

Mendez-Hermida, F., Castro-Hermida, J.A., Ares-Mazas, E., Kehoe, S.C. and McGuigan, K.G. (2005) Effect of batch-process solar disinfection on survival of Cryptosporidium parvum oocysts in drinking water. *Applied and Environmental Microbiology* 71(3), 1653-1654.

Mendez-Hermida, F., Ares-Mazas, E., McGuigan, K.G., Boyle, M., Sichel, C. and Fernandez-Ibanez, P. (2007) Disinfection of drinking water contaminated with Cryptosporidium parvum oocysts under natural sunlight and using the photocatalyst TiO2. *J Photochem Photobiol B* 88(2-3), 105-111.

Mintz, E., Bartram, J., Lochery, P. and Wegelin, M. (2001) Not just a drop in the bucket: Expanding access to point-of-use water treatment systems. *American Journal of Public Health* 91(10), 1565-1570.

Morris, R.D., Audet, A.M., Angelillo, I.F., Chalmers, T.C. and Mosteller, F. (1992) Chlorination, chlorination by-products, and cancer: a meta-analysis. *Am J Public Health* 82(7), 955-963.

Moser, S. and Mosler, H.J. (2008) Differences in influence patterns between groups predicting the adoption of a solar disinfection technology for drinking water in Bolivia. *Soc Sci Med* 67(4), 497-504.

Moss, S.H. and Smith, K.C. (1981) Membrane damage can be a significant factor in the inactivation of Escherichia coli by near-ultraviolet radiation. *Photochem Photobiol* 33(2), 203-210.

Mtapuri-Zinyowera, S., Midzi, N., Muchaneta-Kubara, C.E., Simbini, T. and Mduluza, T. (2009) Impact of solar radiation in disinfecting drinking water contaminated with Giardia

duodenalis and Entamoeba histolytica/dispar at a point-of-use water treatment. *J Appl Microbiol* 106(3), 847-852.

Murray, C.J. (1994) Quantifying the burden of disease: the technical basis for disability-adjusted life years, World Health Organization.

Nair, S. and Finkel, S.E. (2004) Dps protects cells against multiple stresses during stationary phase. *Journal of Bacteriology* 186(13), 4192-4198.

Nam, W. (2007) High-Valent Iron(IV)-Oxo Complexes of Heme and Non-Heme Ligands in Oxygenation Reactions. *Accounts of Chemical Research* 40(7), 522-531.

Navntoft, C., Ubomba-Jaswa, E., McGuigan, K.G. and Fernandez-Ibanez, P. (2008) Effectiveness of solar disinfection using batch reactors with non-imaging aluminium reflectors under real conditions: Natural well-water and solar light. *J Photochem Photobiol B* 93(3), 155-161.

Neal, D.T., Wood, W. and Quinn, J.M. (2006) Habits--A Repeat Performance. *Current Directions in Psychological Science* 15, 198-202.

Neeley, W.L. (2006) Genomic Consequences of DNA Oxidation by Peroxynitrite, Massachusetts Institute of Technology, Cambridge Massachusetts.

Nieto-Juarez, J.I., PierzchÅ‚a, K., Sienkiewicz, A. and Kohn, T. (2010) Inactivation of MS2 coliphage in Fenton and Fenton-like systems: role of transition metals, hydrogen peroxide and sunlight. *Environmental Science & Technology* 44(9), 3351-3356.

Noble, R.T., Lee, I.M. and Schiff, K.C. (2004) Inactivation of indicator micro-organisms from various sources of faecal contamination in seawater and freshwater, pp. 464-472, Blackwell Science Ltd.

Oates, P.M. (2001) Solar Disinfection For Point of Use Water Treatment in Haiti, Massachusetts Institute of Technology.

Oates, P.M., Shanahan, P. and Polz, M.F. (2003) Solar disinfection (SODIS): simulation of solar radiation for global assessment and application for point-of-use water treatment in Haiti. *Water Research* 37(1), 47-54.

Oladepo, S.A. and Loppnow, G.R. (2010) The Effect of Tryptophan on UV-induced DNA Photodamage, pp. 844-851, Blackwell Publishing Ltd.

Orr, C.W.M. (1967a) Studies on Ascorbic Acid .I. Factors Influencing Ascorbate-Mediated Inhibition of Catalase. *Biochemistry* 6(10), 2995-&.

Orr, C.W.M. (1967b) Studies on Ascorbic Acid .2. Physical Changes in Catalase Following Incubation with Ascorbate or Ascorbate and Copper (2). *Biochemistry* 6(10), 3000-&.

Oyanedel-Craver, V.A. and Smith, J.A. (2007) Sustainable Colloidal-Silver-Impregnated Ceramic Filter for Point-of-Use Water Treatment. *Environmental Science & Technology* 42(3), 927-933.

Park, S., You, X. and Imlay, J.A. (2005) Substantial DNA damage from submicromolar intracellular hydrogen peroxide detected in Hpx- mutants of Escherichia coli. *Proceedings of the National Academy of Sciences of the United States of America* 102(26), 9317-9322.

Patterson, C., Waskar, M., Muhammad, N., Sinha, R., Krishnan, E.R. and Shah, N. (2010) Evaluation of a Pour-Through Water Treatment Device for Use as Microbiological Purifier, pp. 33-33, ASCE, Providence, Rhode Island.

Payne, S.M. and Finkelstein, R.A. (1978) The critical role of iron in host-bacterial interactions. *J Clin Invest* 61(6), 1428-1440.

Peak, J.G., Peak, M.J. and Tuveson, R.W. (1983) Ultraviolet action spectra for aerobic and anaerobic inactivation of Escherichia coli strains specifically sensitive and resistant to near ultraviolet radiations. *Photochem Photobiol* 38(5), 541-543.

Peak, M.J. and Peak, J.G. (1978) Action spectra for the ultraviolet and visible light inactivation of phage T7: effect of host-cell reactivation. *Radiat Res* 76(2), 325-330.

Peak, M.J., Peak, J.G., Moehring, M.P. and Webb, R.B. (1984) Ultraviolet Action Spectra for DNA Dimer Induction, Lethality, and Mutagenesis in Escherichia-Coli with Emphasis on the Uvb Region. *Photochemistry and Photobiology* 40(5), 613-620.

Peak, M.J., Johnson, J.S., Tuveson, R.W. and Peak, J.G. (1987) Inactivation by Monochromatic near-Uv Radiation of an Escherichia-Coli Hema8 Mutant Grown with and without Delta-Aminolevulinic-Acid - the Role of DNA Vs Membrane Damage. *Photochemistry and Photobiology* 45(4), 473-478.

Pecson, B.M., Martin, L.V. and Kohn, T. (2009) Quantitative PCR for Determining the Infectivity of Bacteriophage MS2 upon Inactivation by Heat, UV-B Radiation, and Singlet Oxygen: Advantages and Limitations of an Enzymatic Treatment To Reduce False-Positive Results. *Appl. Environ. Microbiol.* 75(17), 5544-5554.

Pedersen, S., Bloch, P.L., Reeh, S. and Neidhardt, F.C. (1978) Patterns of protein synthesis in E. coli: a catalog of the amount of 140 individual proteins at different growth rates. *Cell* 14(1), 179.

Petersen, A.B., Gniadecki, R., Vicanova, J., Thorn, T. and Wulf, H.C. (2000) Hydrogen peroxide is responsible for UVA-induced DNA damage measured by alkaline comet assay in HaCaT keratinocytes. *J Photochem Photobiol B* 59(1-3), 123-131.

Pochon, A., Vaughan, P.P., Gan, D.Q., Vath, P., Blough, N.V. and Falvey, D.E. (2002) Photochemical oxidation of water by 2-methyl-1,4-benzoquinone: Evidence against the formation of free hydroxyl radical. *Journal of Physical Chemistry A* 106(12), 2889-2894.

Powell, W. and Setlow, R. (1956) The effect of monochromatic ultraviolet radiation on the interfering property of influenza virus. *Virology* 2(3), 337-343.

Qualls, R.G., Flynn, M.P. and Johnson, J.D. (1983) The Role of Suspended Particles in Ultraviolet Disinfection. *Journal (Water Pollution Control Federation)* 55(10), 1280-1285.

Quintessa (2009) Graph Grabber, Quintessa Limited, Oxfordshire, UK.

Ragab_depre, N.J. (1982) Water Disinfection with the Hydrogen Peroxide-Ascorbic Acid-Copper(Ii) System. *Applied and Environmental Microbiology* 44(3), 555-560.

Rainey, R.C. and Harding, A.K. (2005a) Acceptability of solar disinfection of drinking water treatment in Kathmandu Valley, Nepal. *Int J Environ Health Res* 15(5), 361-372.

Rainey, R.C. and Harding, A.K. (2005b) Drinking water quality and solar disinfection: effectiveness in peri-urban households in Nepal. *J Water Health* 3(3), 239-248.

Rauth, A. (1965) The physical state of viral nucleic acid and the sensitivity of viruses to ultraviolet light. *Biophysical Journal* 5, 257-273.

Reed, R.H. (1997) Solar inactivation of faecal bacteria in water: The critical role of oxygen. *Letters in Applied Microbiology* 24(4), 276-280.

Reed, R.H., Mani, S.K. and Meyer, V. (2000) Solar photo-oxidative disinfection of drinking water: preliminary field observations. *Lett Appl Microbiol* 30(6), 432-436.

Reed, R.H. (2004) The inactivation of microbes by sunlight: solar disinfection as a water treatment process. *Adv Appl Microbiol* 54, 333-365.

Reygadas, F., Ray, I. and Nelson, K.L. (2009) Field Evaluation of The UV Tube in Baja California Sur, Mexico. *Proceedings of the Water Environment Federation* 2009, 950-952.

Rijal, G.K. and Fujioka, R.S. (2003) Use of reflectors to enhance the synergistic effects of solar heating and solar wavelengths to disinfect drinking water sources. *Water Sci Technol* 48(11-12), 481-488.

Rincon, A.-G. and Pulgarin, C. (2007) Solar Photolytic and Photocatalytic Disinfection of Water at Laboratory and Field Scale. Effect of the Chemical Composition of Water and Study of the Postirradiation Events. *Journal of Solar Energy Engineering* 129(1), 100-110.

Rincón, A.G. and Pulgarin, C. (2003) Photocatalytical inactivation of E. coli: effect of (continuous-intermittent) light intensity and of (suspended-fixed) TiO2 concentration. *Applied Catalysis B: Environmental* 44(3), 263-284.

Rincón, A.G. and Pulgarin, C. (2004a) Bactericidal action of illuminated TiO2 on pure Escherichia coli and natural bacterial consortia: post-irradiation events in the dark and assessment of the effective disinfection time. *Applied Catalysis B: Environmental* 49(2), 99-112.

Rincón, A.G. and Pulgarin, C. (2004b) Effect of pH, inorganic ions, organic matter and H2O2 on E-coli K12 photocatalytic inactivation by TiO2 - Implications in solar water disinfection. *Applied Catalysis B-Environmental* 51(4), 283-302.

Rincón, A.G. and Pulgarin, C. (2007a) Fe3+ and TiO2 solar-light-assisted inactivation of E. coli at field scale: Implications in solar disinfection at low temperature of large quantities of water. *Catalysis Today* 122(1-2), 128-136.

Rincón, A.G. and Pulgarin, C. (2007b) Solar Photolytic and Photocatalytic Disinfection of Water at Laboratory and Field Scale. Effect of the Chemical Composition of Water and Study of the Postirradiation Events. *Journal of Solar Energy Engineering* 129(1), 100-110.

Rincón, A.G. and Pulgarin, C. (2007c) Absence of E. coli regrowth after Fe3+ and TiO2 solar photoassisted disinfection of water in CPC solar photoreactor. *Catalysis Today* 124(3-4), 204-214.

Rincón, A.G. and Pulgarin, C. (2010) Electrochemistry for the Environment. Comninellis, C. and Chen, G. (eds), pp. 443-472, Springer New York.

Rivers, T. and Gates, F. (1928) Ultraviolet light and vaccinia virus. II. The effect of monochromatic ultraviolet light upon vaccine virus. *J Exp Med* 47, 45-49.

Rontó, G., Gáspár, S. and Bérces, A. (1992) Phage T7 in biological UV dose measurement. *J Photochem Photobiol B, Biol* 12(3), 285-294.

Rose, A., Roy, S., Abraham, V., Holmgren, G., George, K., Balraj, V., Abraham, S., Muliyil, J., Joseph, A. and Kang, G. (2006) Solar disinfection of water for diarrhoeal prevention in southern India. *Arch Dis Child* 91(2), 139-141.

Rush, J.D., Maskos, Z. and Koppenol, W.H. (1990) Reactions of Iron(II) Nucleotide Complexes with Hydrogen Peroxide. *Febs Letters* 261(1), 121-123.

Safapour, N. and Metcalf, R.H. (1999) Enhancement of solar water pasteurization with reflectors. *Appl Environ Microbiol* 65(2), 859-861.

Sagripanti, J.L. and Kraemer, K.H. (1989) Site-Specific Oxidative DNA Damage at Polyguanosines Produced by Copper Plus Hydrogen-Peroxide. *Journal of Biological Chemistry* 264(3), 1729-1734.

Sagripanti, J.L., Routson, L.B., Bonifacino, A.C. and Lytle, C.D. (1997) Mechanism of copper-mediated inactivation of herpes simplex virus. *Antimicrobial Agents and Chemotherapy* 41(4), 812-817.

Sak, B.D., Eisenstark, A. and Touati, D. (1989) Exonuclease III and the catalase hydroperoxidase II in Escherichia coli are both regulated by the katF gene product. *Proc Natl Acad Sci U S A* 86(9), 3271-3275.

Salih, F.M. (2002) Enhancement of solar inactivation of Escherichia coli by titanium dioxide photocatalytic oxidation. *Journal of Applied Microbiology* 92(5), 920-926.

Sammartano, L.J. and Tuveson, R.W. (1984) The Effects of Exogenous Catalase on Broad-Spectrum near-UV (300-400 nm) Treated Escherichia Coli Cells. *Photochemistry and Photobiology* 40(5), 607-612.

Sammartano, L.J., Tuveson, R.W. and Davenport, R. (1986) Control of sensitivity to inactivation by H2O2 and broad-spectrum near-UV radiation by the Escherichia coli katF locus. *J. Bacteriol.* 168(1), 13-21.

Sammartano, L.J. and Tuveson, R.W. (1987) Escherichia coli strains carrying the cloned cytochrome d terminal oxidase complex are sensitive to near-UV inactivation. *Journal of Bacteriology* 169(11), 5304-5307.

Sato, K., Taguchi, H., Maeda, T., Minami, H., Asada, Y., Watanabe, Y. and Yoshikawa, K. (1995) The Primary Cytotoxicity in Ultraviolet-A-Irradiated Riboflavin Solution Is Derived from Hydrogen Peroxide. *J Investig Dermatol* 105(4), 608-612.

Schmidt, W.-P. and Cairncross, S. (2009) Household Water Treatment in Poor Populations: Is There Enough Evidence for Scaling up Now? *Environmental Science & Technology* 43(4), 986-992.

Schwartzenbach, R.P.G., P.M.; Imboden, D.M. (2003) Environmental Organic Chemistry, John Wiley and Sons, Hoboken, NJ.

Sciacca, F., Rengifo-Herrera, J.A., Wethe, J. and Pulgarin, C. (2010) Dramatic enhancement of solar disinfection (SODIS) of wild Salmonella sp. in PET bottles by H2O2 addition on natural water of Burkina Faso containing dissolved iron. *Chemosphere* 78(9), 1186-1191.

Seaver, L.C. and Imlay, J.A. (2001a) Hydrogen peroxide fluxes and compartmentalization inside growing Escherichia coli. *Journal of Bacteriology* 183(24), 7182-7189.

Seaver, L.C. and Imlay, J.A. (2001b) Alkyl hydroperoxide reductase is the primary scavenger of endogenous hydrogen peroxide in Escherichia coli. *Journal of Bacteriology* 183(24), 7173-7181.

Shah, S.K., McBean, E.A. and Anderson, W.A. (1996) Preliminary studies into the disinfection of potable water using solar radiation. *Canadian Journal of Civil Engineering* 23(2), 373-380.

Sharpe, M.A., Robb, S.J. and Clark, J.B. (2003) Nitric oxide and Fenton/Haber-Weiss chemistry: nitric oxide is a potent antioxidant at physiological concentrations. *J Neurochem* 87(2), 386-394.

Sichel, C., Blanco, J., Malato, S. and Fernández-Ibáñez, P. (2007a) Effects of experimental conditions on E. coli survival during solar photocatalytic water disinfection. *Journal of Photochemistry and Photobiology A: Chemistry* 189(2-3), 239-246.

Sichel, C., Tello, J., de Cara, M. and Fernández-Ibáñez, P. (2007b) Effect of UV solar intensity and dose on the photocatalytic disinfection of bacteria and fungi. *Catalysis Today* 129(1-2), 152-160.

Sichel, C., Fernandez-Ibanez, P., de Cara, M. and Tello, J. (2009) Lethal synergy of solar UV-radiation and H(2)O(2) on wild Fusarium solani spores in distilled and natural well water. *Water Res* 43(7), 1841-1850.

Sidorkina, O.M., Kuznetsov, S.V., Blais, J.C., Bazin, M., Laval, J. and Santus, R. (1999) Ultraviolet-B-Induced Damage to Escherichia coli Fpg Protein, pp. 658-663, Blackwell Publishing Ltd.

Sies, H. (ed) (1985) Oxidative Stress, Academic Press, London.

Sies, H. (1993) Strategies of antioxidant defense. *European Journal of Biochemistry* 215(2), 213-219.

Sinha, R.P. and Hader, D.P. (2002) UV-induced DNA damage and repair: a review. *Photochemical & Photobiological Sciences* 1(4), 225-236.

Sinton, L., Hall, C., Lynch, P. and Davies-Colley, R. (2002a) Sunlight inactivation of fecal indicator bacteria and bacteriophages from waste stabilization pond effluent in fresh and saline waters. *Applied and Environmental Microbiology* 68(3), 1122-1131.

Sinton, L.W., Finlay, R.K. and Lynch, P.A. (1999) Sunlight inactivation of fecal bacteriophages and bacteria in sewage-polluted seawater. *Applied and Environmental Microbiology* 65(8), 3605-3613.

Sinton, L.W., Hall, C.H., Lynch, P.A. and Davies-Colley, R.J. (2002b) Sunlight inactivation of fecal indicator bacteria and bacteriophages from waste stabilization pond effluent in fresh and saline waters. *Appl Environ Microbiol* 68(3), 1122-1131.

Smith, R.J., Kehoe, S.C., McGuigan, K.G. and Barer, M.R. (2000) Effects of simulated solar disinfection of water on infectivity of Salmonella typhimurium. *Letters in Applied Microbiology* 31(4), 284-288.

Smyk-Randall, E., Brown, O.R., Wilke, A., Eisenstark, A. and Flint, D.H. (1993) Near ultraviolet light inactivation of dihydroxyacid dehydratase in Escherichia coli. *Free Radic Biol Med* 14(6), 609-613.

Sobsey, M.D. (2002) Managing Water in the home: accelerated health gains from improved water supply, World Health Organization, Geneva, Switzerland.

Sobsey, M.D., Stauber, C.E., Casanova, L.M., Brown, J.M. and Elliott, M.A. (2008) Point of Use Household Drinking Water Filtration: A Practical, Effective Solution for Providing Sustained Access to Safe Drinking Water in the Developing World. *Environmental Science & Technology* 42(12), 4261-4267.

Sommer, B., Marino, A., Solarte, Y., Salas, M.L., Dierolf, C., Valiente, C., Mora, D., Rechsteiner, R., Setter, P., Wirojanagud, W., Ajarmeh, H., AlHassan, A. and Wegelin, M. (1997) SODIS - An emerging water treatment process. *Journal of Water Supply Research and Technology-Aqua* 46(3), 127-137.

Spindler, L.A. (1940) Effect of Tropical Sunlight on Eggs of Ascaris suis (Nematoda), the Large Intestinal Roundworm of Swine. *The Journal of Parasitology* 26(4), 323.

Stadler, L.J. and Uber, F.M. (1942) Genetic Effects of Ultraviolet Radiation in Maize. IV. Comparison of Monochromatic Radiations. *Genetics* 27(1), 84-118.

Stauber, C.E., Ortiz, G.M., Loomis, D.P. and Sobsey, M.D. (2009) A randomized controlled trial of the concrete biosand filter and its impact on diarrheal disease in Bonao, Dominican Republic. *Am J Trop Med Hyg* 80(2), 286-293.

Stohs, S.J. and Bagchi, D. (1995) Oxidative Mechanisms in the Toxicity of Metal-Ions. *Free Radical Biology and Medicine* 18(2), 321-336.

Storz, G., Jacobson, F.S., Tartaglia, L.A., Morgan, R.W., Silveira, L.A. and Ames, B.N. (1989) An alkyl hydroperoxide reductase induced by oxidative stress in Salmonella typhimurium and Escherichia coli: genetic characterization and cloning of ahp. *J. Bacteriol.* 171(4), 2049-2055.

Tamas, A., Tobias, R. and Mosler, H.J. (2009) Promotion of solar water disinfection: comparing the effectiveness of different strategies in a longitudinal field study in Bolivia. *Health Commun* 24(8), 711-722.

Termini, J. (2000) Hydroperoxide-induced DNA damage and mutations. *Mutation Research/Fundamental and Molecular Mechanisms of Mutagenesis* 450(1-2), 107-124.

Touati, D. (2000) Iron and oxidative stress in bacteria. *Archives of Biochemistry and Biophysics* 373(1), 1-6.

Tuveson, R.W., Peak, J.G. and Peak, M.J. (1983) Single-strand DNA breaks induced by 365 nm radiation in Escherichia coli strains differing in sensitivity to near and far UV. *Photochem Photobiol* 37(1), 109-112.

Tuveson, R.W. and Sammartano, L.J. (1986a) Sensitivity of Hema Mutant Escherichia-Coli-Cells to Inactivation by near-Uv Light Depends on the Level of Supplementation with Delta-Aminolevulinic-Acid. *Photochemistry and Photobiology* 43(6), 621-626.

Tuveson, R.W. and Sammartano, L.J. (1986b) Sensitivity of hemA mutant Escherichia coli cells to inactivation by near-UV light depends on the level of supplementation with delta-aminolevulinic acid. *Photochem Photobiol* 43(6), 621-626.

Tyrrell, R.M. and Webb, R.B. (1973) Reduced dimer excision in bacteria following near ultraviolet (365 nm) radiation. *Mutat Res* 19(3), 361-364.

Tyrrell, R.M., Ley, R.D. and Webb, R.B. (1974) Induction of single-strand breaks (alkali-labile bonds) in bacterial and phage DNA by near UV (365 nm) radiation. *Photochem Photobiol* 20(5), 395-398.

Tyrrell, R.M. (1978a) Mutagenic interaction between near-(365 nm) and far-(254 nm)ultraviolet radiation in repair-proficient and excision-deficient strains of Escherichia coli. *Mutat Res* 52(1), 25-35.

Tyrrell, R.M. (1978b) Solar dosimetry with repair deficient bacterial spores: action spectra, photoproduct measurements and a comparison with other biological systems. *Photochem Photobiol* 27(5), 571-579.

Tyrrell, R.M. (1980) Mutation induction by and mutational interaction between monochromatic wavelength radiations in the near-ultraviolet and visible ranges. *Photochem Photobiol* 31(1), 37-46.

Tyrrell, R.M. and Pidoux, M. (1989) SINGLET OXYGEN INVOLVEMENT IN THE INACTIVATION OF CULTURED HUMAN FIBROBLASTS BY UVA (334 nm, 365 nm) AND NEAR-VISIBLE (405 nm) RADIATIONS, pp. 407-412, Blackwell Publishing Ltd.

Tyrrell, R.M., Pourzand, C.A., Brown, J., Hejmadi, V., Kvam, V., Ryter, S. and Watkin, R.D. (2000) Cellular Studies with UVA Radiation: A Role for Iron. *Radiation Protection Dosimetry* 91(1-3), 37-39.

Ubomba-Jaswa, E., Navntoft, C., Polo-Lopez, M.I., Fernandez-Ibanez, P. and McGuigan, K.G. (2009) Solar disinfection of drinking water (SODIS): an investigation of the effect of UV-A dose on inactivation efficiency. *Photochem Photobiol Sci* 8(5), 587-595.

Ubomba-Jaswa, E., Fernandez-Ibanez, P. and McGuigan, K.G. (2010) A preliminary Ames fluctuation assay assessment of the genotoxicity of drinking water that has been solar disinfected in polyethylene terephthalate (PET) bottles. *J Water Health* 8(4), 712-719.

United_Nations (2000) United Nations Millennium Declaration, New York.

USEPA (2001) Method 1601: male-specific (F+) and somatic coliphage in water by two-step enrichment procedure. 821-R-01-030, 25.

USEPA (2003) National Primary Drinking Water Standards, USEPA.

USFDA (2009) US Code of Federal Regulations 21CFR184.1366.

Vairavamoorthy, K., Gorantiwar, S.D. and Pathirana, A. (2008) Managing urban water supplies in developing countries - Climate change and water scarcity scenarios. *Physics and Chemistry of the Earth, Parts A/B/C* 33(5), 330-339.

Vermilyea, A.W. and Voelker, B.M. (2009) Photo-Fenton Reaction at Near Neutral pH. *Environmental Science & Technology* 43(18), 6927-6933.

Voelker, B.M. and Sulzberger, B. (1996) Effects of fulvic acid on Fe(II) oxidation by hydrogen peroxide. *Environmental Science & Technology* 30(4), 1106-1114.

Voelker, B.M., Morel, F.o.M.M. and Sulzberger, B. (1997) Iron Redox Cycling in Surface Waters:â€‰ Effects of Humic Substances and Light. *Environmental Science & Technology* 31(4), 1004-1011.

Walker, D.C., Len, S.-V. and Sheehan, B. (2004a) Development and Evaluation of a Reflective Solar Disinfection Pouch for Treatment of Drinking Water. *Appl. Environ. Microbiol.* 70(4), 2545-2550.

Walker, D.C., Len, S.V. and Sheehan, B. (2004b) Development and evaluation of a reflective solar disinfection pouch for treatment of drinking water. *Appl Environ Microbiol* 70(4), 2545-2550.

Webb, R.B. and Lorenz, J.R. (1972) Toxicity of Irradiated Medium for Repair-Deficient Strains of Escherichia coli. *J. Bacteriol.* 112(1), 649-652.

Webb, R.B. and Brown, M.S. (1976) Sensitivity of Strains of Escherichia Coli Differing in Repair Capability to Far UV, near UV and Visible Radiations. *Photochemistry and Photobiology* 24(5), 425-432.

Webb, R.B. and Brown, M.S. (1979) Action Spectra for Oxygen-Dependent and Independent Inactivation of Escherichia Coli Wp2s from 254 nm to 460 nm. *Photochemistry and Photobiology* 29(2), 407-409.

Webb, R.B., Brown, M.S. and Ley, R.D. (1982) Nonreciprocal Synergistic Lethal Interaction between 365-nm and 405-nm Radiation in Wild-Type and Uvra Strains of Escherichia Coli. *Photochemistry and Photobiology* 35(5), 697-703.

Webb, R.B. and Tuveson, R.W. (1982) Differential sensitivity to inactivation of nur and nur+ strains of Escherichia coli at six selected wavelengths in the UVA, UVB and UVC ranges. *Photochem Photobiol* 36(5), 525-530.

Wegelin, M., Canonica, S., Mechsner, K., Fleischmann, T., Pesaro, F. and Metzler, A. (1994) Solar water disinfection; scope of the process and analysis of radiation experiments. *J Water SRT--Aqua* 43(3), 154-169.

Wegelin, M., Canonica, S., Alder, A.C., Marazuela, D., Suter, M.J.F., Bucheli, T.D., Haefliger, O.P., Zenobi, R., McGuigan, K.G., Kelly, M.T., Ibrahim, P. and Larroque, M. (2001) Does sunlight change the material and content of polyethylene terephthalate (PET) bottles? *Journal of Water Supply Research and Technology-Aqua* 50(3), 125-133.

Weisburg, W.G., Barns, S.M., Pelletier, D.A. and Lane, D.J. (1991) 16S ribosomal DNA amplification for phylogenetic study. *J. Bacteriol.* 173(2), 697-703.

Weishaupt, K.R., Gomer, C.J. and Dougherty, T.J. (1976) Identification of Singlet Oxygen as Cytotoxic Agent in Photo-Inactivation of a Murine Tumor. *Cancer Research* 36(7), 2326-2329.

White, D. (2000) The Physiology and Biochemistry of Prokaryotes, Oxford University Press, London, UK.

White, E.M., Vaughan, P.P. and Zepp, R.G. (2003) Role of the photo-Fenton reaction in the production of hydroxyl radicals and photobleaching of colored dissolved organic matter in a coastal river of the southeastern United States. *Aquatic Sciences* 65(4), 402-414.

WHO (2009) Death and disability-adjusted life year (DALY) rates, by WHO region, World Health Organization.

WHO/UNICEF (2010) Progress on Sanitation and Drinking-water: 2010 Update, WHO Press, Geneva, Switzerland.

Wiggington, K.R., Menin, L., Montoya, J.P. and Kohn, T. (2010) Oxidation of Virus Proteins during UV254 and Singlet Oxygen Mediated Inactivation. *Environmental Science & Technology* 44(14), 5437-5443.

Wigginton, K.R., Menin, L., Montoya, J.P. and Kohn, T. (2010) Oxidation of Virus Proteins during UV254 and Singlet Oxygen Mediated Inactivation. *Environmental Science & Technology* 44(14), 5437-5443.

Wilkinson, F., Helman, W.P. and Ross, A.B. (1995) Rate Constants for the Decay and Reactions of the Lowest Electronically Excited Singlet-State of Molecular-Oxygen in Solution - an Expanded and Revised Compilation. *Journal of Physical and Chemical Reference Data* 24(2), 663-1021.

Wilson, A.C. and Pardee, A.B. (1962) Regulation of Flavin Synthesis by Escherichia coli. *J Gen Microbiol* 28(2), 283-303.

Witkin, E.M. (1976) Ultraviolet mutagenesis and inducible DNA repair in Escherichia coli. *Bacteriol Rev* 40(4), 869-907.

Yamanaka, T. (1992) The biochemistry of bacterial cytochromes, Scientific Societes Press; Springer-Verlag, Tokyo, Japan.

Zapata, A., Velegraki, T., Sanchez-Perez, J.A., Mantzavinos, D., Maldonado, M.I. and Malato, S. (2009) Solar photo-Fenton treatment of pesticides in water: Effect of iron concentration on degradation and assessment of ecotoxicity and biodegradability. *Applied Catalysis B-Environmental* 88(3-4), 448-454.

Zepp, R., Schlotzhauer, P., Simmons, M., Miller, G., Baughman, G. and Wolfe, N. (1984) Dynamics of pollutant photoreactions in the hydrosphere. *Fresenius' Journal of Analytical Chemistry* 319(2), 119-125.

Zepp, R.G. and Schlotzhauer, P.F. (1983) Influence of algae on photolysis rates of chemicals in water. *Environmental Science & Technology* 17(8), 462-468.

Zepp, R.G., Schlotzhauer, P.F. and Sink, R.M. (1985) Photosensitized transformations involving electronic energy transfer in natural waters: role of humic substances. *Environmental Science & Technology* 19(1), 74-81.

Zhang, Z., Schwartz, S., Wagner, L. and Miller, W. (2000) A Greedy Algorithm for Aligning DNA Sequences. *Journal of Computational Biology* 7(1-2), 203-214.

Zhao, G., Ceci, P., Ilari, A., Giangiacomo, L., Laue, T.M., Chiancone, E. and Chasteen, N.D. (2002) Iron and Hydrogen Peroxide Detoxification Properties of DNA-binding Protein from Starved Cells. *Journal of Biological Chemistry* 277(31), 27689-27696.

Zheng, M., Wang, X., Templeton, L.J., Smulski, D.R., LaRossa, R.A. and Storz, G. (2001) DNA Microarray-Mediated Transcriptional Profiling of the Escherichia coli Response to Hydrogen Peroxide. *J. Bacteriol.* 183(15), 4562-4570.

Zigman, S. and Hare, J.D. (1976) Inhibition of cell growth by near ultraviolet light photoproducts of tryptophan. *Mol Cell Biochem* 10(3), 131-135.

Zigman, S., Yulo, T. and Griess, G.A. (1976) Inactivation of catalase by near ultraviolet light and tryptophan photoproducts. *Mol Cell Biochem* 11(3), 149-154.

Zwane, A.P., Zinman, J., Van Dusen, E., Pariente, W., Null, C., Miguel, E., Kremer, M., Karlan, D.S., Hornbeck, R., GinÃ©, X., Duflo, E., Devoto, F., Crepon, B. and Banerjee, A. (2011) Being surveyed can change later behavior and related parameter estimates. *Proceedings of the National Academy of Sciences* 108(5), 1821-1826.